46

Novel Dispersion Representation of Rectangular Dielectric Guides with Application to Leaky-Wave Antennas

by

Dean P. Hamilton

A thesis submitted in partial fulfilment of the requirements for the degree of
Doctor of Philosophy in Engineering

University of Warwick, School of Engineering
January 2007

Contents

8. DETERMINING ANTENNA CHARACTERISTICS

List of Tables

List of Figures

Acknowledgements

I would like to express my gratitude to my supervisors Mark Leeson and Roger Green, and to my friend and colleague Philip Shepherd, for all their kind help and encouragement.

Sincere thanks also to my parents, Molly and David, for their love and support.

And finally, thanks must go to my close friends for being there and putting up with me through this process. In no particular order: Doug, Alistair & Tina, Alex, Wendy, Cassida, Chris & Amy, Ali & Pea, Lesley, Vince & Shelly, Matt, Pete, Becky, Lou & Matt, Danny & Chrissy, Graham & Patricia, Will & Nicole, Steve & Mark of Mark's Bar in Pittsburgh P.A, my second home, and especially to Clare for being there the most.

Declaration

The work described in this thesis was conducted by the author except where stated otherwise, in the School of Engineering, University of Warwick between the dates of August 2003 and January 2007. No part of this work has been previously submitted to the University of Warwick or any other academic institution for admission to a higher degree. All publications to date arising from this thesis are listed within Appendix I.

Signed: 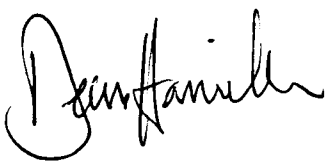 Date 15/06/07

Abstract

A novel method for graphically and mathematically representing the dispersion characteristics of electromagnetic dielectric structures is presented. The method has been used to develop closed-form formulas to find the longitudinal propagation constant and useful frequency range for a number of popular rectangular dielectric waveguide types. These formulas are presented in terms of their material dependency and are guide size and operating frequency independent. Their form is so trivial that these characteristics can now be found in just a few seconds using a basic calculator, yet still with second order accuracy. In addition, improvements have been made to a number of well-known formulas normally associated with periodic grating leaky-wave antennas. These improvements allow the width of the metal strip grating to be taken into consideration to derive the correct main beam angle, array factor pattern and grating limits. Previously, the grating width was neglected by the formulas and the resulting error was unacceptably high.

1. CHAPTER OVERVIEW

A large amount of work has been done on the subject of grating antennas in the last half a century. The periodic metal strip grating leaky-wave antenna variant is perhaps the least well developed of these. A handful of mathematical methods have been developed to analyse these structures. These methods are extremely complex and generally not found in text books perhaps because they are structure-specific. Other published works generally give insufficient detail to be able to reproduce or adapt their method. Each group of authors uses their own preferred method, perhaps because the less familiar alternatives are so laborious.

The results of published work generally furnish dispersion characteristics as well as antenna characteristics, but usually only for one or two sets of parameters. Without significant experience, it is difficult to know how the results might change for other sets of parameters and, particularly, how to adapt the method or results for a different material or operating frequency. However possible, the effort required to reproduce these methods to find the results for parameter changes is tremendous.

It is difficult to navigate through the published work with all its mixed terminology, different structures and limited results and to determine what combinations of guide type, guide dimensions and material can be used to satisfy an antenna specification, and how these choices will affect the antenna characteristics.

The combined effort required to implement one of these methods and then determine suitable parameters seemed excessive for such a simple structure, so there appeared to be an opportunity to reduce the effort. Further, a 3D electromagnetic structure field simulation software tool was available; therefore it appeared both possible and useful to reveal the response to parametric changes for some of the most popular structures so that the results can be used to converge rapidly on the most suitable parameters.

For a theoretical design, once the dispersion characteristics are known, it is then a relatively simple matter to dimension a grating antenna using some well-known formulas. This relationship is reciprocal. Since the methods for obtaining these characteristics for the perturbed structure are so complex and time-consuming there also appeared to be benefit in finding a simpler alternative. Other authors have assumed that the characteristics for the unperturbed waveguide structure are approximately those of the perturbed guide with metal strips on the surface and have used approximate methods to obtain the characteristics. The complexity is an order of magnitude less in these cases but the error and its dependencies are unknown. There was therefore an opportunity to determine what the error was in these cases.

An overview of each chapter follows: Chapter 2 considers the existing literature and reveals what has been done already for this structure and related structures. Then, Chapter 3 presents some essential background information, particularly about the approximate method used in this work. The most important results from a parametric analysis using the structure simulation tool are presented in Chapter 4 to reveal the response to parameter changes and some interesting new findings, like the relationship between the input reflection coefficient and the position of the first strip.

A new general method for graphically and mathematically presenting the dispersion characteristics of electromagnetic and possibly optical structures is presented in Chapters 5 to 7. The method is then used to present these characteristics for a number of types of commonly known rectangular dielectric waveguides of any size, but with a range of fixed aspect cross-sections, and a large range of material dielectric constants that encompass practical materials suitable for use at millimetre wavelengths or smaller. Specifically, both plots and formulas were derived using the method that find the real part of the propagation constant and the single-mode frequency range for *any* size guide. The formulas are of closed-form and are so trivial that these characteristics can be found in just a few seconds using a basic calculator, which more than meets the goal of finding a simpler alternative to existing methods. In

addition, the formulas place no significant restrictions on the guide geometry like some existing methods.

It also represents a significant step forward for both dielectric guide and leaky-wave antenna analysis and design and it is quite feasible that the same steps might be taken to advance other dispersion problems. This author believes that these formulas represent a least two orders of magnitude decrease in the time and effort needed to find these results by any other method, with similar second order accuracy.

A number of previous authors, specifically of the metal strip grating work, have made statements to the effect that the main beam angle is predominantly controlled by the real part of the propagation constant (the phase constant) but also to a small extent by the complex leakage constant part. The simulation results presented in Chapter 4 verify that this is the case, and, since other authors have neglected this leakage constant entirely in their work, it was decided to quantify that error for different parameters in Chapter 8.

It is well-known that the radiation from the antenna is a function of the complex leakage constant and that in turn is a strong function of the strip width and spacing. However, it turned out that the error could be quantified using only the real phase constant part of the propagation constants. This is an important new finding because the real part is significantly easier to obtain than both, especially now that the new dispersion formulas developed in this work allow the real part to be found so trivially. This new finding also enables the guide characteristics and antenna characteristics to be considered and designed separately. This reduces the effort significantly compared to analysing combinations of guide and strip geometry together.

A new perturbed model of a section of guide with strip in series with a section without the strip was used to both find and correct this error, also in Chapter 8. It calculates the average of the two propagation constants over the two sections, using a simple new formula. This result is compared with the propagation constant of the same series length of unperturbed guide to

find the error, and more importantly, allows the lengths of the sections to be adjusted to eliminate the error for any sets of parameters.

The existing well-known grating antenna formulas mentioned above, specifically those for calculating the beam angle, onset of grating lobes and the usual linear array antenna factor for finding the approximate radiation pattern, neglect the strip width and leakage and therefore suffer from the same error. It was found that this error can be eliminated by using the average perturbed propagation constant instead of the constant unperturbed constant in the same formulas.

In chapter 9, some key experimental results are presented to validate some of the theory presented in the earlier chapter of this work. Finally, Chapter 10 concludes and makes some recommendations for further work.

2. REVIEW OF CURRENT LITERATURE

2.1. *Directional antennas*

Highly directional antennas are important in applications such as radar and radiometry systems. Some directivity can easily be achieved by supporting a metal current element above a grounded surface or reflector. Further directivity is generally achieved by making it longer by adding more radiating elements with a periodic spacing, often using dipoles or monopoles. This type is classified as a linear array. In this case, element of the array is actively excited by a system of cables and possibly phase change electronics which can be used to direct or steer the main beam to a given angle. Another way to achieve directivity is to place a radiating element in the bottom of an open-ended metallic tube, typically with a circular or rectangular cross-section, classified as an aperture antenna. In this case, the directivity is increased with length of tube and-or flaring the tube out along its length, and increasing the size of the mouth (aperture) region. Therefore, in general, very high directivity comes at the expense of additional size, and as a result, additional cost and weight.

2.2. *Size reduction*

Once it became clear that adding dielectric materials around a linear radiating structure allowed it to be shrunk in size [1], but that the available analysis and design was complex and time consuming, there appeared to be an excellent opportunity to try to simplify the analysis.

2.3. Considering areas to study

At the beginning of this work, the author decided to investigate the very general category of dielectric antennas. The earliest works are summarized in the first, and one of the only books dedicated to this topic, in [2]. It primarily covered early theoretical and experimental work on circular solid and hollow dielectric rod antennas, and the history dating back to their first known use in German WWII radar systems and unpublished German works. Other investigations centred around dielectric resonant antennas [1] which are essentially radiating probes surrounded by planar dielectric layers of different permittivities or dielectric cylinders of a single material. In terms of interest, dielectric resonant antennas, which are narrowband, were soon surpassed by the category of leaky-wave antennas (LWA). The former dielectric rod antennas fit into this category although no reference is made to the leaky phrase, and they are all endfire radiating. The third of only four dedicated dielectric antenna books was essentially an update to the original dielectric rod work [3]. Finally, the most recent covers dielectric horns, with and without metal surrounds, and with dielectric lenses to correct phase aberrations [4].

2.4. Terminology

At first glance, with so much different nomenclature, and so many structures and methods of analysis used many different researchers, even the task of categorization seems overwhelming. Out of all of these different types, the rectangular dielectric waveguide based periodically perturbed leaky-wave antenna (LWA) appeared to be one of the least well developed subjects, and also one of the most interesting. Choosing this one specific type of antenna for analysis of course cuts down the number of methods and the amount of mixed nomenclature to something more manageable. In theory, its use is most practical at millimetre wavelengths and beyond, where the losses are as low or lower than their metal waveguide equivalents, and where the dimensions become difficult to realize using metals [5].

It soon becomes clear which terms are important in this field: transverse and longitudinal propagation constants, wavenumbers, decay constant, leakage constant, attenuation constant, phase constant, dispersion, dielectric constant, permittivity, waveguide modes, fundamental mode, dominant mode, higher modes, leaky modes, Floquet modes, hybrid modes, antenna modes, E_{pq}^{x} and E_{pq}^{y} modes, evanescent modes, propagating waves, surface waves, space waves, space harmonics, spacial harmonics, spectral harmonics, Floquet harmonics, cutoff frequencies, mode cutoffs, mode-coupling, stop bands, free-space wavelength, guide wavelength, bulk wavelength, dielectric guide, open guide, image guide, trapped image guide, trough guide, inset guide, inverted strip guide, dielectric slab, horn antenna, perturbation, periodic scatterers, dielectric grating, metal grating, stripe, strip, groove, grating period, strip spacing, element spacing, tapers, 2D analysis, 3D analysis, full-wave analysis, spectral harmonic analysis, spectral domain approach, scattering analysis, transverse resonances, effective dielectric constants, Marcatili method, transcendental equations, Goell's method, waveguide model, boundary integral equations, mode-matching, point matching, Eigenvalues, Green's functions, Bessel functions, basis functions, hyperbolic functions, Galerkin technique, dispersion curves, Brillouin diagrams, $k\beta$ diagrams, $k\alpha$ diagrams, linear array theory, collinear array, space factor, array factor, cancelling array, aperture distribution, Cosine distribution, Cos-tapered distribution, Taylor distribution, effective aperture, aperture efficiency, frequency scanning, scan range, beam-steering, line-scanning, analogue scanning, broadside, endfire, backfire, grating lobes. Some of these terms are equivalent and all will be covered in the relevant section of this thesis.

2.5. *Considering LWA types*

One of the most interesting aspects of the general category of LWA is the ability to steer the main beam direction by frequency scanning [6]. Another is the sheer complexity of its analysis and design, which will become obvious through this work, and the comparative simplicity of its structure [7, 8]. Further literature search revealed two more general categories of LWA in addition to the endfire rods covered in [2,4]:

1. Microstrip leaky-wave antennas
2. Dielectric waveguide based leaky-wave antennas:
    a. Uniform
    b. Periodically perturbed
        i. Dielectric grating
        ii. Metal strip grating
    c. Longitudinally perturbed

The microstrip LWA and its radiation mechanisms [9,10] and mode behaviours are well-known [11] and the uniform and dielectric grating types have been very well studied already and good summaries are contained in the text books. The second category is supported by a waveguide which has its travelling wave perturbed in some way so that it leaks (radiates) energy. The uniform type is perturbed by tapering the cross-section and is relatively difficult to experiment with since changes are likely to require a whole new waveguide [12,13]. The longitudinally perturbed type is a more recent addition to this category [14] and publications are appearing at the time of writing. A relatively new subject like longitudinal perturbation leaves scope for overlap with the work of current authors and the present author felt that the subject carried too much risk as a PhD topic.

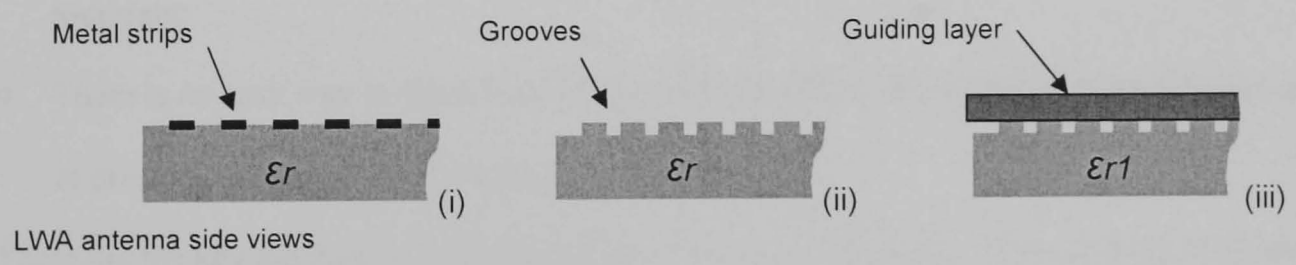

Figure 2.1 Leaky wave antenna side view sections showing various means of perturbing the dielectric guide configurations.

Of the periodic types, the dielectric grating type shown in Figure 2.1(ii) with periodic grooves machined into the surface of a dielectric waveguide have already received significant attention in the past and is well documented. The metal strip type, shown in Figure 2.1(i), has been studied by quite a small number of key people over the past three to four decades. For

this reason, it was chosen for further study here. In particular, following a review of the literature a number of things that drove the current study became apparent:

1. The precise radiation mechanism is undetermined;
2. The analysis is extremely complex for such a simple structure and adequately predicts the main beam shape and position, but poorly predicts the sidelobe levels;
3. The approximate guide and antenna characteristics can be found quite easily once the propagation constant for the guide is known, but this is difficult to obtain [15,16];
4. Dielectric waveguide analysis in general, as published, is very difficult to digest [17]. There is currently no simple way of obtaining the approximate propagation constant;
5. The radiation pattern can be approximated adequately using linear array theory, but the accuracy has only been demonstrated for a few cases;
6. The accuracy of approximate formulas has not been comprehensively compared with the results from rigorous techniques;
7. The respective advantages of the different guiding structures for this type of antenna have not been demonstrated;
8. The affect of the material on the guiding and antenna characteristics is difficult to ascertain;
9. There is no easy way to determine what guiding structure and material combination to use in practice, to meet a set of requirements.

These are the key motivators for choosing this antenna as the subject of the present work and all of these statements will be substantiated in the chapters to come. A key enabler for improving the existing knowledge of this subject was the availability of a general 3D electromagnetic structure software simulation tool and suitably powerful personal computer. This would theoretically enable significant insight to be gained in a relatively short amount of time compared to work carried out decades ago without such a resource. Answering all but the first point turned out to represent the bulk of this work.

2.6. *Review of text books*

Leaky wave antennas have also been treated in early antenna textbooks. The first of these [18] is the perhaps the most comprehensive and covers just about every antenna characteristic and structural variation of the metal waveguide based type. Many of the general characteristics are similar to those for dielectric guide types of interest here and shown in Figure 2.2 but, in general, the mathematical treatment is slight and the graphs are restricted to those individual metal types. Another general antenna text [19] covers the same metal types but also includes an excellent treatment of general travelling wave antenna analysis. It also provides an overview of a number of methods including transverse resonance method and harmonic expansions, which are rigorous solutions for the propagation constant of travelling wave antennas.

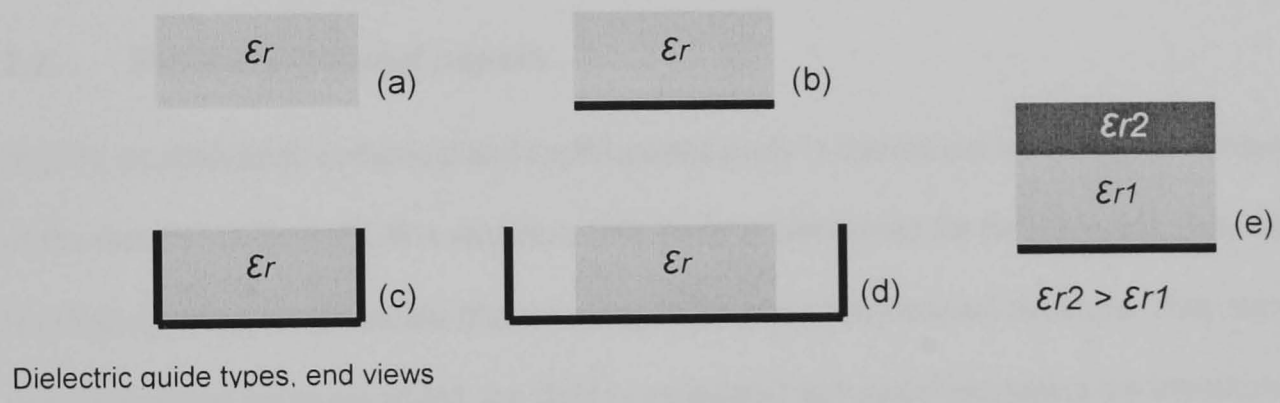

Figure 2.2 Dielectric guide configurations [8] (a) open guide, (b) image guide, (c) inset or trough guide, (d) trapped-image guide and (e) insulated-image guide.

The third edition of the earliest book [8] largely replaces the original leaky wave material with a treatment of dielectric tapered rod or uniform waveguide antennas and a much greater treatment of the periodically perturbed types, including with metal strips. This is the most up to date textbook treatment of these antennas, and is by one of the foremost author's of the subject A.A. Oliner.

[7] gives perhaps the most significant treatment of the dielectric grating type LWA with less than three pages dedicated to the metal strip grating type of interest here. Just a few pertinent

empirical results are given for the latter and these will all be given a fuller treatment in the current work. Although some of the dielectric grating theory applies to both types and so gives good insight, the mathematical treatment and graphs are dielectric grating specific and are of little use here.

While the above mentioned text books are certainly outstanding pieces of work, they provide only very limited insight into the metal strip loaded LWA. In general, they all reference the same handful of key journal papers, and it is only by referring to these directly, and additional work that was not considered in the text books, and performing a parametric analysis on various structures using the simulation tool, that significant insight can be gained.

The key papers give considerable insight and will be given significant attention next. Other papers of course give a lesser insight and will be given the appropriate level of attention.

2.7. *Review of journal papers*

In [20], an analytical, numerical and experimental study is carried out into the guided waves of the metal strip-loaded LWA structure. The study is carried out for the dielectric slab, which is infinitely wide, which means that the study is for a two-dimensional structure. They state that when metal strips are added, the field is modulated and space harmonics are introduced i.e. it radiates.

In the mathematical formulation, approximations are made by assuming that the strips are infinitely thin and infinitely narrow, making it possible to make approximations to the boundary conditions. From these assumptions, it is taken that the current flow is along the length of the strip and that in the longitudinal direction is zero and that the E-mode is unperturbed. Electric and magnetic Hertzian potentials are expanded by Floquet's theorem [21] and the boundary conditions are applied to find the determinental equation. This is then solved numerically and its solution is given as a k-β dispersion plot comparing the perturbed and unperturbed dispersion curve, and the magnitudes of the individual space harmonics. The

perturbed curve is for the main radiated n = -1 harmonic. Curves for the other harmonics are reported to be identical but shifted along the β axis by $n2\pi$ [19]. The results were found to converge for > 31 harmonics, but not quite for 21. The radiation is theoretically strongest when the amplitude of the -1 harmonic is much greater than any other harmonics therefore it is stated that study of the space-harmonic amplitudes is important. The propagation constant has a very small imaginary part caused by the strip perturbations.

The analytical and numerical solution is given in limited detail and is extremely complex and difficult to reproduce. In any case, it can only be used for infinitely wide slabs, and its accuracy as the guide width is reduced to practical proportions is unknown. The theoretical results are shown to agree very well with experimental far-field radiation pattern. Interestingly, the main beam on one side of the structure has a higher gain that on the other, by almost 6dB. This asymmetry will be the subject of a study in the present work. Near field probing results for obtaining the propagation constant are also reported to agree well with theoretical values. Such probing will also be used in the present work. The authors conclude that the propagation constant can also be obtained very accurately from the direction of the measured main beam, presumably using (2-1) which is well-known.

$$\theta_M = \sin^{-1}\left(\frac{\beta}{k_0} + \frac{n\lambda}{d}\right) \qquad (2\text{-}1)$$

[5,22] describe four new dielectric waveguide structures, useful for millimetre-wave and optical integrated circuits, and a method of obtaining their theoretical dispersion characteristics is presented along with their dispersion plots. The structures are based on the simple idea that most energy will propagate in the region of highest dielectric constant. Their precise structures are not important here, but they are effectively variations on the inverted guide shown in Figure 2.1(iii) with the guiding layer on top or bottom. The method of analysis used is of most interest since it has been cited many times in other similar work. Since a solution to Maxwell's equations for these structures would be extremely complex, the

method of effective dielectric constants (EDC) was used to simplify the structure and formulation of the boundary value problem. The EDC method was originally developed by Toulios and Knox [23] and extended by Itoh in [22] for the new guide structures. In this method, the structure and so the solving of the boundary value problem for the dispersion characteristics is simplified by calculating the average or effective dielectric constant (εe) of the different layered parts of the guide cross section, while making them infinitely wide. For example, the structure of Figure 2.3(a) is decomposed into three sections, two of which are identical, to find two effective values (b). These effective dielectric constants are that of single layer hypothetical guides with the same propagation constant.

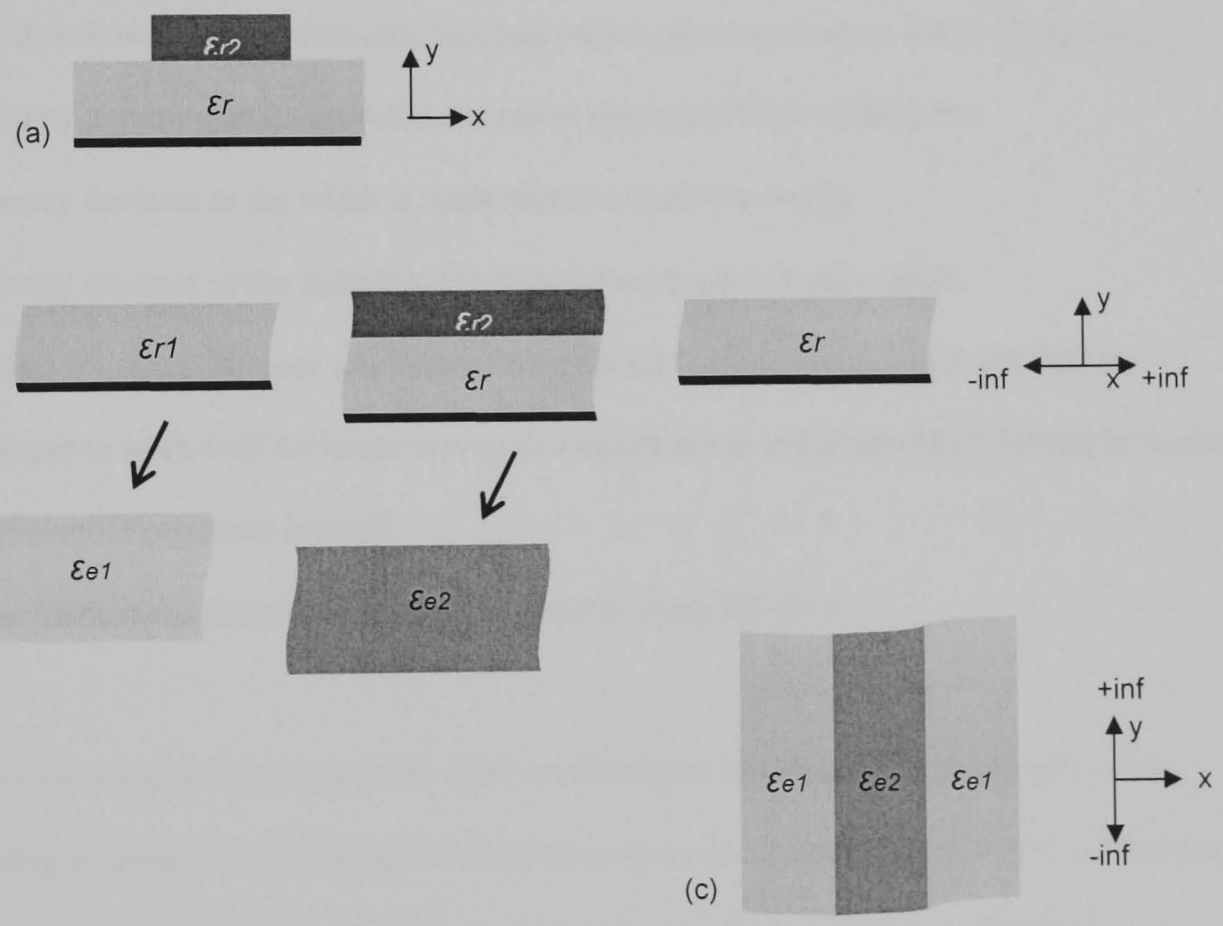

Figure 2.3 Depicts decomposition of ridge-guide structure (a) into its effective dielectric constant parts for deriving the y-direction propagation constant (b) and z-directed longitudinal propagation constant (c).

The boundary conditions are applied at the horizontal boundaries to solve Maxwell's equations for the simplified infinitely wide structures to find the propagation constant in the y-directions of each and the EDC's are then found using $\varepsilon e_n = \varepsilon 1 - ky^2 / k_0^2$ where $\varepsilon 1$ is the

dielectric constant of the highest dielectric constant layer, *ky* is the propagation constant along the vertical axis and k_0 is the free-space propagation constant.

These EDC's are then placed side-by-side as shown in Figure 2.3(c) and the same process is carried out to find the longitudinal z-direction propagation constant of the structure as a whole. This time the tangential E and H fields are matched across the vertical boundaries, assuming that they are infinitely tall. Perfect conductors and lossless dielectrics were assumed.

The results of this approximate method were compared with experimental results at X-band frequencies and showed that the accuracy of the method is geometry dependent and dependent on how close the dielectric constant values are to each other. Since the solution is simplified by assuming infinite widths instead of the actual finite widths, the:

- accuracy deviates as the width is made narrower and vice-versa;
- accuracy deviates as the dielectric constant values become further apart.
- method is general purpose and approximate but the authors report that it can only be expected to work well for larger waveguide aspect ratios and when the difference between the dielectric constants is small.
- dielectric and conductor losses will of course increase the error.

These points about the accuracy of the EDC method must be taken into consideration when considering methods for calculating the dispersion characteristics of guides, which are needed to design antennas based on them. [24] claims that this method is more accurate than Marcatili's method [31]. While this may be true at the less important low frequencies where the wave is less well guided, the Marcatili method suffers from none of the constraints listed above. The inability to study small aspect ratios is a disadvantage for the present work. In addition, the solution of Maxwell's equations for these structures is still very involved and has to be computed for all the structures shown in Figure 2.3 when using the EDC method and is

therefore very time-consuming and prone to error. Of course, this situation is simpler when the structure is a simple unperturbed rectangular guide, such as shown in Figure 2.2(a) to (c). However, Marcatili has already solved Maxwell's equations for these structures, so it is pointless using the EDC method in these rectangular guide cases. Since these simple guide configurations have been used in previous leaky-wave antenna work and will also be considered in the present work, it makes more sense to using the Marcatili method than the EDC method. The Marcatili method will be covered in the next chapter

Knowledge of the guide wavelength and therefore propagation constant is required to design the periodic grating types of leaky-wave antenna. In [25], the authors report an experimental method for finding it experimentally and compare their results with those found using the Marcatili theory. The measurements require quite an elaborate setup and are of little interest in the present work. However, the accuracy of the Marcatili method for calculating the guide wavelength is of importance and is demonstrated to approach 10% at low guide frequencies, decreasing to zero at higher frequencies for a silicon guide.

In [26] an inverted strip (IS) dielectric guide is fabricated with gratings for use as a leaky wave antenna for use at millimetre wave frequencies. This structure, which is compatible with MMICs, consists of a dielectric grating layer (grooves cut transverse to the direction of propagation, which is assumed to be down the length of the guide layer) sandwiched between a higher dielectric constant slab and a ground plane. The IS structure is shown in Figure 2.1(e). This configuration shares the benefits of other periodic LWA and is reported to have some additional advantages over other structures (at millimetre frequencies) [22] but these advantages are not really of interest for antennas. However, this paper is referred to by many LWA authors and contains some important insight. Of particular importance for the present work are that:

1) The grating supports a leaky wave when the phase constant of the nth space harmonic satisfies $\beta_0 / k_0 > 1$. This is interesting because the Marcatili method defines the same point as

the cutoff frequency of the fundamental mode of the guide itself (which does not have a real cutoff per-se).

2) There is a null in the dispersion characteristic of the antenna at the broadside direction (90° to the radiating surface). This is a result of mode-coupling between the forward and reverse travelling first higher space harmonics of the forward and reverse fundamental modes respectively. In the present work, this will be referred to as the broadside null. This is interesting because the Marcatili method does not find the null because it considers the guide without any grating and so it must be assumed to exist for the antenna. This null feature also allows the structure to be designed as a band-reject filter by suitable choice of grating spacing and antenna dimensions to match the design frequency.

3) When the grating is infinitely narrow, the attenuation and therefore radiation per unit cell is small and the amplitude taper over the aperture is also small, the radiation pattern is approximately that of the array factor of a linear array with a constant phase taper between radiating elements of $\beta_0 . d$.

4) Measured radiation patterns compared to theoretical patterns using the simple array factor formula (2-2) show exceptional agreement for two different operating frequencies.

$$AF(\theta) = \frac{1}{N^2}\left[\frac{\sin(N\psi/2)}{\sin(\psi/2)}\right]^2 \qquad \text{where } \psi = k_0 d \sin\theta - \beta_n d \qquad (2\text{-}2)$$

$$\text{and } \beta_n / k_0 < 1 \qquad \text{where} \qquad \beta_n = \beta + 2n\pi / d$$

5) Experiments showed that there was always some radiation from the source and the end of the guides and so the ends of the guide were tapered to a point. This seems to be the first and only time that dissimilar sized tapers have been used in practice.

6) The antenna can be scaled up in size and down in frequency to be compatible with measurement apparatus. This is important to the present work, since equipment was limited to 6 GHz.

[27] proposes a dielectric guide situated in a metal trough as a potential solution to loss due to radiation at curved sections of dielectric guides. They call this structure a trapped-image guide, as shown in Figure 2.2(d). The propagation constant is found using the effective dielectric constant (EDC) method, which was described above. The interesting part from the point of view of the present work is a small section where the trapped image guide has metal strip gratings added periodically to create a leaky wave antenna. The typical experimental radiation pattern for this type of antenna shows a beam width of 6.5° with sidelobes -14dB down, compared to theoretical ones of 6° and -13.5dB using the EDC theory. The high sidelobes were blamed on the constant strip leading to an exponential aperture distribution. Finally, the authors state that, if the attenuation by the grating is small, the main beam angle can be approximated by (2-1), repeated below for convenience

$$\theta_M = \sin^{-1}\left(\frac{\beta}{k_0} + \frac{n\lambda}{d}\right) \qquad (2\text{-}1)$$

where n is the number of grating elements, k_0 is the free-space propagation constant, d is the grating spacing, θ_M is the main beam angle and β is the propagation constant of the nth space harmonic. This formula will be used frequently throughout the present work, where new caveats to its accuracy will be demonstrated, and modifications made.

[28] primarily considers the spacing of the metal strips on the LWA structure, this time an entirely open structure. The ± 1 limits on the right hand side of (2-1) are imposed and rearranged to give (2-3) and then a modification is also made to guarantee to have only one space harmonic in the visible range i.e. a single main beam present. The strip spacing must then satisfy (2-4).

$$\frac{-n}{\left(\frac{\lambda}{\beta}+1\right)} \le \frac{d}{\lambda} \le \frac{-n}{\left(\frac{\lambda}{\beta}-1\right)} \qquad (2\text{-}3)$$

$$\frac{2m-1}{2\left(\frac{\lambda}{\beta}-1\right)} \le \frac{d}{\lambda} \le \frac{2m+1}{2\left(\frac{\lambda}{\beta}+1\right)} \quad \text{where } m = -n \qquad (2\text{-}4)$$

No evidence about the accuracy of (2-3) and (2-4) was provided in the paper. The authors also present experimental results where the LWA dielectric guide is fabricated to fit into a

standard WG26 rectangular metal waveguide for excitation. It is pointed out that care must be taken to properly match the dielectric rod at the feed, but they do not state how, and that a sufficient number of strips must be used to ensure that there is little energy at the end of the rod that can radiate. A larger number of strips leads to a larger antenna aperture and reduced beamwidth. Finally, they point out that the beam from the strip side of the antenna has lower gain than the other side. This beam asymmetry has never been mentioned in any other work, but was noticed in the review of [20], and will be the one of the subjects studied in the present work.

From the point of view of the present work, the next key paper [29] gives great insight into practical strip widths. It reports on theoretical and experimental studies of the same LWA structure as studied by the previous author, but this time mounted on a ground plane. Such a guiding structure is then commonly known as an image-guide, and is pictured in Figure 2.1(b). The authors experimented with the width and number of strips and report that widths of < 0.2 times the guide wavelength radiate an insignificant amount of energy such that even 50 strips leave energy propagating in the guide. Also, widths > 0.5 times the guide wavelength radiate too much so that the effective aperture is very small. They also observed very high sidelobes for the large widths, which is consistent with [30], but suggest that this might be due to a large impedance mismatch at the first strip. In this case, the guide wavelength was calculated using the Marcatili method [31] with minor modifications to his formula to make them specific to the trough type of dielectric waveguide. The modified Marcatili equations were labelled as belonging to the 'trough-guide model' and are given in Appendix C. Dispersion curves show that the single-mode limit is set by the E_{21}^{y} cutoff frequency.

Since the exponential energy leakage along the aperture leads to high sidelobes, they suggest a continuously varying strip width taper and an associated empirical formula to calculate these widths. Strip width tapering, and this formula in particular, is considered in Chapter 8 of this thesis (8-15). The sidelobe levels were claimed to be much lower for the tapered

distribution than the constant strip width. Finally, they state that little benefit was found in experiments for >18 strips, and that a slower taper and more strips gave similar results. The guide height is chosen to provide single-mode operation and the width was chosen to interface to a metal waveguide, for excitation.

In the second part of [29], the authors point out that the H-plane 3dB beamwidth of nearly 180° is too wide for some applications and propose adding a horn type flare along the length of the antenna to make the pattern more directional, as shown in Figure 2.4. In this case the dielectric guide was sunk into an open metal waveguide with longitudinal flares. The optimum flare angle was found to be between 15 and 20 degrees, giving a beamwidth ~ 13°. Such a structure can be mounted into a metal plane surface without significantly modifying the radiation characteristics. No theoretical analysis was provided for this modification.

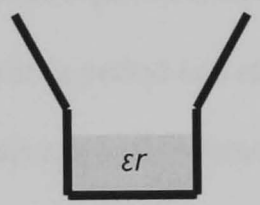

Figure 2.4 Depicts the horn image-guide leaky wave antenna reported in [29], which is effectively the inset guide with metal flares.

A metal strip loaded dielectric slab was theoretically analysed using a technique referred to as mode-expansion [32], as used in [24]. The received power versus strip width is shown to be approximately parabolic, peaking at approximately $W = 0.6\ \lambda_0$ for either normally incident wave. Since εr = 1, this implies that it peaks at $W = 0.6\ \lambda g$ also. This is close to the peak found in [29], which was $W = 0.5\ \lambda g$ but here the power rolls off smoothly and there is no sharp cutoff below 0.2 like [29] suggests. Interestingly, the fundamental mode power peaks for an angle of incidence both around broadside and 25° away from broadside with approximately half power nulls in between. The method is claimed to be relatively simple and computationally very fast, but it is only two dimensional and so its accuracy will be diminished, like the EDC method, as the guide is made narrower.

The same method was also used in [33] in conjunction with the EDC method to analyse thick metal strip gratings on a dielectric slab on a ground plane. It takes into account the higher space harmonics as opposed to just the highest amplitude $n = -1$ harmonic, which determines the main antenna characteristics. The analysis differs to that for thin strips because there is effectively a new layer created in the structure; that of the thick strips with an air gap separating them. The space harmonics are summed for the component E and H fields in the slab, strip layer and above the structure and then boundary conditions are applied. The solution is very involved and was solved numerically by computer with nothing said about the implementation. The method was verified by computing results for thin strips and correlating them with existing results. The results for increasing strip width demonstrate negligible change in the real part of the propagation constant but an exponential increase in the leakage constant. In similar work [34], the authors reported a similar leakage response which peaked off when the thickness equalled the grating period and at peaked $\varepsilon r = 11$. However, the change in the real part was small but not negligible demonstrating a linear increase from $\beta d =$ 5.7 to 5.95 as the dielectric constant was increased from 1 to 9, and then a sharp roll off. This is worth noting, since the present work will consider these high values of εr. An integral equation method was used, with little information to describe it.

Guglielmi and Oliner are two very key contributors to the study of the metal strip-loaded LWA [35] to [39]. As with virtually all of their work, in [35] they use circuit theory, and the transverse equivalent network (TEN) procedure in particular to conduct a parametric analysis of the image guide based antenna in two dimensions and find the dispersion characteristics needed to design the antenna. They report that the simple network that models the n = 0 and -1 harmonics must be supplemented with equivalent networks that represent much higher harmonics when the guide height is small. No experimental results and no evidence about the accuracy of the technique are provided until the following paper [36] when the agreement for the same technique and antenna is shown to be good for both a wide guide width of four times the grating period and a relatively narrow guide equal to a single period.

Of interest to the present work from the former paper is the linear increase in beam angle up to about 6° as the strip width is increased up to about a quarter of a period. In [37] and [38] they apply the same procedure to the inset guide LWA structure shown in Figure 2.2(c) but with high (metal) sidewalls. The circuit representation is noticeably more complex than for the image guide and is based on a circuit for the guide itself [17] with modifications to account for the metal strips [39] by the first author. A direct comparison cannot be made between these results because they are presented differently. However, they both show a theoretically large scanning ability and a sharp leakage peak at the frequency for which the main beam reaches broadside, all without experimental or other verification. The affect of changing the width versus grating period is studied for the inset guide. The broadside null is extremely evident for certain widths because, when the main beam is frequency scanned to broadside it stays at broadside for as much as 200 MHz. For other widths, this null is hardly evident. Interestingly, the null moves up in frequency as the strip width increases. The leakage is extremely high over those periods and comparably low at either side. These plots demonstrate theoretically that the leakage away from the null is very low for very narrow and very wide strips (0.1 and 0.9 times the period p) and relatively high in between ($0.3p$ and $0.6p$). This relationship is shown to be parabolic, peaking when the strip width is half the grating period. The effect of this quite rapid change in leakage is a rapid variation in beamwidth as the antenna is frequency scanned. Since this author finds good leakage between 0.3p and 0.6p and the strip spacing period p is often in the order of one wavelength to get a beam close to broadside, these results correlate closely with those of [29] discussed above. It therefore seems reasonable to assume that a good working strip width range is between 0.2 and $0.5\lambda g$.

The broadside null problem is further investigated in [37] by the same author and using the same TEN technique and inset guide model. Here, it is shown that by adding two metal strips per period and by careful numerical optimisation, the null can be found to be almost vanishingly narrow. However, the evidence is unconvincing because:

a. the authors have not compared like-for-like; they compare the null widths of a single strip of $0.1p$ with two closely-spaced strips of $0.2p$ each;
b. in [38] the authors have already demonstrated that vanishingly narrow nulls were found for various strip widths so there is not enough evidence to suggest that this technique can reduce the null width.

[30] Models the metal strip grating LWA without a ground plane i.e. on an *open* dielectric waveguide. The emphasis of the paper is on showing techniques for achieving low sidelobe levels, by modifying the normal exponential aperture distribution. The author summarises available mathematical techniques for this kind of structure without discussing their particular attributes and then proposes a technique based on Galerkin's method in the Fourier domain applied to a waveguide model that allows both uniform and non-uniform waveguide widths to be evaluated. Sinusoidally varying guide widths and exponentially decreasing widths are explored as shown in Figure 2.5. A very comprehensive set of graphical results are presented in the paper, including for the uniform width guide of interest in the present work, with some comparing theory with experimental results. The claimed benefits of such non-uniform guides are unconvincing. However, since the method is suitable for uniform guide it is worth considering.

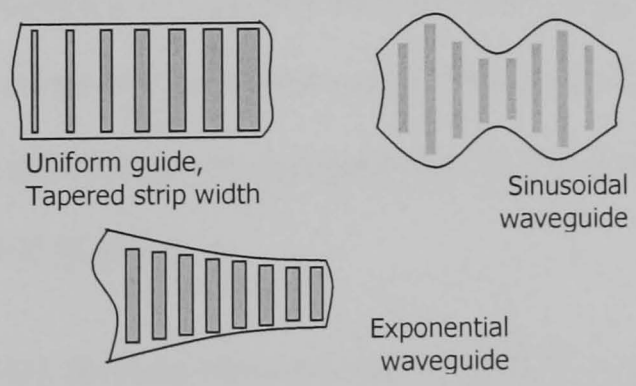

Figure 2.5 Top views of dielectric guides with metal strip gratings on surface.

First, the boundary conditions are expressed in terms of a finite number of Floquet space harmonics for the regions above, below (air) and inside the dielectric guide; enough harmonics for good convergence. Next, the unknown surface current density along the length

of the strips is formulated, using the Galerkin method, by defining and expanding it in terms of known basis functions from [40]. The current is assumed to be constant across the strip width based on the argument that it is narrow. Then, the unknown coefficients of the space harmonics are solved for and expressed in terms of the surface current density. Finally, Galerkin's procedure is applied in the Fourier domain to give an Eigenvalue equation that is solved numerically to determine the complex propagation constant. An approximate method for deriving the radiation pattern from the tangential fields on the plane surface (near fields) in the Fourier-transform domain is used. The plots show near perfect agreement between the results using this method and experimental results. The method presented is extremely complex and would take a very significant amount of time to reproduce.

A large number of results for the uniform width waveguide are directly relevant to the current work, in particular to Chapter 8 of this work, and so it is worth noting them. The key point is that it demonstrates that, while many authors ignore it, the strip width does affect the radiation pattern:

- Shows very minor phase constant decrease with increasing strip width;
- Small linear increase in beamwidth with increased strip width. E.g. the increase is approximately 3 degrees for an increase in width from 0.236 λg to 0.55 λg;
- Linear increase in sidelobe level with increased strip width. E.g. the level increases from about -34 dB to -17 dB for strip widths between 0.158 λg and 0.55 λg;
- Strip width tapering shows about the same pattern as the constant strip width with a reduction from 6° to 3° (E-plane).

By the same author, in [41], the same method is used to perform a full-wave analysis of the uniform waveguide with broad guide width compared to height (ten to thirty times the height), to find the complex dispersion characteristics. The results show that the real part of the propagation constant rolls off at beyond about ten times the height and that the complex leaky part rolls off at about twenty times.

The Marcatili method was used to analyse an electronic phase shifter based on a dielectric rectangular open silicon guide [42]. The device consists of a PIN diode module is fitted to the top surface of the guide to change the propagation constant by simulating a metal plane when forward biased and is proposed for used in millimetre-wave integrated circuits. The theoretical and experimentally derived phased shifts were compared and reported. The reported difference between measured and theoretical phase shift was up to about 16%. However, a significant portion of this error is attributed to the fact the diodes were represented by a perfect metal wall in the Marcatili equations. Finally, the authors state that in the transition from the TE_{10} mode of the metal excitation waveguide to the E_{11}^{y} mode of the silicon guide was made with little probability of a jump to higher E_{mn}^{y} modes and that this assumption had worked well in practice. This is interesting because the same theoretical and experimental setup is used in the present work.

[43] details the rigorous spectral domain approach for computing the complex propagation constant of the metal strip LWA for the first time. The authors state that the real part can be obtained with good accuracy using approximate methods like Marcatili's. The imaginary part was obtained experimentally by near-field probing but no detail was provided about this. The results are shown to agree almost exactly with experimental results, except in the sidelobe region which is blamed on radiation from the feed. This spectral method is extremely complex and difficult to implement.

A leaky wave antenna made from a Silicon open dielectric guide is proposed as an electronically steered alternative to slow and expensive mechanically steered antenna for radar and missile homing applications [6]. The authors recommend keeping the guide dimensions as large as possible to ease fabrication problems. The maximum and minimum dielectric guide dimensions were calculated using Marcatili's equations [31]. The guided wavelength versus operating frequency as calculated by Marcatili's *exact* transcendental equations and his *approximate* closed-form equation were compared. The approximate version was shown to converge with the exact version at the highest guide frequencies.

However, since there is no experimental data, there is no evidence to show how accurate these equations are. However, this rigorous theoretical method demonstrates certain characteristics and errors that are relevant to the present work:

- A smaller guide cross section provides a larger scan range. The extent of this steering capability will form part of the present work, and some interesting conditions will be revealed;
- The theoretical and experimental beam angles were shown to agree only to within about 4° at the high frequency and about 8° at an intermediate frequency. This issue will be discussed and a correction is provided in Chapter 8 of the present work;
- The guide wavelength was also shown to be out by between 7 and 10% over the same frequency range for this Silicon guide. Part of the present work will again be to investigate this error;
- In experiments, an exact broadside beam was found to be difficult to achieve in practice. The experiments used a test fixture where the silicon guide was tapered at both ends and inserted in to the copper plate covered mouth of slightly larger frequency compatible metal waveguide. In the present work, it was found that the copper plate configuration leads to an undesirably highly selective filter.

[44] Custom made PIN diode modules were fitted to one of the sidewalls of a dielectric image guide in the same manner as used for phase shifting as in [42]. However, this time the guide had metal strip gratings to realise a LWA. This structure, depicted in Figure 2.6 (top), gave 10° of steer with full bias. The propagation constant was determined from the measured main beam angle using (2-1). Marcatili's method [31] was used to check these values which were found to be 2% lower than measured. This gives additional confidence in the accuracy of the Marcatili method, for quite a high dielectric constant this time (~12). The authors describe how covering individual walls of the dielectric guide modifies its propagation constant and that these metal walls can be implemented in Marcatili's transcendental equations.

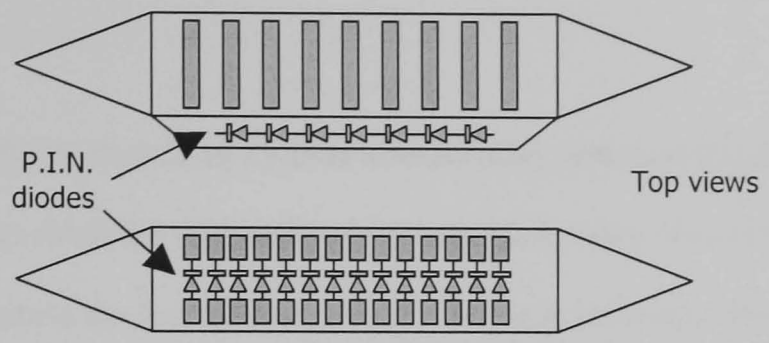

Figure 2.6 Fixed frequency beam-steering mechanisms.

[45] presents an equivalent electronic steering method that uses PIN diodes in the centre of the metal strips themselves, effectively joining two halves of each strip together when biased on. The structure is depicted in Figure 2.6 (bottom). A much greater steer angle of 35° is claimed. The experimental radiation patterns compare very well with theoretical results for the main beam, where the propagation constant is calculated by Marcatili's method again. Another author achieves fixed-frequency steering using a tunable ferroelectric material with a dielectric constant in the order of $\varepsilon r = 19$ [21]. The metal strip LWA in the image guide configuration is implemented and a very high DC voltage (low current) is applied between the strips and the ground plane to effectively tune the dielectric constant and therefore propagation constant of the guide. A beam steer of up to 6° was experimentally demonstrated for a voltage of 0 to 19kVcm^{-1}. The propagation constant was calculated using the EDC method and is shown to be only within about 5° of experimental values. Again, the EDC method appears less accurate than the Marcatili method.

[24] states that periodic dielectric grating (corrugated) waveguides have been analysed for integrated optics applications for such as beam-to-surface wave couplers, distributed feedback amplifiers and filters. Since the same physical principles that apply to the couplers also apply to the analysis of periodic leaky wave antennas, the authors of this paper apply the results known for the optical counterpart to the design of LWA's. One main difference between the optics case and the present antenna type is that the dielectric constant of the latter is much higher. The image-guide type which has a metal plane on the bottom surface of the dielectric

guide is used to create a LWA. The purpose of the ground plane is to redirect downward energy upwards.

The authors report that compared to an ideal antenna array structure, radiation pattern distortions and larger sidelobes reportedly occur as a result of the discontinuities at the ends of the guide and because the field extends outside the guide sidewalls. Plots are provided to determine the propagation constant of the grating type antenna. The following characteristics, which are also relevant to metal strip grating leaky wave antennas were presented:

- The choice of waveguide height will depend on the required tradeoff between fabrication tolerances and scan range;
- There is an optimum dielectric guide height and frequency at which the radiation will peak. This is due to the fact the field is mostly travelling outside the guide at low frequencies near cutoff and entirely contained within the guide at much higher (unspecified) frequencies and, as a consequence, the field strength at the grating, and therefore the radiation, is very weak;
- The authors state that the grating period has a determining influence on the propagation constant of the structure;
- The guide length required to radiate 90% of the power in is one half of that required to radiate 99%.

In [46], it is claimed that significant conductor loss can occur for the image-guide LWA configuration. Therefore, in order to improve the efficiency of this type of antenna they propose placing a lower dielectric constant layer between the dielectric and the ground plane. Such a technique was already proposed for other structures in [5, 22, 26]. In addition, they state that reflections occur between the metal strip gratings and the ground plane that distort the radiation pattern, especially in the sidelobe region. To combat this, they propose a cancelling technique where the metal strips are mirrored on the back side of the main guide

section. Reflections are then of similar amplitude but 180° out of phase and cancel. This is shown graphically to almost completely eliminate these reflections.

Of major importance to the present work is a statement by the authors that's states that the beam direction depends not only on the spacing as other authors have reported, but also on the strip width. And, that the radiation leakage depends not only on the strip width, but also on the spacing. They state that these secondary effects should be taken into account in an antenna design. The extent to which these secondary effects affect the beam direction was not shown and will be the subject of investigations in the present work.

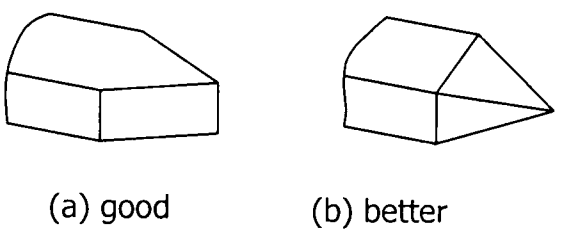

Figure 2.7 Dielectric guide taper patterns to improve insertion loss in the metal waveguide to dielectric guide transition.

Experiments are conducted in [47] on an open guide based LWA for potential use in an airborne imaging radiometer. The authors not surprisingly point out that the fabrication of two inch long silicon rods with a cross section in the order of $0.4mm^2$ was difficult. The rod was supported in a channel machined in a thick Teflon rod, and a copper clad Teflon printed circuit board was etched with the strip pattern and placed over the surface. The ends of the rod were tapered and inserted in a standard metal waveguide. Experiments conducted without these tapers showed high insertion losses over the frequency range from 206 to 218 GHz, which decreased from -20dB to < -10dB for a guide width of 2mm or more. The performance with a taper on the sides of the rod, as per Figure 2.7(a) still showed high insertion loss at the high end of the frequency range, but tapering all four sides to a point as in (b) levels it to approximately -4dB over the whole frequency range. In the present work, experiments revealed the same high insertion loss issue and since HFSS simulations had indicated zero benefit in tapering and the machining process was difficult, the lower performance was

accepted. The authors also used the HFSS simulation tool to show that only the dominant mode had significant power. No further information was provided about the apparent accuracy of HFSS.

In one of the earliest works on leaky wave antennas [16] reports on an inductive grid antenna consisting of periodically spaced wires stretched over a slightly curved metal surface in one model and a printed circuit with the equivalent strip pattern suspended over the surface by foam in a second model. Although this particular LWA structure is not the subject of the present work, it is worth pointing out that this was the first time that the aperture distribution had been tapered in order to minimise the sidelobe level and decrease beamwidth. In that case, the curvature of the surface with respect to the wires or strips was used to achieve this. The TEN technique was used for the study and experimental results showed almost perfect agreement over a wide frequency range. Earlier, in [29] a simple taper expression was reported based on experimental evidence for the metal strip LWA of interest. Also, since the authors of [35] had showed that the leakage rate varies strongly as a function of the ratio of strip width versus grating period, they also make a statement that the distribution could theoretically be controlled by varying the ratio accordingly along the length of the antenna. The author's of [48] give some insight into how this might be achieved in practice; first choose the required aperture distribution and then determine the changes necessary to the antenna geometry to obtain the required leakage and maintain the real part of the propagation constant at the same value in each unit cell. They do not report on how the geometry should be modified in this case. However, in [49], the same author provides a full account, including a table listing the geometry in each unit cell. This time, the author uses the mode-matching and EDC methods so that the effects of incorporating the higher space harmonics can be demonstrated compared to using only the n = -1 harmonic. These results demonstrate that, although this rigorous method accurately determines the shape and position of the main beam, according to experimental results the sidelobe region cannot be predicted with any degree of accuracy even when many harmonics are included and state that only a moderate

improvement in sidelobe level is found when the geometry is modified to control the aperture distribution. Control of the aperture distribution is one of the subjects of Chapter 8 of the present work, which also argues that the author of [49] appears to have made a mistake that perhaps contributed to the lack of improvement reported.

2.8. References

[1] K.M. Luk and K.W. Leung, *Dielectric resonator antennas,* Research Studies Press, 2003.

[2] D.G. Kiely (Ed), *Dielectric Aerials*, Methuen & Co., London, 1953.

[3] R. Chatterjee, *Dielectric and dielectric loaded antennas*, Research Studies Press Ltd., England, 1985.

[4] C. Salema, C. Fernandes and R.K. Jha, *Solid dielectric horn antennas*, Arctech House, 1998.

[5] W.V. McLevige, T. Itoh and R. Mittra, "New waveguide structures for millimeter-wave and optical integrated circuits," *IEEE Trans. Microwave Theory and Techniques*, vol. MTT-23, no. 10, pp. 788-794, Oct. 1975.

[6] K. L. Klohn, R. E. Horn, H. Jacobs and E. Freibergs, "Silicon waveguide frequency scanning linear array antenna," *IEEE Trans. Microwave Theory and Techniques*, vol. MTT-26, no. 10, pp. 764–773, Oct. 1978.

[7] F. Schwering and A.A. Oliner, *Millimeter-wave antennas* in Antenna Handbook, Eds. Y.T. Lo and S.W. Lee, Van Nostrand Reinhold, New York, Chapter 17, 1988.

[8] A.A. Oliner, *Leaky-wave antennas* in Antenna Engineering Handbook (Third edition), Ed. R.C. Johnson, McGraw-Hill, Chapter 10, 1993.

[9] Y.D. Lin, J.W. Sheen and C.K.C. Tzuang, "Analysis and design of feeding structures for microstrip leaky wave antenna," *IEEE Trans. Microwave Theory and Techniques*, vol. 44, no. 9, pp. 1540-1547, Sept. 1996.

[10] C. Luxey and J.M. Laheurte, "Simple design of dual-beam leaky-wave antennas in microstrips," *IEE Proc. Microwaves Antennas and Propagation*, vol. 144, no. 6, pp. 397-402, Dec. 1997.

[11] Y.D. Lin and J.W. Sheen, "Mode distinction and radiation efficiency analysis of planar leaky-wave line source," *IEEE Trans. Microwave Theory and Techniques*, vol. 45, no. 10, pp. 1672-1680, Oct. 1997.

[12] H. Schrank and N. Herscovici, "The shaped-beam polyrod antenna," *IEEE Antennas and Propagation Magazine*, vol. 36, no. 2, pp. 55-57, Apr. 1994.

[13] Y. Shiau, "Dielectric rod antennas for millimeter-wave integrated circuits," *IEEE Trans. Microwave Theory and Techniques*, Short Papers, pp. 869–872, Nov. 1976.

[14] J.L Gomez-Tornero, A.T Martinez, D.C. Rebenaque, M. Guglielmi and A.A. Melcon, "Design of tapered leaky-wave antennas in hybrid waveguide-planar technology for millimeter waveband applications," *IEEE Trans. Antennas and Propagation*, vol. 53, no. 8, pp. 2563-2577, Aug. 2005.

[15] M. Guglielmi and A.A Oliner, "Practical theory for dielectric image guide leaky-wave antennas loaded by periodic metal strips," *Proc. 17th European microwave conference*, Rome, Italy, pp. 549-554, Sep, 1987.

[16] R.C. Honey, "A flush-mounted leaky-wave antenna with predictable patterns," *IRE Trans. Antennas and Propagation*, vol. 7, iss. 4, pp. 320-329, Oct. 1959.

[17] N. Marcuvitz (Ed), *Waveguide handbook*, vol. 10, McGraw-Hill, 1951.

[18] F.J Zucker, *Surface and leaky-wave antennas* in Antenna Engineering Handbook (First edition), Ed. H. Jasik, McGraw-Hill, Chapter 16, 1961.

[19] A. Hessel and T. Tamir, *General characteristics of travelling-wave antennas* and *Leaky-wave antennas* in Antenna Theory, part 2, Eds. R.E. Collin and F.J. Zucker, McGraw-Hill, Chapters 19 & 20, 1969.

[20] J. Jacobsen, "Analytical, numerical, and experimental investigation of guided waves on a periodically strip-loaded dielectric slab," *IEEE Trans. Antennas and Propagation*, vol. AP-18, no. 3, pp. 379-388, May. 1970.

[21] V.K. Varadan, V.V. Varadan, K.A. Jose and J.F Kelly, "Electronically steerable leaky wave antenna using a tunable ferroelectric material," *Smart Materials & Structures*, vol. 3, pp. 470-475, Jun. 1994.

[22] T. Itoh, "Inverted strip dielectric waveguide for millimeter-wave integrated circuits," *IEEE Trans. Microwave Theory and Techniques*, vol. MTT-24, no. 11, pp. 821-827, Nov. 1976.

[23] P.P. Toulios and R.M. Knox, "Image line integrated circuits for system applications at millimeter wavelengths," U.S. Army Electronics Command, Final Report, Rept. No. ECOM-73-0217-F, Jul. 1974.

[24] F.K. Schwering and S.T. Peng, "Design of dielectric grating antennas for millimeter-wave applications," *IEEE Trans. Microwave Theory and Techniques*, vol. MTT-31, no. 2, pp. 199-208, Feb. 1983.

[25] H. Jacobs, G. Novick, C. M. LoCascio and M. M. Chrepta, "Measurement of guide wavelength in rectangular dielectric waveguide," *IEEE Trans. Microwave Theory and Techniques*, vol. MTT-24, no. 11, pp. 815–820, Nov. 1976.

[26] T. Itoh, "Application of gratings in a dielectric waveguide for leaky-wave antennas and band-reject filters," *IEEE Trans. Microwave Theory and Techniques*, vol. MTT-25, no. 12, pp. 1134-1138, Dec. 1977.

[27] T. Itoh and B. Adelseck, "Trapped image guide for millimeter-wave circuits," *IEEE Trans. Microwave Theory and Techniques*, vol. MTT-28, no. 12, pp. 1433-1436, Dec. 1980.

[28] S. Kobayashi, R. Lampe, R. Mittra and S. Ray, "Dielectric rod leaky-wave antennas for millimeter-wave applications," *IEEE Trans. Antennas and Propagation*, vol. AP-29, no. 5, pp. 822–824, Sep. 1981.

[29] T.N. Trinh, R. Mittra and R.J. Paleta, "Horn image-guide leaky-wave antenna," *IEEE Trans. Microwave Theory and Techniques*, vol. MTT-29, no. 12, pp. 1310-1314, Dec. 1981.

[30] M. Ghomi, B. Lejay, J.L. Amalric and H. Baudrand, "Radiation characteristics of uniform and nonuniform dielectric leaky-wave antennas," *IEEE Trans. Antennas and Propagation*, vol. 41, no. 9, pp. 1177-1185, Sep. 1993.

[31] E. A. J. Marcatili, "Dielectric rectangular waveguide and directional coupler for integrated optics," *Bell Syst. Tech. J.*, vol. 48, no. 7, pp. 2071–2095, Sep. 1969.

[32] H.A. Kalhor, "Electromagnetic scattering by a dielectric slab loaded with a periodic array of strips over a ground plane," *IEEE Trans. Antennas and Propagation*, vol. AP-36, no. 1, pp. 147-151, Jan. 1988.

[33] J. Encinar, "Mode-matching and pont-matching techniques applied to the analysis of metal-strip-loaded dielectric antennas," *IEEE Trans. Antennas and Propagation*, vol. 38, no. 9, pp. 1405-1412, Sep. 1990.

[34] M. Matsumoto, M. Tsutsumi and N. Kumagai, "Radiation characteristics of a dielectric slab waveguide periodically loaded with thick metal strips," *IEEE Trans. Microwave Theory and Techniques*, vol. MTT-35, no. 2, pp. 89-95, Feb.

[35] M. Guglielmi and A.A Oliner, "Practical theory for dielectric image guide leaky-wave antennas loaded by periodic metal strips," *Proc.17th European microwave conference*, Rome, Italy, pp. 549-554, Sep, 1987.

[36] M. Guglielmi, Z.M. Lu, J. Encinar, S.T. Peng and A.A Oliner, "Metal-strip-loaded rectangular dielectric rod leaky-wave antennas : experimental verification of new simple theory," *IEEE AP-S International Symposium*, Dallas, pp. 1922-1925, May. 1990.

[37] M. Guglielmi and D.R. Jackson, "Broadside radiation from periodic leaky-wave antennas," *IEEE Trans. Antennas and Propagation*, vol. 41, no. 1, pp. 31-37, Jan. 1993.

[38] M. Guglielmi and G. Boccalone, "A novel theory for dielectric-inset waveguide leaky-wave antennas," *IEEE Trans. Antennas and Propagation*, vol. 39, no. 4, pp. 497-504, Apr. 1991.

[39] M. Guglielmi and A.A Oliner, "Multimode network description of planar periodic metal-strip grating at a dielectric interface – Part III: Rigorous solution," *IEEE Trans. Microwave Theory and Techniques*, vol. MTT-37, pp. 902–909, Mar. 1989.

[40] T. Itoh and W. Menzel, "A full-wave analysis method for open microstrip structures," *IEEE Trans. Antennas and Propagation*, vol. AP-29, no. 1, pp. 63–67, Jan. 1981.

[41] M. Ghomi and H. Baudrand, "Full-wave analysis of microstrip leaky-wave antenna," *Electronics Letters*, vol. 25, no. 13, pp. 870-871. Jun. 1989.

[42] H. Jacobs and M. M. Chrepta, "Electronic phase shifter for millimeter-wave semiconductor dielectric integrated circuits," *IEEE Trans. Microwave Theory and Techniques*, vol. MTT-22, no. 4, pp. 411–417, Apr. 1974.

[43] R. Mittra and R. Kastner, "A spectral domain approach for computing the radiation characteristics of a leaky wave antenna for millimeter waves," *IEEE Trans. Antennas and Propagation*, vol. AP-29, no. 4, pp. 652–654, Jul. 1981.

[44] R. E. Horn, H. Jacobs, E. Freibergs and K. L. Klohn, "Electronic modulated beam-steerable silicon waveguide array antenna," *IEEE Trans. Microwave Theory and Techniques*, vol. MTT-28, no. 6, pp. 647–653, Jun. 1980.

[45] L. Huang, J.C. Chiao and M.P. De Lisio, "An electronically switchable leaky wave antenna," *IEEE Trans. Antennas and Propagation*, vol. AP-48, no. 11, pp. 1769-1772, Nov. 2000.

[46] T. Teshirogi, Y. Kawahara, A. Yamamoto, Y. Sekine, N. Baba and M. Kobayashi, "High efficiency dielectric slab leaky-wave antennas," *IEICE Trans. Communications*, vol. E84-B, no. 9, pp. 2387-2394, Sep. 2001.

[47] A. Basu and T. Itoh, "Dielectric waveguide-based leaky-wave antenna at 212 GHz," *IEEE Trans. Antennas and Propagation*, vol. 46, no. 11, pp. 1665-1673, Nov. 1998.

[48] J. Encinar, M. Guglielmi and A.A Oliner, "Taper optimization for sidelobe control in millimeter-wave metal strip-loaded dielectric antennas," *URSI Radio Science meeting*, Syracuse, New York, pp. 379. Jun. 1988.

[49] J. Encinar, "Analysis and CAD techniques for periodic leaky-wave printed antennas: numerical and experimental results," International journal of Microwave and Millimetre-wave Computer-aided Engineering, vol. 4, no 1, pp. 88, 99. 1994.

3 BACKGROUND MATERIAL

3.1 Introduction

The previous chapter, which is a review of previous works, necessarily presumes certain background knowledge. This chapter is included to add additional context for the chapters that follow and includes a brief review of some key background material. The latter will help the less familiar reader to cut through the large amount of terminology associated with this subject.

3.2 Antenna classification

3.2.1 Familiar leaky-wave antennas

The LWA comes in many forms, some of which might be familiar. The wire and rhombic antennas could be classified as two such examples. Periodic-slotted and longitudinally-slotted hollow metal waveguide antennas are also relatively well-known examples. From about the late 1970's and for around a decade, the dielectric waveguide-based leaky-wave antennas,

particularly dielectric grating antennas, became the subject of a certain amount of interest. These dielectric guide based antennas became interesting because the metal waveguide based versions are known to suffer from undesirably high conduction losses at millimetre-wave frequencies and are relatively difficult to manufacture with smooth surfaces and internal dimensions in the order of less than a few millimetres. In general, the dielectric waveguide structure is suited to these frequencies because they are low loss and, being of solid construction, are easier to manufacture than their hollow metal counterparts.

3.2.2 Causing the leaky-wave structure to radiate

Radiation from the LWA structure is caused by disturbing or 'perturbing' the travelling wave field. For the wire-based versions this is caused by bending the structure. For waveguide-based structures, this is achieved by varying the cross-section either continuously or periodically, or causing an abrupt change to the boundary conditions. For the type of LWA under study here the air-dielectric boundary is changed periodically by adding conducting sections. These are usually fixed to the wide surface of the rectangular dielectric guide so that they are as long as possible, to minimise the H-plane beamwidth and maximise the directivity. Equally, these could have been dielectric groove gratings but the dielectric grating version has already been well documented [1].

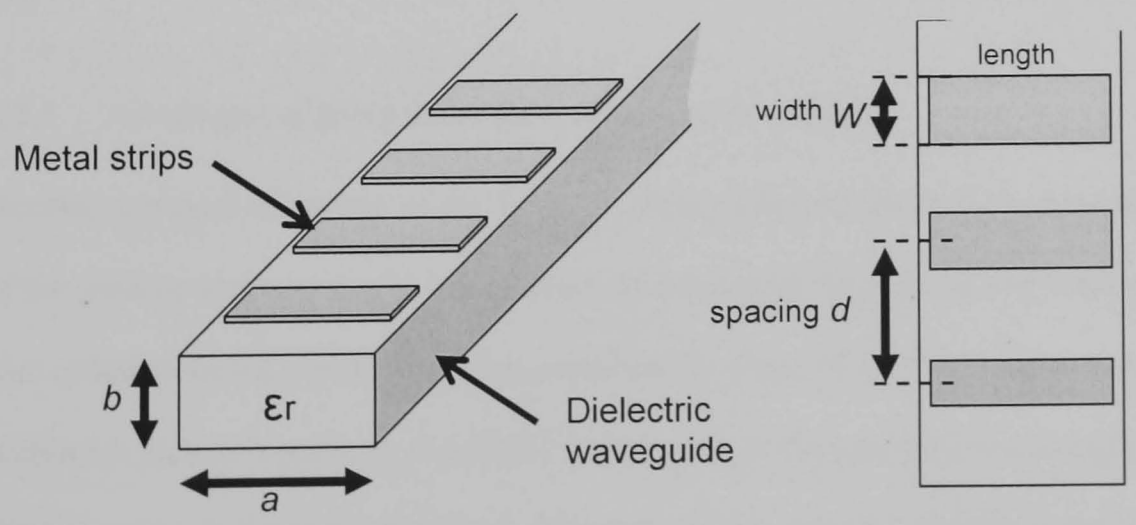

Figure 3.1 Basic metal strip grating leaky-wave antenna (LWA)

3.2.3 Travelling-wave antennas

The antenna of interest in this work fits into the category of travelling-wave antennas along with surface-wave and log-periodic antennas. The class of travelling wave antennas are similar to linear dipole arrays in a great many respects, but instead of each element of the array being excited individually, they are excited by a wave travelling down the guiding structure from a *single* source, exciting each element in term. In both cases, the goal is the same; to form an aperture illumination along its length.

3.2.4 Waveguides and waveguide based antennas

The earliest waveguide based LWA were the uniform or periodically slotted metal guides. These have the same antenna characteristics as the dielectric waveguide based versions i.e. narrow E-plane beamwidth, wide H-plane beamwidth and frequency scanning capability. Since only part of the energy within the dielectric guide is radiated per unit length by the elements, the rest being bound within the guide, this provides an electrically long antenna with a large effective aperture, and the resultant high E-plane directivity. In addition to its use in antenna work, the dielectric waveguide, or dielguide as it is sometimes known, has also been shown to be useful in millimetre-wave integrated circuits, phase-shifting, optical periodic couplers, material measurements and antenna applications at these frequencies [2] to [5].

3.2.5 Advantages of using dielectric waveguides for antennas

Another principal advantage of the dielectric waveguide over the metal version is that the size of the guiding structure can be scaled down by increasing the material electrical permittivity, also called dielectric constant εr. This is enabled by virtue of the fact that the wavelength within the dielectric guide λg is reduced with respect to the operating wavelength λo. In general, when λo is greater than the guide cross-section, which is usually at the low frequencies at which the guide is still useful, much more field travels outside the guide than inside and $\lambda g \sim \lambda o$. The opposite is true at the high frequencies and when the one or more of

the dielectric guide walls are metalised; and then $\lambda g < \lambda o$. There is also a material / εr dependency. It was discovered in the current work that a dielectric guide with an $\varepsilon r \sim 2$ is essentially equivalent to the metal waveguide guide in terms of its geometry and working frequency range, but this and the other guide characteristics change rapidly above two. Simplifying the actual quantification of λg under all these circumstances will form a significant part of the current work. This will effectively enable the user to understand the tradeoffs and to choose and characterize a dielectric guide suited to the application. Another interesting attribute of the dielectric guide is the inherent weather protection, and the low cost offered by some dielectric materials.

3.2.6 Main beam scanning

One of the most interesting LWA attributes is the ability to steer the main beam angle by changing the operating frequency. This is generally referred to as frequency scanning and, for the LWA under study here, the scanning takes place in just one plane, the E-plane. In the last chapter, it was revealed than other authors had reported beam-steering at a fixed frequency. In all cases, it is the modification of the guided wavelength with respect to a fixed radiating element spacing that redirects the beam. Beside the most obvious visual physical differences between the three travelling-wave antenna types, part of what differentiates them from each other is the extent to which the main beam can be directed between the backfire direction and the endfire direction (same direction as the forward propagating wave), and this in turn depends upon whether the wave travels faster or slower than the free-space propagation constant. In general, the LWA radiates along its entire length with a bound-wave travelling slower than the free-space propagation constant and the beam may be pointed anywhere between the backfire and endfire directions. In contrast, the surface-wave antenna only radiates from its source and termination in the endfire direction, with the wave travelling faster than the free-space propagation constant [6].

3.3 *Waveguide modes and propagation constant*

The solid dielectric waveguide supports a finite set of waveguide modes, like its hollow metal counterpart. The main attribute of interest associated with each mode is its propagation constant, which can be broken down into real and imaginary components usually known as the phase and leakage constants respectively in dielectric guide theory. When the strips are added, the wave is perturbed and an infinite spectrum of radiated spacial harmonics is generated, per mode, with different amplitudes.

3.3.1 Mode expansion

The fields of a periodically perturbed dielectric waveguide can be expanded into a discrete spectrum of normal (proper) modes, which exist within the confines of the guide (bound) and propagate without attenuation, and a continuous spectrum of spatial modes which represent the radiation outside [7,8]. The boundary conditions are such that the normal modes propagate without attenuation, whereas the spatial ones decay exponentially toward infinity. In addition, and in contrast to the metal waveguide, additional discrete modes termed 'improper' represent the various leaky waves supported by the structure. In this case, the associated fields grow in magnitude away from the structure, hence the label.

3.3.2 Propagation constants

From traditional metal waveguide and transmission line theory, it is well known that the propagation constant is given by $\gamma = \alpha + j\beta$ where α is the attenuation constant and $j\beta$ is the complex phase constant.

However, in dielectric antenna theory there is an equivalent: $k = \beta - j\alpha$ where k is the propagation constant or wavenumber along the longitudinal axis. The latter can be decomposed further into a complex propagation constant when considering radiated spatial harmonics resulting from the periodic perturbation of each guided mode (wave):

$$kz_n = \beta_0 + \frac{2n\pi}{d} - j\alpha$$

Here, the z axis has been chosen as the direction of propagation, β_0 is the phase constant of the fundamental *bound* mode, d is the metal strip spacing and n the number of the nth spacial harmonic. It was shown in Section 2.7 that the $n = -1$ harmonic is the main radiating harmonic, with additional harmonics radiating at significantly lower amplitudes and existing in pairs e.g. 0 and -1 [8] and only in the vicinity of the near field. The additional harmonics have been shown, at least theoretically, not to affect the main beam angle found from the -1 harmonic [9]. However, the same author demonstrated theoretically how the designed sidelobe level for a Taylor amplitude distribution beam pattern is raised and degraded compared to a very nice -1 pattern when the additional harmonics are taken into account. Of paramount interest, the same author also reveals that an experimental version appeared to be no better than a design with no sidelobe level control. No further elaboration was given.

3.3.3 Neglecting the complex part of the propagation constant

When strips are added, the excited wave attenuates as a constant along the length due to radiation. This is the leakage constant, also commonly termed the attenuation or decay constant and denoted by α. This constant is what makes the wave and its associated propagation constant complex. This attenuation can be made to vary along the length of the antenna to effectively control the aperture distribution and the associated radiation pattern. This type of non-uniform distribution has been the subject of study by previous authors as presented in the previous chapter.

Other authors have shown this complex part to be extremely low compared to the real part [10]. In this work, a simplification is used such that the imaginary part is zero, and the term propagation constant is used throughout this work except where it is necessary to mention the component parts. Technically, the notation would be kz_0 but this is shortened to kz throughout this work.

The present author provides some new formulas in chapter 8 for a non-uniform distribution that effectively allows the phase and leakage constants to be considered separately. Only the dominant phase part, which is significantly easier to estimate, is computed in this work.

3.3.4 Relationship between key attributes

It was discussed above in general terms how the guide wavelength λg is related to the size of the dielectric guide and the material εr. The guide wavelength is of course normally related directly to the propagation constant $k = 2\pi / \lambda g$. However, in this work it will be demonstrated that this relationship becomes invalid when k is made to vary within the wavelength. For this antenna work the total phase change over a give length of the dielectric guide section between adjacent metal strips become the most important attributes.

3.3.5 Mode field containment and cutoff frequencies

According to Marcatili [4], for a rectangular dielectric waveguide of finite dimensions, the field distribution is partly contained within the waveguide and extends partly outside. These are non-radiating fields of proper bound modes. For any of the bound modes, the associated wave becomes unguided when the field extends to infinity outside of the guide. Under these circumstances, there is negligible field inside the guide. This occurs when the longitudinal propagation constant (kz) of the guide equals the free-space propagation constant (k_0) and the frequency at which a wave becomes unguided is known as its cutoff frequency, or mode cutoff when considering a specific waveguide mode. This field containment was shown earlier in this chapter to be the cause of the variation in guide wavelength, which of course is related to the propagation constant. Equally then, the modes cut off when their guide wavelengths increase to equal the operating wavelength.

3.3.6 Modes, harmonics and main beams

An important point that is rarely mentioned is that radiation is leaked for every spacial harmonic associated with every bound mode that propagates down the guide. This means that multiple main beams might exist at different angles according to the propagation constant of

each mode, and spurious beams might exist according to the propagation constant of each spacial harmonic of each mode. Such a situation would not make a good antenna, since the power would be spread thinly. For this reason, a single beam is the normal requirement and requires that only the lowest waveguide mode propagates, common phrased as 'single-mode operation'. As in metal waveguide theory, this condition is achieved by limiting the operating frequency to a point below which the first higher mode (or modes) is completely cut off, leaving only the lowest 'fundamental' mode to propagate.

The guide dimensions also have to be chosen to be compatible with the operating frequency. Since there is a direct relationship between the guide dimensions and that cutoff point, the dimensions may also be chosen so that only the fundamental mode can propagate [11]. In this work however, it will be assumed that the frequency can be limited, as in practical cases, eliminating the dimensional constraint.

3.3.7 Floquet modes and grating lobes

Although, for LWA based on most types of dielectric guides, the spacial harmonics cannot be prevented they can fortunately be put out of range by careful dimensioning. This means that even after careful choice of the guide dimensions to ensure single-mode operation, it is still possible for multiple significant and unwanted beams to exist. Since the $n = -1$ harmonic has the highest amplitude, it is normal to dimension the antenna and direct the beam based on just that harmonic [8]. Then, to prevent the higher harmonics from radiating the operating frequency must limited to limit the guide wavelength or propagation constant. These special harmonics are strongly related to grating lobes which will be treated later in Chapters 4 and 7.

Floquet developed an extremely useful mathematical expansion of the waveguide modes into a fundamental mode and an infinite spectrum of harmonics. These harmonics, also commonly referred to as 'spectral harmonics', 'leaky modes' or 'Floquet modes' and are used in the mode-expansion method by other authors, as described in Section 2.7.

3.3.8 Dispersion relations

The proper and improper modes, which together represent an expansion of the fields, have an associated propagation constant kz. This is determined from the dispersion relation, also called characteristic equation, for the structure at a given operating frequency. The derivation of the dispersion relation is extremely difficult because the superposition of the contributions from the continuous spectrum cannot be solved in closed form [4]. However, if only the far-field representation is taken instead, only the single dominant leaky wave mode is needed to adequately describe the radiated field [9].

3.3.9 Methods for deriving the dispersion relation

A number of approaches, all of them very challenging and tailored to an individual type of structure, have been used to derive the dispersion relation or the propagation constant directly. The main ones associated with this type of LWA were described with the work of other authors in Chapter 2. Two of these methods will be elaborated on here because they are directly related to the current work. They are interesting because they derive the dispersion characteristics and demonstrate the field intensity of the modes for unperturbed rectangular dielectric waveguides respectively. The relative simplicity of the second method has lead to its widespread use, including throughout the current work.

3.3.9.1 Method by Goell

Goell used a circular harmonic analysis and point-matching to solve for the modes of a rectangular dielectric waveguide and produced diagrams showing the relative field intensity of the first few waveguide modes over the rectangular cross-section [12]. For the fundamental mode that is of most interest in this paper, the highest field strength is concentrated in an oval section around the centre of the rectangular cross-section as depicted in Figure 3.2(a), with rapidly decreasing intensity outside that region.

If the area around the guide cross-section is divided up as in Figure 3.2(b), where region-1 represents the guide cross-section, it is immediately obvious from this example that the field intensity is lowest in the corner regions 6 to 9. Now, if the interface is considered between regions 1 and 2, it can be seen that the field strength is relatively high. Of course, the actual field strength at any point will depend on the excitation amplitude and the operating frequency as described earlier.

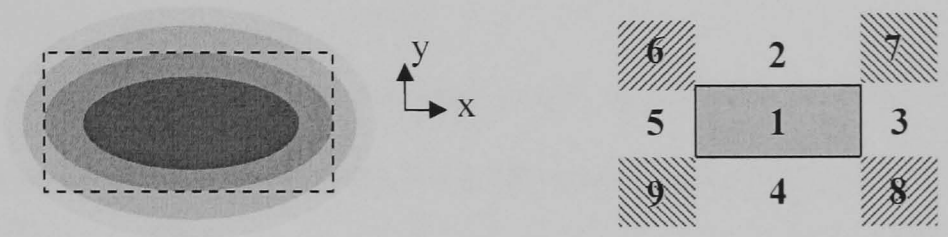

Figure 3.2 (a) Depicts E_{11}^{y} mode field intensity (darker is higher intensity), (b) boundary regions of the rectangular dielectric guide.

3.3.9.2 Method by Marcatili

Marcatili solved Maxwell's Equations in closed form to find the approximate transmission properties of rectangular dielectric waveguide structures [4]. The boundary conditions cannot be matched simultaneously in the x and y directions in the corner regions, thus making the solution for the fields extremely complicated. To solve this, those regions are ignored and the solution becomes approximate with its accuracy increasing with operating frequency as the field is better contained.

Marcatili also assumes that a symmetrical and sinusoidal field distribution exists in the guide material region 1, on both the x and y axes, while the field is assumed to attenuate exponentially in regions 2-5 away from the guide. The solution is therefore developed by solving only for the interfaces between these four remaining regions and their boundary with region 1.

Using these assumptions, Marcatili developed a pair of transcendental equations (3-1), organised in terms of the transverse propagation constants, which describe the rate of change

of phase along the x and y axis. The nomenclature used by Marcatili for these constants is k_x, and k_y respectively. The solutions k_x, and k_y are found in terms of the width (a) and height (b) of the rectangular dielectric guide cross section, and in terms of the difference between dielectric constant(s) between the guide and its surrounding material or materials. The four sides may individually form a boundary with a different material but in this work it is assumed to be air since the guide will be used for a standalone antenna.

Although the transverse constants provide great insight, especially to quantify the distance that the fields penetrate outside the guide walls, the most useful quantity derived by this method is the longitudinal constant, here denoted by k_z. This can be found simply using (3-2) once k_x, and k_y are known. For the well-guided case defined in his paper, where most of the field is confined inside the dielguide, closed-form expressions are also provided.

$$k_x a = p\pi - \tan^{-1}\left(\frac{k_x}{k_{x3}}\right) - \tan^{-1}\left(\frac{k_x}{k_{x5}}\right)$$

$$k_y b = q\pi - \tan^{-1}\left(\frac{k_y}{\varepsilon_r k_{y2}}\right) - \tan^{-1}\left(\frac{k_y}{\varepsilon_r k_{y4}}\right) \qquad (3\text{-}1)$$

where $\frac{1}{k_{x3,5}} = \left[\left(\frac{\pi}{A_{3,5}}\right)^2 - k_x{}^2\right]^{-0.5}$ and $\frac{1}{k_{y2,4}} = \left[\left(\frac{\pi}{A_{2,4}}\right)^2 - k_y{}^2\right]^{-0.5}$

and $$A_{2,3,4,5} = \left(\frac{f}{2c(\varepsilon_r - \varepsilon_{2,3,4,5})^{0.5}}\right)$$

$$k_z = \sqrt{k_0{}^2\varepsilon_r - k_x{}^2 - k_y{}^2} \qquad \text{where} \quad k_0 = \frac{2\pi f}{c} \qquad (3\text{-}2)$$

where a and b are the dielectric waveguide width and height, p and q are the mode numbers, f is the operating frequency and c is the speed of light and 2,3,4,5 are the region numbers opposite the four dielectric guide walls shown in Figure 3.2.

The method is also generalised so that it can solve for the propagation constants of any proper mode, including the fundamental and any of the higher modes. According to Marcatili, the rectangular dielectric waveguide structure supports pseudo TEM modes, where the largest field components are perpendicular to the direction of propagation. He has grouped these modes into two families and given them the nomaclature E_{pq}^{x} and E_{pq}^{y}, where p and q represent the number of extrema of the electric and magnetic field in the dielectric guide in the x and y directions respectively. The main field components are Ex and Hy for the E_{pq}^{x} family and Ey and Hx for the E_{pq}^{y} family. As an example, E_{11}^{x} and E_{11}^{y} represent the fundamental modes of the rectangular guide. E_{11} is depicted in Figure 3.2(a). The next higher modes are E_{12}^{y} and E_{21}^{y} for the y-polarised case, and so on.

Marcatili compares the results of his approximate method in a set of dispersion plots with those of Goell, who used the exact method. One of these plots is reproduced in Figure 3.3. The cutoff occurs when $kz = k_0$ for any of these modes. It can be seen that ignoring the corner regions has resulted in an error for the fundamental E_{11} mode cutoff frequency between points G and M, but this error decreases with increased operating frequency and Marcatili's results start to show good agreement with Goell's about half way toward the end of the single-mode frequency range, labelled G'. Point G' represents the value of k_z when the E_{21} mode starts to propagate at point G''according to Goell. The difference is about 5% between Point G'' and point-M'' which are the Goell and Marcatili E_{21} cutoff frequencies respectively. Since the Marcatili method will be used in the present work, the propagation constant will only be computed up to the Goell cutoff by limiting the upper frequency to point G'' instead of M''. In other words, the propagation constant will only be computed along the dark line from point M to point G'.

The Marcatili E_{21} error will be eliminated so that the method will be accurate at the more useful higher single-mode guide frequency range. The comparisons by Marcatili of his results with those of Goell show excellent agreement for well guided case and good agreement

elsewhere. Experimental results by other authors have confirmed these expectations [5,11,13,14]. The method is useful for experimenting or a preliminary design, and arguably for a precise design because modern EM structure field solver software makes it possible to quickly tune the model to compensate for any error. This process would be required even if a more rigorous and time consuming method was utilized. Perhaps more due to the *relative* simplicity of the method, Marcatili's equations have been used and validated by numerous authors through experimental work on both microwave and millimetre wave leaky-wave antennas and phase shifters [3,5,11,13,14] amongst other things.

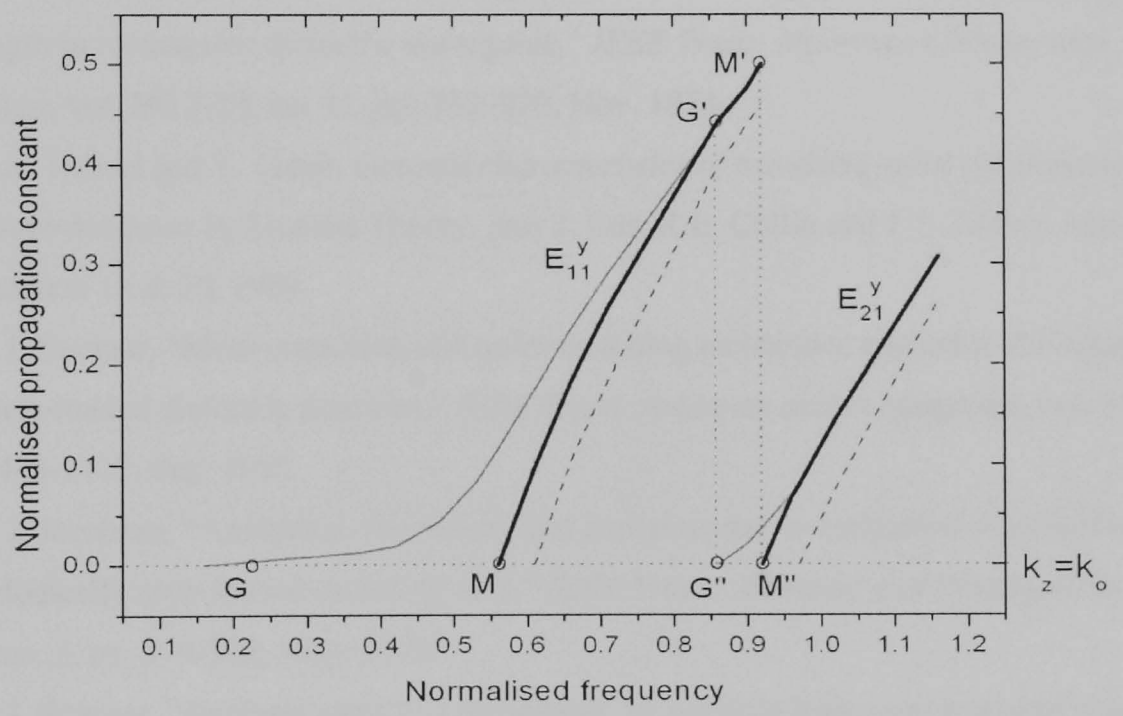

Figure 3.3 Dispersion plot for a rectangular dielectric waveguide (gray curves Goell, black curves by Marcatili transcendental equations, dashed curves by Marcatili closed-form approximation formula).

3.4 References

[1] F. Schwering and A.A. Oliner, *Millimeter-wave antennas* in Antenna Handbook. Eds. Y.T. Lo and S.W. Lee, Van Nostrand Reinhold, New York, Chapter 17, 1988.

[2] W.V. McLevige, T. Itoh and R. Mittra, "New waveguide structures for millimeter-wave and optical integrated circuits," *IEEE Trans. Microwave Theory and Techniques*, vol. MTT-23, no. 10, pp. 788-794, Oct. 1975.

[3] H. Jacobs and M. M. Chrepta, "Electronic phase shifter for millimeter-wave semiconductor dielectric integrated circuits," *IEEE Trans. Microwave Theory and Techniques*, vol. MTT-22, no. 4, pp. 411–417, Apr. 1974.

[4] E. A. J. Marcatili, "Dielectric rectangular waveguide and directional coupler for integrated optics," *Bell Syst. Tech. J.*, vol. 48, no. 7, pp. 2071–2095, Sep. 1969.

[5] H. Jacobs, G. Novick, C. M. LoCascio and M. M. Chrepta, "Measurement of guide wavelength in rectangular dielectric waveguide," *IEEE Trans. Microwave Theory and Techniques*, vol. MTT-24, no. 11, pp. 815–820, Nov. 1976.

[6] A. Hessel and T. Tamir, *General characteristics of travelling-wave antennas* and *Leaky-wave antennas* in Antenna Theory, part 2, Eds. R.E. Collin and F.J. Zucker, McGraw-Hill, Chapters 19 & 20, 1969.

[7] J. Encinar, "Mode-matching and point-matching techniques applied to the analysis of metal-strip-loaded dielectric antennas," *IEEE Trans. Antennas and Propagation*, vol. 38, no. 9, pp. 1405-1412, Sep. 1990.

[8] J. Jacobsen, "Analytical, numerical, and experimental investigation of guided waves on a periodically strip-loaded dielectric slab," *IEEE Trans. Antennas and Propagation*, vol. AP-18, no. 3, pp. 379-388, May. 1970.

[9] J. Encinar, "Analysis and CAD techniques for periodic leaky-wave printed antennas: numerical and experimental results," International journal of Microwave and Millimetre-wave Computer-aided Engineering, vol. 4, no 1, pp. 88, 99. 1994.

[10] R. Mittra and R. Kastner, "A spectral domain approach for computing the radiation characteristics of a leaky wave antenna for millimeter waves," *IEEE Trans. Antennas and Propagation*, vol. AP-29, no. 4, pp. 652–654, Jul. 1981.

[11] K. L. Klohn, R. E. Horn, H. Jacobs and E. Freibergs, "Silicon waveguide frequency scanning linear array antenna," *IEEE Trans. Microwave Theory and Techniques*, vol. MTT-26, no. 10, pp. 764–773, Oct. 1978.

[12] J. E. Goell, "A circular-harmonic computer analysis of rectangular dielectric waveguides," *Bell Syst. Tech. J.*, vol. 48, no. 7, pp. 2133–2159, Sep. 1969.

[13] T.N. Trinh, R. Mittra and R.J. Paleta, "Horn image-guide leaky-wave antenna," *IEEE Trans. Microwave Theory and Techniques*, vol. MTT-29, no. 12, pp. 1310-1314, Dec. 1981.

[14] R. E. Horn, H. Jacobs, E. Freibergs and K. L. Klohn, "Electronic modulated beam-steerable silicon waveguide array antenna," *IEEE Trans. Microwave Theory and Techniques*, vol. MTT-28, no. 6, pp. 647–653, Jun. 1980.

4 PARAMETRIC ANALYSIS USING FIELD SIMULATOR

4.1 Introduction

The main purpose of this chapter is to demonstrate some of the key results found as a result of many hundreds of simulated leaky-wave antenna (LWA) models. These results will serve as an introduction to specific effects that are investigated in the subsequent chapters of this work.

It is prudent to mention here at the beginning that it was found to be near impossible to find a working leaky-wave antenna model by trial and error modification of geometry and guide materials. A relatively significant understanding of the design process was required because a working design falls between strict and quite narrow bounds. Further, even when the supporting guide geometry has been carefully designed for a particular material, the variation in antenna characteristics can still vary quite markedly. For example, some models gave unpredictably very high directivity in the order of >40 while some were low in the order of <<10 despite having almost identical beamwidths. The directivity was also found to vary significantly as the main beam was scanned. After running many simulations for many structures with different geometries, materials and frequencies, it became very clear that the effective aperture A_e is *extremely* sensitive to parametric changes.

4.2 High Frequency Structure simulator (HFSS)

HFSS is a three-dimensional electromagnetic structure software simulation tool with a schematic input. It uses finite element analysis to solve for the fields and has a range of different outputs. The outputs include graphical visualisation of the radiated fields or power, and some basic numerical results including S_{11} and peak directivity.

The 3D LWA models, each consisting of a scale rectangular guide with scale rectangular strips were constructed in the schematic editor. A new model had to be created or modified from an existing model where appropriate to realize parametric changes to the dimensions. For example, to simulate a different strip width or different guide dimensions, a new model had to be created for every case. The simulation results from tens of antenna models are summarised on a small number of graphs in this chapter, where each point represents a single simulation or model.

4.3 Initial simulation model and results

The initial simulated LWA model was based on [1] but without the horn flares. Small changes in the strip spacing and dielectric constant εr were made to capture the change in radiation pattern. The results, shown in Figure 4.1 demonstrate the expected main beam steer towards endfire 0° with advance in strip spacing *d* or εr. These patterns reveal some interesting trends:

1. The original εr = 2.47 model, which is the only model that works within the single-mode range of the guide, has 2 to 3 times lower gain than the higher εr overmoded models;
2. The main beam radiated from the strip-covered guide surface (0° to +180°) has lower magnitude than the beam radiated from the opposite back side surface. This asymmetry was pointed out in [1] but to the best of this author's knowledge has never been investigated. However, it will be investigated in the present work;
3. The half-power beamwidths remain relatively constant for each value of *d* as εr is increased:
4. The onset of grating lobes is apparent as *d* or εr is advanced.

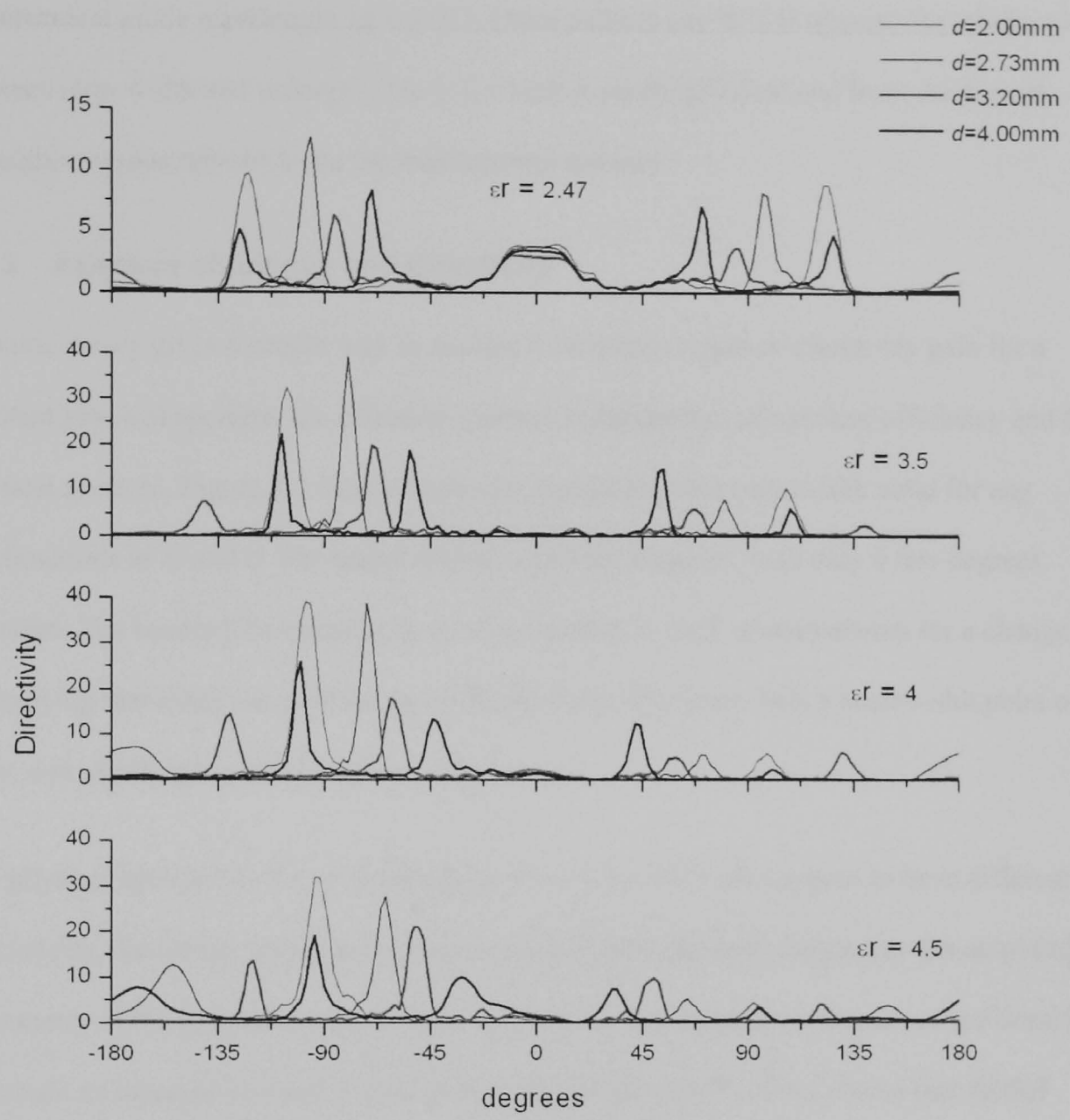

Figure 4.1 Simulated E-plane radiation patterns for LWA parametric study with varying strip spacing d and material dielectric constant εr. The E-plane is the YZ or θ-plane seen from the side of the antenna.

4.3.1 Correct way of expressing leakage

There is no obvious explanation for the sudden increase in gain, and obvious increase in aperture efficiency with εr. Other authors have reported that the beamwidth is controlled by the strip leakage [2]. Assuming that is the case and since the beamwidth is essentially constant, then the leakage must be constant. This is not surprising since the physical strip width is a constant in this model. It implies that the leakage is geometry dependent, but εr-independent. It is interesting that many previous authors, knowing that the leakage is a

function of the strip width, express the strip width in electrical terms as a fraction of the very εr-dependent guide wavelength λg e.g. [1]. Other authors use W/d to express the relationship between strip width and leakage [3] to [5], which is purely physical and from the present simulation results appears to be the most appropriate way.

4.3.2 Aperture efficiency and directivity

Antenna theory gives a simple way to express a variation in gain or directivity gain for a constant physical aperture; the effective aperture is the product of aperture efficiency and the physical aperture. Figure 4.2 demonstrates the typical H-plane beamwidth valid for any combinations of εr and *d*. The beamwidth is relatively constant, with only a few degrees variation. The beamwidth variation is more noticeable in the E-plane patterns for a change in *d*, implying that *d* has some influence on the aperture efficiency from a beamwidth point of view, and significantly more influence than εr.

The physical aperture on the strip and back sides of the LWA also appear to have different efficiencies, the former seeing much more variation than the latter judging by the amplitude asymmetry of the respective main beams. In general, this asymmetry increases significantly with both an increase in *d* and *εr* (not shown), although later it will be shown that further increases cause the asymmetry to increase and decrease in a cycle.

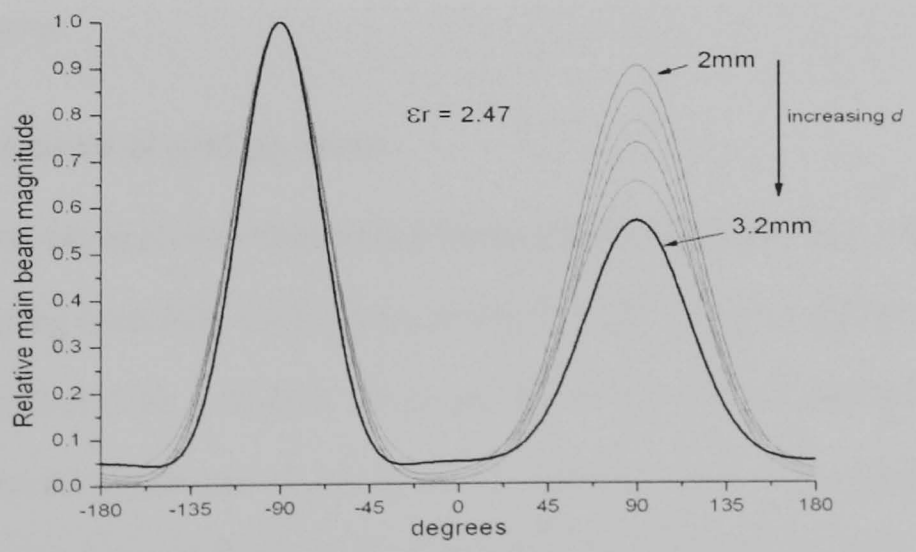

Figure 4.2 Typical simulated H-plane radiation pattern for LWA parametric study with varying strip spacing d and material dielectric constant εr.

This chapter will also demonstrate that it would not be possible to have a single aperture efficiency for this antenna in the same way that it is possible for other types of antenna [6]. Instead, the efficiency will vary significantly with just about any small parameter change. This can also be proven very easily by deriving the efficiency from the standard formula: $D_0 = \eta_a A_p(4\pi / \lambda_o^2)$ for the main beam directivity for any of the plotted patterns, where D_0 is the directivity gain, η_a is the aperture efficiency, A_p is the physical aperture size and λ_o is the operating wavelength.

4.3.3 Overmoding

The models of εr = 3.5 and higher have been simulated above the single-mode frequency of the guides. It is interesting that all these models see a step increase in gain over the εr = 2.47 model which is simulated within its single-mode frequency range. [2] has stated generally that the field intensity around the gratings peaks somewhere between the low frequencies, where the field extends well outside of the guide walls, and the very high frequencies where it is well contained and guided. These simulation results tend to suggest that the field intensity at the strips is closer to its peak value in the overmoded models.

Radiation at the endfire angle 0° is also noticeably reduced for the overmoded models, presumably due to the fact that these models are radiating more efficiently in the upper and lower hemispheres.

4.3.4 Appearance of grating lobes

The approximate physical limits that prevent higher special harmonics from radiating undesirable grating lobes have already been defined in [7,8]. The latter author's formula was given in chapter 2 as (2-4). A study by the present author tested these formulas by comparing their results with the appearance of grating lobes in radiation patterns generated using the usual antenna array factor (2-1) for the same physical and electrical characteristics. The derivation of such characteristics will be the subject of further chapters.

These results are compared with the simulated radiation patterns of Figure 4.1 where, for the εr = 2.47 case, the grating lobe can be seen appearing at -180° when the spacing is increased to d = 3.2mm. The main beam is at -86° in that case.

The Marcatili method was used to derive the normalised propagation constant, giving 1.1927. Plotting the radiation pattern, shown in Figure 4.3, using the array factor shows that the grating lobe starts to appear when the spacing reaches d = 3.255mm with the main lobe at 86.4°, almost identical to the simulation result. This main beam angle itself can be found using the well-known formula (2-2) and n = -1.

4.3.4.1 Testing accuracy of existing grating lobe formulas

The formula presented in [7] and reproduced below as (4-1) is a simplification of (2-2) and finds the spacing d that produces a grating lobe with magnitude *equal* to the main beam. It is derived by solving for d when (2-2) = -1 and using n = -2 and gives a value of d = 3.355mm at 81.5 GHz. This result is also plotted in Figure 4.3 for comparison, where a problem becomes apparent; the grating lobe that (4-1) predicts actually started earlier for a lower spacing value, making this formula inaccurate. This occurs because (2-2) and its simplification (4-1) only predict *maxima*. The difference in main beam angle between the grating starting to appear and reaching full magnitude is only 1.9° in theory for this example. Figure 4.1 demonstrates quite clearly that the grating lobes never really become maxima per-se. It therefore appears prudent to tackle this error and so this will be done in Chapter 7.

$$\frac{\lambda_0}{\frac{\beta}{k_0}+1} \le d \le \frac{\lambda_0}{\frac{\beta}{k_0}-1} \qquad \text{for } \beta/k_0 > 3$$

$$\frac{\lambda_0}{\frac{\beta}{k_0}+1} \le d \le \frac{2\lambda_0}{\frac{\beta}{k_0}+1} \qquad \text{for } \beta/k_0 < 3 \qquad (4\text{-}1)$$

where β is the propagation constant of the fundamental E_{11} mode.

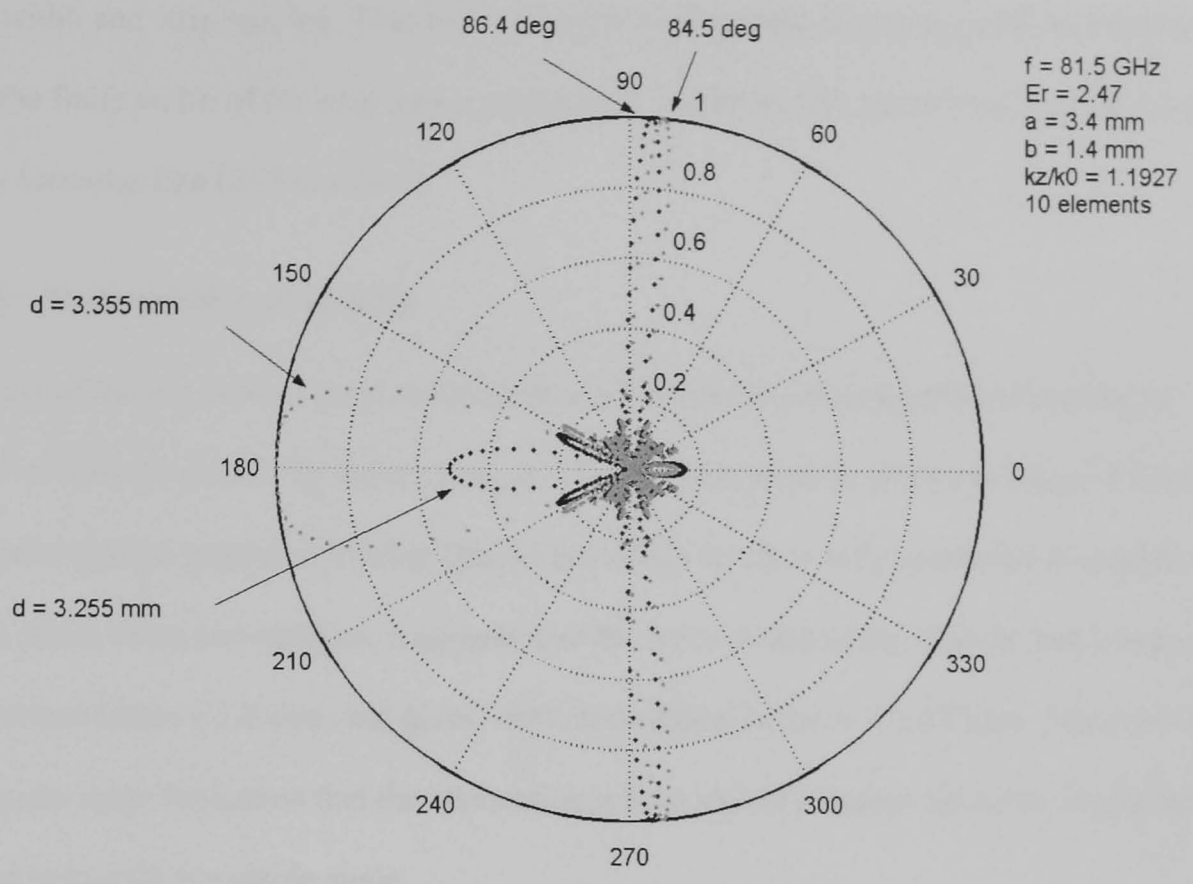

Figure 4.3 Theoretical E-plane radiation pattern computed using linear array factor formula (2-1) showing onset of grating lobe and full magnitude grating lobe for the εr = 2.47 model.

The second formula (2-4) compensates for the inability of the first formula to predict the spacing for the early appearance (onset) of the grating lobe by adding an arbitrary margin. However, the present author found that this margin overcompensates quite severely, giving d = 2.516mm as the maximum spacing without a grating lobe appearing, which is almost 23% lower than simulated.

Comparing theory and simulation results shows almost perfect agreement for the pointing angle of the main beam at the onset of the grating. However, the theoretical strip spacing is almost 5% higher than simulations suggest. It is the present author's opinion that this error is due to the fact that the theory does not incorporate the strip width.

This appears to be the first time that the inaccuracy of these existing formulas has been demonstrated. While these errors are quite small, it will be shown in Chapter 8 that the beam angle error increases significantly under certain circumstances like higher values of dielectric constant, and a new correction formula will be provided that incorporates the actual physical

strip width and strip spacing. This will use a new average value of propagation constant to take the finite width of the strip into consideration, which can be entered into any of the well-know formulas like (2-2) and (4-1).

4.3.5 Broadside null effects

Additional models were created and simulated with smaller incremental strip spacing to discover how the directivity values change. The resultant patterns shown in Figure 4.4 tend to suggest a smooth parabolic looking change but with a notch or null around the broadside ±90° angle. From these two samples, it appears that the notch is both quite shallow and narrow in the overmoded $\varepsilon r = 3.5$ case, but gives ~50% attenuation in the $\varepsilon r = 2.47$ case. The latter case also gives some indication that the attenuation is held almost constant for some considerable period below the broadside angle.

Other authors have demonstrated the effects of this null on the leakage constant. In particular [2] shows that an almost step change theoretically occurs within about 1° of broadside (91° or -1°) and then increases slightly more slowly so that the leakage is restored to about the original value at approximately +3° to +4°. It appears that, within that region of change, the beam angle is held at broadside. Other authors have presented techniques to reduce the null depth or width [9,10] and have presented alleged improvements on leakage or beam angle versus frequency plots. This appears to be the first time that this effect has been presented for the radiation pattern of a leaky-wave antenna.

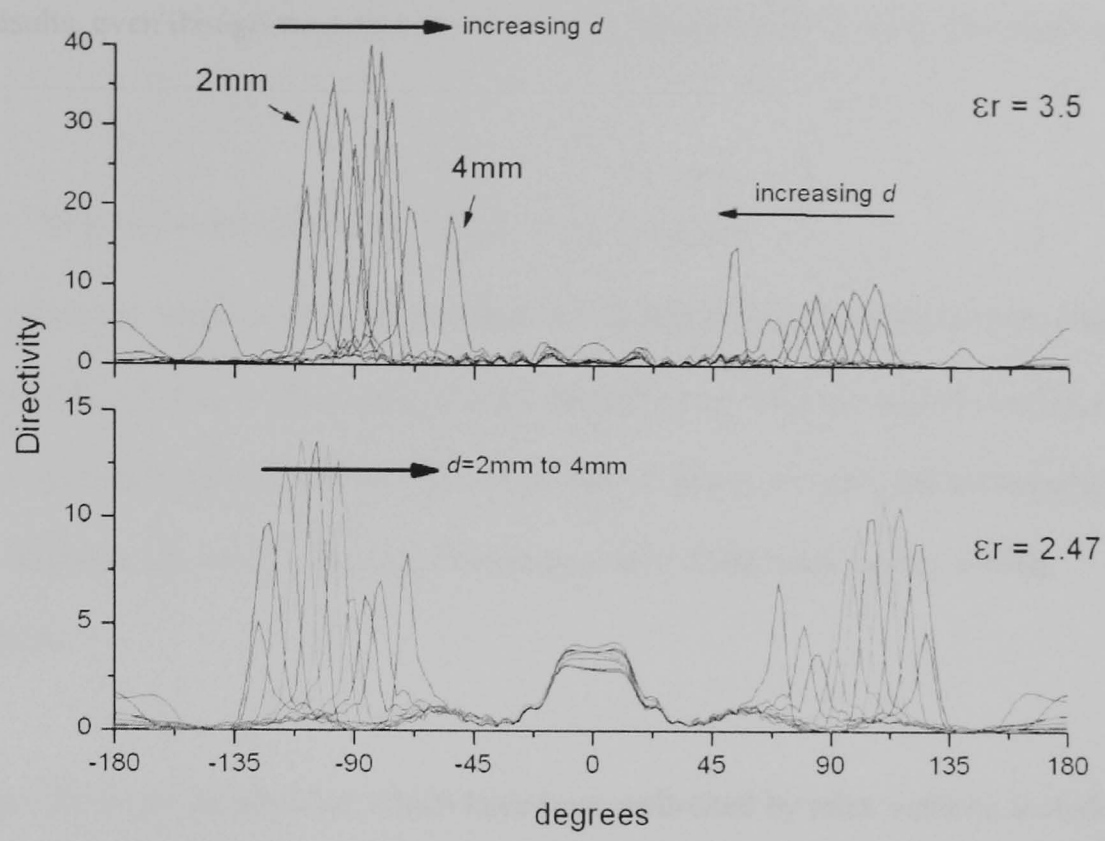

Figure 4.4 Sample E-plane radiation patterns versus strip spacing demonstrates reduction in directivity for main beams around the broadside angle ±90°.

4.3.6 Varying the strip width and operating frequency

Additional models were created with various strip widths, constant strip spacing, and the same dielectric guide geometry as previous models. The effect on the directivity can be seen from the results shown in Figure 4.5 for three frequencies near the limits and middle of the single mode range for the εr = 2.47 guide and in Figure 4.6 for frequencies in the upper half of the εr = 15.8 frequency range. The lower of the two εr = 2.47 plots simply shows the results for models with a smaller width increment so that the curvature could be captured more accurately. This kind of curvature can be safely assumed for the other results. A notch is evident in the results for both models at 74 GHz and 5.6 GHz / 5.8 GHz respectively. By cross-reference with Figure 4.7 and 4.8 which show the variation in simulated main beam angle versus strip width, it can be seen that the directivity notches are due to the beam passing through the broadside null angle, where it remains for all the narrowest strip widths. At 5.6 GHz, the beam only passes within say 8° however the notch is very evident in its directivity curve. Interestingly, only the wider widths seem to be more affected by the null according to

these results, even though the narrowest widths clearly generate the same broadside beam angle.

4.3.6.1 Strip width and frequency versus directivity gain

[1] on which the model is based declare that the highest gain is found for a strip width of $W=0.4\lambda g$ with $< 0.2\lambda g$ widths leading to poor radiation and $> 0.5\lambda g$ widths reducing the effective aperture (implies that the radiation would be poor). It is perhaps not surprising then that the response shown for the same frequency of 81.5 GHz leads to very similar conclusions.

However, the same declarations, which have been well-cited by other authors, including in text books [7] do not appear to apply quite as well to the higher and lower frequency results. For example it appears that the gain is continuing to increase even at $W=0.55\lambda g$ at various frequencies. This is also despite the fact that the physical strip width is narrower at that point than at the lower frequencies, because the guide wavelength is lower. The leakage has been shown by other authors to be strongly frequency dependent and dependent on W/d [10].

4.3.6.1.1 Optimum strip width

The present results also tend to verify the frequency dependence on the leakage. Moreover, given the variations shown in Figure 4.5, it appears that the highest possible operating frequency is the key to achieving maximum gain along with a wide physical strip width W/d = 0.5. Interestingly, this is the same optimum ratio as reported for the dielectric grating type LWA [2]. It is relatively straightforward to optimise with ratios around 0.5 using a simulation tool like HFSS. The very high directivity of the overmoded models also tends to reinforce the indication that a high operating frequency is important to achieving high gain.

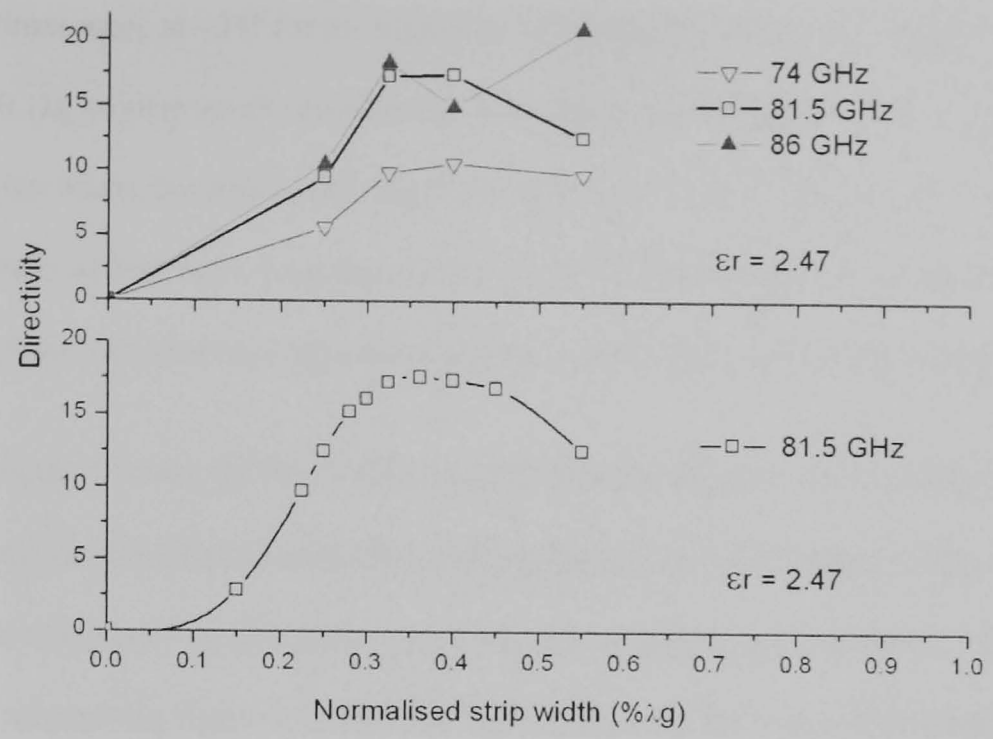

Figure 4.5 Simulated directivity gain versus strip width for three frequencies in the single-mode range.

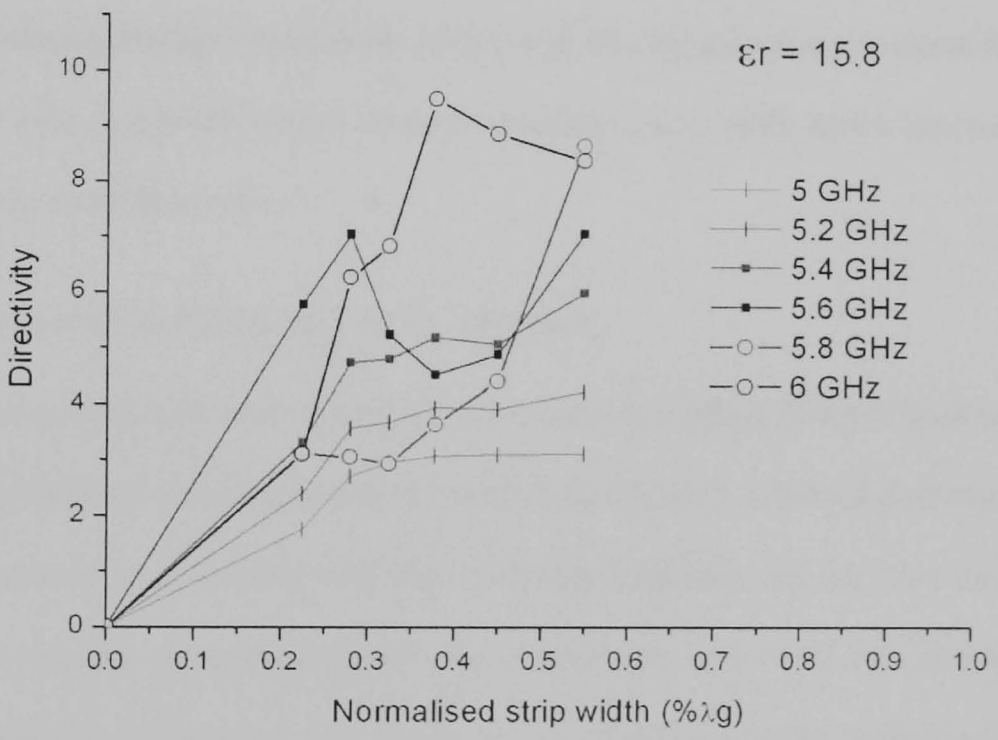

Figure 4.6 Simulated directivity gain versus strip width for frequencies in the upper half of the single-mode range for the high dielectric constant model.

4.3.6.2 Strip width and frequency versus main beam angle

Figures 4.7 and 4.8 demonstrate a very important point as far as this work is concerned; the main beam is quite a strong function of the strip width. The main beam moves in the endfire direction as the strip width is increased. For the εr = 2.47 model, the change in main beam angle over the range of strip widths is in the order of ~6°. The rate of change is slightly more

than fours times more at ~21° for the higher εr = 15.8 model. These rates equate to about 2° and 7° per 0.1λg of strip width respectively. It is easy to see that neglecting the strip width in a LWA design where the strip width might typically be ~0.5λg would appear to be a grave error, but some authors have done exactly that [1,11,12]. There appeared to be an opportunity to quantify these variations for any model and this will be done in Chapter 8 of this work.

A key observation is that, for the 74 GHz and 5.8 GHz frequencies where the main beam reaches broadside, the beam remains at broadside for the narrowest strips. It is not clear whether this effect is a function of the broadside null width and the unaffected wider strips just happen to steer the beam outside of the null region, or if the wide width simply overcomes the broadside null effect. Although the former explanation seems quite credible, the fact that the wide strips appear to draw the beam away from broadside also seems more than a coincidence. Further experiments with a strip spacing adjustment to move the main beam of the wide strip width models through broadside could verify which explanation best fits this newly found behaviour.

4.3.6.3 Strip width and frequency versus asymmetry

The strip side to back side beam magnitude asymmetry is a strong factor of both strip spacing and material dielectric constant, as already mentioned. Figure 4.7 and 4.8 demonstrate the simulated variation in asymmetry with strip width and frequency, for the low εr and high εr models. The variation of asymmetry with strip width is very minor at < 10% in most cases and only about 20% in the worst case. However, the asymmetry varies strongly with frequency. The change in asymmetry with frequency is extremely significant for the high εr model, reducing by ~70% even though only the upper half of the single mode range has been used. The low εr model shows an average of ~35% change over its entire single-mode range. It is not apparent what might cause this difference. In general, the asymmetry is highest at the highest frequencies.

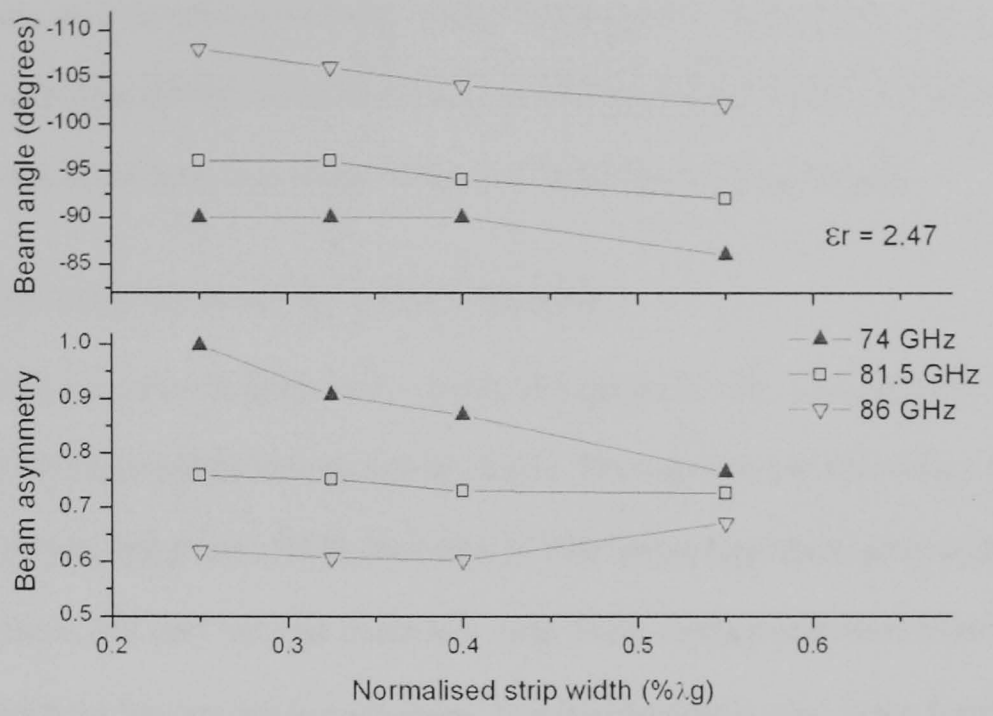

Figure 4.7 Simulated beam angles and strip-side to back-side beam magnitude asymmetry versus strip width for three frequencies in the single-mode range.

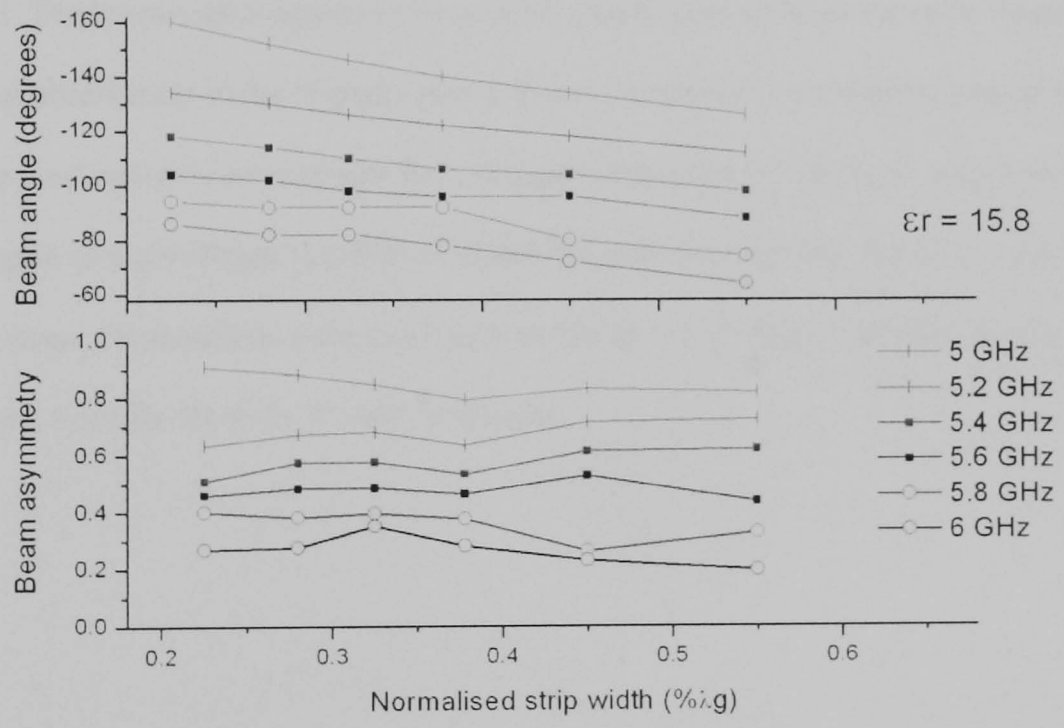

Figure 4.8 Simulated beam angles and strip-side to back-side beam magnitude asymmetry versus strip width for the high dielectric constant model.

It is interesting to see that for the two frequencies 74 GHz and 5.8 GHz where the main beam passes through the broadside null and stays there for a period, the results appear to show that the change in asymmetry with strip width sees the largest variation. This is certainly the case for the $\varepsilon r = 2.47$ model, but it could simply be a coincidence that it happens for both models.

This does raise an interesting possibility: since the variation in beam angle with strip width is mostly zero at broadside but varies elsewhere, and the asymmetry varies at broadside but is mostly constant elsewhere, then these effects are potentially complementary.

4.3.6.4 Strip width and frequency versus beamwidth

The E and H-plane radiation patterns are shown in Figures 4.9 and 4.10, primarily to demonstrate the beamwidths and associated effects. The rapid movement of the main beams over the frequency range can also be seen clearly. The interesting observation in the E and H-planes patterns is that they become essentially strip width independent close to broadside, but at slightly different frequencies in each plane. It is also interesting that in the E-plane pattern at 6 GHz, the beams representing the different strip width models appear to have their trailing edges stuck at broadside, implying that the null is still taking effect at angles less than broadside. The beamwidths appear to be widening with strip width at the same frequency. The interesting observation in the H-plane plot is that it is essentially omnidirectional at the lowest frequency, and becomes increasingly less so as the frequency is increased, until eventually the classic figure of eight shaper is achieved where the nulls between the front and back side lobes are deep. These effects were not found for the $\varepsilon r = 2.47$ model, perhaps because the main beams were far from the 0° and 180°limits.

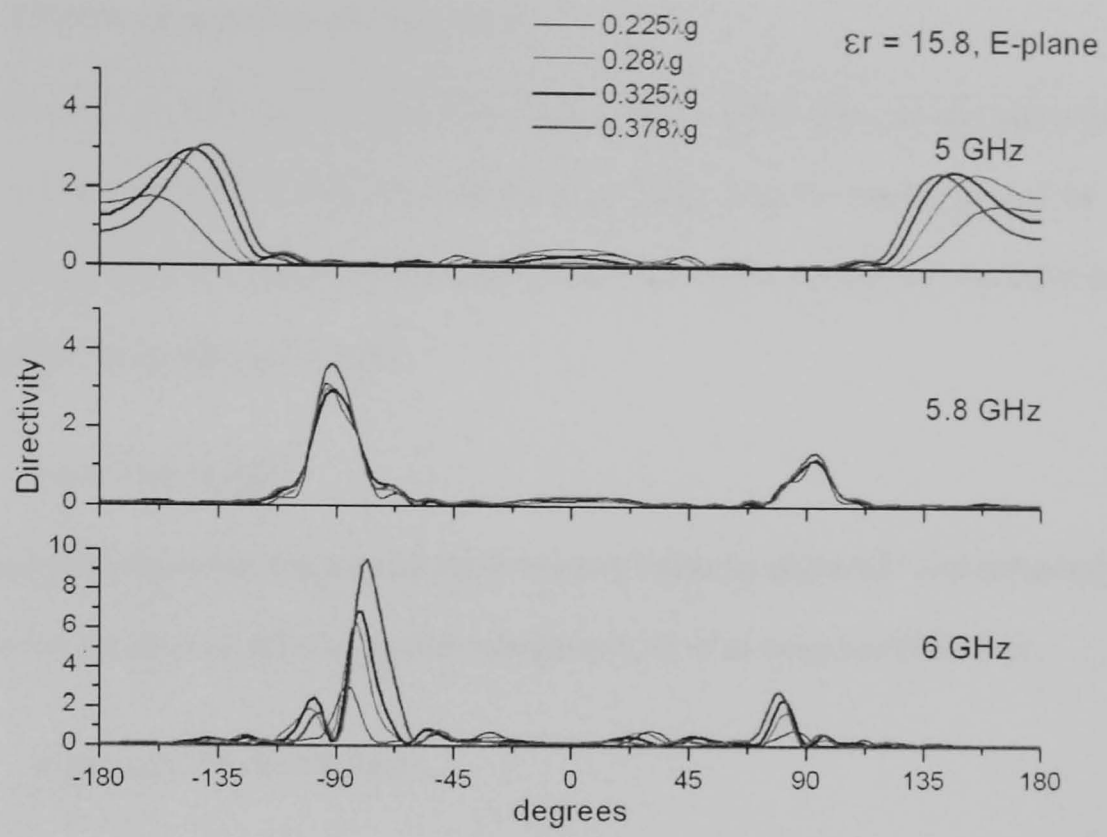

Figure 4.9 Simulated E-plane radiation patterns showing effects of variation of strip width for 3 frequencies for the high dielectric constant model.

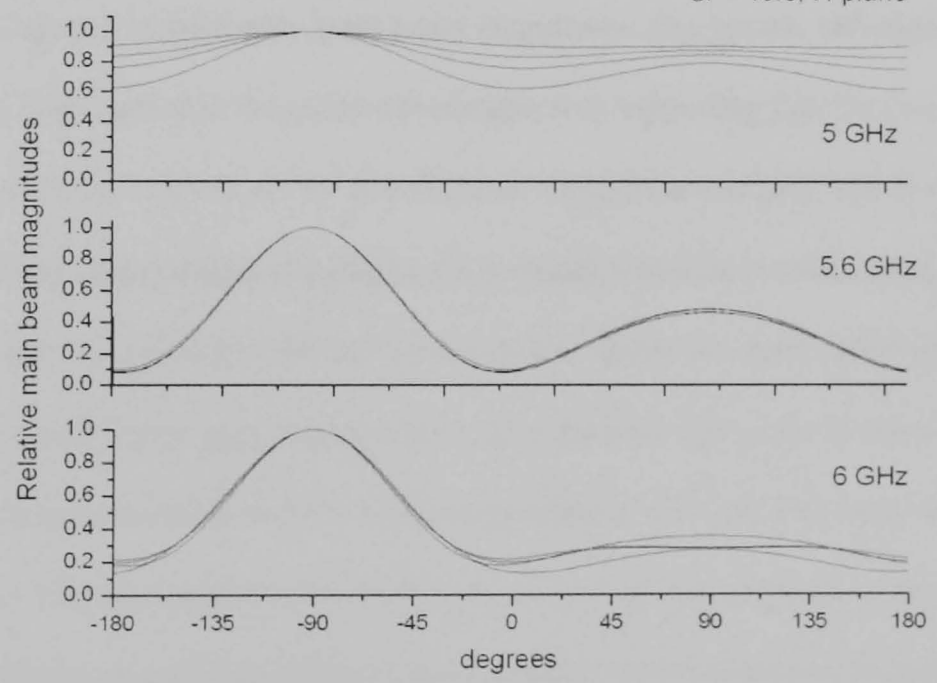

Figure 4.10 Simulated H-plane radiation patterns showing effects of variation of strip width for 3 frequencies for the high dielectric constant model.

4.3.7 Effects of position of first strip

Using the same εr = 2.47 and 3.5 models as a basis, new models were created and simulated with the position of the first strip, the start spacing, varied from the starting end of the guide. The resulting effects are presented next in Figures 4.11 to 4.13, where the vertical lines are spaced at half the guide wavelength.

4.3.7.1 Main beam angle

Of obvious interest is that angle cycles between two limits by about ±1° and apparently with a period approximately equal to one guide wavelength λg or at twice the frequency.

4.3.7.2 Input reflection coefficient

S_{11} also cycles as the start spacing is increased, between similar limits for all three basic models. In all these cases, it cycles at almost precisely half the guide wavelength.

4.3.7.3 Asymmetry

The ratio of strip-side to back-side main beam magnitudes also cycles, although not so clearly, at the same period as the guide wavelength. It is interesting that the two models for which the asymmetry is given are for two different dielectric constants. The εr = 2.47 model has low directivity gain compared to the εr = 3.5 model, which is overmoded as pointed out earlier. It is interesting then that the asymmetry is low for the low gain model and much higher for the much higher gain overmoded model, although this could be coincidence. The strip-side beam has as little as < 20 % of the magnitude of the back-side beam in the latter case. In Figure 4.8, this same level of asymmetry was seen at the high frequency for the εr = 15.8 model. The asymmetry therefore appears to increase with increased frequency.

4.3.7.4 Directivity gain

The directivity also cycles with increasing strip spacing and, in addition, it gradually reduces in amplitude in all three models. This time, the period is not very clear, and appears to be different for each model.

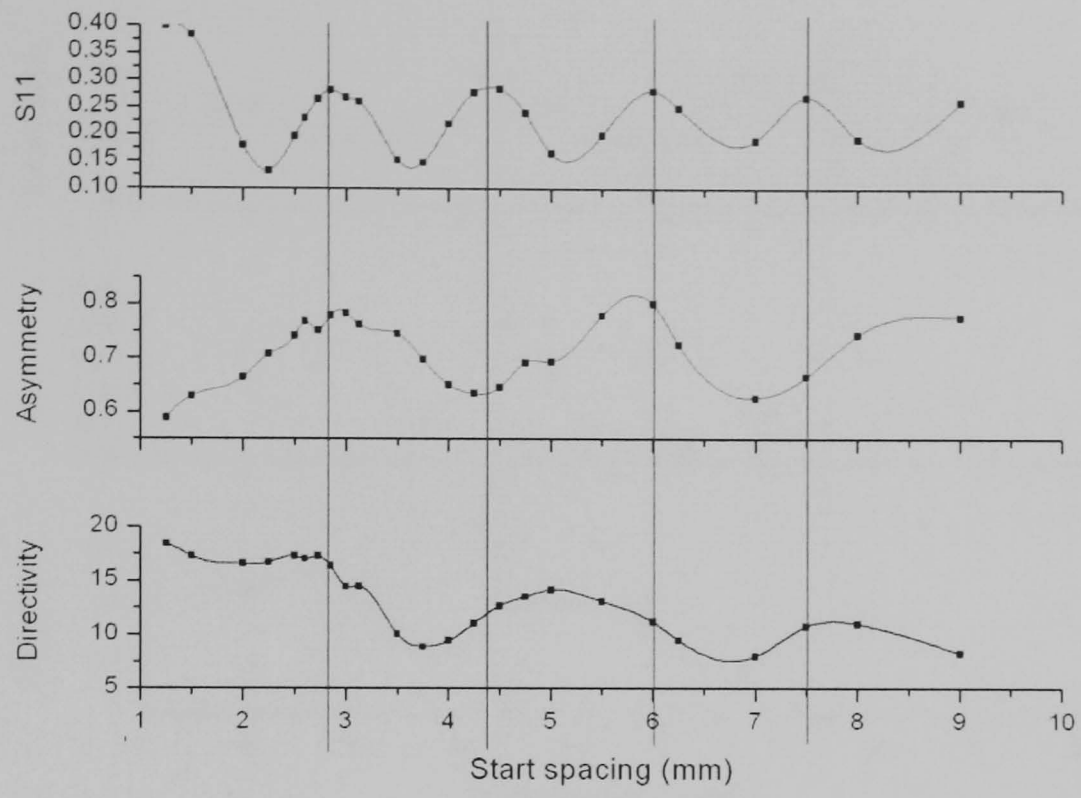

Figure 4.11 Start spacing effects for the simulation model with parameters: εr = 2.47, d = 2.73mm, f_o = 81.5 GHz, λg ~ 3.1 mm

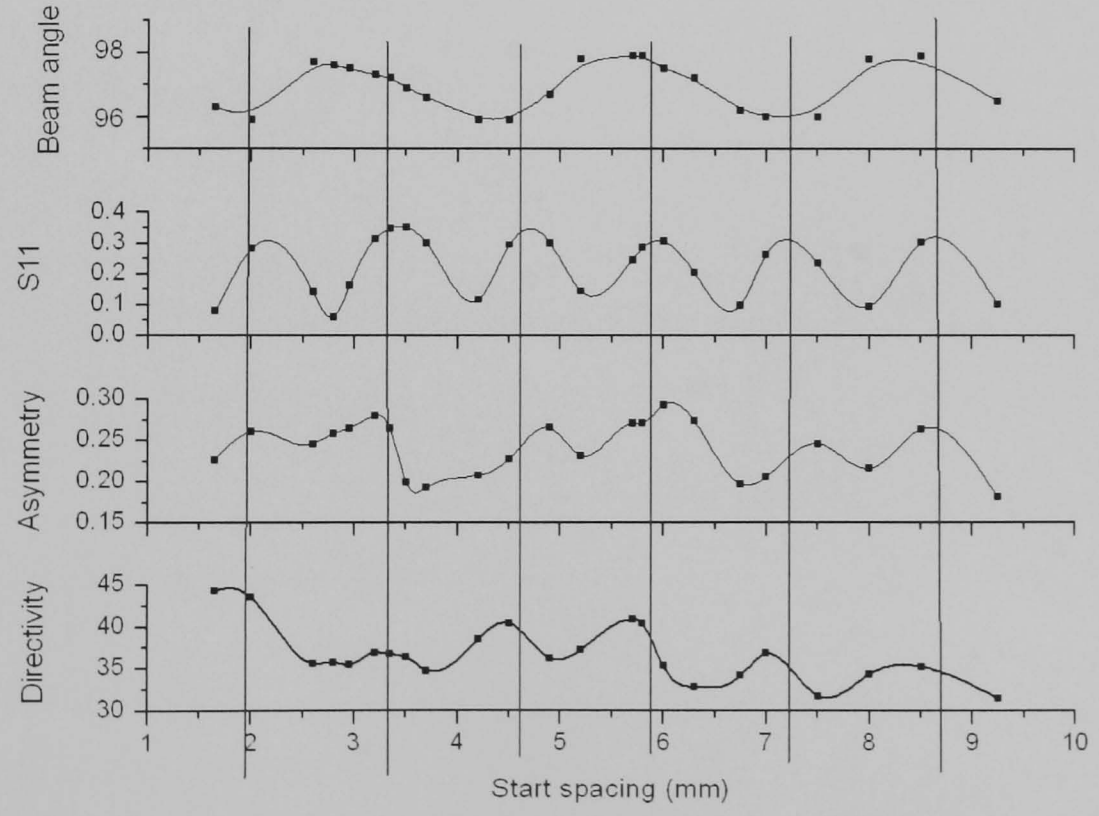

Figure 4.12 Start spacing effects for the simulation model with parameters: εr = 3.5, d = 2.6mm, f_o = 81.5 GHz, λg ~ 2.53 mm

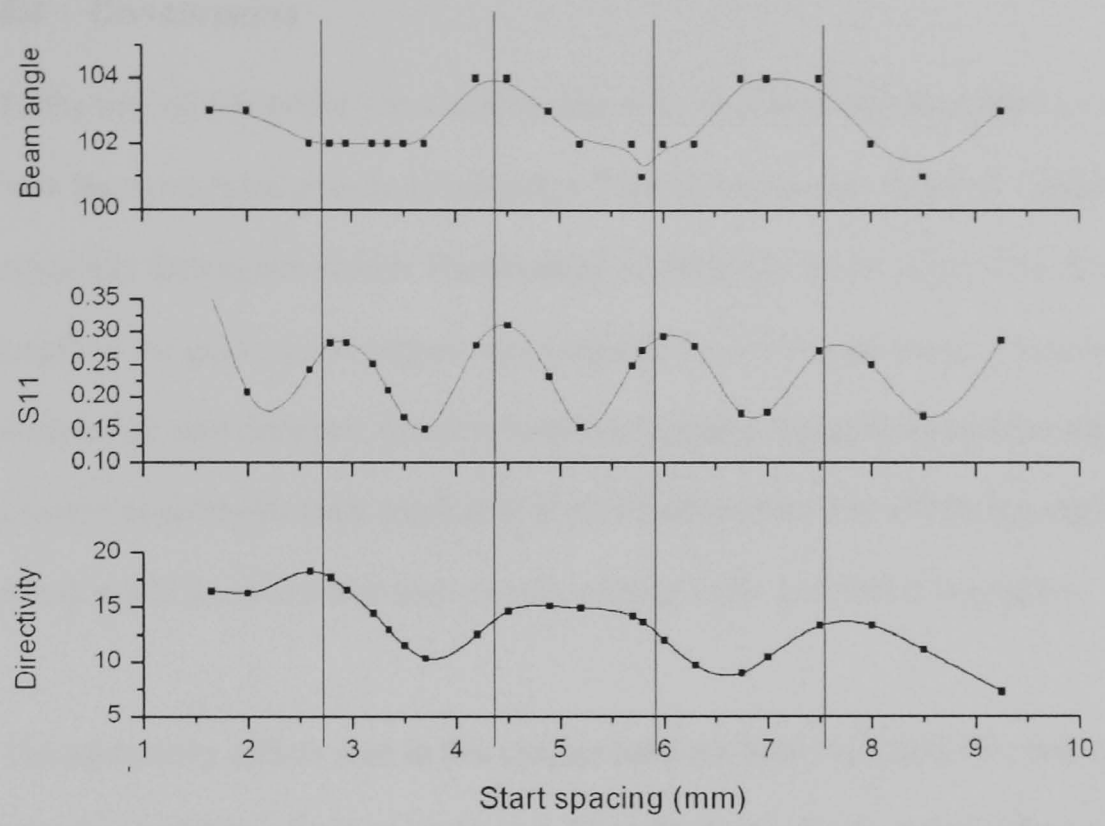

Figure 4.13 Start spacing effects for the simulation model with parameters: εr = 3.5, d = 2.6mm, f_o = 70 GHz, λg ~ 3.2 mm

4.4 Conclusions

To the best of this author's knowledge, this is the first time that these start spacing effects have been presented or even investigated. There is no obvious theory to support the effects, especially their cyclic nature. The decrease in directivity as the strips are moved down the length of the guide might suggest that the guide itself is losing energy. However, since the models had zero dielectric loss, this tends to suggest a reduction in aperture efficiency instead. Limited experiments were conducted as verification and these will be reported in Chapter 9 where it will be shown that such a cyclic change in S_{11} was found in practice.

The asymmetry effects seen in this chapter have not been studied before and the mechanisms associated with its causes are unknown. The effects are simply reported here without offering any explanation. The key influences on the asymmetry were found to be primarily operating frequency. In general, at the lowest frequencies it is almost symmetrical and at the highest frequencies there is > 5:1 asymmetry. The asymmetry also varies strongly with changes in dielectric constant and strip spacing. Its variation with strip width and start position is minor in comparison. This is quite puzzling because if the variation was large with a change in strip width, the effect could have been associated with leakage. However, as it stands, there appears to be no other explanation. The existence of the main beam asymmetry is also proven in practice in Chapter 9.

These simulations also demonstrated how sensitive the directivity is to parametric changes. This time however, the impact of the strip width was shown to be very important. A high operating frequency was again shown to be important. It was found that the directivity could be maximised for any given model by setting the strip width and gap between the strips to be approximately equal. The general response for directivity versus strip width was found to be very parabolic around this peak. Despite this, large directivity variations were found between models. It is thought that this is a function of the guide dimensions, material and operating

frequency, and that some combinations give good overall leakage while others do not. Perhaps the most important point about this is that it appears to be both possible and valid to treat the strip width and spacing on the guide surface separate from the guide itself as far as optimum leakage is concerned. However, this assertion must be validated and is discussed in Chapter 10 among the further recommendations.

4.5 References

[1] T.N. Trinh, R. Mittra and R.J. Paleta, "Horn image-guide leaky-wave antenna," *IEEE Trans. Microwave Theory and Techniques*, vol. MTT-29, no. 12, pp. 1310-1314, Dec. 1981.

[2] F.K. Schwering and S.T. Peng, "Design of dielectric grating antennas for millimeter-wave applications," *IEEE Trans. Microwave Theory and Techniques*, vol. MTT-31, no. 2, pp. 199-208, Feb. 1983.

[3] M. Matsumoto, M. Tsutsumi and N. Kumagai, "Radiation characteristics of a dielectric slab waveguide periodically loaded with thick metal strips," *IEEE Trans. Microwave Theory and Techniques*, vol. MTT-35, no. 2, pp. 89-95, Feb. 1987.

[4] M. Guglielmi and G. Boccalone, "A novel theory for dielectric-inset waveguide leaky-wave antennas," *IEEE Trans. Antennas and Propagation*, vol. 39, no. 4, pp. 497-504, Apr. 1991.

[5] J. Encinar, "Mode-matching and point-matching techniques applied to the analysis of metal-strip-loaded dielectric antennas," *IEEE Trans. Antennas and Propagation*, vol. 38, no. 9, pp. 1405-1412, Sep. 1990.

[6] C.A. Balanis, "*Aperture Antennas*,"in Antenna Theory, Second edition, John Wiley & Sons, Ch. 12, p600, 1997.

[7] F. Schwering and A.A. Oliner, *Millimeter-wave antennas* in Antenna Handbook, Eds. Y.T. Lo and S.W. Lee, Van Nostrand Reinhold, New York, Chapter 17, 1988.

[8] S. Kobayashi, R. Lampe, R. Mittra and S. Ray, "Dielectric rod leaky-wave antennas for millimeter-wave applications," *IEEE Trans. Antennas and Propagation*, vol. AP-29, no. 5, pp. 822–824, Sep. 1981.

[9] K. Solbach and B. Adelseck, "Dielectric image line leaky-wave antennas for broadside radiation," *Electronic Letters*, vol. 19, pp. 640–644, Aug. 1983.

[10] M. Guglielmi and D.R. Jackson, "Broadside radiation from periodic leaky-wave antennas," *IEEE Trans. Antennas and Propagation*, vol. 41, no. 1, pp. 31-37, Jan. 1993.

[11] K. L. Klohn, R. E. Horn, H. Jacobs and E. Freibergs, "Silicon waveguide frequency scanning linear array antenna," *IEEE Trans. Microwave Theory and Techniques*, vol. MTT-26, no. 10, pp. 764–773, Oct. 1978.

[12] L. Huang, J.C. Chiao and M.P. De Lisio, "An electronically switchable leaky wave antenna," *IEEE Trans. Antennas and Propagation*, vol. AP-48, no. 11, pp. 1769-1772, Nov. 2000.

5 DETERMINING DIELECTRIC GUIDE CHARACTERISTICS

5.1 Introduction

5.1.1 Rectangular dielectric waveguides

Unlike their hollow metal rectangular waveguide counterparts, the solid rectangular dielectric waveguide has no standardised specification chart listing the guiding characteristics such as guide dimensions, frequency range, fundamental mode cutoff and power handling capabilities etc. In the dielectric guide case, all these parameters are highly material dependent [1]; therefore such a table would have to have one set of characteristics for every material, and every standard guide size. In addition, since the *standard* guide dimensions only really apply to metal waveguides and not to dielectric guides, there would be a potentially infinite number of sizes and therefore entries in a hypothetical specification chart for dielectric waveguides. There are also many other possible dielectric waveguide types/structures, in addition to the simple rectangular rod of dielectric material, commonly known as an 'open' dielectric guide. Other simple dielectric guide types can be produced by covering one or more of the dielectric guide walls with conducting planes, thereby partially 'closing' the guide. Each type would have to have its own unique specification table, again, with a potentially infinite number of entries.

5.1.2 Analysis and numerical methods

When beginning a new design using a dielectric guide, the engineer of course would need to have many of these specifications at hand. Determining suitable guide dimensions for a particular target operating frequency or frequency range, for example, and for a given material and guide type, is an essential task that will be extremely difficult and cumbersome for the uninitiated, and tedious and time-consuming at best for the expert. The methods available to obtain such information include [2-24]:

- Transverse resonance method;
- Spectral harmonic expansions;
- Mode expansion method;
- Method of moments.

It is certainly possible to program these methods for a given structure, but it would be an extremely time-consuming programming task, perhaps taking many months to complete.

5.1.3 Dispersion plots

For a very limited number of guiding structures there exist dispersion plots that will allow the designer to find an approximate size and material permittivity combination for one of those structures at a given frequency [8, 13, 14, 25-27]. If the designer knows how to read such plots, this will potentially help to reduce the number of design cycles with the code. Such plots normally furnish the normalised longitudinal propagation constant, one of the most important guide characteristics used in this thesis. The plots quantify this for any given material permittivity (dielectric constant) and size, but most published plots are based on a fixed frequency, guide material and size and are therefore of no use unless one of them happens to match the new requirements. Other, more generic, dispersion plots of the type published in [28,29] are also available, but in practice, despite being much more flexible in terms of guide size and frequency, are specific to a particular guide material dielectric constant (permittivity) and surrounding material ratio. If the surrounding material is free space, these plots become material specific and so again, have limited use.

5.1.4 Finding a size and material compromise

Ultimately, the designer will need to choose a material, out of the finite number of suitable and available types with satisfactory physical and electrical characteristics, and form it into a size such that the design frequency falls well within the valid frequency range for those dimensions. Alternatively, the engineer can work the other way around and choose a material that meets particular maximum size requirements and meets the frequency requirements simultaneously. In practice, even if the code exists, without the guidance of suitable dispersion plots, the designer will spend a great deal of time running the code to in an iterative and potentially extremely time-consuming manner to try to find the best compromise of size, material and guide type.

The guiding characteristics of dielectric guides have not been presented before comprehensively covering many possible combinations of sizes, materials and guide types in a simple format where the reader can immediately see their geometric and material. Perhaps this is because there are a theoretically infinite number of possible combinations.

5.1.5 Objectives

A good understanding and, in particular, the ability to quantify these dependencies are essential prerequisites to finding a working compromise suited to a new dielectric guide based design. This is of course the case for the dielectric rectangular guide based leaky wave antenna (LWA) which is the primary focus of this thesis. Therefore, in the current section, the objectives are to first find and quantify the dependencies, and then to find a better way to present them such that the final product simplifies and shortens the design cycle for finding a suitable dielectric guide configuration for any application, including the LWA.

5.2 Computing the guide characterisitcs

5.2.1 Overview

The derivation of the guiding characteristics of a dielectric waveguide is significantly more difficult to solve than for the metal waveguide because the fields spread outside the guide walls (dielectric/air boundaries). As pointed out earlier, available analytical and numerical methods are extremely rigorous and time-consuming to develop so an approximate method is chosen. The method by Marcatili [28] is a well-known approximate method that is specific to rectangular dielectric waveguides, which are of interest in this antenna work. The method is easier to program than rigorous methods, but still challenging.

Although the Marcatili method, introduced in chapter 2, was conceived to aid integrated optical circuit development, it is equally suited to electrical frequency problems, including the microwave region and the full region in between. The method has been shown to provide enough accuracy to serve as the basis for real designs with dielectric waveguides, as proven by a great many journal paper authors since its publication in the Bell Labs Journal in 1969 [13, 25, 26, 30, 31]. Here, it will be used to carry out this parametric study to investigate various unperturbed rectangular dielectric waveguide structures and determine their geometric and material dependencies.

5.2.2 Computing the frequency range

In a real design with a dielectric waveguide, one of the most important characteristics required is the possible working frequency range. Of course, this information is essential to ensure that the required operating frequency or range and a particular guide or guide design are compatible. This range is dependent on the polarisation of the wave and the waveguide modes under consideration: therefore these conditions are defined first.

5.2.2.1 *Choice of polarization*

In this work, the Y-polarised case, where the primary component of the electric field is orientated along the Y-axis (see Figure 3.2), will be primarily considered. It is assumed that the guided wave is travelling along the length of the guide, along the positive Z axis. Only the fundamental bound waveguide mode is considered because this is known to excite the modes that radiate [27, 30]. This latter selection was made because the primary interest is in the application of guides for antenna designs. The guide will be excited by a standard metal waveguide or horn, which inherently supports both X and Y polarisations (by rotation).

5.2.2.2 *Dielectric waveguide modes*

The nomenclature first used by Marcatili and now in common use will be used to identify the individual waveguide modes. Only the first radiated mode E_{11}^{y} is of interest, which has one field maximum approximately centred along both the X and Y axis, which are aligned with the guide width *a* and height *b* respectively. Additional 'higher' modes can be excited by frequencies above the required frequency range. For antennas, these higher modes, E_{21}, E_{12}, E_{22} and so on, lead to the generation of additional (undesired) beams. It is desirable therefore to stay within the frequency range for which only the E_{11} mode is excited and the point up to where the first higher mode begins is commonly referred to as the *single-mode frequency range*. The frequencies at which the higher modes start to propagate are termed 'cutoff' frequencies.

5.2.2.3 *Enforcing a low frequency cutoff*

Although sometimes suggested otherwise in literature, there is no defined fundamental E_{11} cutoff because the fundamental mode never cuts off in the same definite manner that the higher modes do. However, as the frequency is lowered well below the first higher mode cutoff for any given dielectric guide, the field spreads outwards such that the field intensity within the guide walls is lowered and the field outside is increasingly susceptible to

disturbance by surrounding objects. Under such circumstances, the wave is often referred to loosely as being 'poorly guided'. Further, at some indefinable point, the fields become evanescent [17]. Since such conditions represent uncertainty and poor guiding performance, to avoid these conditions an E_{11} cutoff frequency will effectively be defined and enforced and then simply referred to as the *low frequency* throughout this work.

5.2.2.4 Useful single-mode range

The Marcatili formulas do not give the correct results under the poorly guided conditions described above [31]. Instead, they produce a definite cutoff for the E_{11} mode. This is considered an advantage here and will be chosen as a suitable point for the definition of the minimum useful low frequency of the available dielectric waveguide frequency range.

It is common knowledge that the limit of the single mode range is the onset of the next higher mode (E_{21} in most cases). It can be determined directly from the Marcatili dispersion plots for the types of guide under study here, that his method finds the first higher mode approximately 5% high, even for large differences between the guide material permittivity and the permittivity of the surrounding material [28]. Therefore, it was decided to eliminate this error and define the high frequency of the single mode range as 95% of the Marcatili value. The low and high frequency points defined here will be assigned the labels *fL* and *fH* from here on and the region in between will be described as the useful single-mode frequency range *fL* to *fH* for each guide sample.

5.2.2.5 Reducing the problem space

Focusing on practical and specific sizes and materials, and types of guiding structure allows this potentially infinite problem to be reduced to a finite one that can be solved using the latest personal computer equipment.

5.2.2.6 Practical constraints

At lower frequencies e.g. < 1GHz the guides begin to get physically very bulky. In practice, some materials might be difficult to manufacture beyond a certain size, are not obtainable in large sizes, or simply might be expensive, too heavy or both. At high millimetre frequencies, there will come a point where small sizes are difficult to cut with acceptable tolerance, too fragile, or have too many imperfections for example. In this study, it was decided to work in terms of the dielectric constant or electrical permittivity rather than with specific materials and do not set sizes limits. It will certainly be the case that not all values of permittivity will be furnished by the actual materials available, but no particular values will be excluded on that basis. It is feasible that an artificial material can be made with any value of intermediate permittivity, although the cost of doing this might be prohibitive in practice.

The assumption is made, as with all work cited in this thesis, that the guide material is lossless. This has proven to be a safe assumption provided that the conductivity loss, usually referred to as the tan-delta loss (electrical version) is negligible i.e. less than about 0.001. It is assumed that if this condition is met by the material that the results presented in this work are valid for that material.

5.2.2.7 Types of guiding structure

In waveguide terms, the guide size is defined as the dimensions of the cross section. Usually, the width of a rectangular guide section is given the label *a* and the height is labelled *b*. This same nomenclature will be used throughout this thesis. Of course, there are a theoretically infinite number of possible cross sections as pointed out already.

A number of different types of dielectric guide structures that are amenable to the mathematical treatment that will be used here, and also suited as the basis of a LWA design, will be considered. It should be noted that the final choice of structure might in some cases be

motivated by the mounting environment, as opposed to its guiding characteristics. For example, if the guide is part of an antenna that has to be flush-mounted onto an aircraft body, it might be necessary to choose the 'inset guide' structure which has only one open guide wall. This choice will prevent the guiding characteristics from being modified when fixed in place onto the metallic body. After completion, one would use the code to obtain guiding or radiating characteristics for each sample input and, eventually, converge on a size, material and structure that best meets the requirements.

5.2.2.8 Materials

A suitable material, in this case, is one that has low enough losses at the design frequency to meet the performance requirements, while meeting all other requirements; for example, mechanical and environmental requirements. A practical range of dielectric constants with integer number values from 2 to 16 were chosen for this study. This range covers most practical non-magnetic materials that can be used up to millimetre wavelengths, as can be seen from Table 5.1 [32].

Table 5.1 Low-loss materials suitable for use at millimetre wavelengths.

	Loss factor	***εr***
Teflon (PTFE)	0.0006	2.08
PTFE-glass	0.0009	2.17
Polyethylene	0.0006	2.26
Quartz-Teflon	0.0006	2.47
Polystyrene	0.0012	2.54
Fused quartz	0.00025	3.78
Boron Nitride	0.0003	4.40
Sapphire	0.0001	9.0
Alumina	0.0001	9.8
Silicon	0.00001	11.8
Gallium arsenide	0.001	13.2
Magnesium titanate	0.0002	16.1

The same dimensions as standard metal waveguides (internal dimensions used with width *a* and height *b*) were used in this initial stages of the study, for reasons that will be explained later in Section 5.2.4.3.

5.2.3 *Programming task*

The transcendental Marcatili formula were programmed in Matlab to solve for the frequency range and longitudinal propagation constant *kz*, for this range of dielectric constants (integer values) and the range of guide cross section sizes. Deriving this information for a basic open dielectric guide with no metal sidewalls was used as the starting point for the study. The Matlab program listing is given in Appendix A. Aspects of its implementation will be discussed in the following sections.

From a practical point of view, in order to find *kz*, one must first choose a guide size, structure and material and then find the working frequency range. Or perhaps more likely, find a suitable guide size, material and structure combination (compromise) to suit a required operating frequency or range. The Marcatili method may be used to select a suitable dielectric waveguide by repeatedly solving the transcendental equations to find the fundamental mode E_{11} and first higher mode E_{21} cutoffs for increasingly smaller guide sizes and for one or more materials i.e. practical values of dielectric constant (permittivity) εr, until a suitable compromise is found. The useful working frequency range for any guide falls between these cutoff frequencies, and each occurs when *kz* for the respective mode is equal to the free space propagation constant k_0 where $k_0 = 2\pi f_0 / c$. These points can be found for each sample size and material by repeatedly solving for *kz* at an increasingly higher operating frequency until $kz \leq k_0$. The associated pseudo code, also provided in Appendix A, will help to reinforce an understanding of this procedure.

5.2.4 *Computed frequency range*

The resulting curves for *fL* and *fH* versus εr are shown in Figure 5.1 for three different size guides first of all. These curves are made up from the results of the computed high and low frequency cutoff's for each guide size and integer value εr combination. For example, Figure 5.1 contains sixty-six points, consisting of 3 types x 2 points x 11 values of dielectric constant. Each sample converges to a minimum of 10 MHz accuracy, which at least 1%

accuracy for the largest guide sizes (the larger of which will likely only ever be used in metal form to deliver signals to antennas on warships), and typically better than 0.1% for the smaller, more practical sizes that might be used for antennas running at frequencies of say ≥ 5 GHz.

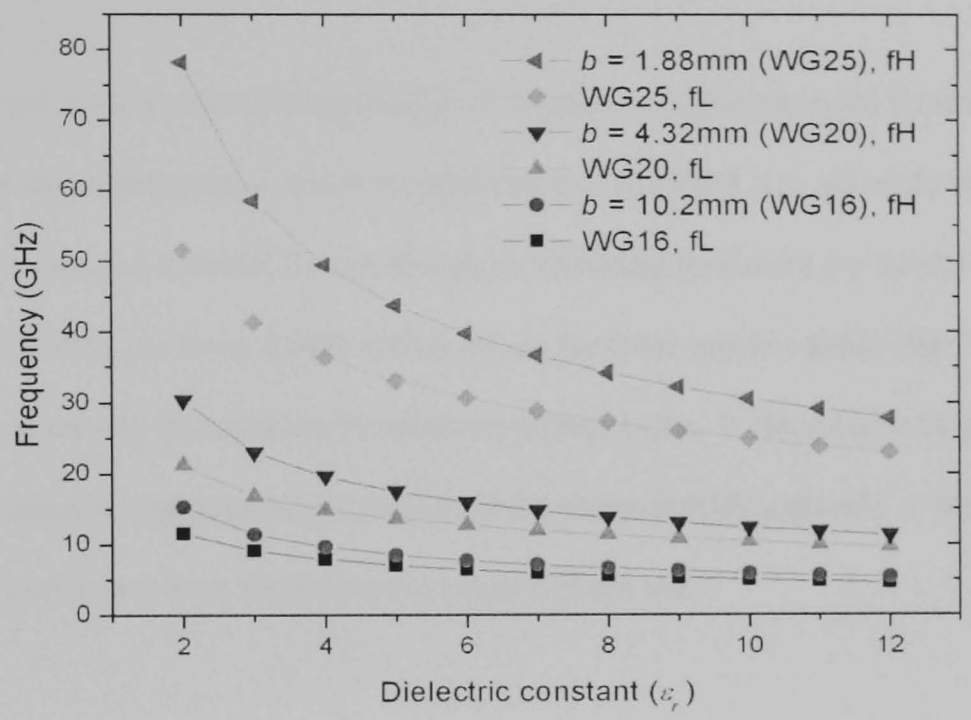

Figure 5.1 Shows the approximate working frequency range (*fL* to *fH*) for a selection of rectangular dielectric open waveguides over a range of dielectric constants. The guide dimensions are the same as the internal dimensions of standard (WG) metal waveguides.

5.2.4.1 Frequency range results analysis

The material dependencies for each guide size can be seen from this plot. The main points to note are that:

- As the reader might understand intuitively, the frequencies at which any of these guides will operate increases as the waveguide cross section size is reduced (from WG16 to WG20 to WG25 size), and vice-versa.
- For any given size, the frequencies at which it will operate decreases with an increase in εr, and vice-versa.

- The guides are more broadband at the lower half of the εr scale, and vice-versa. This decrease appears to be extremely rapid below $\varepsilon r = 2$ (not shown) and at the other end of this εr scale it sees diminishing returns, demonstrating an overall exponential decay.
- The smaller guides are much more sensitive to a change in εr, and vice-versa.

This type of information cannot be gained from inspection of the Marcatili formulas, or by inspection of any other method, and it is important to understand it to aid in the selection of a suitable guide size and material for use at a given operating frequency (or band). Of course, the plot is of limited use since it only shows results for three specific guide sizes; however, the intention is only to demonstrate the material dependencies. It should also be pointed out that in some cases it might not be possible to find a material with a specific εr that will work with low enough losses over the frequency range defined here.

5.2.4.2 Frequency range coverage

One of the most interesting features of the dielectric waveguide is the ability to scale the guide down in size by choosing a higher value εr material, while supporting the same frequency. This feature can also be seen directly from Figure 5.1. For example, the guide made of material with $\varepsilon r = 2$ that operates up to approximately 30 GHz can be replaced by a smaller guide of εr greater than about 6, depending on the actual operating frequency or range required.

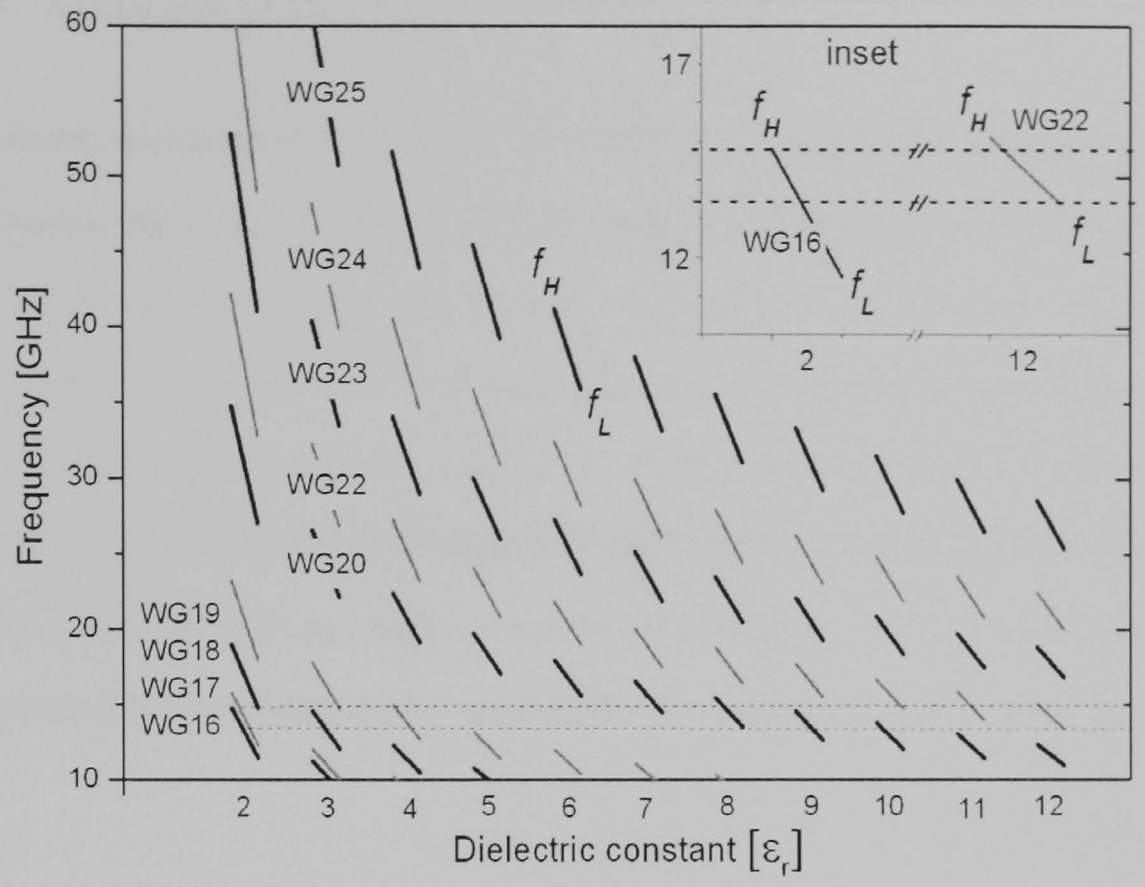

Figure 5.2 Useful frequency range for a selection of different size open dielectric waveguides. Diagram Inset shows the frequency overlap for two samples.

5.2.4.3 Utilizing standard sizes for dielectric guides

Because the standard set of metal waveguides cover the full frequency spectrum from a few gigahertz to a few hundred gigahertz, and also cover a full spectrum of physical sizes, it is interesting to look at how the same size dielectric guides would fill this same spectrum.

A good way of visualising this is with the new type of plot shown in Figure 5.2. Here, the computed useful single-mode frequency range has been plotted for integer values of εr, and for a contiguous range of these guide sizes. Each size is labelled according to the label used by its corresponding metal guide size. From this plot, it is easy to see the material dependency on the frequency ranges for all these sizes. In particular, it is possible to immediately see how the many different alternatives, for any given frequency or range.

5.2.4.4 *Special case for low values of permittivity ~ 2*

The dielectric waveguide of $\varepsilon r \sim 2$ presents an interesting case; the useful frequency range is approximately the same as the equivalent sized standard metal waveguide. It is therefore easy to find its approximate frequency range from the metal guide standard specification chart. However, this is not the case as εr is increased; the same size dielectric waveguide can be seen to work at progressively lower frequencies and a progressively narrower useful guide bandwidth. A smaller dielectric waveguide size may be used to compensate for the frequency reduction yielded by choosing a higher εr material. In these cases, there is no lookup table and the determination of its characteristics requires the type of analysis carried out in this chapter.

5.2.4.5 *Example: using alternative guide sizes*

Figure 5.2 (inset) shows how a WG16 size Teflon dielectric waveguide of $\varepsilon r = 2.08$ that covers almost the whole X-band frequency range of its metal counterpart can be substituted by a much smaller WG22 size guide made from Silicon of $\varepsilon r = 12$. This would only cover the upper half of the X-band, but its cross-section would be 285% smaller. An interesting side note however is that, in this example, the guide wavelength also increases by 15%. This implies that the guide length might also have to be increased by 15% if it has to be the same number of wavelengths long.

5.2.4.6 *Justification for using standard sizes*

Although it is known that there is no such thing as a *standard* dielectric waveguide, for reasons which should now be apparent, the adoption of the exact same sizes as the standard metal waveguides (with aspect ratios in the order of 2:1), can be justified in a number of ways:

- Having a standard enables a level of commonality and re-use;
- Because the single-mode frequency range for $\varepsilon r \sim 2$ is approximately the same as that of the same size metal waveguide, it can be excited by simply inserting one end directly into a metal coaxial to waveguide adaptor or a horn antenna [26, 27, 33-36].
- These sizes are well known, cover a very large range of physical sizes, and conveniently, already have standardized labels e.g. WG25;
- The sizes, in conjunction with a range of materials (and material dielectric constants), can cover the same frequency spectrum as the complete set of standard metal waveguides.

5.2.5 Slight variations in guide aspect ratio

An important feature of standard metal guides, that is not immediately obvious, is the fact that some of the internal cross-sectional dimensions have an aspect ratio (width a x height b) that deviates slightly from the majority 2:1 aspect. It was found that the guides in any standard metal guide specification table actually share six different aspect ratios from 2:1 to 2.47:1, with the large majority at exactly 2:1.

Further analysis determined that these slight deviations in the aspect ratio were the main cause of the slight offsets between the curves seen in Figure 5.3. Figure 5.4 highlights the impact of the precise aspect ratio by displaying only the curves for the guide sizes that have an exactly 2:1 aspect. Here, the small deviations along the smooth line are due to very minor differences in convergence for each solved guide size.

5.2.6 Useful guide bandwidth

The plots presented so far have demonstrated that the dielectric guide working frequency range, which is between the low frequency curves and high frequency curves, reduces as εr is increased and vice-versa, as shown in Figure 5.3. For a large selection of open dielectric

guides that again use the same internal cross section dimensions as standard metal waveguides.

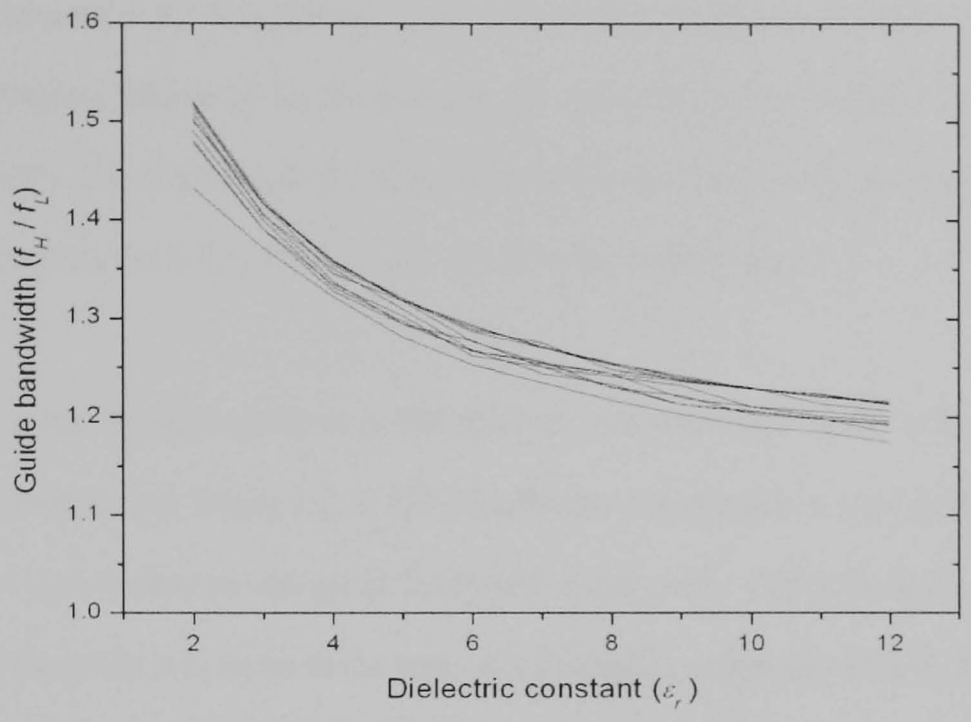

Figure 5.3 Shows the guide bandwidth (*fH* / *fL*) for a large selection of dielectric open waveguide sizes over a range of dielectric constants. In all cases, the guide dimensions are the same as the internal dimensions of standard WG metal waveguides i.e. with aspect ratio between 2:1 and 2.47:1.

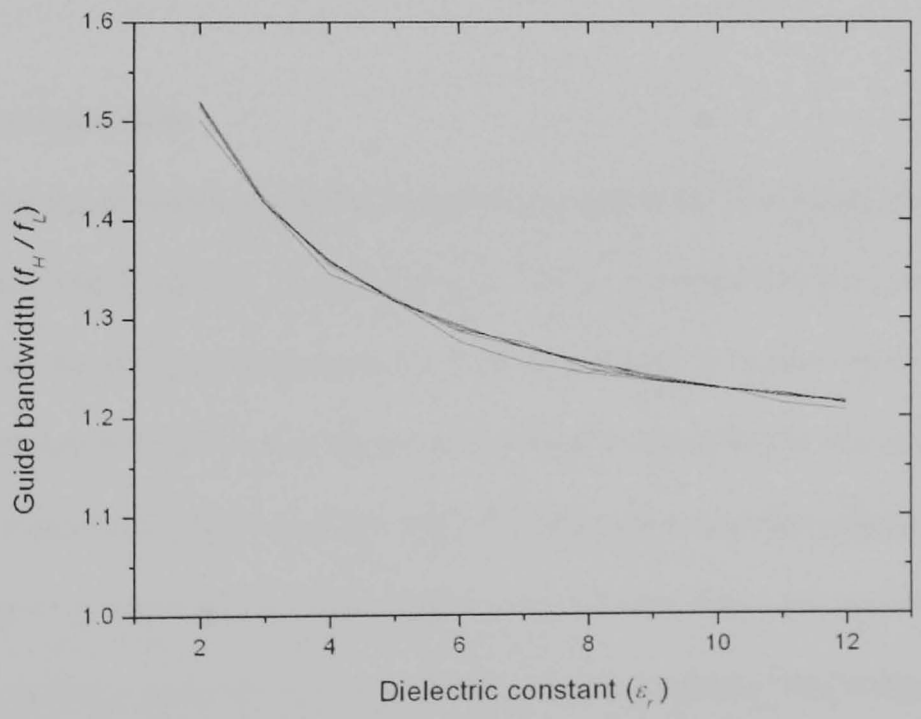

Figure 5.4 Shows the guide bandwidth (*fH* / *fL*) for a large selection of dielectric open waveguide sizes with exactly 2:1 aspect ratio, over a range of dielectric constants. In all cases, the guide dimensions are the same as the internal dimensions of standard WG metal waveguides.

This range will be referred to in this work as the *useful guide bandwidth* and is quantified in the usual way as fH / fL. So, from Figure 5.1, it can be seen for example that for a dielectric guide material with $\varepsilon r \approx 2$ (e.g. Teflon, $\varepsilon r \approx 2.08$), the high frequency is approximately 50% higher than the low frequency. In this example, the guide is of course referred to as having 50% bandwidth. The other standard bandwidth notation used in practice normalises with respect to unity to give 1.5 / 1 in this case, as expressed in the Figure 5.3.

It can be seen that for high values of εr like Silicon (~12), the bandwidth is only a little over 20% higher than the low frequency, or 20% bandwidth. For a guide or antenna designed to operate at a single frequency, the guide bandwidth might not be very relevant in practice. However, if the guide is to serve as the basis of a frequency scanning antenna, the bandwidth capabilities, and the choice of material, is likely to be very important.

Also of interest in this plot is the offset between the curves representing the different guide sizes used in this part of the study. This will be discussed in the following section.

5.2.7 Antenna bandwidth

While discussing the dielectric guide bandwidth, it is worthwhile discussing the bandwidth of a dielectric guide based antenna; these two characteristics are related in this case. In theory, the bandwidth of the antenna could equal the guide bandwidth. However, the elevation angle of the radiated beam from this type of antenna is primarily controlled by the exact operating frequency, the material dielectric constant and the distance between perturbations [1.32]. It can only radiate over a limited part of the upper two quadrants above the perturbed guide surface. Under certain conditions then, it is possible that the antenna bandwidth could be slightly less than the guide bandwidth. What is really meant by this is that it might not be possible to utilise the entire guide bandwidth in practice. This situation will be described later in this chapter.

5.2.8 Computing the propagation constant

The next thing to be studied is how the longitudinal propagation constant *kz* is affected by the same geometric and material values. This parameter, which is related to the important guide wavelength λg of the dielectric guide by (5-1), can be found by computing Marcatili`s transcendental equations for a given waveguide size, dielectric constant and operating frequency, as introduced in Chapter-3.

$$k_z = \frac{2\pi}{\lambda g} \qquad (5\text{-}1)$$

The same range of dielectric constants and waveguide sizes that were used in the frequency range analysis above were used in the present analysis. The choice of operating frequencies for calculating the propagation constants were chosen to be the limits found for the useful single-mode frequency range just determined for each size and εr combination because this will then highlight the limits of *kz*, and so the limits of the guide wavelengths. From the antenna point of view, this will set the limits of frequency scanning range, as will be seen in an example shortly.

5.2.8.1 Propagation constant results analysis

Matlab was again programmed to compute the results, which were then plotted for analysis. A selection of the resulting curves is shown in Figure 5.5. The following points can be observed from these:

- The rate of change of phase in the longitudinal Z-direction (*kz*) is higher for smaller waveguide cross-sections, and vice-versa;
- The guided wavelength (λg), which is the distance over which the phase undergoes one complete 360° or 2π radians cycle is therefore correspondingly shorter;
- *kz* decreases with an increase in εr, and vice-versa;

- For each size, the slopes of *kz* at each end of the frequency range are approximately the same;
- Each pair of slopes is approximately equidistant apart over the whole *εr* range;
- The range of *kz* is highest for the smallest guide size, and vice-versa.

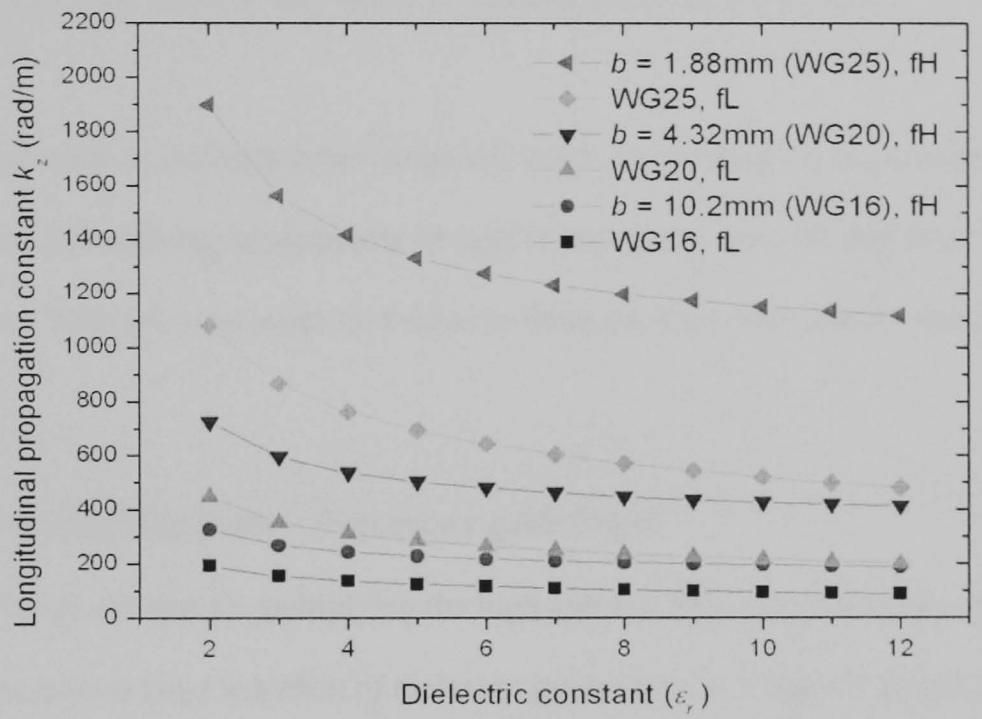

Figure 5.5 Shows the approximate longitudinal propagation constant range (*kzfL* to *kzfH*) for single mode over a range of dielectric constants.

One of the most interesting observations to be made here is that, although the frequency and *kz* plots look very similar in terms of the pairs of slopes for each size guide, while the frequency pairs converge at high *εr*, the *kz* pairs remain approximately equidistant over the full *εr* range. This demonstrates that the change of *kz* between the low and high frequencies (kz_{fL} to kz_{fH}) is essentially constant and independent of *εr*.

5.3 *Normalising the guide characteristics*

5.3.1 Review

The plots presented thus far are useful from the point of view of visualising the size and material dependencies on the propagation constant, frequency range and bandwidth etc., but they are of limited use because they are only valid for the three sizes shown.

Attempts were made to normalise the computed data to try to bring the associated curves closer together and deriving a reasonable (rough, if necessary) curve fit that fits a larger range of guide sizes. Different normalization factors to those used by other authors were applied to these curves.

5.3.2 New normalizing factors: frequency x guide height

This author has found that by multiplying the high and low frequencies found using the Matlab program for a large selection of dielectric guide sizes by the guide height essentially produces two guide height independent curves. One of these curves represents the normalised upper frequency *fH* and one representing the normalised lower frequency *fL* of the useful frequency range, as shown in Figure 5.6.

5.3.2.1 Resulting normalized frequency curves

It is evident from inspection of this plot that although many of the curves representing the different guide sizes do overlap, others deviate slightly above or below the two main curves as was seen in Figure 5.3 earlier. Further analysis showed that these curves are again aspect ratio dependent (most of the curves overlap because the majority of the standard metal guide sizes use a 2:1 internal aspect ratio for their rectangular cross sections).

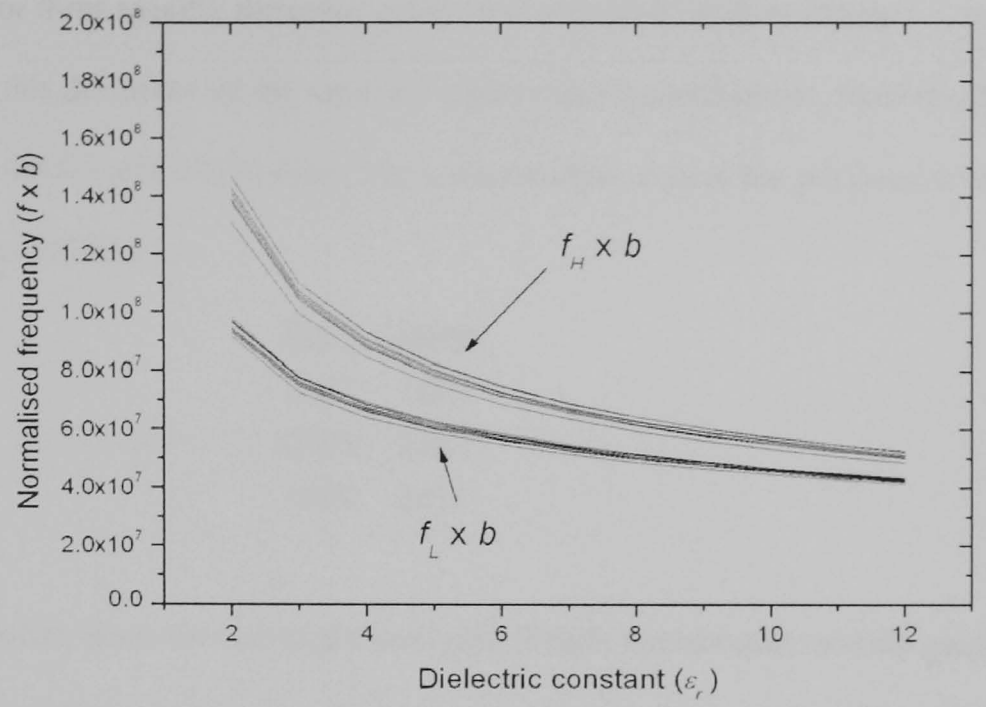

Figure 5.6 Shows the normalised frequency range *(fL x b to fH x b)* for a large selection of rectangular dielectric open waveguide sizes over a range of dielectric constants. Here, the dimensions are the same as the internal dimensions of standard WG metal waveguides i.e. approx 2:1 aspect ratio.

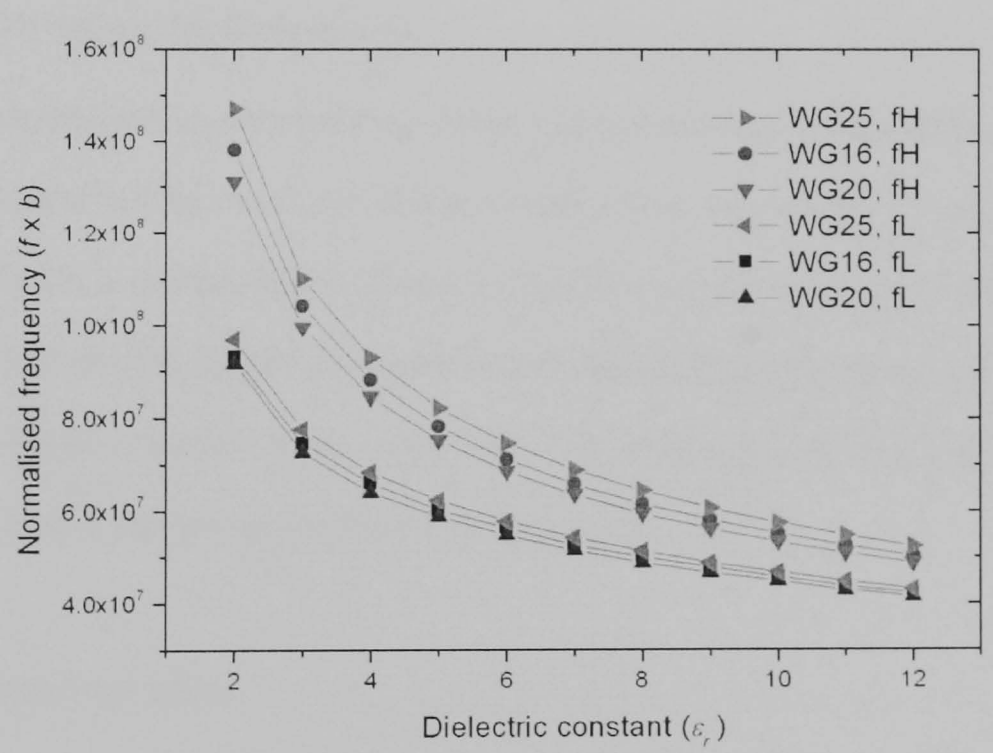

Figure 5.7 Shows the normalised frequency range *(fL x b to fH x b)* for three specific dielectric open waveguide sizes over a range of dielectric constants. Here, the effect of the slightly different guide aspect ratios can be seen. The aspect ratios are: WG16 – 2.25 to 1, WG20 – 2.47 to 1, WG25 – 2 to 1.

The curves for three specific dielectric guide sizes are also plotted in Figure 5.7, to demonstrate this deviation for the same six aspect ratios as used above. Note the change in order for the WG16 and WG20 sizes. The normalisation process has put them in order of aspect ratio as follows:

Size	Aspect
WG25	2.00:1
WG16	2.25:1
WG20	2.47:1

This makes sense, since the curves are now guide height independent, and the guide width is all that separates them. In any case, this means that provided the width of the guide is chosen to give one of these aspect ratios, then the cutoff frequencies for *any* height open dielectric waveguide can be found from this plot.

5.3.2.2 Alternative normalizing factors

The same normalisation process was also applied to the guide width a instead of height b but the results showed that the curves deviated even further from those for the 2:1 aspect. In this normalised figure, is still possible to see most of the important dependencies demonstrated by its unnormalised version. Similar attempts were also made to make the curves aspect ratio independent but these attempts were unsuccessful. The resulting curves from some of these other normalisation attempts are included in Appendix B.

5.3.3 Other considerations

It is also worth pointing out that mechanical robustness and cost may influence the decision on which material to use in practice. For example, although it might be possible to make the 1.88 mm Silicon guide, it might be that there are doubts about its robustness in the application, or the that larger Teflon option is more desirable because it is cheaper to manufacture.

5.3.4 *Fixing the aspect ratio*

To the best of the present author's knowledge, this is the first time that the useful frequency range versus εr has been presented in this height independent format that has immediate practical use. It will be useful for quickly determining the range for any material with any value, including non-integer values, of εr in the range 2 to 12. This has only been possible, because the aspect ratio has been fixed.

Of course, only a limited number of aspect ratios have been used so far but the following sections of this chapter will derive and present guide-height independent guide characteristics for additional aspects and additional guide types beyond the simple open type.

5.3.5 *Examples: using the normalized frequency plots*

A set of examples will serve as an illustration: **Find the single mode frequency range for a WG25 size dielectric guide made from Silicon with a permittivity of $\varepsilon r = 12$.** From Figure 5.8, $fL*b \sim 4.2 \times 10^7$ and $fH*b \sim 5.3 \times 10^7$. Since the guide height for a WG25 is known to be 1.88 mm, the range is computed as 22.34 to 28.19 GHz. Comparison with Figure 5.1 shows that these values are approximately correct. **What if Teflon is used instead with $\varepsilon r = 2.5$?** From Figure 5.8, $fL*b \sim 8.8 \times 10^7$ and $fH*b \sim 1.3 \times 10^8$. The new range is therefore 46.8 to 69.15 GHz. **How can the Teflon guide be resized to work at 25 GHz?** Take the same $fH*b$ value and solve for b by dividing by 25 GHz. This gives $b = 5.2$ mm. Equally, this could have been solved for b with $fL = 25$ GHz to get $b = 3.52$ mm but, as will be seen later, it is better to operate close to the guide's high frequency because the wave is better guided than at its low frequency.

To further highlight the flexibility of the new method, the example could have been presented the other way round by finding the frequency range for a Teflon guide and then demonstrating that the guide dimensions can be reduced by using Silicon instead. Alternatively, suitable

combinations of εr and guide height could have been found for a required high or low frequency, and then the most suitable option could be chosen or optimized. The following section attempts to normalise the propagation constant data and curves in a similar manner to that carried out for the frequencies.

5.3.6 Traditional propagation constant normalizing factor

Traditionally, the longitudinal propagation constant kz, which quantifies the rate of change of phase of the travelling wave propagating through the material, is normalised with respect to the free-space propagation constant k_0.

Since kz is frequency dependent and the valid frequency range is proportional to the waveguide cross section and the dielectric constant, then it is valid to normalise the values of kz with respect to the free-space propagation constant in this study (i.e. kz / k_0) still allows the goal of demonstrating and quantifying the material and size dependencies of the dielectric guides to be met.

5.3.6.1 Computed results

Naturally, since the low frequency fL is taken in this work as the point at which $kz = k_0$, then $kz / k_0 = 1$ for all guide sizes and εr. The normalised kz values found at the high frequency fH are therefore greater than one. These were found for each sample directly using a slight modification to the Matlab program to perform the division by k_0 and store the new results. The results are plotted in Figure 5.8 for the same selection of guide sizes used earlier. The curves are again guide height independent, even though this time the height is not part of the normalisation factor. However, these values are calculated purely at the frequency range limits, and they are guide height dependent. In other words, the guide-height dependence is built in to the particular value of kz / k_0.

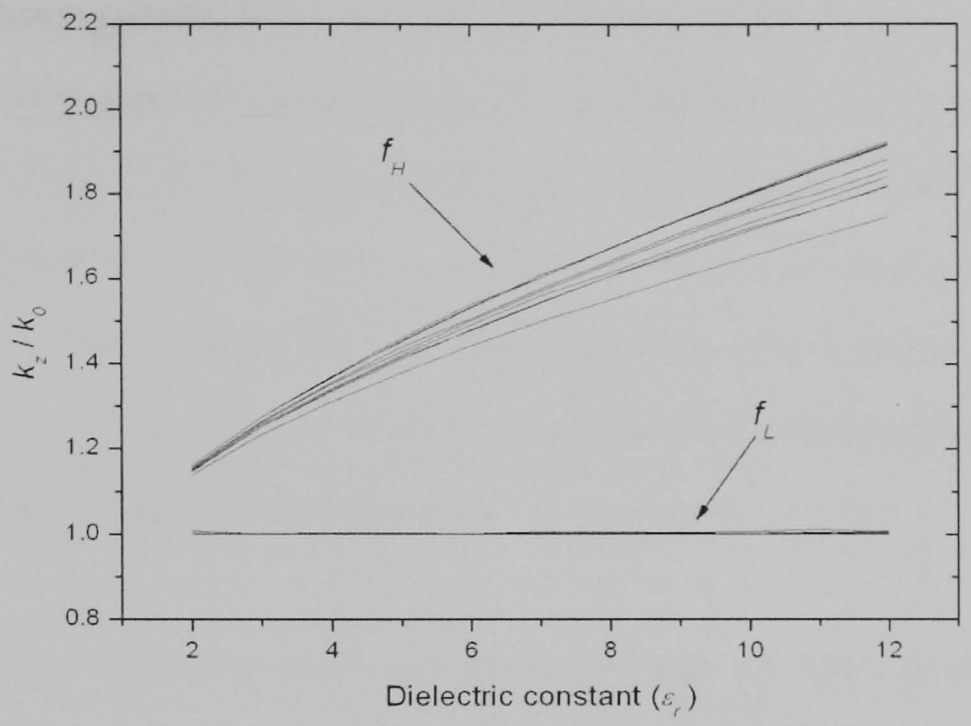

Figure 5.8 Shows the normalised longitudinal propagation constant for a large selection of dielectric guides at the two ends of the useful single mode frequency range (*fL* and *fH*) and over a range of dielectric constants. Here, the guide dimensions are the same as the internal dimensions of standard WG metal waveguides.

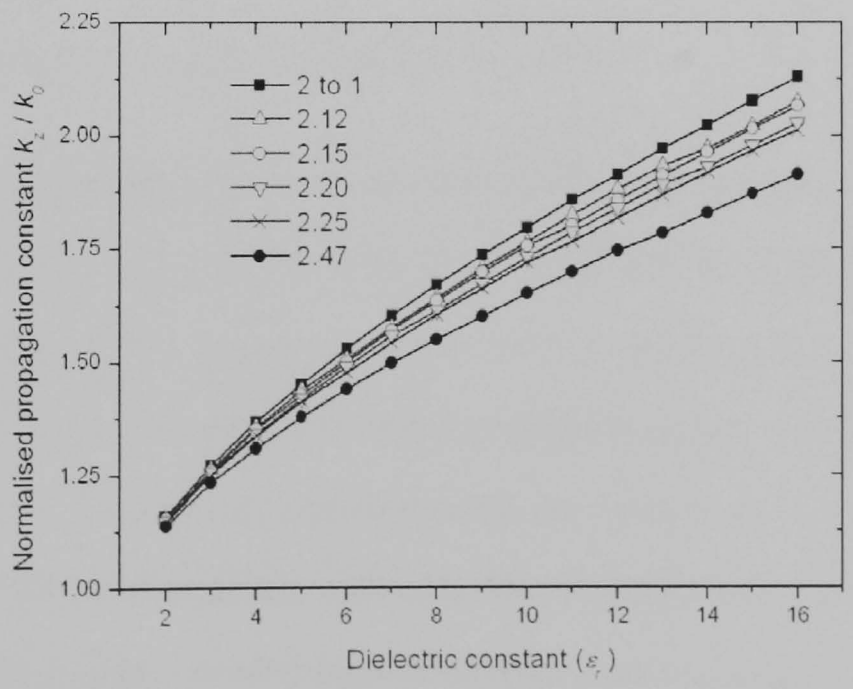

Figure 5.9 Shows the normalised longitudinal propagation constant at the high frequency of single mode operation (*fH*), for a selection of dielectric guides using all six standard aspect ratios.

Immediately then, from this plot, it is possible to get a reasonable estimate for the value of kz for any dielectric guide height, any intermediate frequency, and any εr. for a guide with one of these standard aspects (additional aspects will be covered in the next section). The operating frequency that defines the value of k_0 takes the high frequency value fH of the useful single mode range for the upper curves and fL for those at unity. The values of fL and fH were defined and plotted earlier, and must be found first in order to find the value of kz / k_0. The normalisation by k_0 as used here is not new, but its material dependence has not been presented in this practical manner before.

Not surprisingly, when the aspect ratios are precisely the same e.g. 2.00:1, the curves representing the different guide heights overlap perfectly, and those aspects that differ have a slightly different slope in the same way as seen before. The affect of the slight difference in aspect ratios is clearer from Figure 5.9. Note from the curves the large jump from 2.25:1 to 2.47:1 and the associated space between these two curves. It appears from this plot that the change in kz / k_0 versus aspect is approximately linear over this small range of aspect ratios.

5.3.7 New propagation constant normalizing factor: kz x b

An alternative to the traditional normalisation factor for kz is developed next. Even though it is unconventional, the propagation constant will be normalised by the guide height in the same manner as done for the frequency range i.e. the f*b plots. This is done with a view to enabling the designer to find a value of kz based on the guide height rather than the working frequency i.e. k*b. By finding such a quantity for the same guide samples, the designer can use it to trade off the guide height and value of kz. The chosen guide height can then be used to find the frequency range. The advantages of the resulting plot of Figure 5.10 and the associated procedure will be demonstrated in an example later in this chapter. For example, it could be that the designer has already found the frequency range and height compromise but then decides to fine tune the value of kz then subsequently found, perhaps to fix the guided

wavelength at the nearest integer value. It is interesting that the Y-axis turns out to have units of Radians, but this fact offers no real benefits except for its use as a relative quantity.

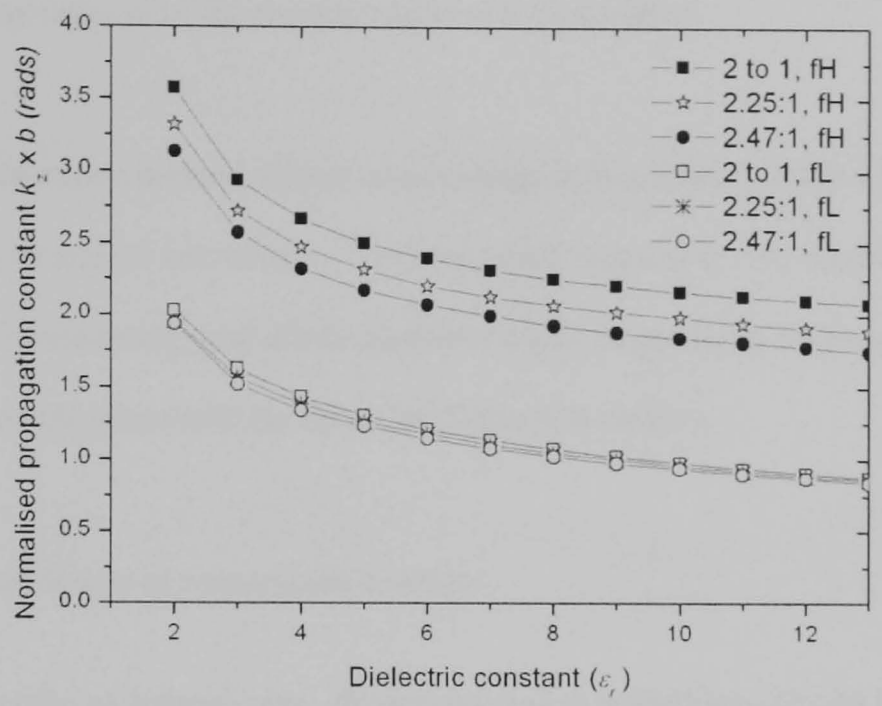

Figure 5.10 Shows the new alternative normalised longitudinal propagation constant at the limits of the single mode frequency range for a selection of dielectric guide sizes with slightly different aspect ratios.

5.3.8 Examples: using the normalized propagation constant plots

Find the range of *kz* for a WG25 size guide made of Silicon with $\varepsilon r = 12$. The WG25 size is known to have an aspect ratio of 2:1. In the last example the frequency range was found to be approximately 22.34 to 28.19 GHz which corresponds to a range of k_0 from 468.21 to 590.82. From Figure 5.9, $kz / k_0 = 1.83$ for the high frequency (always unity for the low frequency), giving an associated range of *kz* of 468 to 1081 rads/m. This corresponds to a range of guide wavelengths (λg) of 13.42 mm and 5.81 mm respectively. According to Figure 5.5, these values are quite accurate.

In the above example, it was not necessary to specify the guide dimensions. These were defined earlier and the frequency range was derived based on those dimensions. The chosen material εr is also carried forward with the associated frequency range. The only way to modify *kz* or λg if that were a requirement, would be to go back and change the εr and

dimensions, and to then recalculate based on the new frequency range (it is assumed that this will be similar, but not exactly the same). This procedure will have to be carried out iteratively many times until the required value of *kz* is achieved.

The new normalisation method affords an advantage in this respect. With this method, the guide size can be altered immediately for the required value of *kz*. The approximate range of *kz* can also be immediately read off without knowledge of operating frequency, as can the range of achievable phase shift (*kz* times the distance in metres).

5.3.9 Rate of change of propagation constant

Given that the ratio of antenna array element spacing to guided wavelength ($\lambda g = 2\pi / kz$) sets the beam angle, of interest for frequency steered antenna designs is the amount of change in *kz* that occurs over the useful guide frequency range. This will be measured over 1 GHz to give a relative measure of this change for each value of material dielectric constant εr.

This is again inherently guide height independent and the resulting curves produced by the suitably modified Matlab program are plotted in Figure 5.11 for the same standard sizes and aspect ratios as used so far. It is simply calculated, for each value of εr, by dividing the difference between the upper and lower values of *kz* by the difference between the upper and lower values of the frequency range in GHz i.e.

$$kz / GHz = \frac{kz_{fH} - kz_{fL}}{(fH - fL).10^{-9}} \qquad (5\text{-}2)$$

From inspection of this plot, it is clear that this change versus εr occurs linearly, and increases with increased εr. It can immediately be deduced that choosing a guide material with a high value of εr will steer the beam significantly faster than for a low value of εr, for any change in

frequency. It will be seen next how, due to this linearity, this quantity can be used to accurately find values of *kz* at intermediate frequencies between *fL* and *fH*, or even outside of this range. Of course, this value can also be expressed in Hertz, rather than GigaHertz by eliminating the 10^{-9} from expression (5-2).

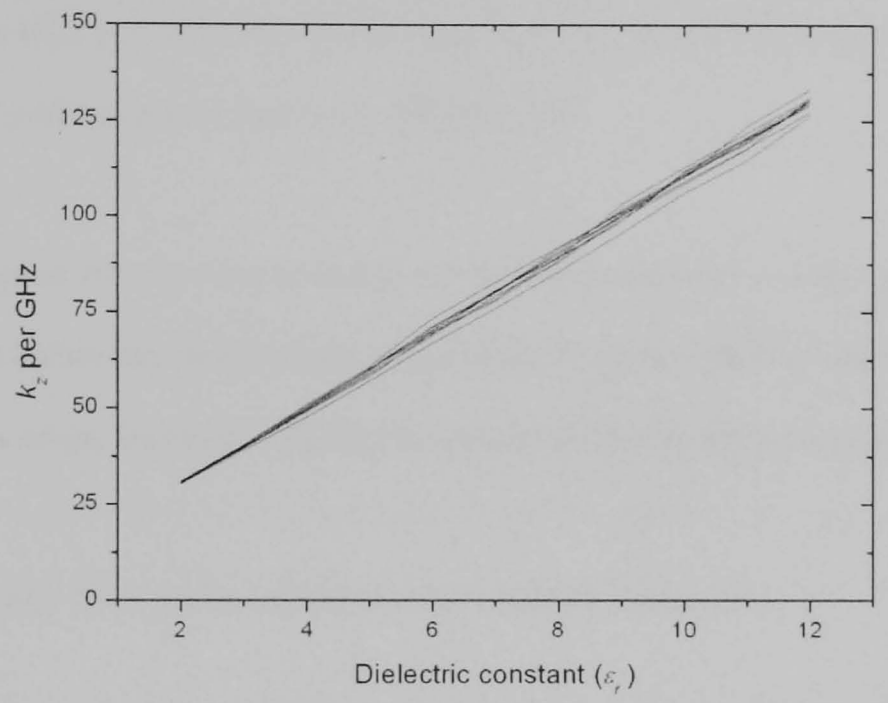

Figure 5.11 Shows rate of change of *kz* per 1GHz of bandwidth versus the material dielectric constant.

5.3.10 Linearity of propagation constant over frequency range

Now that a method has been programmed to find the frequency range and the propagation constant at the limits of that range, it is necessary to add to this by quantifying how the propagation constant changes between these limits. The existing Matlab implementation was extended to find and store discrete values of *kz* between the computed useful single-mode frequency limits using the Marcatili transcendental formulas again for the same large sample of guide sizes. The results demonstrated a perfectly linear change in *kz* between the frequency limits, thus making it possible to find intermediate values of *kz* by projection. A selection of these results are plotted in Figure 5.12 to complement the existing frequency and *kz* plots (same guide sizes) shown earlier in this chapter. A simple expression will now be derived to find intermediate values of *kz* using the limits of *kz* (kzfL and kzfH) at the associated frequency limits (*fL* and *fH*):

$$kz_o = kz_{fL} + (f_o - f_L).\Delta kz \qquad (5\text{-}3)$$

where f_o is the operating frequency at which the value kz_o must be determined, and Δkz is the rate of change of *kz* per Hertz for a given value of εr between the frequency limits imposed by the particular guide geometry and εr i.e. *kz*/GHz x 10^{-9}.

While the original intention was to find *kz* for operating frequencies in the useful frequency range defined earlier, the formula does not preclude its use for finding values for frequencies outside of this range. However, it is not known how far this linearity extends.

5.3.11 Example: Propagation constant at intermediate frequencies

Following on from the above examples: **find the value of *kz* and its associated value of λg for an intermediate frequency of 27 GHz.** Using (5-2) gives a value of *kz*/GHz = 104.79 and using (5-3) gives kz_o = 956.3 rads/m, equivalent to λg = 6.57 mm.

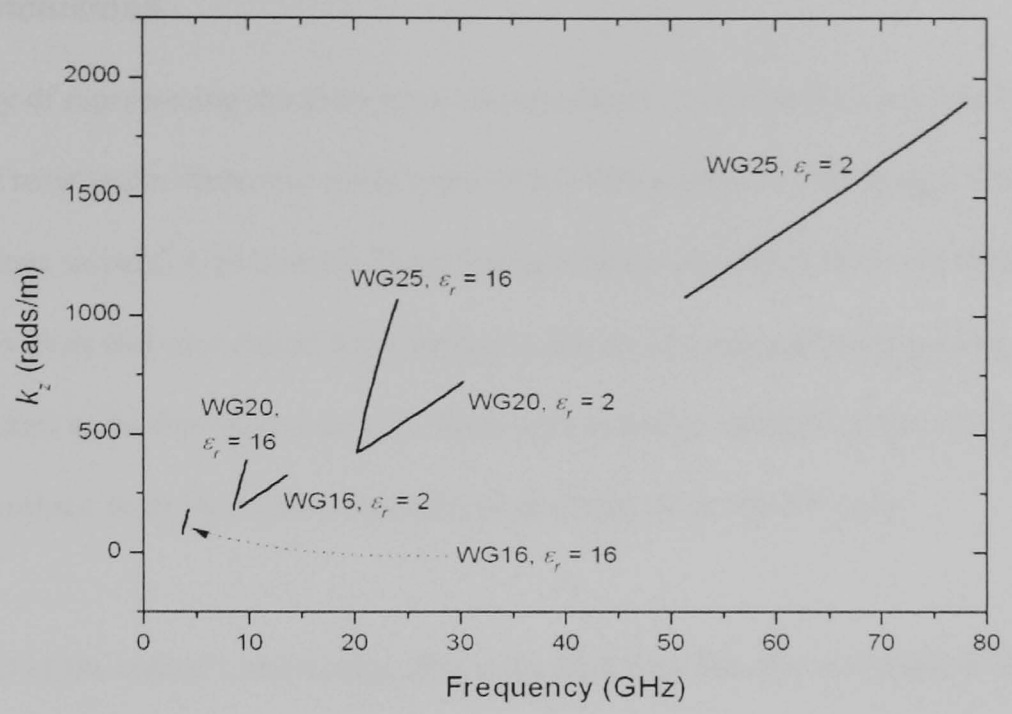

Figure 5.12 Demonstrates the linear change with frequency of the longitudinal propagation constant *kz* for a selection of dielectric guides over the calculated frequency range for single mode operation (*fL* and *fH*).

5.4 Conclusions

A new way of representing the dispersion characteristics for the fundamental bound mode of a number of rectangular dielectric guide types of any size and for a wide range of fixed guide cross sections (aspect) is presented. These characteristics are presented in the form of new normalized plots and new closed form formulas that enable the important guiding characteristics to be determined quickly from a guide design (analysis case) or a guide design to be determined from the required guiding characteristics (synthesis case).

To the best of the author's knowledge, this is the first time that this information has been presented in this simple to use and intuitive manner, where the material dependency can be seen directly. This also appears to be the first time that a formula has been produced to derive the frequency range of all of these dielectric guides directly. This new information represents a significant improvement in the speed and ease of selecting a dielectric guide configuration for any given application, and being able to quickly quantify and optimize its characteristics.

For frequency-scanning antennas, like the leaky wave antenna that is the main focus of this thesis, the calculated range of propagations constants can be used to determine the angles that represent the limits of beam (angle) steering, the rate at which it steers with change in frequency, and the angle and propagation constant for any intermediate frequency. This new information also, therefore, represents a significant speeding up of the process of both analysis and synthesis of the scanning characteristics of the leaky wave antenna. The new methods are demonstrated by example.

5.5 References

[1] A. Basu and T. Itoh, "Dielectric waveguide-based leaky-wave antenna at 212 GHz," *IEEE Trans. Antennas and Propagation*, vol. 46, no. 11, pp. 1665-1673, Nov. 1998.

[2] L.O. Goldstone and A.A. Oliner, "Leaky wave antennas I: rectangular waveguides," *IRE Trans. Antennas and Propagation*, vol. AP-7, pp. 307, Oct.1959.

[3] M. Ghomi, H. Baudrand and C. Cavalli, "New approach for computing radiation pattern of dielectric leaky-wave antenna," *Electronics Letters*, vol. 25, no. 5, pp. 345-346, 1989.

[4] M. Ghomi, B. Lejay, J.L. Amalric and H. Baudrand, "Radiation characteristics of uniform and nonuniform dielectric leaky-wave antennas," *IEEE Trans. Antennas and Propagation*, vol. 41, no. 9, pp. 1177-1185, Sep. 1993.

[5] M. Guglielmi and D.R. Jackson, "Broadside radiation from periodic leaky-wave antennas," *IEEE Trans. Antennas and Propagation*, vol. 41, no. 1, pp. 31-37, Jan. 1993.

[6] M. Guglielmi and G. Boccalone, "A novel theory for dielectric-inset waveguide leaky-wave antennas," *IEEE Trans. Antennas and Propagation*, vol. 39, no. 4, pp. 497-504, Apr. 1991.

[7] A. Hessel and T. Tamir, *Antenna Theory*, vol. 2, Eds. R.E. Collin and F.J. Zucker, McGraw-Hill, 1969.

[8] J. Encinar, "Mode-matching and pont-matching techniques applied to the analysis of metal-strip-loaded dielectric antennas," *IEEE Trans. Antennas and Propagation*, vol. 38, no. 9, pp. 1405-1412, Sep. 1990.

[9] M. Matsumoto, M. Tsutsumi and N. Kumagai, "Radiation characteristics of a dielectric slab waveguide periodically loaded with thick metal strips," *IEEE Trans. Microwave Theory and Techniques*, vol. MTT-35, no. 2, pp. 89-95, Feb. 1987.

[10] M. Ghomi and H. Baudrand, "Full-wave analysis of microstrip leaky-wave antenna," *Electronics Letters*, vol. 25, no. 13, pp. 870-871, Jun. 1989.

[11] W.V. McLevige, T. Itoh and R. Mittra, "New waveguide structures for millimeter-wave and optical integrated circuits," *IEEE Trans. Microwave Theory and Techniques*, vol. MTT-23, no. 10, pp. 788-794, Oct. 1975.

[12] T. Itoh and W. Menzel, "A full-wave analysis method for open microstrip structures," *IEEE Trans. Antennas and Propagation*, vol. AP-29, no. 1, pp. 63–67, Jan. 1981.

[13] T. Itoh and B. Adelseck, "Trapped image guide for millimeter-wave circuits," *IEEE Trans. Microwave Theory and Techniques*, vol. MTT-28, no. 12, pp. 1433-1436, Dec. 1980.

[14] J. Jacobsen, "Analytical, numerical, and experimental investigation of guided waves on a periodically strip-loaded dielectric slab," *IEEE Trans. Antennas and Propagation*, vol. AP-18, no. 3, pp. 379-388, May. 1970.

[15] R. Mittra and R. Kastner, "A spectral domain approach for computing the radiation characteristics of a leaky wave antenna for millimeter waves," *IEEE Trans. Antennas and Propagation*, vol. AP-29, no. 4, pp. 652–654, Jul. 1981.

[16] H.A. Kalhor, "Electromagnetic scattering by a dielectric slab loaded with a periodic array of strips over a ground plane," *IEEE Trans. Antennas and Propagation*, vol. AP-36, no. 1, pp. 147-151, Jan. 1988.

[17] J.L Gomez-Tornero, A.T Martinez, D.C. Rebenaque, M. Guglielmi and A.A. Melcon, "Design of tapered leaky-wave antennas in hybrid waveguide-planar technology for millimeter waveband applications," *IEEE Trans. Antennas and Propagation*, vol. 53, no. 8, pp. 2563-2577, Aug. 2005.

[18] T. Itoh, "Inverted strip dielectric waveguide for millimeter-wave integrated circuits," *IEEE Trans. Microwave Theory and Techniques*, vol. MTT-24, no. 11, pp. 821-827, Nov. 1976.

[19] M. Guglielmi, Z.M. Lu, J. Encinar, S.T. Peng and A.A Oliner, "Metal-strip-loaded rectangular dielectric rod leaky-wave antennas : experimental verification of new simple theory," *IEEE AP-S International Symposium*, Dallas, pp. 1922-1925, May. 1990.

[20] M. Guglielmi and A.A Oliner, "Practical theory for dielectric image guide leaky-wave antennas loaded by periodic metal strips," *Proc.17th European microwave conference*, Rome, Italy, pp. 549-554, Sep. 1987.

[21] M. Guglielmi and A.A Oliner, "Multimode network description of planar periodic metal-strip grating at a dielectric interface – Part I: Network formulations," *IEEE Trans. Microwave Theory and Techniques*, vol. MTT-37, pp. 534–541, Mar. 1989.

[22] M. Guglielmi and A.A Oliner, "Multimode network description of planar periodic metal-strip grating at a dielectric interface – Part II: Small aperture and small obstacle solutions," *IEEE Trans. Microwave Theory and Techniques*, vol. MTT-37, pp. 542–552, Mar. 1989.

[23] M. Guglielmi and A.A Oliner, "Multimode network description of planar periodic metal-strip grating at a dielectric interface – Part III: Rigorous solution," *IEEE Trans. Microwave Theory and Techniques*, vol. MTT-37, pp. 902–909, Mar. 1989.

[24] T. Rozzi and S.J. Hedges, "Rigorous analysis and network modelling of the inset dielectric guide," *IEEE Trans. Microwave Theory and Techniques*, vol. MTT-35, no. 9, pp. 823–834, Sep. 1987.

[25] T.N. Trinh, R. Mittra and R.J. Paleta, "Horn image-guide leaky-wave antenna," *IEEE Trans. Microwave Theory and Techniques*, vol. MTT-29, no. 12, pp. 1310-1314, Dec. 1981.

[26] K. L. Klohn, R. E. Horn, H. Jacobs and E. Freibergs, "Silicon waveguide frequency scanning linear array antenna," *IEEE Trans. Microwave Theory and Techniques*, vol. MTT-26, no. 10, pp. 764–773, Oct. 1978.

[27] H. Jacobs and M. M. Chrepta, "Electronic phase shifter for millimeter-wave semiconductor dielectric integrated circuits," *IEEE Trans. Microwave Theory and Techniques*, vol. MTT-22, no. 4, pp. 411–417, Apr. 1974.

[28] E. A. J. Marcatili, "Dielectric rectangular waveguide and directional coupler for integrated optics," *Bell Syst. Tech. J.*, vol. 48, no. 7, pp. 2071–2095, Sep. 1969.

[29] J. E. Goell, "A circular-harmonic computer analysis of rectangular dielectric waveguides," *Bell Syst. Tech. J.*, vol. 48, no. 7, pp. 2133–2159, Sep. 1969.

[30] R. E. Horn, H. Jacobs, E. Freibergs and K. L. Klohn, "Electronic modulated beam-steerable silicon waveguide array antenna," *IEEE Trans. Microwave Theory and Techniques*, vol. MTT-28, no. 6, pp. 647–653, Jun. 1980.

[31] H. Jacobs, G. Novick, C. M. LoCascio and M. M. Chrepta, "Measurement of guide wavelength in rectangular dielectric waveguide," *IEEE Trans. Microwave Theory and Techniques*, vol. MTT-24, no. 11, pp. 815–820, Nov. 1976.

[32] F. Schwering and A.A. Oliner, *Antenna Handbook*, Eds. Y.T. Lo and S.W. Lee, Van Nostrand Reinhold, New York, 1988.

[33] T. Teshirogi, Y. Kawahara, A. Yamamoto, Y. Sekine, N. Baba and M. Kobayashi, "High efficiency dielectric slab leaky-wave antennas," *IEICE Trans. Communications*, vol. E84-B, no. 9, pp. 2387-2394, Sep. 2001.

[34] L. Huang, J.C. Chiao and M.P. De Lisio, "An electronically switchable leaky wave antenna," *IEEE Trans. Antennas and Propagation*, vol. AP-48, no. 11, pp. 1769-1772, Nov. 2000.

[35] H. Schrank and N. Herscovici, "The shaped-beam polyrod antenna," *IEEE Antennas and Propagation Magazine*, vol. 36, no. 2, pp. 55-57, Apr. 1994.

[36] K. Solbach, "Slots in dielectric image-line as mode launchers and circuit elements," *IEEE Trans. Microwave Theory and Techniques*, vol. MTT-29, pp. 10–16, Jan. 1981.

6 CHARACTERISTICS OF ADDITIONAL GUIDE CONFIGURATIONS

6.1 Introduction

By fixing the aspect ratio, it has made it possible to express the most important guiding characteristics of a dielectric waveguide in the simple and practical manner presented in the previous chapter. The plots are intuitive to understand and will enable the designer to quickly determine what guide dimensions and material dielectric constant they will need to fulfil a particular design requirement. It might also be used for design purposes, as the method is quite accurate. Of course, the aspect ratio has been limited to a very small range around 2:1 so far, and only a single open guide type. The methods used to ascertain the guide characteristics presented so far are in theory applicable to any other aspect ratio and guide type. These methods are applied to a range of aspect ratios and other guide types in the present chapter.

6.2 Characteristics for additional guide aspect ratios

Of course there are a potentially infinite number of possible aspect ratios. The affects that this parameter has on the standard size guides, which use six slightly different aspects altogether, have already been seen and quantified in this work to some extent. However, it is not clear how much the guide characteristics will change for other much larger or much smaller dielectric guides. Further studies have therefore focused on a finite number of practical values of aspect ratio in order to understand and quantify these effects.

Again, the Marcatili method was programmed in Matlab to compute the same characteristics as before, but this time for a selection of different aspect ratios. In this case, the guide heights were made to be the same as before, and the guide widths were varied according to the required aspect. To a great extent, the program is identical to that used to compute the earlier results because only the dimensions used as program inputs have changed.

6.2.1 Suitable range of aspects

From initial experiments, it quickly became apparent that increasing the aspect ratio beyond 10:1 gave very little change therefore this was chosen as the highest aspect. The 2:1 aspect is included here for comparison and the additional values 1:1 and 5:1 were found to be good final choices. Of course, an aspect of less than one does not make practical sense because this would simply be equivalent to turning a higher aspect guide on its side. The Matlab program was used to generate results based on these four aspects, to again ascertain the guide size and material dependencies on the guiding characteristics of the open type dielectric guide. The unnormalised plots will be dispensed with from here on in now that a practical way to normalise the results has been found. Results are presented next for the useful normalised frequency range and normalised propagation constant, in the forms used earlier. These variations with respect to aspect are also demonstrated for values of εr at the two ends of the scale.

6.2.2 Computed frequency results for all aspects

The values computed for the normalised high frequency versus εr are plotted in Figure 6.1. This has also been plotted to show the curve versus aspect ratio directly in Figure 6.2 for two different materials. The advantages of one aspect over another can be seen immediately from these plots. For example, it can be seen that the values found for the 2:1 aspect are the same as found earlier. Now, it is possible to immediately see the affects caused by the selection of aspect ratio for any open guide made of any dielectric material that falls within the computed εr range. Clearly, the main effect of lowering the aspect ratio to 1:1 aspect is increased $f*b$ with respect to that of the 2:1 aspect. Conversely, f*b is decreased as the aspect is increased.

This means that an increasingly larger aspect ratio enables both lower frequency operation and smaller guide height b. Of course, either parameter can be minimised and all compromises are possible. The opposite is true for the smaller aspects.

6.2.2.1 *Flexibility of f*b quantity*

Having the quantity *f*b* enables a great deal of flexibility when it comes to guide selection for a practical application. It enables the designer to make the guide as large as possible (low aspect and low εr) when the operating frequency is so high that it might otherwise make the guide impractically small or fragile, and allows the guide size to be made as small as possible when the frequency is in the low microwave range (high aspect and high *εr*). The large guide is also less susceptible to manufacturing tolerances. The low frequency curves will be presented later. It is sufficient to say at this point that the low frequency curves have precisely the same characteristics, but at lower frequencies.

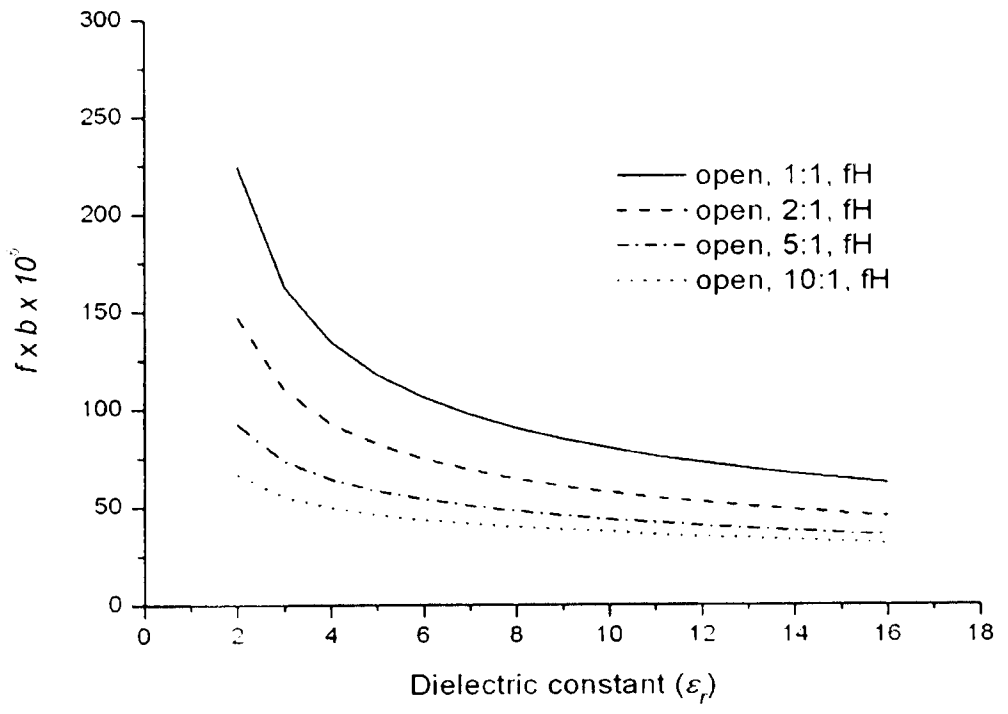

Figure 6.1 Normalised high frequency versus Er for the range of aspect ratios.

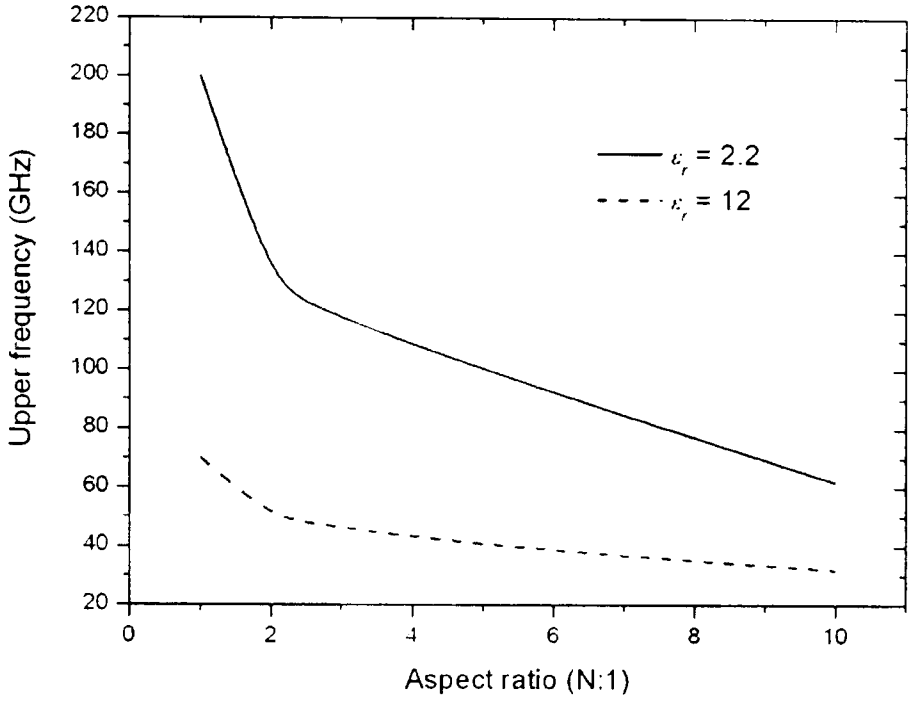

Figure 6.2 Example quantifies the useful high frequency limit (fH) versus guide aspect for hypothetical guides made from materials with high and low values of dielectric constant (permittivity εr) respectively, both with a guide height *b* of 1 mm. The waveguide width *a* varies from 1 to 10 mm.

6.2.2.2 Example: frequency and size versus aspect compromises

A substrate of εr=2.2, 1mm thick and 1mm wide (1:1 aspect) would allow operation at around 200GHz while making it 10mm wide (10:1 aspect) would allow operation at up to around 60GHz. However, if the dielectric constant material is chosen, the guide allows operation at up to 60GHz using a lower aspect ratio, here approximately 1.5:1. Therefore, it can be concluded that lower frequency operation is achieved, not only by increasing the overall cross-section and by using materials with higher permittivity (εr), but also by selecting a larger waveguide aspect ratio. Of course, the opposite also applies.

6.2.3 Computed propagation constants for all aspect ratios

The normalised propagation constant has also been computed and is presented next in both the traditional form and the new form for all the new aspects. Again, the changes are simply pointed out with respect to the new aspects, beginning with the results normalised to k_0 presented in Figure 6.3.

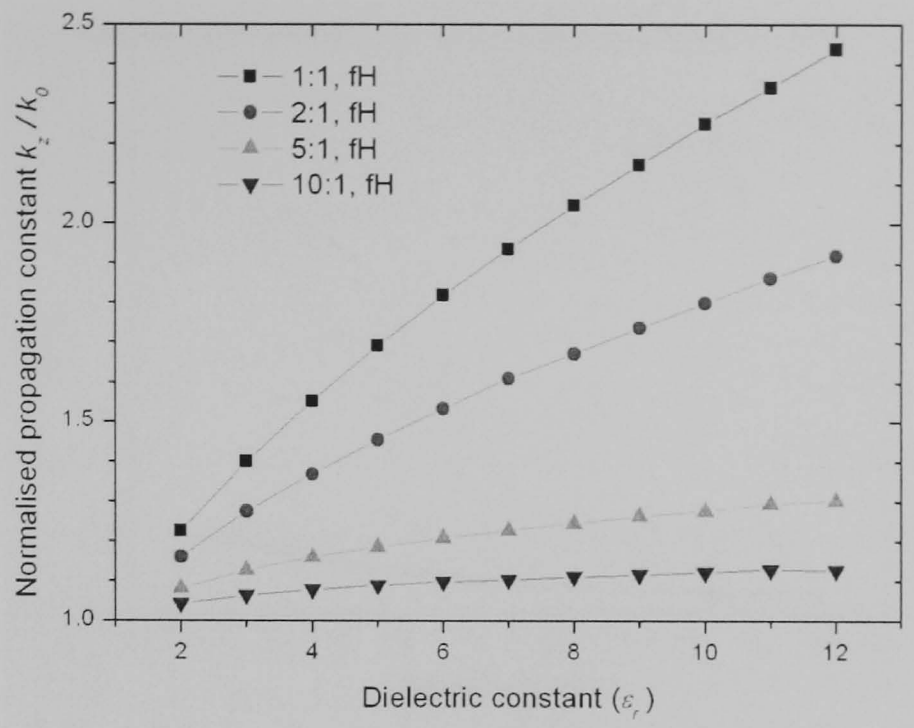

Figure 6.3 Traditional form for normalised kz for a range of εr.

6.2.3.1 Traditional normalising factor

It is clear that the lower aspect provides the greatest values of kz for any value of εr, and the value increases with εr. The highest aspects have considerably lower values, not far above unity. Finally, it can be seen that the impact of changing from 10:1 to 5:1 is much less than from 5:1 to 2:1 and 2:1 to 1:1. This effect is much clearer when the results are plotted for the two ends of the εr range versus aspect ratio, as in Figure 6.4. The material and aspect dependency on the change in phase along the guide with respect to that in free space (i.e. dispersion) can be seen immediately from this plot. The main observation is that this change is significantly more rapid at higher values or εr and aspect ratios below about 5:1. The aspect is not as important at very low values of εr.

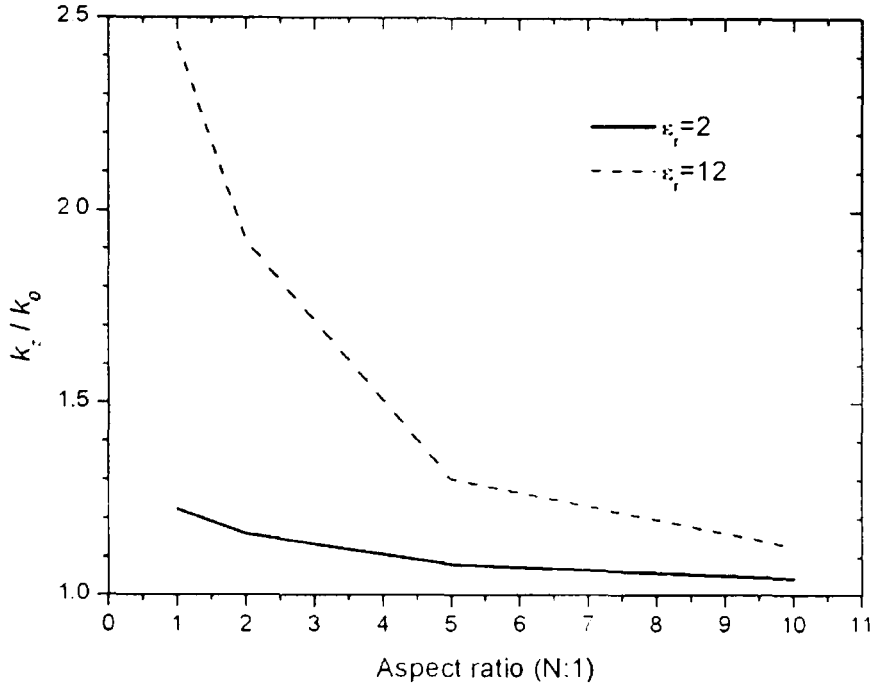

Figure 6.4 Normalised kz versus aspect ratio for two values of εr.

*6.2.3.2 New normalizing factor; kz*b*

Computed results subjected to the new normalisation in terms of guide height *b* are presented next in Figure 6.5. The resulting curves take exactly the same form as their unnormalised counterparts like that of Figure 5.5 from the previous chapter. It is easy then to deduce the behaviour with respect to changes in material directly from the *kz*b* normalised plot. Here, the shape of the curve for each aspect is almost identical i.e. large change up to about $\varepsilon r \leq 4$, and gently sloping off, almost flat, for higher εr materials. The most obvious effect caused by the differences in aspect ratio is the large vertical shift between the respective curves. Of minor interest is that the 2:1 aspect falls almost dead centre between the 1:1 and 10:1 aspects; these three curves are separated by approximately $kz*b = 2$. The slopes also move in the same direction as the *f*b* curves such that *kz*b* is highest for low εr and low aspect and lowest for high εr and high aspect. These facts might potentially be used as a memory aids or rules of thumb.

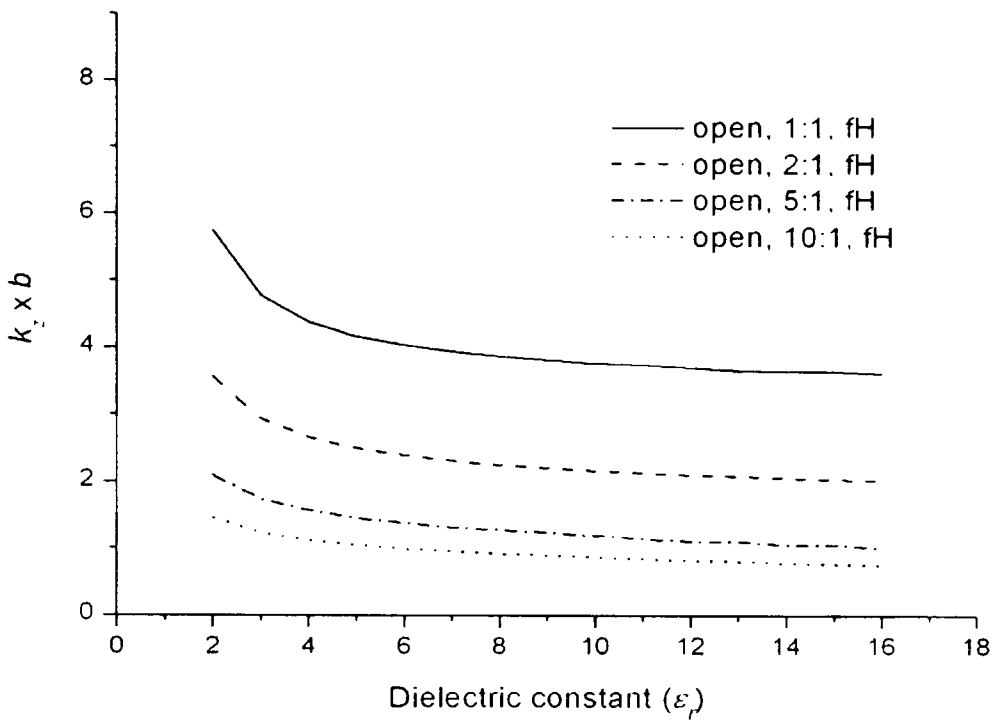

Figure 6.5 Normalised kz versus εr for the full range of aspect ratios.

*6.2.3.3 Flexibility of kz*b quantity*

This new type of normalisation factor and its associated plot has some advantages its kz/k_0 counterpart. Namely, that:

- the range of kz can be seen immediately for any size guide or material;
- The phase change can be read off immediately (in Radians);
- A compromise for kz or guide height b can be found and quickly fine-tuned to meet any practical constraints, including for a fixed phase change (the frequency range must be recalculated if the height is modified).

The kz/k_0 plot allows the relationship between kz and the frequency to be seen; both electrical characteristics. This does not help to dimension a guide for a particular requirement. On the other hand, $kz*b$ plot does. However, these two plots are considered here to be slightly complementary as opposed to complete alternatives.

6.2.4 *Other issues relating to the aspect ratios*

Before moving on to investigate the guiding characteristics of other dielectric guide types, there are a number of points to be made about the different aspect ratios used in this part of the study.

6.2.4.1 *One-to-one aspect ratio*

Marcatili points out that for the 1:1 aspect ratio guide, the modes are degenerate [1]. This means that the Y-polarised mode and the X-polarised mode are the same and have exactly the same guiding characteristics i.e. E_{11}^{x} is the same as E_{11}^{y} and $E_{12} = E_{21}$. It is assumed here that only one of these modes is excited in practice, depending on the orientation of the exciting probe. It is understood this degeneracy has no bearing on the results presented here for the E_{11}^{y} mode, except that the same results would be produced if the E_{11}^{x} mode was computed. The next higher E_{21} mode cutoff would also be joined at the same frequency by the E_{12} mode cutoff, but again this has no bearing on the validity of the results presented so far because the E_{21} mode cutoff was computed anyway.

6.2.4.2 *Five-to-one and ten-to-one aspect ratios*

Another possible motivation for using the higher 5:1 or 10:1 aspect ratios, in addition to their guiding characteristics may come from a need to use an existing substrate. Since a substrate is generally relatively thin, if it was made into a guide with a low cross section aspect, it would probably only guide at very high frequencies. In contrast, making it five or ten times wider than the substrate thickness (guide height) allows significantly lower frequency operation. Later in Section 6.5, an example will illustrate the magnitude of these advantages versus dielectric guide aspect.

6.3 Characteristics for additional dielectric guide types

6.3.1 Open and closed waveguides

A rectangular dielectric rod without any metallic walls is generally known as an 'open' guide, because its walls cannot contain the fields, and it may therefore radiate. Conversely, a metal waveguide is a 'closed' guide, because its walls are impervious to radiation, the fields being contained entirely within. Up to this point, only the completely open guide has been considered. In this section, the same analysis as considered above will be applied to additional types. Although strictly, all of the dielectric guide types considered could be classed as types of open guide, this term will be used to describe the entirely open guide, to differentiate it from the other types to be considered next.

6.3.2 Three additional types under study

Three other possible types, that are hybrids of the pure open dielectric guide and dielectric-filled metal guide that are all amenable to the same analysis using the Marcatili method, have also all been used as the basis of leaky wave antennas of the type studied in this thesis [2-5]. They are the:

1. **image guide**; a dielectric open guide with one metallic wall, usually perpendicular to the polarisation plane;
2. **inset guide**; a dielectric open guide with three metallic walls:
3. **trapped image guide**; same as an inset guide but with an air gap between the dielectric guide sidewalls and the metallic side walls.

As per the open guide work carried out so far, the main objective here is to quantify the material dependencies on the waveguiding characteristics of these other types of guide. Namely, the useful frequency range, propagation constant and other characteristics. The 2:1 aspect ratio is considered here. The other combinations of aspect and guide type will be

considered in the next section, where all of the different combinations are considered together to highlight the advantages with respect to their characteristics and other factors.

6.3.3 Modifications to computational method

A new extension to the Matlab implementation of the Marcatili method was programmed (see Appendix A) to incorporate the ability to simulate metallic walls on any of the four guide sidewalls. These new extensions to Marcatili's transcendental formulas (C.1, C.2 of Appendix-C), developed by Horn et al [3] also allow for a finite gap to be introduced between the dielectric guide sidewalls and the metal sidewalls. This latter feature will be useful for the study of the trapped image guide case. As these gaps (*h3, h5, t2, and t4*) are extended to infinity, the new formulas reduce to Marcatili's original formulas (C.3, C.4).

The new guide types were represented using a guide model with metal on all four walls, then setting the gaps to be either zero or infinity (a large value in practice) according to the guide type. For example, the inset guide was programmed with *t2*=infinity and *h3= h5= t4=0* so that the top wall is effectively uncovered and the base and two sidewalls are covered with metal. The guiding characteristics were then computed, using the new transcendental formulas, for all combinations of material permittivity (εr), aspects and guide types.

6.3.4 Additional considerations for the trapped guide type

The setup is not so simple for the trapped image guide because it introduces an additional variable: the size of the gaps *h3* and *h5* between the dielectric guide sidewalls and the associated metal sidewalls. Intuitively, it can be seen that the inset guide case is approached as the gap on both sides tends to zero. Conversely, as the gaps tend to infinity, the image guide case is approached. In the latter case, one can only guess about what gap constitutes an approximation to the image guide case. Since it would be pointless to present results for a random selection of different gaps, programming experiments were conducted instead to ascertain what gaps constitute an approximation to the two limiting cases, and the shape of the

response at a number of discrete points in between was captured. To eliminate the guide size dependency here too, the various gap sizes used in these experiments were normalised to fractions of the guide height *b*. The trapped guide has been shown to be useful for traversing bends [6]. The results will be presented in the next section but it was worth pointing out the derivation here alongside with the image and inset guides.

6.3.5 Computed frequency results for the new types

The computed results for the useful frequency range of WG25-size dielectric open, image and inset guides as generated by the Matlab program are compared in Figure 6.6. The relevant normalised plot will be shown in the next section with all other combinations of guide type and aspects. In that case, the curves are precisely the same; only the Y-axis will be different. The most important characteristics evident from the current plot are that:

- The guide type has a significant impact on the useful frequency range;
- In general, the frequency range for the new types shifts down below the open guide;
- The image guide frequency range is lowest, about one third less than the open guide;
- The inset useful guide bandwidth is widest, particularly at the low frequency;
- The open and inset useful guide bandwidth reduces significantly as the permittivity (dielectric constant, εr) is increased;
- The bandwidth reduction for the image guide is much less; The guide bandwidth is almost constant across the full range of εr;
- There is some crossover of these characteristics at around $\varepsilon r = 3.5$. It is apparent that this is due to the slopes of the curves, especially at the low εr end of the scale.

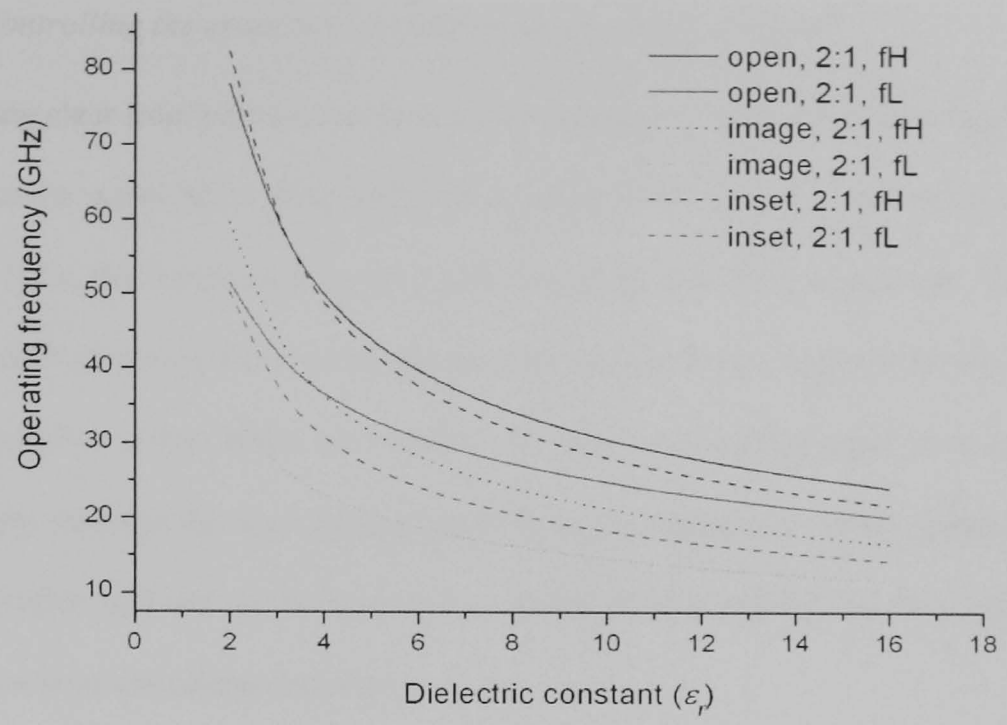

Figure 6.6 Material dependency on frequency range (fL to fH) of WG25-size rectangular open, image and inset dielectric waveguides. Uses WG25 internal dimensions (3.76mm wide x 1.88mm high).

6.3.5.1 Comparing the frequency range with standard metal guides

Now that a multidimensional approach to controlling the frequency range and guide bandwidth has been created, it is instructive to compare these (unnormalised) results with the specifications for the closed metal TE_{10} waveguide of the same size, which has a standard frequency range of 50GHz to 75GHz [7]. From Figure 6.6, it can be seen that for a dielectric constant of εr=2, both the open and inset guides offer the same or better range than the standard metal guide. However, this is not the case for the image guide; this covers only about 35GHz to 60GHz, approximately equivalent to that of the smaller standard WG24 metal waveguide. This implies that an image guide is slightly larger than a metal guide, for approximately the same frequency range (this condition requires εr ~ 2). In this example, the difference in size is about 20%.

6.3.5.2 *Controlling the cross section dimensions by choice of aspect*

It was already clear from previous sections where the open guide was studied, that size reduction can be achieved by using higher εr materials, but only at the expense of guide bandwidth. Here, the dependency on the type of guide has also been discovered. The most important result is that inset and image guide types support lower frequencies than the open guide studied prior to this. When the smallest waveguide cross section and or widest guide bandwidth are required, the inset guide appears to be the best choice. Normalisation and further discussion will wait to the next section, where all combinations of size, aspect, εr and guide types will be considered together.

6.3.6 *Computed propagation constants for the new types*

Next, the longitudinal propagation constants kz of the same guides are computed and compared in Figure 6.7. Again, the unnormalised plot is presented to quantitively highlight the interesting attributes, which are that:

- The guide type has a significant impact on the useful kz range;
- The kz range for the inset guide is extended considerably outside that of the open guide;
- The kz range for the image guide is almost the same width as the open guide, but has shifted down the scale by about 25%;
- The kz range is almost independent or insensitive to changes in $\varepsilon r > 8$;

Again, further discussion and normalisation will wait for the next section.

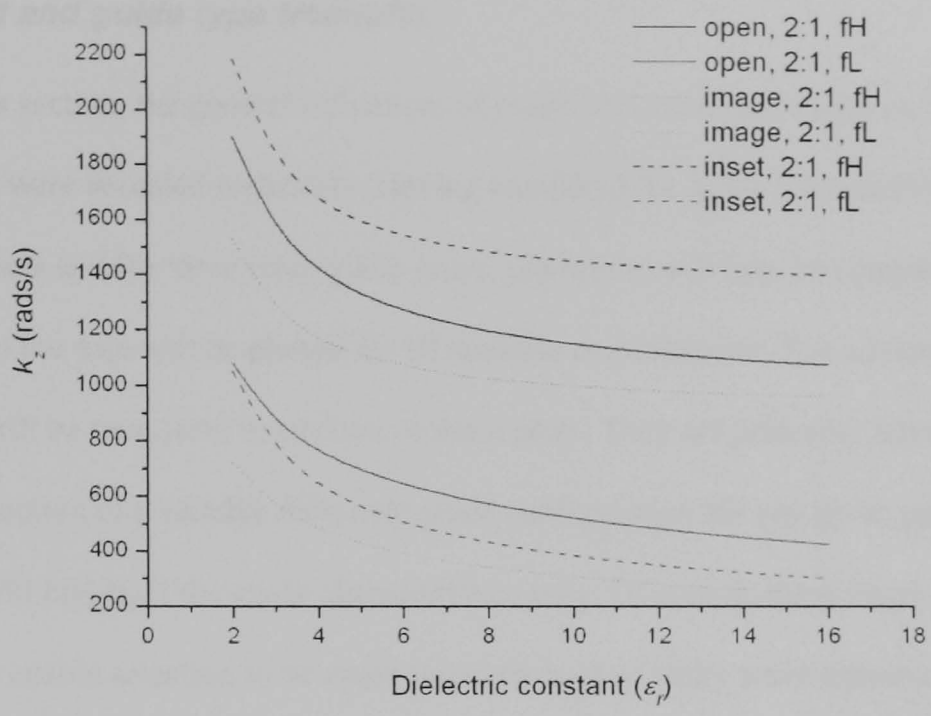

Figure 6.7 Material dependency on propagation constant of WG25-size rectangular open, image and inset dielectric waveguides. Uses WG25 internal dimensions (3.76mm wide x 1.88mm high).

6.4 *Aspect and guide type tradeoffs*

In the previous section, the general influences of aspect ratio and guide type on the guide characteristics were revealed separately. Having computed the guide characteristics for the four main aspects and the three main guide types, the results will now be compared and contrasted, and the data will be plotted for all possible combinations. The advantages of each combination will be seen from inspection of these plots. They are primarily intended to be used to aid selection of a suitable dielectric guide configuration for any given application. This section will highlight the guide characteristics only. Of course, the primary interest in this work is to enable selection to be made based on a set of leaky wave antenna requirements; that relationship between the guide and antenna will be developed in the next section. Since it is not possible to present more than a handful of curves on a single plot, the guide data will be presented in a systematic fashion using two sets of plots as follows:

- Individual aspect, all guide types
- Individual type, all guide aspects (Appendix D)

6.4.1 Comparing normalized frequency characteristics

Relative f^*b values can be seen from inspection of the plots in Figure 6.8. There are no real surprises, but they do furnish the normalised quantitive information for all types and aspects together. There are however some less obvious features as follows:

- From a frequency range perspective, there are no gaps in coverage;
- The inset 1:1 guide gives the highest f^*b values;
- The inset frequency range is shifting down faster than the other two types as the aspect increases above 1:1, so that the open guide gives the highest values for all higher aspects;
- The image and inset guides achieve the lowest f^*b values. For aspects > 5, there is little difference between these two types. In that case, physical rather than electrical considerations may determine which one to use when lowest f^*b is the requirement:

- The image guide consistently gives the lowest $f*b$ values;
- The bandwidth of all types is decreasing with increased εr as expected according to earlier results, but the 5:1 aspect gives some interesting results; the bandwidth is roughly constant for the open guide and similarly for the image guide. Investigations showed that this is not due to a mistake;
- The inset guide bandwidth decreases much less over the εr range. It is relatively constant over the second half of this εr range.

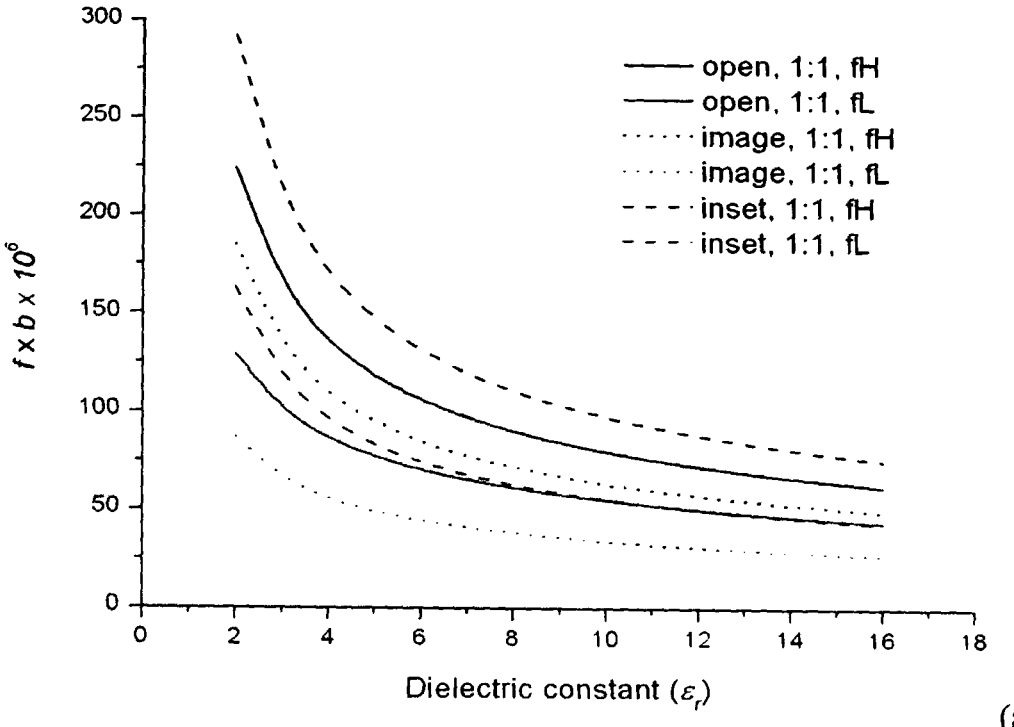

(a)

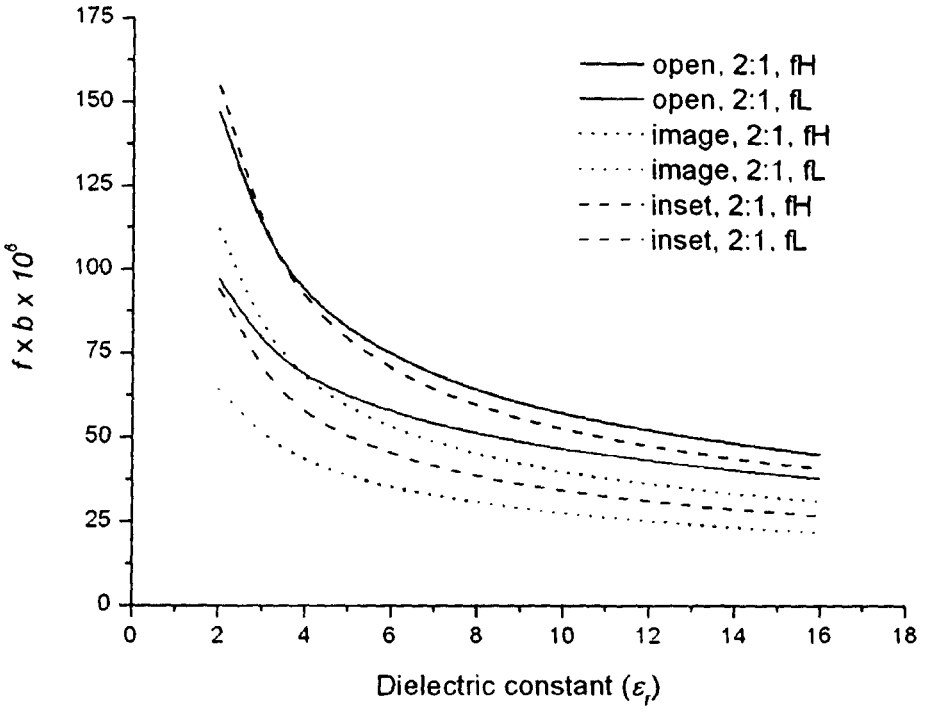

(b)

Figure 6.8 Height-independent frequency range (fL to fH) for rectangular open, image and inset dielectric waveguides with fixed aspect ratio (a) 1:1 (b) 2:1 (c) 5:1 (d) 10:1 aspect.

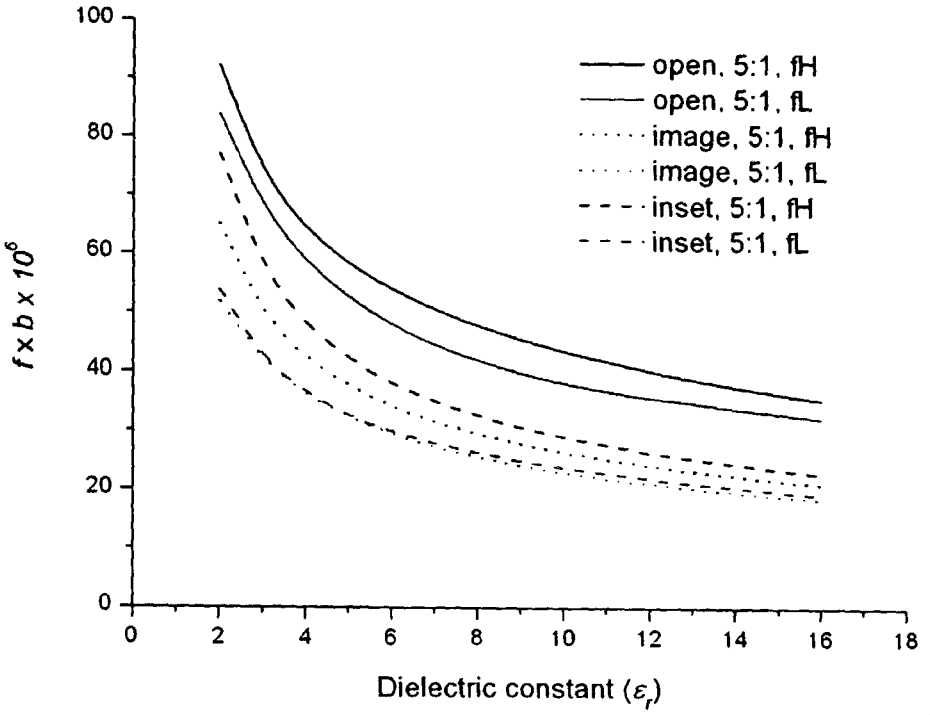

(c)

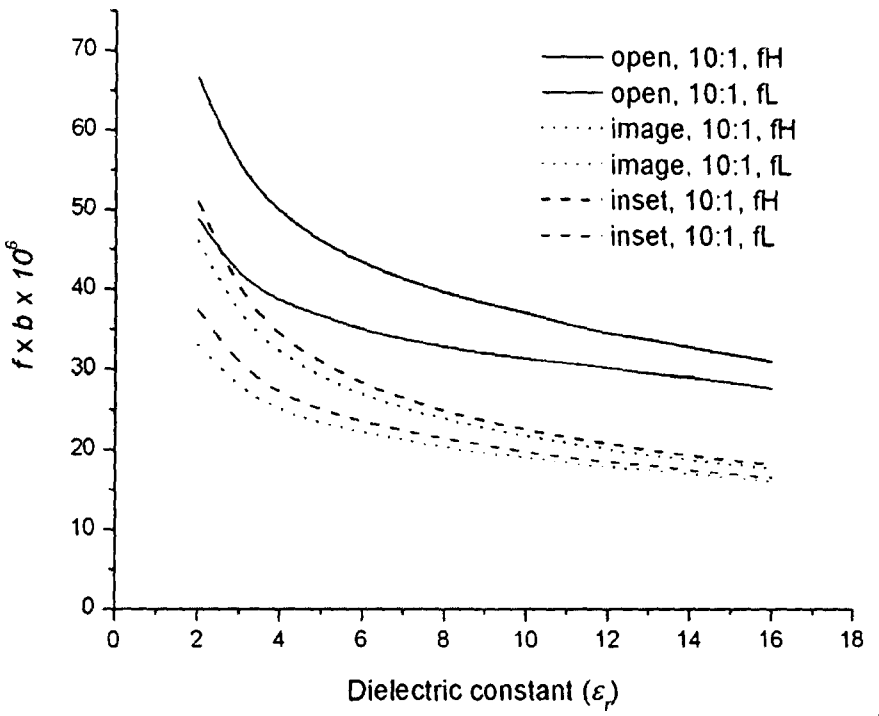

(d)

Figure 6.8 Height-independent frequency range (fL to fH) for rectangular open, image and inset dielectric waveguides with fixed aspect ratio (a) 1:1 (b) 2:1 (c) 5:1 (d) 10:1 aspect.

6.4.2 *Comparing normalized propagation constant characteristics*

Plots of the normalised propagation constant *kz*b* for have been plotted side-by-side in Figure 6.9. The following points are of most interest:

- The lowest aspect ratio provides the highest values of kz for any height *b*. Since *kz*b* is in radians, these curves also represent the range of change of phase over the frequency range. This means that the vertical axis could also be replaced or supplemented with an axis displaying *kz*b* directly in units of degrees. The rate of change of phase is also therefore highest for the lowest aspect. The opposite is true for the highest aspect.;
- As per the useful guide bandwidth, the range of propagation constants is broader for the lowest aspect. The lowest aspect therefore gives the largest phase change. The opposite is true for the highest aspect;
- In all cases except the highest aspect, the inset guide type provides by far the broadest range of propagation constants and phase change over its useful frequency range. In terms of phase, this represents a change in phase approaching two cycles;
- For the highest aspects, and at the high frequency of the useful range, the change of phase is relatively constant;
- For materials with permittivity greater than about 5 and any of the aspect and guide type combinations, the change in *kz*b* or phase is not very sensitive to a change in the material permittivity. The maximum phase change is roughly ‹ 3 degrees per integer increase in permittivity over the designed value. This means that a change of material will not have a significant effect on the design as long as the new material has a similar permittivity;
- These plots can be used to find the range of guided wavelength directly, or intermediate values can be found by extrapolation using (5-3).

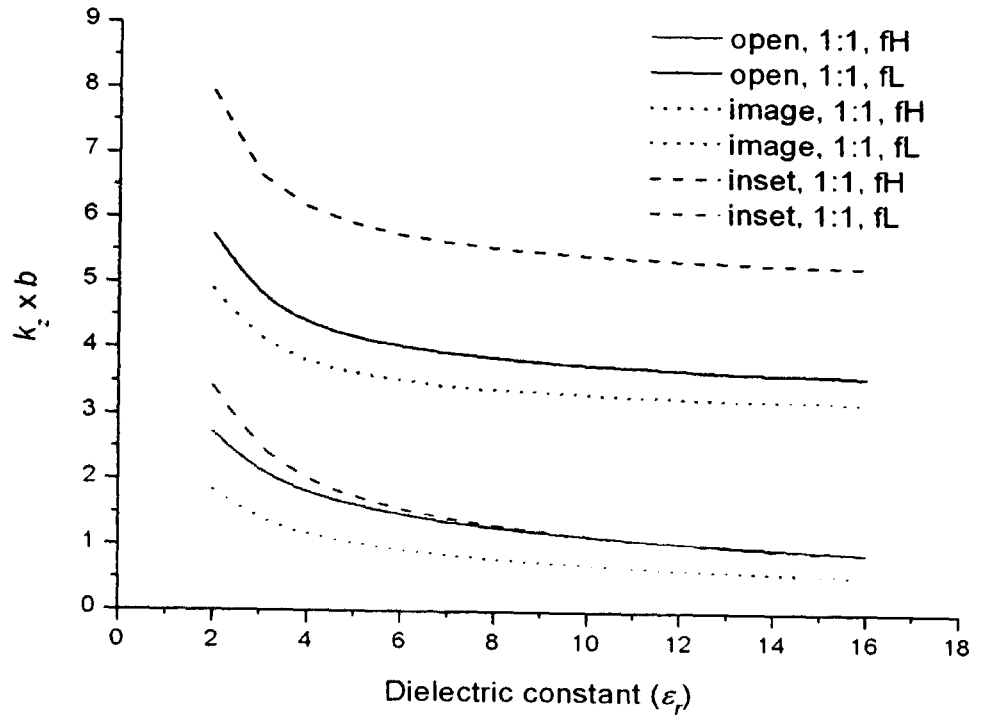

(a)

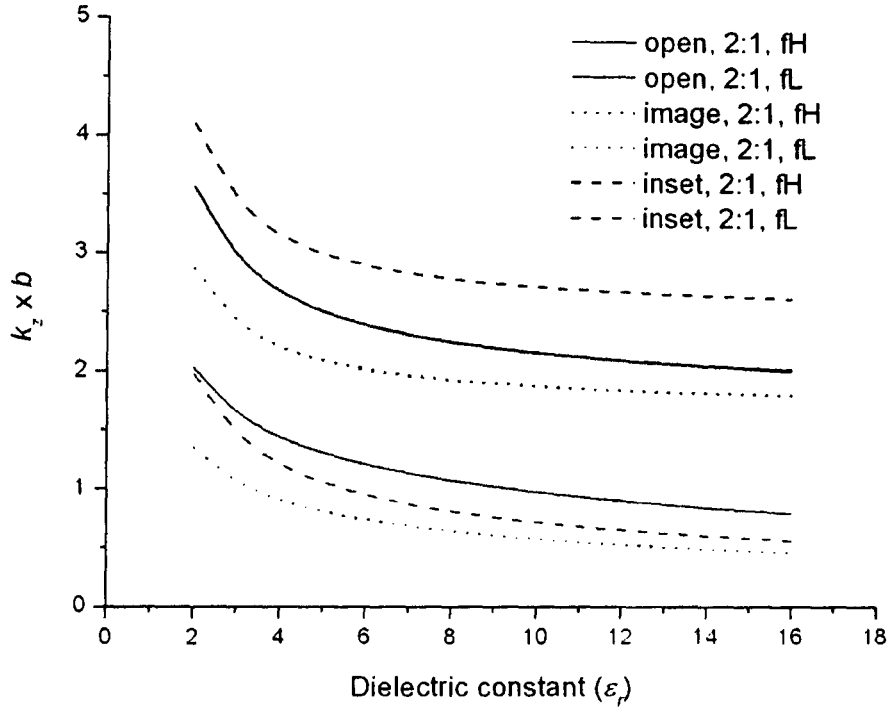

(b)

Figure 6.9 Height-independent longitudinal propagation constant kz at both ends of the frequency range (fL to fH) for rectangular open, image and inset dielectric waveguides with fixed aspect ratio (a) 1:1 (b) 2:1 (c) 5:1 (d) 10:1 aspect.

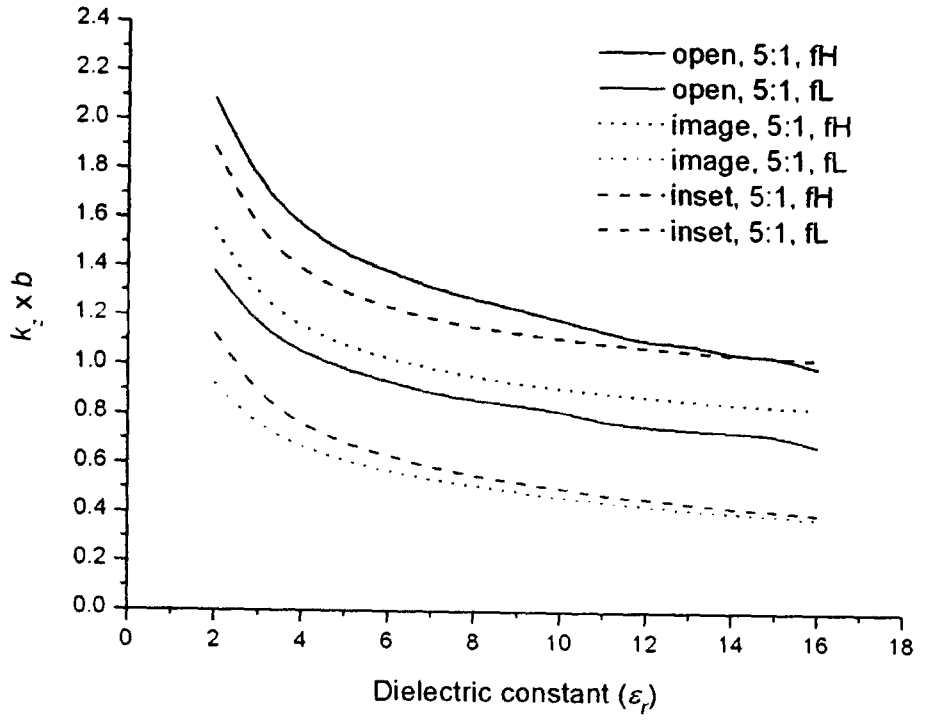

(c)

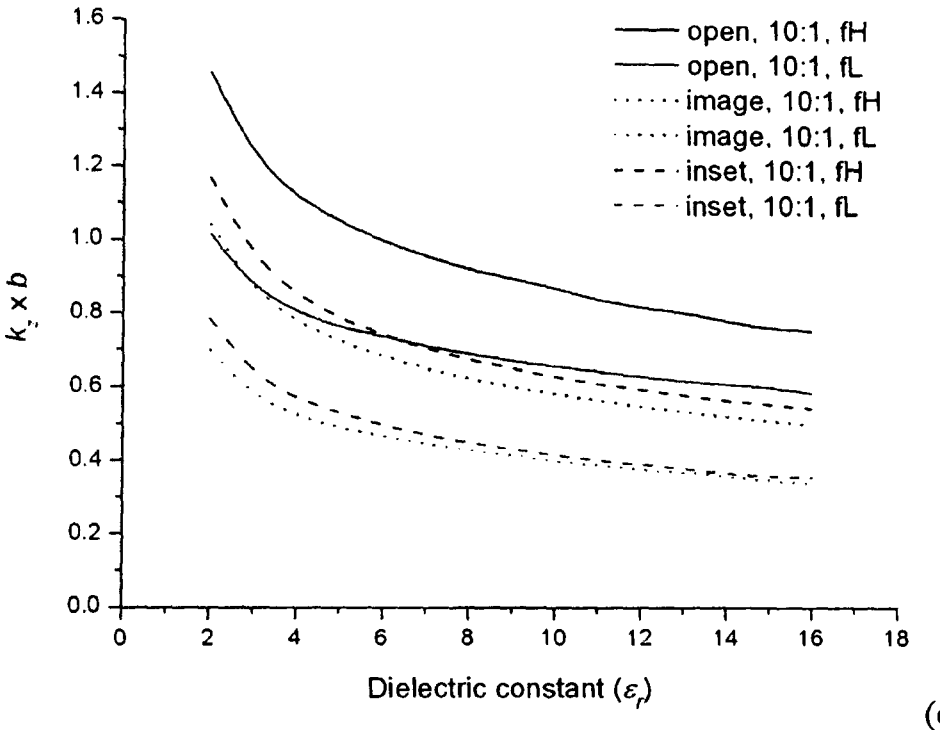

(d)

Figure 6.9 Height-independent longitudinal propagation constant kz at both ends of the frequency range (fL to fH) for rectangular open, image and inset dielectric waveguides with fixed aspect ratio (a) 1:1 (b) 2:1 (c) 5:1 (d) 10:1 aspect.

6.4.3 *Guide frequency range / bandwidth*

The useful guide frequency range from *fL* to *fH*, here called the *guide bandwidth*, varies between 10% and 110%, depending on the waveguide type, aspect ratio and dielectric constant. It is highest for the smallest aspect ratio and smallest dielectric constant and vice-versa, as depicted in Figure 6.10. This figure is simply derived from the computed high and low frequency data. As can be seen from the plot:

- These characteristics are guide height independent;
- The waveguide type has a significant effect on the bandwidth at low aspects;
- The 1:1 aspect ratio image guide provides the highest bandwidth, followed by the 1:1 inset guide and then the 2:1 inset guide;
- The guide type has a significant effect on variation in bandwidth versus εr at low aspects. Specifically, the variation is an almost zero for the 1:1 aspect inset guide and only about 10% for the 2:1 aspect. These can be approximated to a constant εr-independent 75% and 60% bandwidth respectively. The variation is approximately 30% over the range of εr for all open and image guides;
- As expected, the equivalence for the open 1:1 and image 2:1, and the open 5:1 and image 10:1 can be seen as overlapping curves.
- Two unexplained inconsistencies occur for the highest aspect ratios for the open guide type: the bandwidth for the 10:1 aspect is higher than for 5:1, and the variation with increase in εr is less than that for the image guide;
- The bandwidths are significantly narrower for the 5:1 and 10:1 aspects, but nevertheless plenty wide enough for practical uses.

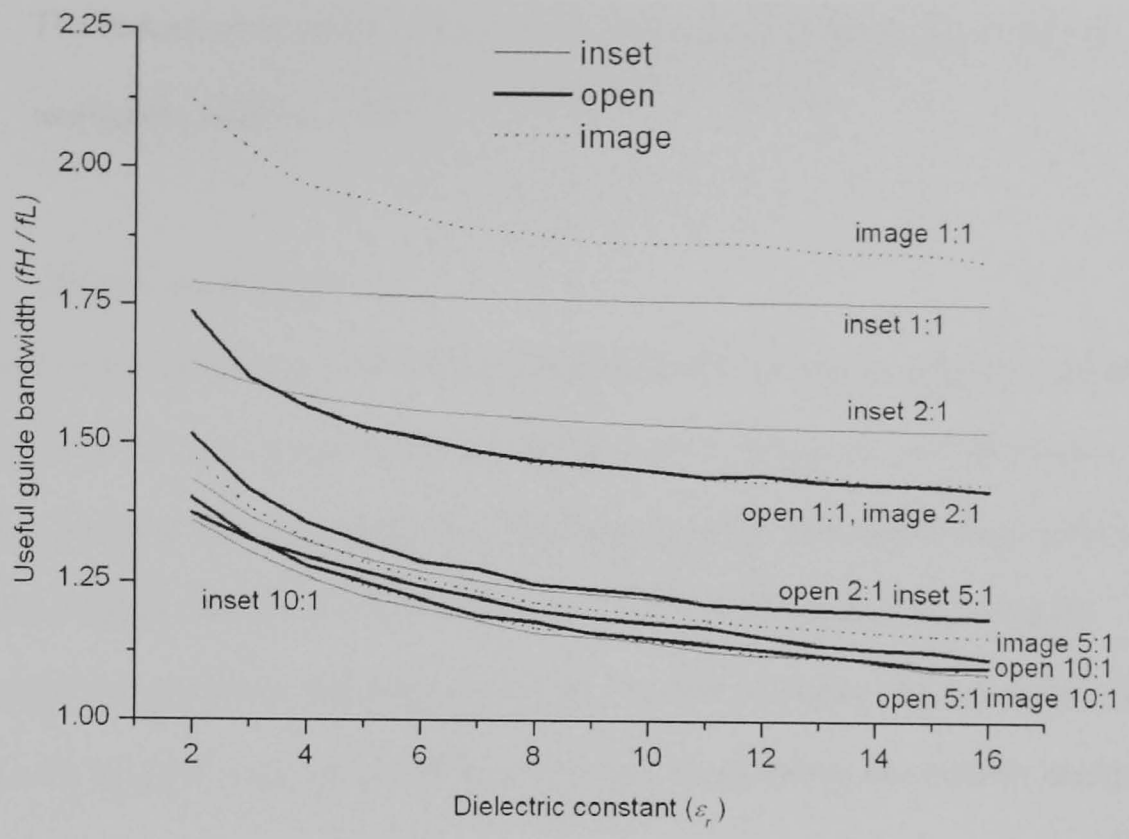

Figure 6.10 Material dependence on guide bandwidths for all guide types and aspect ratios.

6.4.4 Diminishing gains of higher permittivity materials

In antenna theory, it is commonly known that selecting a higher εr material over a lower εr material enables a smaller structure to be realized for the same operating frequency. So, perhaps one of the most important findings in this work is quantification of the extent to which the dimensions and the guide characteristics of dielectric guides (of the types studied) can be influenced by the dielectric constant. Only the electrical permittivity, the real part of the dielectric constant, is considered. From the plots above it is easy to see that, in general, there is little gain to be made from choosing a dielectric constant much above εr = 16. The guide type and aspect has no significant effect on this number, except that the lowest aspect could be argued to roll off at a slightly lower εr. To cover all combinations, and to take into consideration that large scale of the 1:1 aspect plots, it is proposed that:

- The reduction in guide cross-section and change in guide characteristics is negligible when $\varepsilon r \geq 20$.

6.4.5 Trapped image guide case

As mentioned in Sections 6.3.3 and 6.3.4, the gaps between the metal sidewalls and the dielectric sidewalls varies and approaches the inset and image guide cases at the two extremes, zero and infinity, respectively. The characteristics were captured using the extended Marcatili program, and following experiments to find out what gaps approximately represented the two limits, data was captured at a number of increments in between. Fractions of the guide height *b* were used to represent the gap because this is the variable used to normalise the data. The results are plotted in Figures 6.11 and 6.12 for the two extremes of εr. The results have only been captured at the high frequencies of the useful guide range, and only the low aspects because these curves would be almost entirely flat at the higher aspects because of the associated small differences in inset and image characteristics. The main points to note are that:

- A gap equal to *b* is essentially large enough to approximate an image guide;
- A gap equal to *b/32* or smaller is enough to approximate an inset guide, except for the 1:1 aspect guide with low εr which would ideally be *b/64* or thereabouts ;
- If a gap equal to *b* takes the value of the image guide characteristics, and gap of *b/64* takes the value of the inset characteristic, a linear approximation could be taken between these values in all cases with little loss of accuracy.

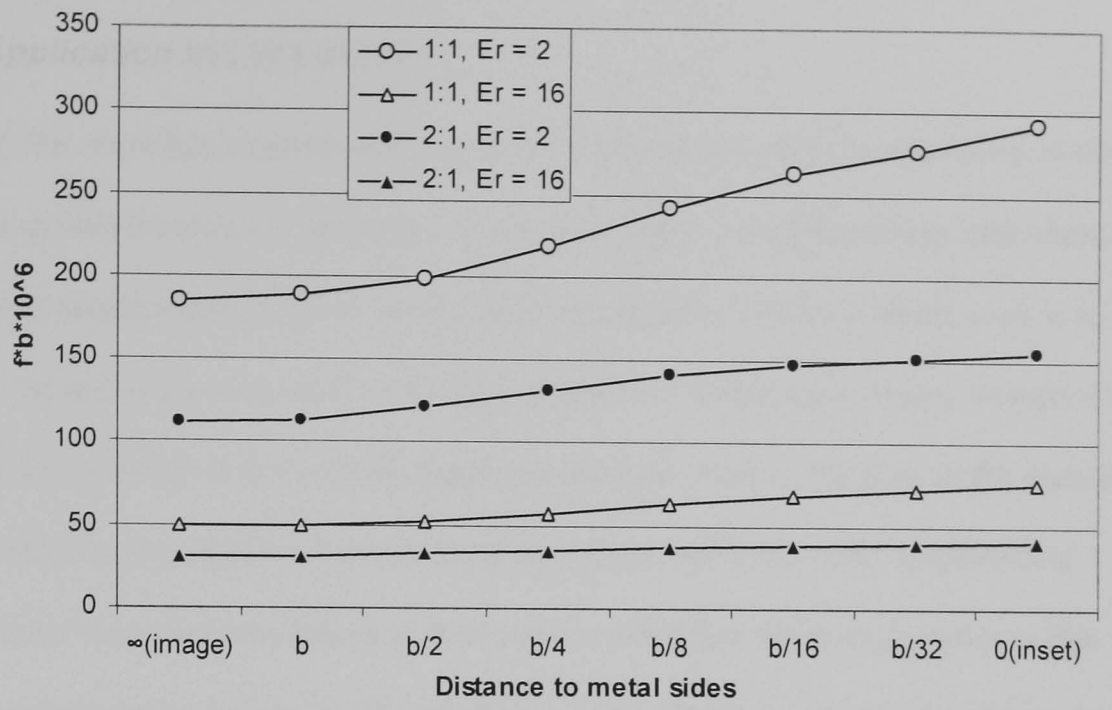

Figure 6.11 Trapped image frequency characteristics as a function of the proximity of the metal sidewalls to the dielectric guide sidewalls.

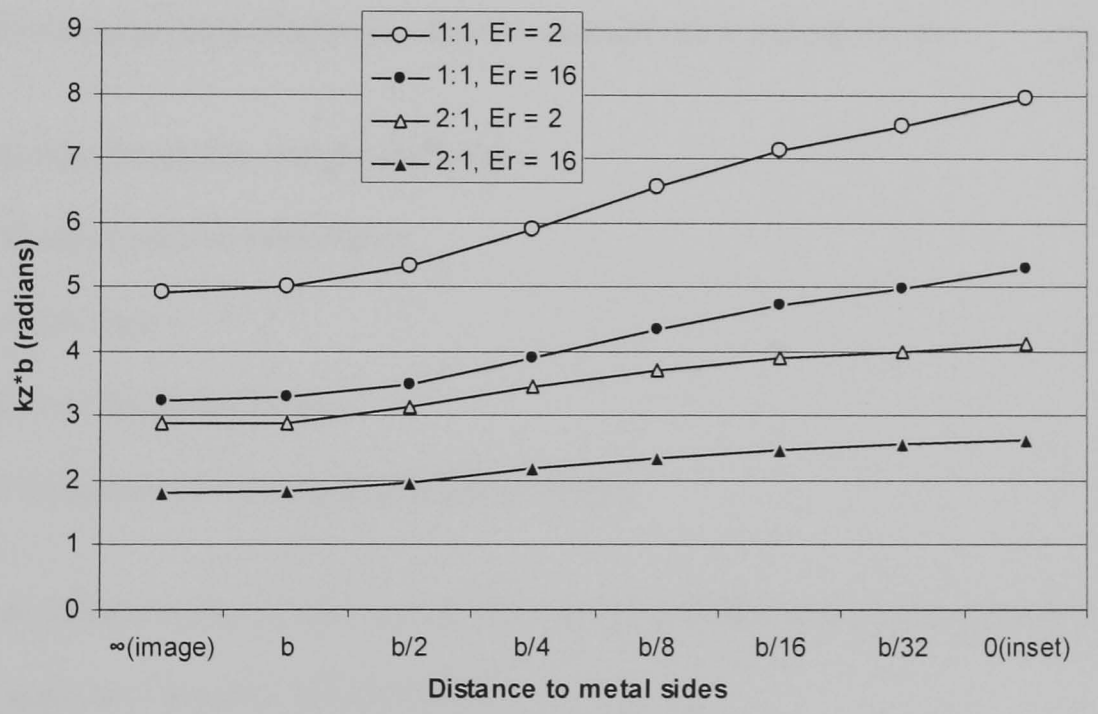

Figure 6.12 Trapped image guide propagation constant characteristics as a function of the proximity of the metal sidewalls to the dielectric guide sidewalls.

6.5 *Application to LWA design*

Thus far, this work has concentrated primarily on determining the characteristics of the dielectric guides themselves, with only a superficial look at their respective influences on the leaky wave antenna design. Since, one of the main objectives of the present work is to simplify the analytical treatment of this type of antenna; attentions will now be turned to illustrate and quantify how the guide characteristics presented in the plots in the preceding section influence the important antenna characteristics, and vice-versa. Hypothetical requirements for an antenna design will be used to develop a number of examples that demonstrate the many tradeoffs. The emphasis of this chapter is on enabling the designer to make an informed choice of guide material and geometry based on antenna requirements.

6.5.1 Relevant characteristics

The guide characteristics of relevance here are both physical and electrical:

- Guide dimensions (height and width)
- Material relative permittivity
- Guide type
- Useful frequency range
- Propagation at working frequency (or range)

Additional characteristics of relevance to the metal strip loaded leaky wave antenna of interest here are again both physical and electrical:

- Strip dimensions
- Strip spacing
- Length of antenna / guide
- Main beam angle
- Frequency scanning rate
- Scanning limits

6.5.2 *Other characteristics*

Some additional guide characteristics will be gathered as a result of this analysis but other antenna characteristics such as gain, beamwidth, impedances and efficiencies are outside the scope of this chapter. The polarisation is assumed to be linear, with the main component of electric field Y-polarised, as per the preceding work.

6.5.3 *Analysis and synthesis*

This will essentially be an analysis exercise, where the antenna characteristics are found based on a set of guide characteristics. It could be argued that there is also synthesis, since the operating frequency has been fixed and a number of guides are designed to work at that frequency; guides of all possible combinations of aspect and type. Analysis is the applied to all these guides to demonstrate the tradeoffs with respect to antenna characteristics for two extremes of (non-magnetic) relative permittivity; $\varepsilon r = 2$ and 12.

6.5.4 *Demonstrating by example*

The examples use a fixed upper frequency (*fH*) as a reference to demonstrate the variation in guide cross section. The aim of these examples is to allow the reader to gain a working understanding of the information furnished by the previous plots, and to highlight some additional issues. The examples are developed in a spreadsheet program and the results are presented in tables for reference in Appendix E, one for the high value of dielectric constant and one for the low value. Open, inset and image guide types are compared for all four aspects, at both ends of their respective useful frequency ranges. Each table is labelled with row and column identifiers to aid discussion of individual results.

In general, the results are intended, not only to provide quantification and to help reinforce the ideas presented so far, but to highlight the possible advantages of selecting a particular guide for the basis of a leaky wave antenna design of the type studied in this thesis.

6.5.4.1 Validity of unperturbed approach

The antenna characteristics are calculated assuming that the array elements (metal strips) are infinitely narrow and therefore do not perturb the value of propagation constant kz (or guide wavelength λg). Two sets of element spacing d are taken and the results are shown side by side in a separate table section. Many researchers have taken this unperturbed approach and proved its validity in specific cases [2-3, 8-9]. Later in Chapter 8 of this thesis, it will be demonstrated that a correction factor is required for the element spacing d when finite width metal strip elements are placed on the surface of a dielectric guide. In any case, all the analysis presented next is still completely valid. In other words, it is not necessary to apply that correction at this point.

6.5.4.2 Scope

Although, a single frequency, 10 GHz, has been chosen as the upper frequency (fH) for these examples, the full working range will be analysed below that frequency. This will allow the capabilities in terms of beam steering (frequency scanning) and rate of scan to be demonstrated, for example.

6.5.5 Determining the antenna characteristics

The guide characteristics used in this section are found directly from the data used to create the normalised guide characteristics plots. Each guide and antenna characteristic listed above will be considered next.

6.5.5.1 Choices of antenna cross section

The specific results can be seen in the appendix under columns A to C. Here, the guide heights have been chosen to fix the high frequency at 10 GHz. Because this frequency is fixed and the aspect ratio is varied across the example, then the guide height must vary also. The

cross-section is then a function of the height and the aspect. It is only necessary here to discuss one or two examples and explain the resulting trends which are that the:

- approximate guide cross sections can be read directly from the $f*b$ plots;
- guide height can be found for a fixed frequency;
- frequency can be found for a fixed guide height;
- tradeoffs with respect to guide type, aspect and permittivity can be determined immediately by inspection of the plots;
- plots have a practical application.

The relative guide dimensions for each aspect, type and any εr can be found by inspection of the plots; the highest $f*b$ value will give the largest guide height and the lowest $f*b$ value will give the lowest guide height. These results give a quantitative idea about how the choice of guide aspect, type and material can influence the size of the antenna, such as:

- for the low εr case the maximum $f*b$ is over 7 times the minimum;
- this is reduced to 4 times for the high εr case.

There are some other trends worth mentioning:

- the image guide of any aspect consistently supports the lowest $f*b$;
- in general, the inset guide supports the highest $f*b$ values for low aspects and the open guide supports the highest $f*b$ at high aspects.

The first bullet makes sense since an image guide is equivalent to an open guide of twice the height [10] which, electrically, makes it twice as big as the open guide. Of course, intuitively, one would expect a larger guide to support lower frequencies. The crossover noted in bullet 2 occurs because the inset $f*b$ curves move to lower frequencies more rapidly than the open guide as the aspect increases, as can be seen from the plots.

Practical considerations like available dimensions of off-the-shelf materials, weight, cost, or robustness might influence the final choice of guide geometry for an antenna design. It is important to consider the whole cross-section in that case.

For **example**, the guide height for a 1:1 open guide is found at fH and $\varepsilon r = 2$ from the data as $f*b*10^6 = 224$. This can be seen immediately in Figure 6.8(a). Since the frequency has been specified as 10 GHz, the height b must therefore be set to 22.4 mm. Since this lookup has been determined for a 1:1 aspect, the guide width a must also be 22.4 mm. Similarly, for a 10:1 image guide at $\varepsilon r = 12$ and fH, the data gives $f*b*10^6 = 20.5$. Figure 6.8(d) confirms this. The necessary guide cross section to put fH at 10 GHz in this case is $b = 2.05$ mm and $a =$ 20.5 mm. The cross-sectional dimensions are therefore 31.68 mm and 20.6 mm respectively; about a 50% difference.

Of course, the length of the guide might also be of practical importance. This will be found shortly.

6.5.5.2 Trapped case and adjusting band of operation

Earlier, it was shown that the trapped guide case approaches the image guide case when the metal planes are far from the sidewalls of the dielectric guide, and approaches the inset case as the metal approaches the guide sidewalls. Inspection of the low aspect ratio $f*b$ results in column B (rows 1, 5 & 9) reveals an intriguing possibility; the frequency band of operation for the guide can be shifted quite significantly by implementing either a trapped guide with adjustable distance metal side planes, or an open guide with a single adjustable distance metal base. According to these results, the former will maintain approximately the same bandwidth, while the latter will see a significant increase in bandwidth. Similar configurations have been developed before for specific geometries and materials [3, 8-9, 11-12]. The tradeoffs for all common geometries and materials can now be studied easily using the new plots. The precise

change in guide characteristics as the metal approaches the guide sidewalls is studied shortly in this chapter.

6.5.5.3 Antenna bandwidth and limits

Under certain circumstances the antenna bandwidth, defined here as the frequency range over which the main beam is present, will be equal to the guide bandwidth itself. From the results in column *F*, which is just $fH - fL$ in gigahertz, it is clear that the 5:1 aspect ratio has the narrowest guide bandwidth in almost all cases. Only the 10:1 inset case is lower. It is not known whether this offers any advantages.

For unknown reasons, the 5:1 open guide case with $\varepsilon r = 2$ is extremely narrow band. Similar notches are also evident in column *F* for the 5:1 aspect ratio low frequency for the open and image guide cases at $\varepsilon r = 2$, and for the open guide case at $\varepsilon r = 12$. Interestingly, the low frequency value for the 5:1 open guide case is essentially the same for both values of εr.

The relative guide bandwidths be seen by inspection of Figure 6.10 for all guide combinations or the bandwidth and limits can be quickly derived from the f^*b plots of Figure 6.8. In that case the limits are found by inspection and the bandwidths can be found from $f^*b_{(fH)} / f^*b_{(fL)}$ with guide height *b* constant.

Since the guide does not really cut off at the low frequency, it could be argued that the guide bandwidth is actually equal to fH. This would mean that, provided that the main beam is sufficiently within the forward and backward directions, the antenna bandwidth could be slightly higher in practice than the useful guide bandwidth found here. This is an extremely complicated corner-case, and will not be discussed further here. The absolute limit imposed here is either the useful guide bandwidth or the band over which both the forward and backward scanning limits are reached; whichever comes first. The scanning characteristics will be considered shortly.

6.5.5.4 *Main beam scan range and limits*

Except in the cases where the scan range is limited by close proximity to the forward and backward directions (i.e. ends of the guide, ± 90° from broadside), it was discovered that the range of propagation constant (*kz_fH - kz_fL*) is what determines the maximum scan range of the main beam given in column *S*. The strip spacing *d* will then, of course, position this range in the elevation plane. It can be seen from columns *Q* and *R* of the results which combinations of aspect, guide type and material do and do not reach these antenna scan limits. These limits can be obtained from the *kz*b* plots, by fixing the guide height *b*. The relative kz range can be obtained in the in exactly the same way as the relative bandwidths are derived from the *f*b* plots i.e. from *kz_fH / kz_fL*.

One might expect that, for a given material, the guide bandwidth might dictate the size of the propagation constant range. However, although the relative values are similarly ordered with respect to the different aspect and guide types, they are not in exactly the same order, as can be seen by comparing across columns *F* and *I*. The exact order is also a function of εr. For example, for a guide material with εr = 12 (e.g. Silicon) the 1:1 image guide has the highest overall guide bandwidth but only the second largest kz range.

The results from the example demonstrate that:

- For the lowest aspects (especially 1:1) and high εr value the main beam can be scanned all the way up to its ± 90° scan limits.
- Conversely, a high aspect and low εr might only reach one or two tens of degrees of angular scan;
- In all cases, the inset guide provides the largest scan range, followed by the image guide and then open guide;
- Typically, the high εr material gives about 50% to 100% more range than the low εr material and the inset guide about 100% more than the open guide, with the image guide somewhere in between.

6.5.5.4.1 Appearance of grating lobes

According to [13], additional main lobes called grating lobes appear when the spacing in linear or planar arrays is sufficiently large to allow the in-phase addition of radiated fields in more than one direction. The theoretical bounds on the spacing, to avoid the onset on grating lobes for this type of leaky wave antenna have been derived in [14] as a function of the propagation constant and operating frequency. The previous author's formula (2-4) for deriving these bounds appears to over compensate and is not really very useful in its current form in practice. This author has found that these grating beams appear with very low magnitude as the main beam direction scans to, say, within ten to twenty degrees of the forward or backward limits, and rapidly grow in magnitude as the limits are reached. Of course, the main beam direction is a direct function of the antenna parameters specified by that author, therefore there is a direct link between these respective findings.

The information needed to predict the onset of grating lobes is difficult to obtain by inspection of the *f*b* and *kz*b* plots directly. In the next chapter, a more detailed investigation will be conducted and closed form formula will be provided to derive these bounds based on the dielectric guide geometry and material.

6.5.5.5 Scan rate

The scan rate is the rate of beam scan (sometimes referred to as steer) versus change in frequency. In the majority of cases, it is practical to state this in degrees per gigahertz as seen from column T. It can be seen from these results that the:

- guide type has little influence on the scan rate, especially for the low εr material;
- scan rate for the high εr is roughly 100% higher than for the low εr material. For a 1:1 aspect, it peaks at about 25°/GHz for low εr and 60°/GHz for high εr, and for the 10:1 aspect drops to between about 10°/GHz and 20°/GHz;
- inset guide has highest scan rate by a very small margin over the other two types.

The relative scan rate for all the different combinations of guide type and size versus εr was found to have the same order as the amount of change in kz versus frequency. This information is difficult to obtain by inspection of the *f*b* and *kz*b* plots. In Chapter 5, this was quantified for the 2:1 aspect ratios and an open guide. Here, it is shown in Figure 6.13 for all combinations. The highest values of kz /GHz give the highest scan rates and vice-versa.

The image guide with a 5:1 aspect gives the highest scan rate for all εr, followed closely by the inset 5:1. The order of these curves is consistent with the tabled results from the example. The order is interesting; there are a number of anomalies, like the open 1:1 combination falling between the open 2:1 and 5:1, and a number of crossovers and bumps. No attempt will be made to explain these here.

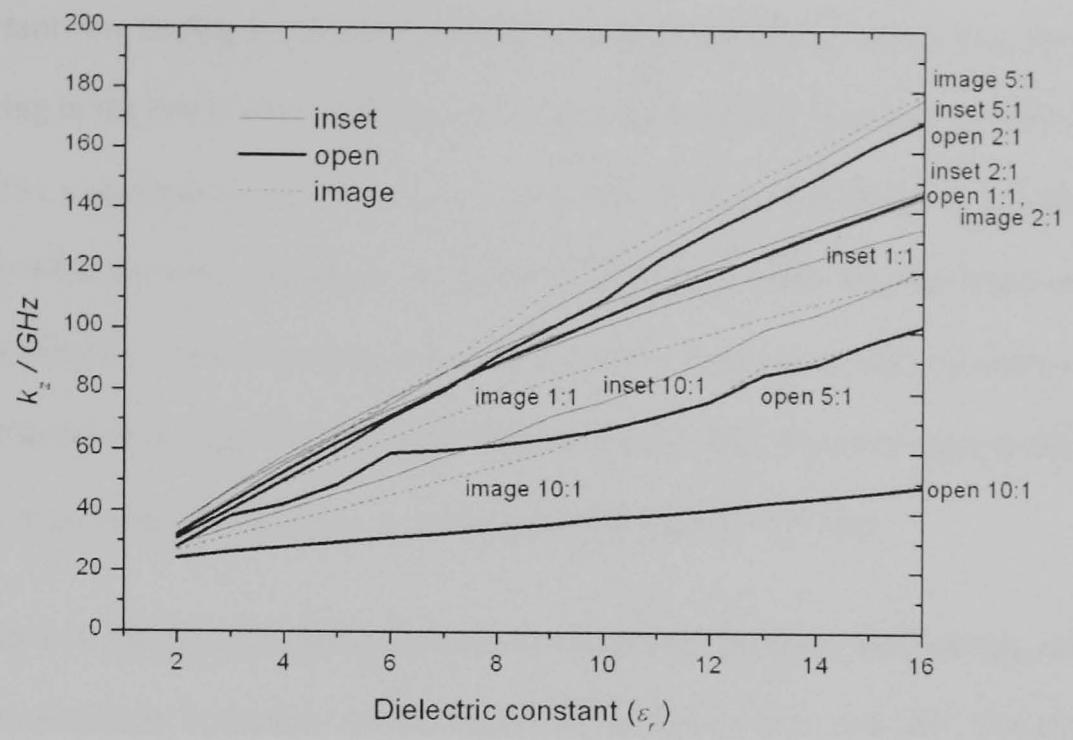

Figure 6.13 kz/GHz level for all guide combinations. The relative levels were also found to dictate the beam angle scanning rate as a function of a change in operating frequency.

6.5.5.6 Centreing and rotating the angular scan

From columns Q and R of the results given in Appendix-E, it was observed in some cases that the beam angle set by the high frequency and the beam angle set by the low frequency were asymmetrical with respect to the centre angle, broadside 90°. Further investigations revealed some interesting compromises. Of course, the beam angle is a function of the strip spacing *d* and so as the spacing is changed, so the beam angle changes accordingly. The beam angle versus spacing was computed and plotted for both the low εr case and the high εr case at both ends of their respective frequency ranges, and at their respective mid frequency, as shown in Figures 6.14 and 6.15.

The most immediate observations to be made are that, while the whole range from 0° to 180° can be covered in the high εr case, by careful choice of spacing, only a small fraction of the whole angular range can be covered in the low εr case.

An important new finding is that the maximum possible scan range is also a function of the strip spacing in the low εr case, and not just the frequency at which the angular limits are reached. The range reduces as the spacing is increased, but becomes relatively constant, apparently when the *whole* frequency range falls sufficiently within the scan limits of Figure 6.15. This behavior cannot be seen in the high εr case in Figure 6.14, and is put down to the fact the scan rate is so high that the whole frequency range only becomes close to fitting within the scan limits at one point i.e. through point B when $d \sim 21$ mm.

It is also easy to see the relationship between the operating frequency and spacing and their subsequent proximity to the forward and backward scan limits at 0° and 180°. For example, by inspecting Figure 6.15, if the spacing is set to 18 mm, the beam angle will hit the backward limit and generates a grating lobe as the operating frequency is reduced and approaches the centre frequency.

From both plots, it can be seen that the centre frequency and the broadside beam angle do not coincide. In that case, over the useful frequency range, the beam may be scanned over almost twice the number of degrees in the backward direction than the forward direction (asymmetrical scan case). Analysis shows that, by careful selection of the spacing distance e.g. increasing it from points A to B or C to D, that the scan range at either side of broadside can be equalized (symmetrical scan case), but the centre frequency f_C and beam angle will no longer coincide at broadside, as per points A and C. Figure 6.16 demonstrates this situation graphically for the present example and for both values of εr. Each vertical line represents the possible beam scanning range over the full frequency range, for a number of values of strip spacing.

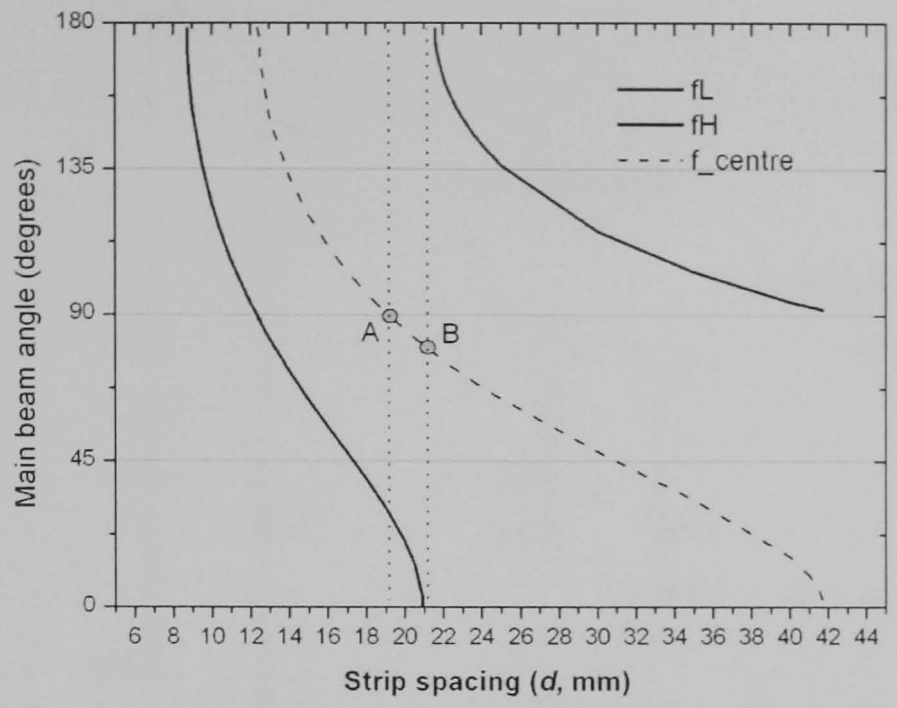

Figure 6.14 Beam angle versus strip spacing for the εr = 12 case, at both ends of the useful single-mode frequency range.

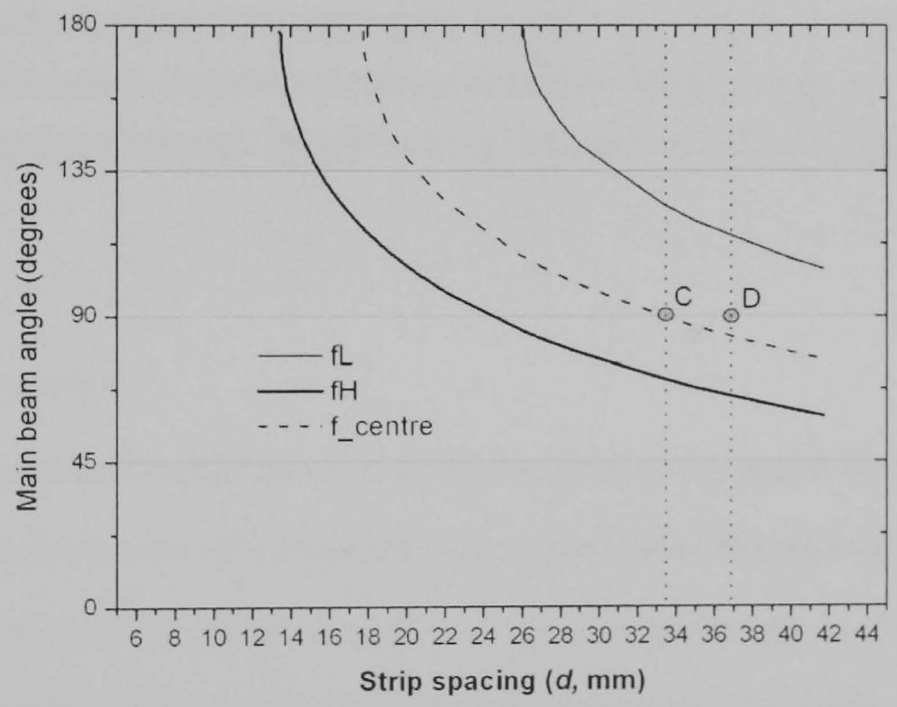

Figure 6.15 Beam angle versus strip spacing for the εr = 2 case, at both ends of the useful single-mode frequency range.

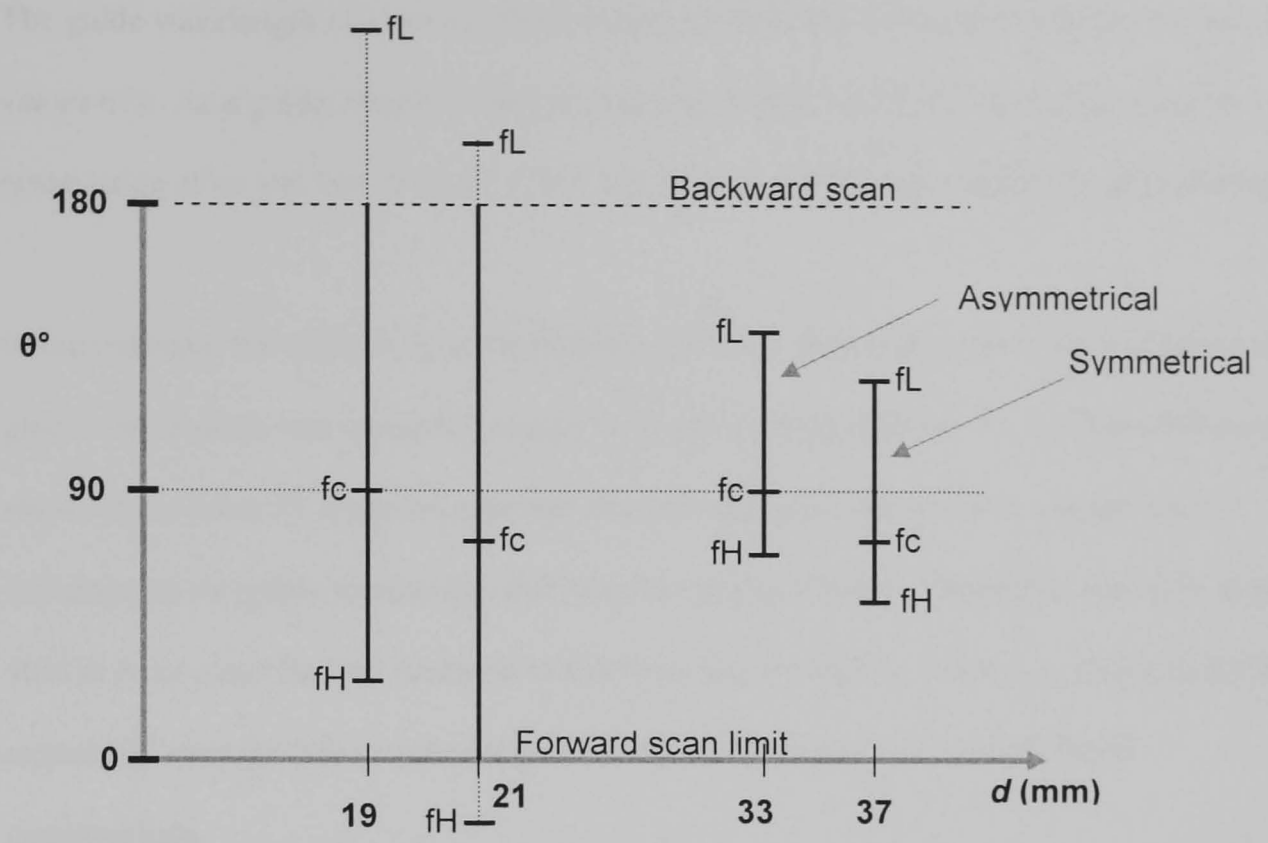

Figure 6.16 Depicts the effects of changing the strip spacing *d* to position the centre frequency of the range (fL to fH) at broadside (asymmetrical case), or centring the frequency range and scan range about broadside (symmetrical case). The εr =2 and εr = 12 cases are both shown, from Figures 6.14 and 6.15.

6.5.5.7 Antenna length

The results, in columns *L* and *M* demonstrate that the guide wavelength at the low frequency can be very high compared to at the high frequency. This implies that the antenna length *(l)* is highly dependent on what frequency is used to set the centre beam angle i.e. depends on what value of strip spacing *d* is used. It is also highly dependent on how many strips are needed. This in turn depends on the gain / beamwidth requirements. These latter dependencies are complex issues and outside the scope of this present chapter. However, based on the present author's simulation results and theoretical analysis, and the work of previous authors, it is sufficient here to say that 20 to 30 times the strip spacing will typically be required. In general, the lower the working frequency, the longer the antenna will need to be.

The guide wavelength (λ_g) can be obtained directly from the $kz*b$ plots of Figure 6.9 for fixed values of b. As a guide, simply letting the spacing d equal the guide bandwidth taken at the mean value of kz and then letting $l = 30d$ will allow a realistic and relative length to be found.

In the example, the value of λ_g at the centre of the respective useful frequency range for each guide combination was computed using (5-1) to (5-3), and allowing $d = \lambda_g$. From the results shown in (column P), it can be seen that the type of guide does not have a great deal of influence on the guide wavelength and therefore antenna length, varying by less than about 10% in most cases for low values of εr and even less for high εr. However, selecting the high εr material over the low εr material gives about a 50% reduction in length for all combinations.

6.5.5.8 Volume of material

The volume of material for the high εr material is only approximately 10% of that required for the low εr for a 1:1 aspect, as can be seen from column AD. This increases slowly to about 25% as the aspect is increased. In other words, there are substantial savings to be made by choosing high εr materials.

Of course, this information cannot be read straight from the plots. However, since the volume is a function of the guide cross section and length, whose derivation was described above, it can of course easily be calculated. A good way of comparing the relative volumes for each combination is to compare $a*b*\lambda_g$ at the centre frequency of their respective ranges.

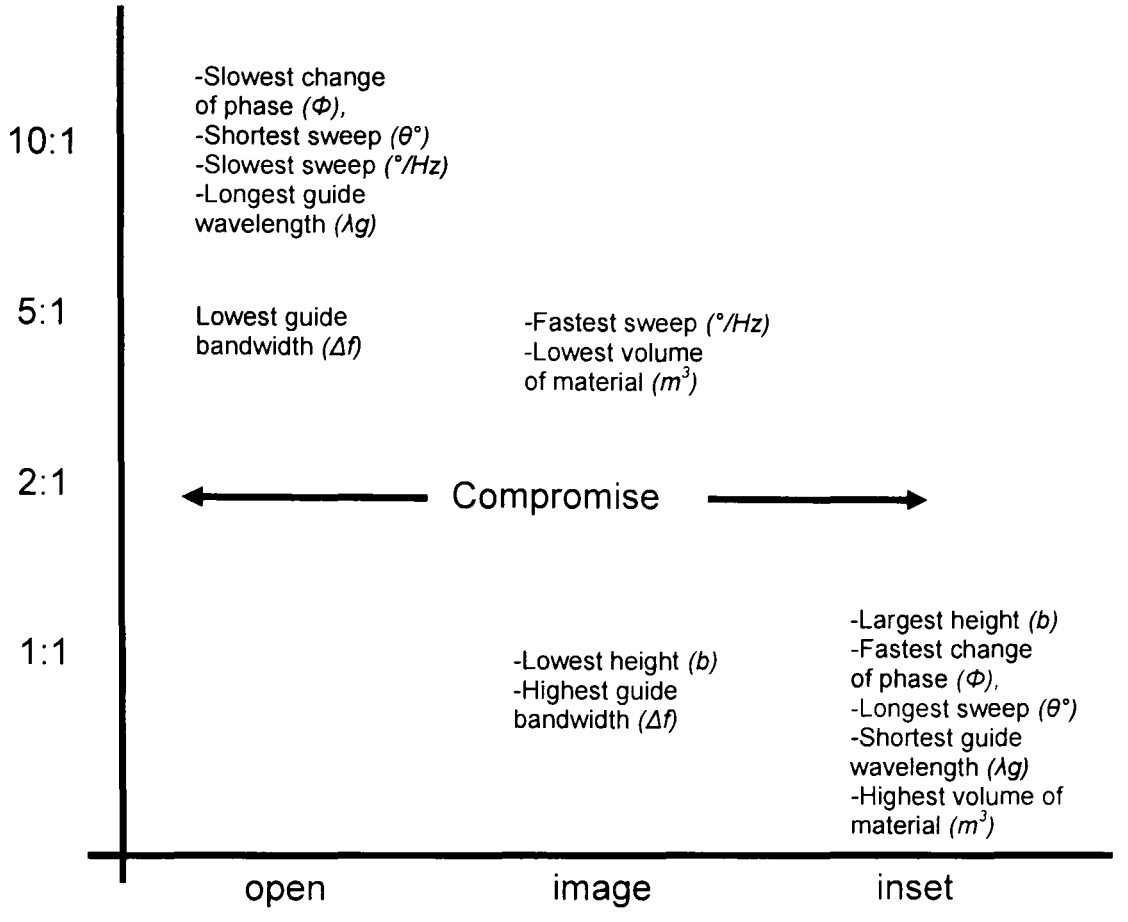

Figure 6.17 Summarises the antenna and guide characteristics and advantages for each combination of guide type and aspect ratio.

6.5.6 Guide and antenna characteristics compromises

For an antenna, the 2:1 aspect ratio guide represents a practical compromise between overall dimensions, weight and material cost, and the useful single-mode frequency range, scan range and scan rate. Figure 6.17 summarizes the advantages of each guide type and aspect ratio studied in this work, as detailed in the preceding sections of this chapter.

6.6 Conclusions

A new way of representing dispersion characteristics was developed in Chapter 5. In that case, the method was applied to rectangular dielectric waveguides, which are the structure of interest in this work. The British Standard sizes designated to metal waveguides was used as a basis to develop the idea. The method normalises the dispersion data to remove the size and frequency dependency of the structure and presents the results so that their dependencies on the material dielectric constant can be seen by inspection from the resulting plotted data. The same method may also be applied to the dispersion characteristics of other structures and materials.

In the present chapter, this method was applied in exactly the same way to represent the dispersion characteristics of the largest practical range of waveguide cross-section aspect ratios for a number of common dielectric guide types, namely the completely open guide, the image guide and inset (trough) guide. Here, the results are shown graphically and together so that the characteristics of each combination of aspect and guide type can be found by inspection for a large practical range of dielectric constants that encompasses most non-magnetic materials. This is the first time that such a comprehensive set of results have been produced and it fills the gaps between existing published works that only give results for a small number of specific sizes or materials and for a specific frequency.

The trapped image guide is a special case that is a hybrid of the image and inset guides, and its transition from one to the other was demonstrated. Finally, its application to leaky-wave antenna analysis and design was demonstrated, and to specific antenna characteristics. The tradeoffs of each combination of aspect ratio and guide type were also presented in terms of the main antenna physical and electrical

characteristics such as bandwidth, beam scan rate and range and volume of dielectric material.

It is anticipated that this information can be used as both a selection aid for selecting a suitable waveguide configuration for non-antenna applications as well as for a specific antenna design specification. In the following chapter, simple closed-form formulas will be developed to represent these same guide dispersion characteristics to reduce the burden normally associated with detailed design of the guide to just a few minutes. The leaky-wave antenna may also be designed once the guide has been selected and its characteristics have been found using these new formulas.

6.7 References

[1] E. A. J. Marcatili, "Dielectric rectangular waveguide and directional coupler for integrated optics," *Bell Syst. Tech. J.*, vol. 48, no. 7, pp. 2071–2095, Sep. 1969.

[2] T.N. Trinh, R. Mittra and R.J. Paleta, "Horn image-guide leaky-wave antenna," *IEEE Trans. Microwave Theory and Techniques*, vol. MTT-29, no. 12, pp. 1310-1314, Dec. 1981.

[3] R. E. Horn, H. Jacobs, E. Freibergs and K. L. Klohn, "Electronic modulated beam-steerable silicon waveguide array antenna," *IEEE Trans. Microwave Theory and Techniques*, vol. MTT-28, no. 6, pp. 647–653, Jun. 1980.

[4] H. Jacobs and M. M. Chrepta, "Electronic phase shifter for millimeter-wave semiconductor dielectric integrated circuits," *IEEE Trans. Microwave Theory and Techniques*, vol. MTT-22, no. 4, pp. 411–417, Apr. 1974.

[5] H. Jacobs, G. Novick, C. M. LoCascio and M. M. Chrepta, "Measurement of guide wavelength in rectangular dielectric waveguide," *IEEE Trans. Microwave Theory and Techniques*, vol. MTT-24, no. 11, pp. 815–820, Nov. 1976.

[6] T. Itoh and B. Adelseck, "Trapped image guide for millimeter-wave circuits," *IEEE Trans. Microwave Theory and Techniques*, vol. MTT-28, no. 12, pp. 1433-1436, Dec. 1980.

[7] Detail specification for ordinary rectangular waveguides, British Standard Institute standard number BS 9220.

[8] K. L. Klohn, R. E. Horn, H. Jacobs and E. Freibergs, "Silicon waveguide frequency scanning linear array antenna," *IEEE Trans. Microwave Theory and Techniques*, vol. MTT-26, no. 10, pp. 764–773, Oct. 1978.

[9] V.K. Varadan, V.V. Varadan, K.A. Jose and J.F Kelly, "Electronically steerable leaky wave antenna using a tunable ferroelectric material," *Smart Materials & Structures*, vol. 3, pp. 470-475, Jun. 1994.

[10] S.P. Schlesinger and D.D. King, "Dielectric image lines," *IRE Trans. Microwave Theory and Techniques*, vol. MTT-6, pp. 291-299, Jul.1958.

[11] R. E. Horn, H. Jacobs, K. L. Klohn and E. Freibergs, "Silicon frequency electronic modulated analog line scanning using a dielectric antenna," *IEEE Trans. Microwave Theory and Techniques*, vol. MTT-30, pp. 816–820, May. 1982.

[12] I.J. Bahl and P. Bhartia, "Leaky-wave antennas using artificial dielectrics at millimeter-wave frequencies," *IEEE Trans. Microwave Theory and Techniques*, vol. MTT-28, pp. 1205–1212, Nov. 1980.

[13] C.A. Balanis, "*Arrays*," in Antenna Theory, Second edition, John Wiley & Sons, Ch. 6, p311, 1997.

[14] S. Kobayashi, R. Lampe, R. Mittra and S. Ray, "Dielectric rod leaky-wave antennas for millimeter-wave applications," *IEEE Trans. Antennas and Propagation*, vol. AP-29, no. 5, pp. 822–824, Sep. 1981.

7 NEW CLOSED FORM EXPRESSIONS FOR THE GUIDE CHARACTERISTICS

7.1 Introduction

The information derived from the plots presented in the previous chapters, and by graphical methods in general, is useful from the point of view of gaining insight into the operation, but it is often difficult to derive quantitive information with better accuracy than ~10%. It is far better of course to have a mathematical description, with enough accuracy so that the information derived can be used as the basis for a real design. Such mathematical descriptions will be derived in this chapter to satisfy the goal of simplifying the existing mathematical treatment of metal strip loaded leaky wave antennas. Specifically, formulas will be derived to find the useful frequency range and real part of the longitudinal propagation constant of the host dielectric waveguide, as described graphically in the previous two chapters, and formulas will also be presented for determining the important antenna characteristics described in the latter half of the last chapter.

7.2 Curve fitting exercise

Since it now appears to be both useful and possible to find the most important guide characteristics for a large practical range dielectric waveguides of any size from the new normalised plots, it then makes sense to perform a curve-fitting exercise on the curves in an attempt to describe these mathematically. If a reasonable curve fit could be found with good enough accuracy over a high proportion of the εr range, then the resulting expressions could represent a much simpler solution to finding the approximate characteristics than provided by Marcatili and other authors. It is assumed and accepted that accuracy might have to be traded for simplicity in this process.

7.2.1 Early attempts at curve fitting

Judging by the curvature seen in the current plots of Chapter 6, it would appear to be impossible in most cases to find a good curve fit that would be accurate enough to represent the full length of the curve. However, various attempts were made using both the Matlab and Microsoft Excel curve-fitting features, and these were optimized manually to average out the

error. However, the fit to a curve was either unacceptable because of a very poor representation at one end of the curves or the other, or the resulting curve function needed to be third-order or higher even for a moderate fit, and mostly ended up being almost as complicated as the Marcatili formulas.

7.2.2 Further normalization of plot data

As an alternative, further normalisation was applied to the curve data to try to reshape the curves for a better curve function fit. After this procedure was completed, the final curves were essentially almost perfect straight lines. This process will be described in the next section. Of course, this meant that an almost perfect curve fit was achieved, and from these, trivial straight line formulas could be derived.

These formulas are the primary output from the present chapter, along with their implementation in some common leaky wave antenna formula that significantly simplify that analysis. The existence of these new formulas was only possible because the normalisation experiments resulted in such straight lines, and because the Marcatili equations have the incorrect low frequency dispersion curve behaviour, as was described in Chapter 5.

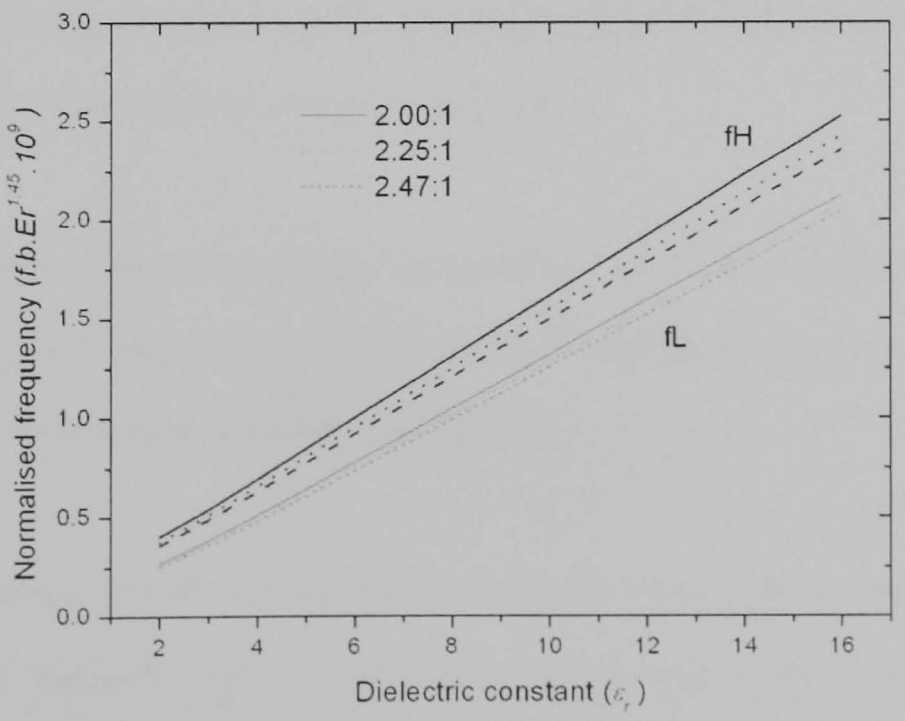

Figure 7.1 Optimized normalised frequency curves for standard aspect ratio open guides.

7.3 *Derivation of formulas*

7.3.1 Normalizing factors for open guide and standard sizes

The normalised frequency data ($f*b$), derived using the Marcatili formula software implementation, for a large range of open dielectric guides with cross-sections the same as the internal dimensions of the standard metal waveguides, were copied into a graphing program and the curves were plotted. Additional normalising factors were applied to the frequency data. It was found that multiplying the $f*b$ curves by a linear function of εr e.g. $f*b*\varepsilon r$, $f*b*sqrt(\varepsilon r)$ made the curves much straighter and therefore much more amenable to a good curve fit. A sample of the resulting curves is shown in Appendix B to demonstrate these effects. Further optimisation allowed the best compromise to be found for all the curves, which was: $f*b*Er^{1.45}$. The resulting curves are shown in Figure 7.1 as evidence of the effectiveness of this technique.

7.3.2 Frequency formulas and coefficients

Trivial straight-line formulae have been derived from the end points of these lines. Because the position of the lines was found to be a function of the aspect ratio, there is one pair of straight lines and therefore one pair of straight line coefficients for each aspect ratio. Each pair represents the high frequency and low frequency limits of the approximate useful frequency range for any value of εr in the range 2 to 16.

The slope and start values for the straight line equations were worked out for all six standard size aspects at both the high and low frequencies. These coefficients were then given the labels U and V respectively and are listed in Table 7.1.

To arrive back at the original frequency or $f*b$ values, with a much greater degree of accuracy than possible by reading from the $f*b$ plots, the normalising factor is applied to the straight line equations. Since the normalisation factor satisfied all cases, the result is a single formula

(7-1). The associated formula, including denormalization factor, is a direct mathematical representation of any of the frequency curves from Chapter 5 and curves for any other size guide as long as it uses one of these aspect ratios.

It can be seen immediately by inspection of (7-1) what the effect will be for an increase or decrease in parameters εr, b, and fH (or fL) or any combination. Accurate values for a single parameter can be found by fixing the other two. In practice, it is most likely that the operating frequency will be known, probably the high frequency. A suitable combination or εr and b can then be found to satisfy the equation and other practical considerations to do with available materials. Of course, either the guide height b or guide width a can be used in (7-1) even though the new formulas have been derived based on b. For example, $b = 1/2a$ for the 2:1 aspect, and $b = 1/10a$ for the 10:1 aspect and so on.

$$f_{L,H} = \frac{(U\varepsilon_r + V)\times 10^6}{b\varepsilon_r^{\,1.45}} \qquad (7\text{-}1)$$

$$k_{z\,fL} = \frac{2\pi f_L}{c} \qquad (7\text{-}2)$$

$$k_{z\,fH} = \frac{2\pi f_H}{c\varepsilon_r^{\,0.6}}(P\varepsilon_r + Q) \qquad (7\text{-}3)$$

Table 7.1 Coefficients for (7-1) to (7-3), valid for dielectric guides using standard WG sizes only.

Aspect ratio	f_L coefficients		f_H coefficients		kz_{fH} coefficients	
	U	*V*	*U*	*V*	*P*	*Q*
2 : 1	131	4	152	93	0.68	0.45
2.12 : 1	129	4	149	90	0.66	0.45
2.15 : 1	128	4	148	89	0.65	0.46
2.20 : 1	127	4	147	85	0.64	0.49
2.25 : 1	127	6	146	82	0.64	0.47
2.47 : 1	124	7	142	72	0.60	0.56

7.3.2.1 Simple example

Find the frequency range and range of propagation constant for the εr = 2.47 model used in Chapter 4. **Answer**: the guide cross section was 3.4 x 1.4 mm, which equates to a 2.43:1 aspect. Using the coefficients for the 2.47:1 will give good accuracy. Using (7-1) to (7-3) gives fL = 60.31 GHz, fH = 81.38 GHz, kz_fL = 1264 rad/m and kz_fH = 2024.56 rad/m. At these frequencies, the Marcatili method gives 1307.6 and 2033 rad/m which are within 3% and 0.5% respectively.

7.3.3 Deriving propagation constant expressions

Using the same techniques, it was also found that the normalised propagation constant data could be manipulated in the same way using different normalization factors and so it becomes immediately obvious that these too might be well represented by curve-fit formula. In chapter 5, the kz data was normalised in the traditional manner by k_0 to produce Figure 5.7. There it was seen that the low frequency kz curve was at $kz / k_0 = 1$ for all values of εr. From inspection of these formulas, note that (7-2) is εr independent. This occurs because the low frequency cutoff of the fundamental propagating mode in the guide occurs when $kz = k_0$ for any guide configuration or material In other words, kz at the low frequency (kz_fL) is given by (7-2) and no additional normalisation is required. Note that (7-2) is therefore εr independent.

Various attempts were made at normalising the high frequency kz data. Some of these results are shown in Appendix B to demonstrate the effects of different normalisation factors. It was interesting to note that dividing the data by the guide height (i.e. $kz\ b$) produced the same shape response as for the kz / k_0 plot, but with a different and less convenient Y-axis scale. The high frequency data was normalised by the more convenient k_0 but the resulting high frequency kz curves are far from straight, as was see in Figure 5.7. After further normalisation attempts and optimisation, it was found that multiplying the kz data by $Er^{0.6} / k_0$ again

produced almost perfect straight lines, as shown in Figure 7.2 clearly shows the different slopes due to the differing aspect ratios used in the standard guide size sample. The plots also demonstrate the deviation from a perfect straight line for a part optimised case (a) where the normalisation factor is slightly different, and demonstrates almost perfect straightness for the actual factor (b) used to derive the new formulas. These same effects were seen for the frequency normalisation.

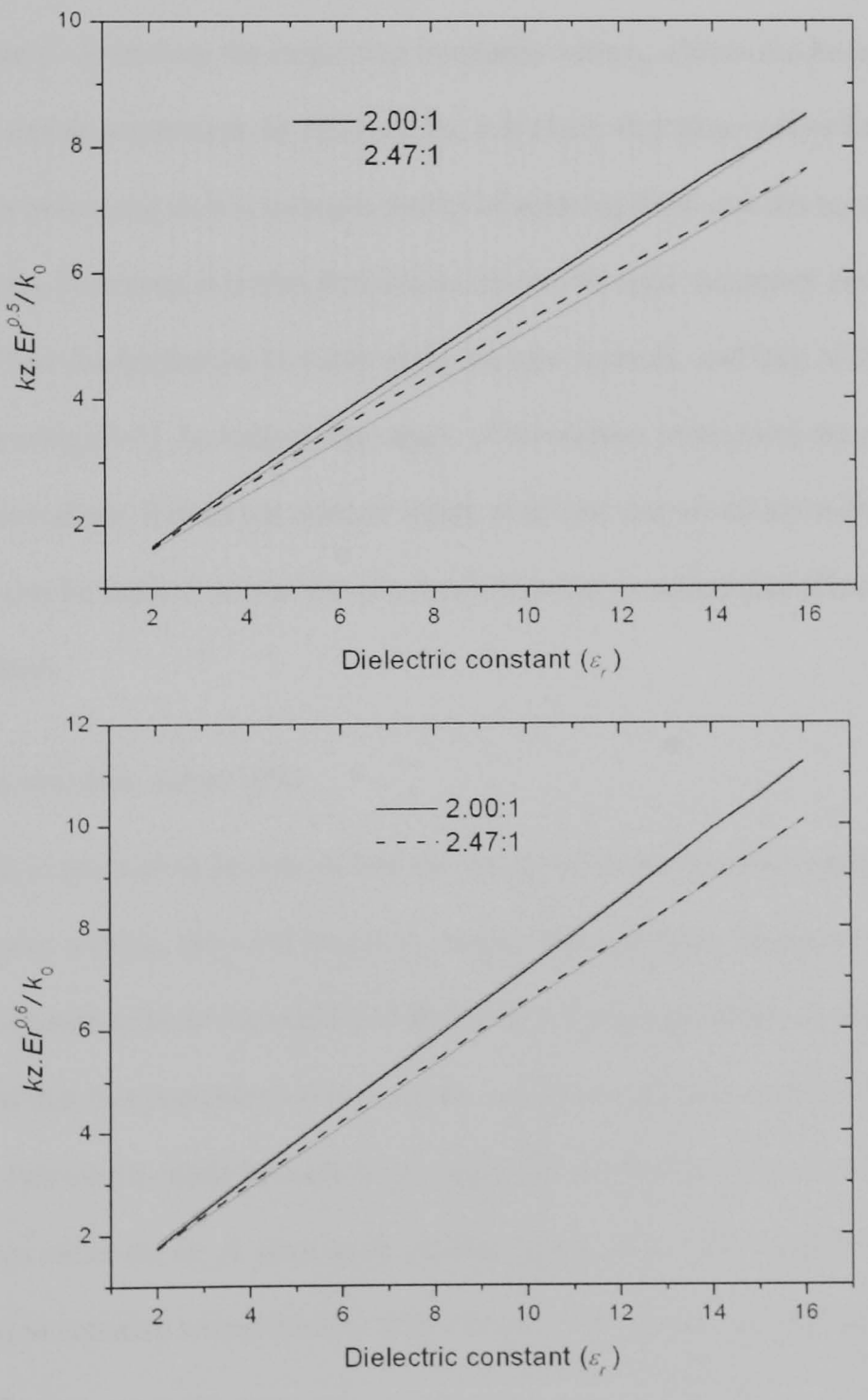

Figure 7.2 Part (a) and fully optimized (b) normalised propagation constant curves for standard aspect ratio open guides. The light coloured lines are perfect straight lines drawn through the two ends of each curve to demonstrate the effectiveness of the respective normalisation factors.

7.3.4 Propagation constant expressions and coefficients

Formulas were again derived from the straight lines and the relevant denormalization factors were applied to produce a new formula (7-3) for the high frequency propagation constant that derives values for any size dielectric guide, and any εr in the range. The slope and start values for the straight lines have been given the labels *P* and *Q* and the subsequent coefficients for all six standard aspect ratios are included in Table 7.1.

Both (7-2) and (7-3) include the respective frequency values, which of course incorporate the guide height and εr parameters. In other words, it is likely that these values have already been chosen at this point, and so it is a simple matter of entering them into the equations along with the coefficients. However, it is also possible to choose the high frequency and a material at this point to find the respective kz value using the new formula, and then to find the necessary guide height using (7-1). As long as the values of the chosen parameters are maintained consistent throughout, it does not manner which order the unknowns are found. In addition, adjustments can be made to any of the chosen parameters provided that all of the unknowns are recalculated.

7.3.4.1 Intermediate values of kz

It is desirable in practice to be able to find the values of kz for any intermediate frequency inside, and even outside, the valid frequency range. The operating frequency might, for example, be chosen to be in the middle of the guide's frequency range. In chapter 5 it was demonstrated that it is possible to find accurate values of k_z for any intermediate frequency between the two single-mode boundaries *fL* and *fH* by simple interpolation backwards or forwards from either the *kz_fL* limit or *kz_fH* limit using (5-3). This is enabled by the fact that the propagation constant varies linearly with change of frequency, as was demonstrated in Figure5.12. In fact, since the intermediate values are on a straight line, it is possible to project beyond these two single-mode boundaries using the same formulation. Some previous authors have used frequencies much higher than the single-mode range without considering the higher

modes that might propagate [1] while others have found that the higher modes do not couple into the excitation metal waveguide [2]. The ability to project, enabled by the new formulas, allows such cases to be analysed quickly and easily.

The relevant procedure is included here to complete the mathematical treatment. It finds both intermediate values and projected values:

1. divide the total number of radians per metre between *kz_fL* and *kz_fH* by the guide bandwidth *fL* to *fH* in Hertz or gigahertz, to find kz/Hz or kz/GHz (5-2);
2. calculate the difference between the low frequency *fL* as per (5-3) or the high frequency *fH* as per (7-4) and the actual operating frequency f_o;
3. take the product of the results from steps 1 and 2 to find the offset value δkz;
4. calculate the sum of either *kz_fL* or *kz_fH* and δkz, as appropriate, as (5.3) or (7-4).

$$kz_o = kz_{fH} + (f_H - f_o).\delta kz \qquad (7\text{-}4)$$

7.3.4.2 Simple kz/GHz formula

It turns out, after having tried to make a more compact expression out of (5-2), that a neat simplification is possible that can be used as a simple approximation for any of the six standard aspect ratios from 2:1 to 2.47:1 (7-5a, b). Since only the *rate* of change is needed, this was simply derived from the approximate slope of the curves of Figure 5.11. Note that (7.5a) and (7.5b) are interchangeable, except that one is in terms of gigahertz and the other Hertz.

$$k_{z/GHz} \approx 10(\varepsilon_r + 1) \quad \sim 2{:}1 \text{ aspects} \qquad (7\text{-}5)$$

$$\Delta kz \approx (\varepsilon_r + 1) \times 10^{-8} \qquad (7\text{-}5b)$$

7.3.5 Quantifying the error

The results presented in the previous two chapters were derived from many thousands of computations of the Marcatili transcendental formulas. These earlier chapters have also demonstrated and validated the accuracy of the Marcatili method. Its accuracy was shown to increase above the low frequency of the useful single-mode range and many authors have shown the results to correlate closely with experimental findings [3] to [7].

Since the new formulas are a direct empirical representation of those results, they will produce the same error, plus or minus any error introduced by the differences between the subsequent normalised results curves and the straight lines from which the new equations were derived.

Here, it was deemed sufficient to validate the accuracy of the new formulas simply by comparing their results with those calculated using the Marcatili formulas. The error was calculated as a percentage of the difference between *fL, fH, kz_fL* and *kz_fH* for a sample of standard guide sizes covering all six standard aspect ratios and for the same range of εr. The errors can be attributed largely to minor curvature in the straight lines, and to a smaller to rounding errors.

7.3.5.1 Frequency error

To begin with the new frequency range formula produced results that were slightly higher than those produced by the Marcatili formulas, with the error peaking at approximately +5% at around εr = 4 and reducing to almost zero at higher values. It was decided to average out the error across the range of εr. To achieve this, the original straight line formula coefficients were manually adjusted to achieve the best results. This process resulted in an average error of around ± 2% for the low frequency results. Since the Marcatili values at the low frequency end, as the E_{11} cutoff frequency is approached, are known to be relatively inaccurate anyway as described in Chapter3, this small amount of error is satisfactory. Since the error for the

original high frequency coefficients was already relatively low, these were not adjusted and the error is typically less than ± 0.5% except for a peak of 1.5% around εr = 4 again. The worst case results for a range of aspects are shown in Figure 7.3. From these, it can be seen that the error appears to increase with aspect ratio. The relative errors can be explained by inspection of Figure 7.1, where it is clear that the low frequency curves all suffer from more curvature, especially at the low εr end than the high frequency counterparts. Less evident is the fact that the higher aspect curves suffer from more curvature than the lower aspects.

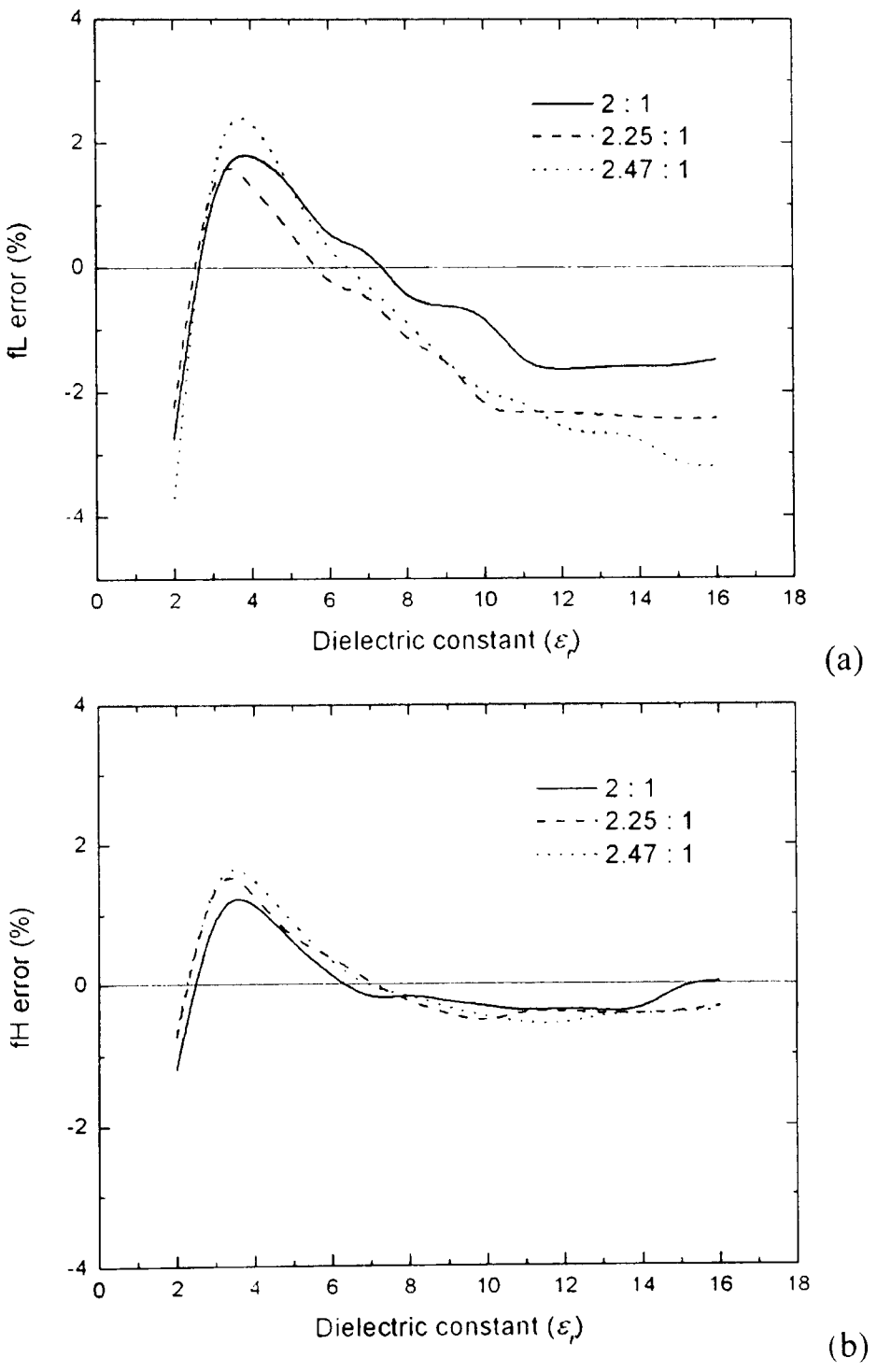

Figure 7.3 Typical worst case difference between f_L (a) and f_H (b) calculated by the new formula (7-1) and by the full Marcatili transcendental formulas for a selection of aspect ratios.

7.3.5.2 *Propagation constant error*

The same procedure used for quantifying the difference between actual Marcatili formula derived single-mode frequency limits results and those as derived from the new formula is used to find the propagation constant error at the same frequencies. Worst-case results are again shown in Figure 7.4 for two cases:

1. Marcatili derived frequencies substituted into (7-3);
2. New formula (7-1) derived frequencies substituted into (7-3).

In the first case, the error as shown in Figure 7.4(c) is entirely attributed to (7-3), since the frequency calculation obviously has zero error. The error is again aspect ratio dependent, with the lowest aspect showing on average less than ±1% error, with the highest aspect approaching ±2%. However, in the second case, both (7-1) and (7-3) contribute errors when compared to purely Marcatili method derived values. The can be seen to produce slightly less error, which is interesting since there is an additional error source. It can easily be seen from inspection of the frequency plots in Figure 7.3 that the error is positive at the low εr end of the scale and so compensates a little for the error found by (7-3), bringing it closer to ±1% for all aspects. The error is therefore additive i.e. fH error + kz_fH error = total kz_fH error. For the low frequency value of propagation constant, the error is always zero because the propagation constant in the guide at that frequency is equal to the free-space propagation constant k_0.

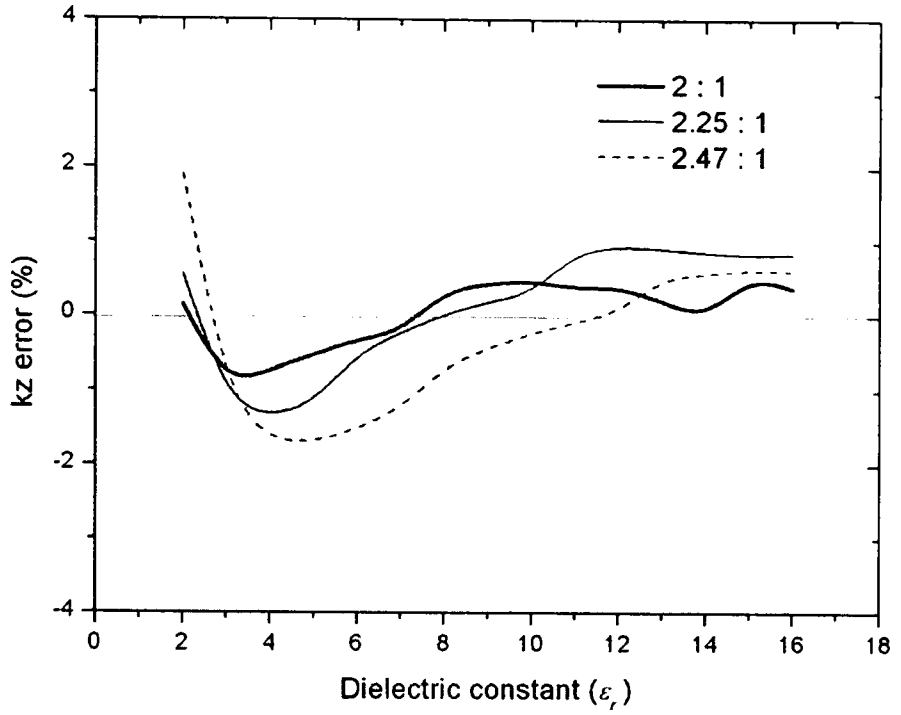

(c)

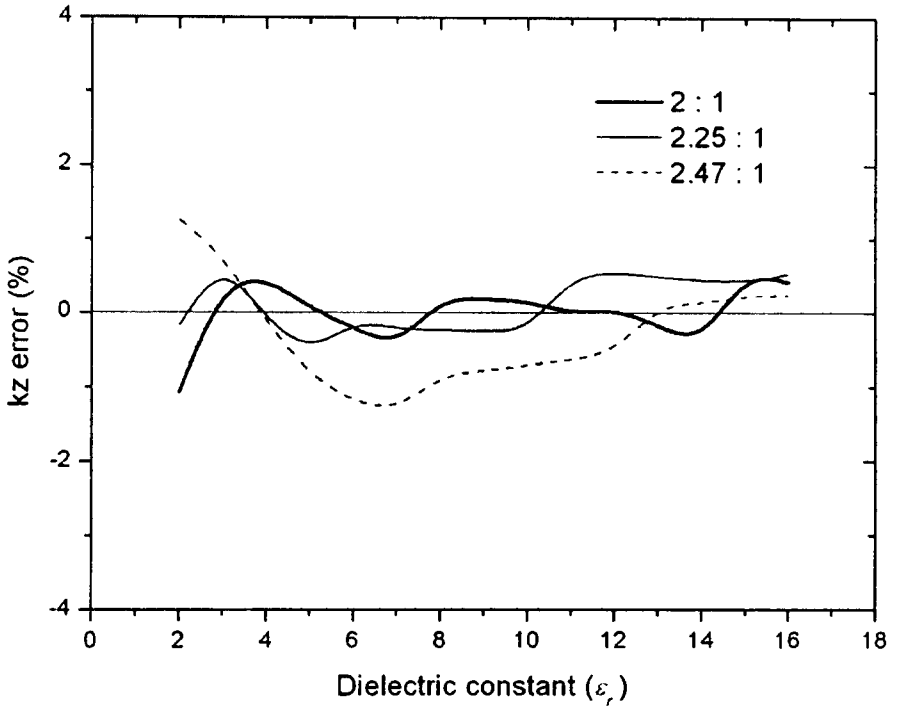

(d)

Figure 7.4 Typical worst case difference between kz_f_H calculated by the new formula (7-3) incorporating the frequency values derived using (c) the Marcatili formulas and (d) by the new formula (7-1).

7.3.5.3 Error for standard aspect ratios

Interestingly, if the coefficients for an exactly 2:1 aspect ratio are chosen to represent all aspect ratios from 2:1 to 2.47:1, then the worst-case error for the calculated single-mode frequency range will be between 7% (εr = 16) and 10% high (εr = 2), and the k_z error 16.4% and 10.3% low respectively. Of course, these worst-case errors are for the 2.47:1 aspect.

7.3.6 New waveguide specification table

Chapter 5 described why it was not possible to create a set of standard waveguide specifications for dielectric waveguides, as available for the metal waveguides. The biggest reason is the material dependency. However, the new formulas effectively now make this achievable. Chapter 6 demonstrated that the 2:1 aspect ratio represents a compromise between the advantages and disadvantages of the other aspect ratios studied in this work. Here, it is proposed that such a table could be constructed with the standard frequency range being represented by the fL and fH coefficients for the respective aspect ratio for every standard size waveguide, as shown in Appendix F.

The standard metal waveguide chart also includes the dB loss. For the dielectric version, the loss is of course material dependent and so it is not practical or necessary to include it in the new table. Since, the propagation constant is of interest in dielectric guides, and a new compact formula is now available, the relevant coefficients are also included in the new table. The relevant formulas are (7-1) to (7-3) and (7-4) or (7-5).

Some justification for using standard guide sizes was given in section 5.3. For example, that sizes must be decided in order to create standards, and that the existing standards sizes are well known and have been shown to cover a contiguous part of the frequency spectrum. Figure 5.2 demonstrated part of the frequency overlap and Appendix G shows the full range.

However, it could also be argued that the slight deviations from the 2:1 aspect are essentially unnecessary and that it would make more sense to simply use the exact 2:1 aspect. The same argument was perhaps had when the standard guides were defined. It is not clear but from an analysis of the standard chart, it looks like the precise dimensions were decided to neatly align the frequency ranges of alternate size guides. If that is the case, then the same justification cannot be applied to dielectric guides because the range is material dependent and so could not be aligned neatly for more than one material, even it were possible.

7.4 *Expressions suitable for all guide configurations*

7.4.1 Change of normalizing factors

The normalisation factors have, to this point, been validated for the standard aspect ratios and a completely open guide type. The final goal is to derive formula for all aspect ratios and guide types studied in the previous chapter. These combinations represent the widest practical range, and so the same procedures described above were used to find formulas to represent all of them.

As it turns out, normalisation factors derived for the standard waveguide sizes above were not optimum for the other aspect ratios. After further analysis, $fH*b*Er^{1.5}$ and $Er^{0.5}*kz / k_0$ were found to be suitable compromises and the resulting straight lines are shown in Figures 7.5 and 7.6 as verification. The bend in the curve seen in Figure 7.1 at around $\varepsilon r = 3$ is evident in Figure 7.5 to about the same extent. The actual lines are again essentially straight otherwise and the error is expected to be within about ±2% again.

However, the propagation constant curves have more curvature than before, and this can be seen to increase with aspect ratio in Figure 7.6. The level of curvature for the open 2:1 guide has already been seen from Figure 7.2(a) for this new best-fit normalisation factor.

Here, it was decided that, although each individual aspect could definitely have its own independent and optimal normalisation factor, it would be better to have a single best-fit normalisation factor so that one formula fits all the guide combinations. In this case, the propagation constant error has not been quantified. However, as a rough guide and from inspection, it peaks at approximately ±1% for 1:1, ±2% for 2:1, ±5% for 5:1 and ±10% for 10:1 near the centre of the εr range. Here, a larger error is traded for simplicity but there is definitely scope for manually averaging out the error. This can be done by drawing the perfect straight line through intermediate points on the curve to get the best fit rather than through the

endpoints, which was done primarily done for speed. In that case, the error will likely be just a few percent over most of the range.

The straight line coefficients were captured for the curves shown in Figure 7.5 and 7.6, and the normalisation factors were added to create the formulas, which take the same form as before. These are listed in Table 7.2.

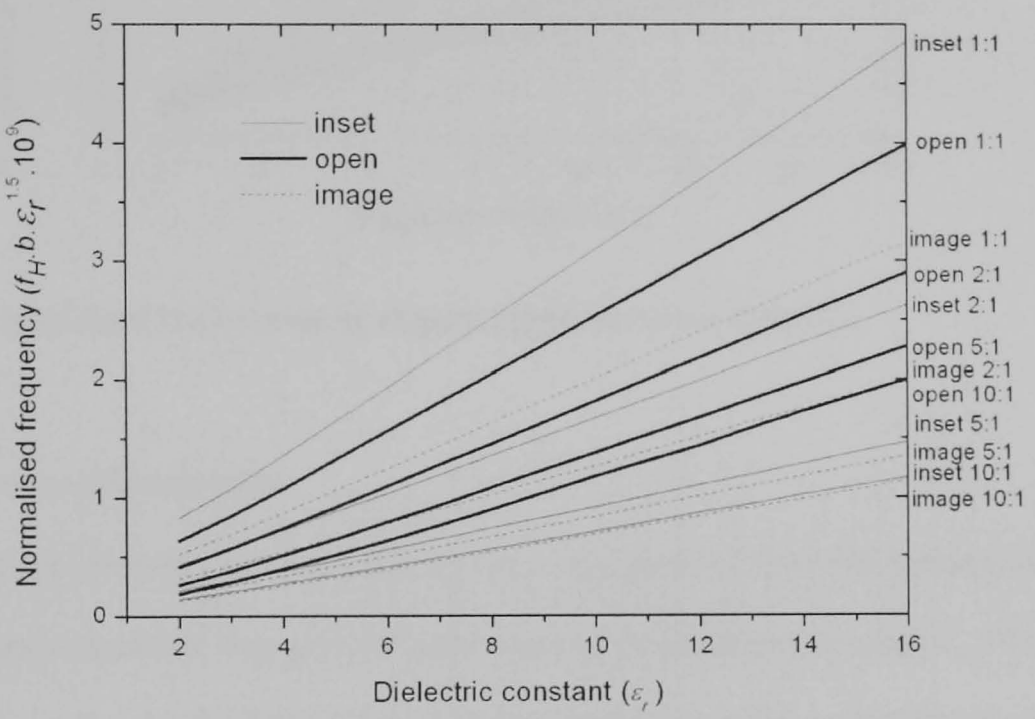

Figure 7.5 Normalized *f*b* curves for all guide combinations and material εr.

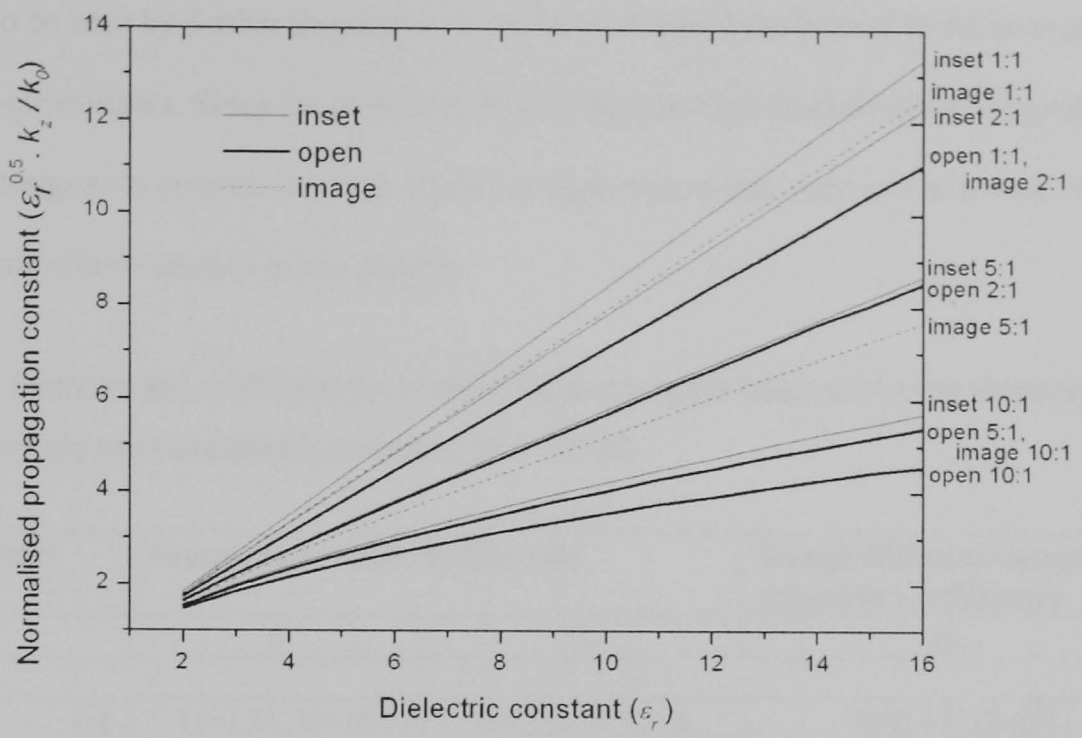

Figure 7.6 Normalized kz / k_0 curves for all guide combinations and material εr.

7.4.2 New coefficients table

The equivalence between an open guide and an image guide of twice the aspect is well known from a guide perspective; they give the same value of propagation constant [8]. This equivalence can be seen in Table 7.2 for both the image 2:1 / open 1:1 and the image 10:1 / open 5:1 coefficients. The frequency coefficients for the image guides are twice that of their open guide equivalents and the propagation constant coefficients are the same. The same equivalence was seen in the relative guide bandwidths plot of Figure 6.10 and the rate of change of propagation constant in Figure 6.13. This all gives further validation of the methods used in the current work.

This raises an interesting possibility: coefficients for a 2.5:1 open guide can be found by doubling the 5:1 image guide frequency coefficients and taking the image guide propagation constant coefficients. Equally, it is valid to find coefficients for a 20:1 image guide from the 10:1 open guide coefficients. However, it was already shown that there is little benefit to be gained from aspects greater than 10:1, and this will be demonstrated again next.

It can also be seen by further inspection of the last column of the table that the inset guide has no such equivalences. Since the plots presented in the previous chapter allow the guide or antenna designer to determine which guide configuration to use, only one or two of the coefficients will be needed in any design.

Table 7.2 Formulas and coefficients for all aspect ratios and guide type, valid for any dielectric guide height b and any value of dielectric constant εr from 2 to 16.

Aspect ratio ***a:b***	**Frequency range coefficients**		**Longitudinal propagation constant coefficients**
	f_L	f_H	kz_{fH}
Open			
1:1	U=174, V=16	U=239, V=156	P=0.67, Q=0.4
2:1	U=154, V=-35	U=177, V=61	P=0.49, Q=0.66
5:1	U=131, V=-25	U=143, V=-27	P=0.28, Q=0.98
10:1	U=117, V=-98	U=129, V=-70	P=0.22, Q=1
Image			
1:1	U=105 V=37	U=187, V=149	P=0.76, Q=0.26
2:1	U=87, V=8.7	U=120, V=76	P=0.67, Q=0.39
5:1	U=74, V=-2.2	U=83, V=17	P=0.43, Q=0.75
10:1	U=67, V=-41	U=72, V=-13.5	P=0.27, Q=0.97
Inset			
1:1	U=164, V=133	U=287, V=252	P=0.82, Q=0.19
2:1	U=103, V=60	U=155, V=127	P=0.75, Q=0.28
5:1	U=77, V=-2.5	U=89, V=39	P=0.5, Q=0.65
10:1	U=68, V=-31	U=73, V=-2.5	P=0.3, Q=0.95

$$f_{L,H} = \frac{(U\varepsilon_r + V)\times 10^6}{b\varepsilon_r\sqrt{\varepsilon_r}} \quad (7\text{-}1b) \qquad kz_{fL} = \frac{2\pi f_L}{c} \quad (7\text{-}2b) \qquad kz_{fH} = \frac{2\pi f_H}{c\sqrt{\varepsilon_r}}(P\varepsilon_r + Q) \quad (7\text{-}3b)$$

b is the dielectric waveguide height in mm
ε_r is the relative dielectric constant of the dielectric waveguide material
c is the speed of light, approximately $299.79\text{x}10^6$m/s

7.4.3 Intermediate aspects

Although the choices of aspect ratio taken in this work were shown to cover a large practical range, it is interesting to consider intermediate aspects. To begin with, the frequency coefficients U and V were plotted versus the aspect ratios in Figure 7.7.

Again, the benefits of increasing the aspect ratio can be seen to diminish beyond 10:1 for the important *U* coefficient, and especially for the image and inset guide types. The slopes of the curves between the actual data points have been filled in by the graphing program. However, for the slopes between the 1:1 and 2:1 aspects and the 5:1 and 10:1 aspect, there is little scope for error in this curvature and so those curves are assumed to be accurate and suitable coefficients for intermediate aspects e.g. 1.5:1 can therefore be read off. In fact, a linear interpolation could be taken between the frequency coefficients in Table 7.2 without introducing significant error.

For the curves between the 2:1 and 5:1 aspect there is potentially scope for incorrect curvature because those segments contains the transition from a steep slope to a shallow slope. Fortunately, there is one test that can be used without generating data for an intermediate aspect: the 2.5:1 open guide aspect can be obtained by doubling the 5:1 image *U* coefficients to 148 and 166 to check the position of the *fL* and *fH* curves at that important juncture. It can be seen from inspection that the curves are quite close at those points for the open guide case. There is greater scope for error in the inset case, but this has not been checked and the associated curve segments are assumed to be close enough.

Under certain circumstances the *V* coefficients can be ignored when only a rough approximation is required. This is obviously the case when the *V* coefficient is low compared to *U*. and as $\varepsilon r \rightarrow 16$.

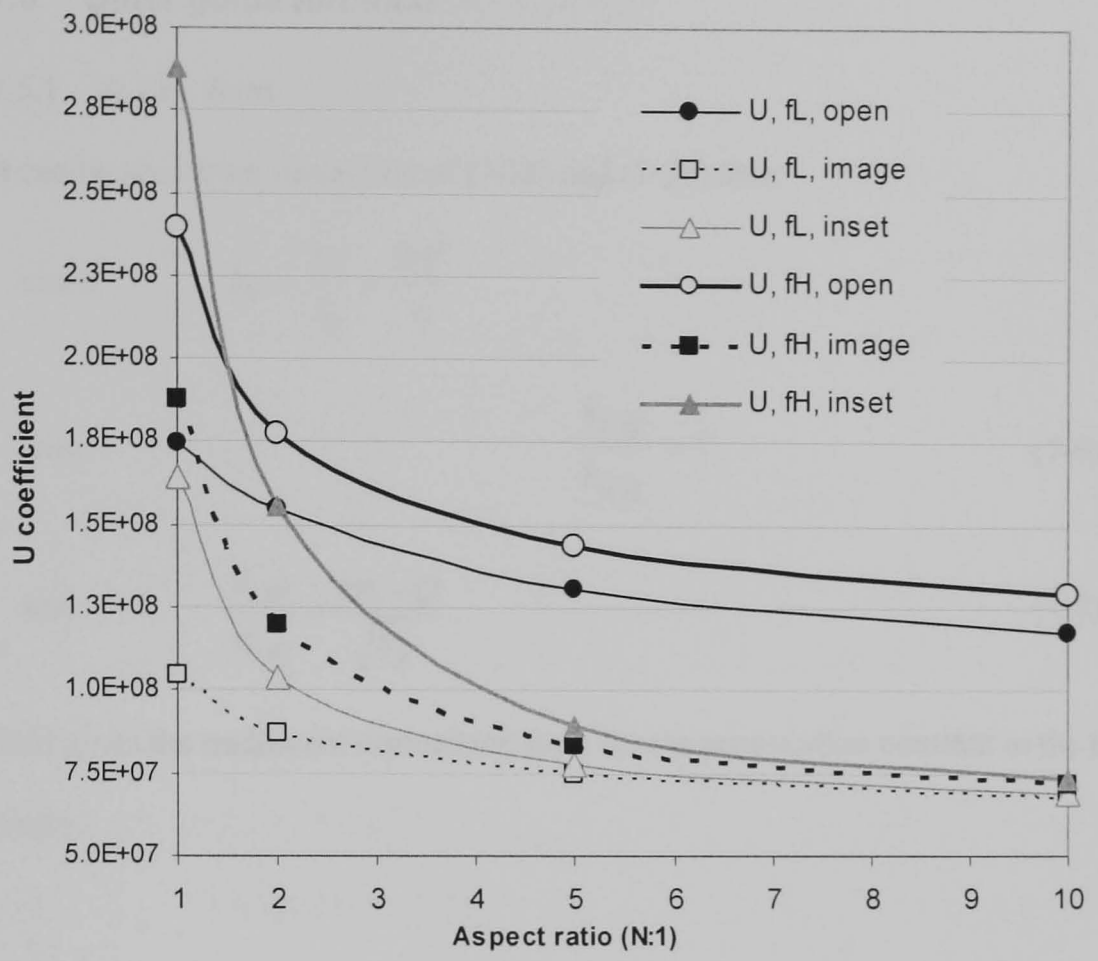

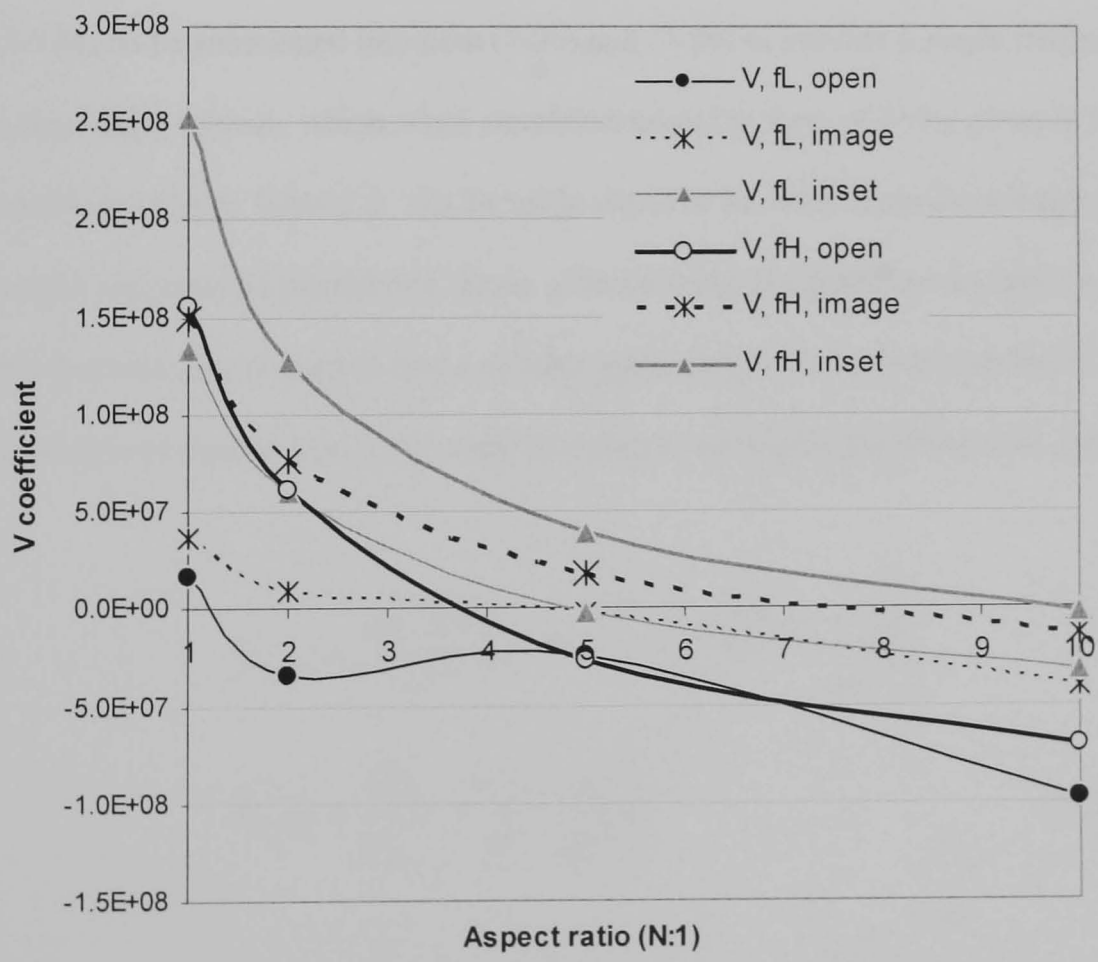

Figure 7.7 U and V frequency limit coefficients for (7-1b) for all aspect ratios and guide type, valid for any dielectric guide height b and any value of dielectric constant εr from 2 to 16.

7.5 *Other guide formulas*

7.5.1 k_z / k_0 form

It can be seen from inspection of (7-2b) and (7-2b) that:

since $$k_0 = \frac{2\pi}{\lambda_0} = \frac{2\pi f}{c}$$

then $$\frac{k_{z\,fL}}{k_{0\,fL}} = 1 \qquad (7\text{-}6)$$

and $$\frac{k_{z\,fH}}{k_{0\,fH}} = \frac{P\varepsilon_r + Q}{\sqrt{\varepsilon_r}} \qquad (7\text{-}7)$$

This gives the traditional normalized form for the propagation constant at the two frequency limits.

7.5.2 Frequency independent kz form

(7-1b) can be substituted into both (7-2b) and (7-3b) to provide a single frequency independent formula which when simplified takes the form of (7-8), given in terms of the coefficients from Table 7.2. The kz range can then be found from knowledge of the guide height and material permittivity alone. Alternatively, if a particular kz range is the goal, then this formula can be used to find a suitable guide height for a given material or vice-versa. A new table of coefficients XYZ could be constructed to give the alternative form (7-8b).

$$k_{z\,fH} = \frac{2\pi.10^6}{c.b}\left[U.P + \frac{(V.P + Q.U)}{\varepsilon r} + \frac{V.Q}{\varepsilon r^2}\right] \qquad (7\text{-}8)$$

$$k_{z\,fH} = \frac{1}{b}\left[X + \frac{Y}{\varepsilon r} + \frac{Z}{\varepsilon r^2}\right] \qquad (7\text{-}8b)$$

where $X = \frac{2\pi}{c}U.P.10^6$ $Y = \frac{2\pi}{c}(V.P + Q.U).10^6$ $Z = \frac{2\pi}{c}V.Q.10^6$

7.6 *New leaky wave antenna formulas*

7.6.1 New beam angle formulas

The formula for the determination of the main beam angle is well-known, and is repeated in its various forms in (7-9) for convenience. Of course, ordinarily, the difficult to find parameter is kz. However, now that a very compact closed form solution has been found, it is possible to substitute it directly into the angle formula to give formulas that derive the main beam angle at the low frequency (7-10) and the high frequency (7-11). They are simple enough to enter directly into a simple calculator and can be used to find the scan range directly, provided that the angle does not reach the 0° and 180° end limits. If the 180° limit is reached before the low frequency limit, as demonstrated in Figure 7.8, it is possible to find the hypothetical angle by adding 90° to the L.H.S and 1 to the R.H.S of (7.9) or (7-10). For the 0° limit, it is possible to subtract 90° and subtract 1. This might be done to see how far the strip grating spacing parameter d has moved the complete angular scan.

$$\cos\theta = \frac{\lambda_o}{\lambda_g} + \frac{n\lambda_o}{d} \qquad \cos\theta = \frac{k_z}{k_o} + \frac{2n\pi}{k_o d} \qquad \cos\theta = \frac{k_z c}{2\pi f_o} + \frac{nc}{f_o d} \tag{7-9}$$

Substituting (7-6) and (7-7) into (7-9):

$$\cos\theta_{fL} = 1 + \frac{nc}{f_L d} \qquad \cos\theta_{fL} = 1 + \frac{ncb\varepsilon_r^{\frac{3}{2}}}{(U\varepsilon_r + V)\times 10^6 d} \tag{7-10}$$

$$\cos\theta_{fH} = \frac{k_{z\,fH}}{k_{0\,fH}} + \frac{nc}{f_H d} \qquad \cos\theta_{fH} = \frac{P\varepsilon_r + Q}{\sqrt{\varepsilon_r}} + \frac{ncb\varepsilon_r^{\frac{3}{2}}}{(U\varepsilon_r + V)\times 10^6 d} \tag{7-11}$$

where n is the nth radiated harmonic and the main harmonic is $n = -1$.

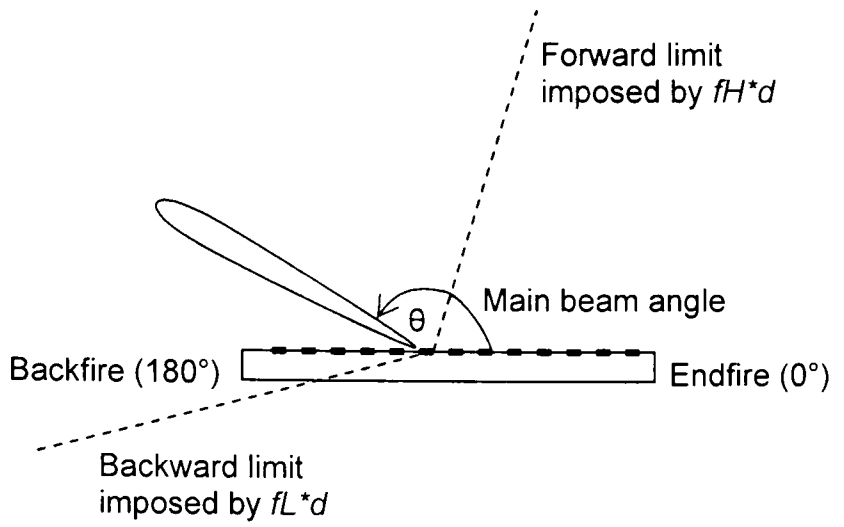

Figure 7.8 Demonstrates main beam angle scan sector with a hypothetical backward limit that exceeds the physical 180 degree limit.

7.6.2 Scanning limits formulas

The conditions that cause the antenna to point its main beam at either of the physical scan limits can be found by letting the L.H.S of (7-9) to (7-11) equal ±1. Solving for the operating frequency and strip spacing that leads to this condition:

$$\pm 1 = 1 + \frac{nc}{f_L d} \qquad \text{so} \qquad f_L d = \frac{-nc}{2} \quad \text{(or infinity)} \qquad (7\text{-}12)$$

$$\pm 1 = \frac{k_{z\,fH}}{k_{0\,fH}} + \frac{nc}{f_H d} \qquad \text{so} \qquad f_H d = \frac{-nc}{(s+1)} \text{ or } \frac{nc}{(1-s)} \qquad (7\text{-}13)$$

where $s = \dfrac{k_{z\,fH}}{k_{0\,fH}}$ is given by (7-7) and fL and fH are given by (7-1b).

It can be seen that (7-13) reduces to (7-12) when $s = 1$. For $s > 1$ and n = -1, which is the usual case for radiation, the $nc/(1\text{-}s)$ form must be used.

7.6.3 Grating limits formulas

The limit formula (7-13) above becomes the equivalent of the well-known grating lobe formula (4-1) when $n = -2$ and $s > 1$ (7-14).

$$f_H d = \frac{2c}{(s+1)} \qquad (7\text{-}14)$$

Chapter 4 demonstrated that it only detects the grating when it becomes a maxima, and could both be considered as somewhat inaccurate because the grating starts earlier, or safe. The other well-know formula (2-4) was also shown to overcompensate. The actual conditions for the onset of a grating lobe lay somewhere between those predicted by (7-14) and those predicted by (2-4). The only way of deriving this point accurately is to plot the radiation pattern using the array factor (2-1) and adjust the conditions until the grating lobe appears / disappears. However, (7-14) is a good starting point.

7.7 Examples

7.7.1 Guide design

A rectangular dielectric waveguide made of Quartz Teflon of $\varepsilon r = 2.47$ is required to operate over as wide a band as possible, up to an operating frequency $f_o = 65$ GHz. The guide cross-section should not be so small as impossible to machine from a block of material and the antenna should only radiate a single main beam. Define the guide dimensions, assuming that a suitable guide length L is a minimum of 20 guide wavelengths at 60GHz, which will be the primary operating frequency, and ensuring that all these operating frequencies are well within the single-mode range. State the guide wavelength at the limits of the useful single-mode range.

Solution - Chapter 6 demonstrated the relative characteristics of the various guide combinations studied in this work. In particular, in section 6.4.3, it was shown that the image guide has the highest bandwidth of all. The image guide also satisfies the requirement for a single beam. Choosing the high frequency to be $f_H = 65$GHz will put this well within the single-mode range because, in this work, f_H has been fixed at 5% below the first higher mode cutoff frequency, as per metal waveguides. Now, using (7-1b) and the coefficients for a 1:1 aspect ratio image guide from Table 7.2:

$$f_H \times b = \frac{(187\varepsilon_r + 149)\times 10^6}{\varepsilon_r^{1.5}} = 157.37\times 10^6$$

Therefore, at 65GHz, the required guide height b is: $$b = \frac{157.37\times 10^6}{65\times 10^9} = 2.42mm$$

Clearly, this cross-section will be fragile and therefore difficult to machine successfully. In order to increase its size, some bandwidth might have to be sacrificed. The 1:1 inset guide has the next highest bandwidth, and since its coefficients are much higher than its image counterpart, it will naturally produce a higher $f*b$ value, and so for the same frequency will be correspondingly bigger. Recalculating using the inset guide coefficients:

$$f_H \times b = \frac{(287\varepsilon_r + 252)\times 10^6}{\varepsilon_r^{1.5}} = 247.53\times 10^6 \quad \text{and} \quad b = \frac{247.53\times 10^6}{65\times 10^9} = 3.81mm$$

This value will be rounded up to b = 4mm, therefore a = 4mm. which is more robust. Quickly recalculating f_H for b = 4mm, 247.53x10^6 / 4x10^{-3} gives f_H = 61.88 GHz. This upper frequency is much lower than specified; therefore the original dimensions of 3.8 x 3.8 mm will be used.

Now, using (7-8b) and its associated high frequency coefficients to find kz at b = 3.8mm and εr = 2.47:

$$k_{z\,fH} = \frac{1}{b}\left[4.932 + \frac{5.474}{\varepsilon r} + \frac{1.003}{\varepsilon r^2}\right] = 1924 rad/m$$

Or 1881 rad/m if the the last term is neglected. Alternatively, using (7-3b):

$$k_{z\,fH} = \frac{2\pi f_H}{c\sqrt{\varepsilon_r}}(0.82\varepsilon_r + 0.19) = 1920 rad/m$$

At the low frequency, using (7-1b) and (7-2b):

$$f_L = \frac{(164\varepsilon_r + 133)\times 10^6}{b\varepsilon_r^{1.5}} = 36.5GHz \quad \text{therefore} \quad k_{z\,fL} = 7645 rad/m$$

To find kz and the guide wavelength at 60 GHz, first the rate of change of kz must be found using (5-2):

$$\delta kz = \frac{\Delta kz}{\Delta f} = \frac{1922 - 764.5}{65 - 36.5} = 35.09$$

Then the interpolation / projection formula (7-5) is used. The number of gigahertz δf between f_H and the primary operating frequency f_o is 5, therefore kz is:

$$k_{zo} = 1922 - (\delta f \times \delta kz) = 1746.5 rad/s$$

Finally, using (5-1) for the guide wavelengths gives:

λ_{gfL} = 8.22 mm

λ_{gfH} = 3.27 mm

λ_{go} = 3.6 mm, therefore $L = 20\lambda_g$ = 72 mm

A suitable guide size is therefore 3.8mm high x 3.8mm wide x 72mm long.

7.8 *Validation and application*

Although the present results are effectively derived from the independently proven Marcatili formulas, and have been shown to produce results to within one or two percent of Marcatili's, it is appropriate to test them against published theoretical and experimental works.

7.8.1 Validating against existing LWA works

Mittra [9] used the well known but rigorous spectral domain method to compute the radiation characteristics of a periodic leaky-wave antenna (LWA) built around a 2:1 aspect ratio open dielectric waveguide. In Example-1, the same physical characteristics are entered into the new formulas to check that the operating frequency is within the single-mode range and find and compare the radiated beam angle for the antenna. The results show even better agreement with their experimental results than the spectral domain method.

Kobayashi [10] published experimental results for a LWA based on a WG26 size dielectric waveguide. Example-2 compares these results with those calculated using the present method, based on the same inputs. Here, the agreement is quite good, showing 5% error.

***Example** 1: $f = 80$ GHz, $a = 3$ mm, $b = 1.4465$ mm, $\varepsilon r = 2.46$, $d = 2.5$ mm*

The new equations employed and the coefficients for a 2:1 aspect ratio from Table 7.1 produce: f_L =61.15 GHz, f_H = 87.51 GHz, $k_{z\,fL}$ = 1280 and $k_{z\,GHz}$ = 34.6. At 80 GHz, $k_z = f_L + k_{z\,GHz}(f - f_L)$ = 1932, equivalent to a guide wavelength (λ_g) of 3.25 mm. Using (2-2) gives a beam angle (θ) in the E-plane 101° from the end fire direction. Mittra predicts an angle of 103° by the rigorous spectral domain method and finds 98 degs by experiment [9].

***Example** 2: $f = 81.5$ GHz, $a = 3.1$ mm, $b = 1.55$ mm, $\varepsilon r = 2.33$, d = 2.09 mm*

At 81.5 GHz, k_z = 1992.3 and $\lambda_g = 2\pi/k_z$ = 3.154 mm, giving θ = 126.42°. Kobayashi finds θ =120° by experiment [10].

7.9 Conclusions

Existing methods for obtaining the guide characteristics of dielectric guides are extremely rigorous, and usually very structure dependent, as detailed in Chapter 5 section 5.2. In general, even the most rigorous methods turn out to provide only an approximation to experimental results [11] to [13]. The great lack of understandable information, vast number of possible guide configurations, the difficulty of deriving their guiding characteristics, and the fact that the field is not fully contained and can easily be perturbed are perhaps some of the reasons why dielectric guides have not been used as much as their metal counterparts commercially. This is despite the fact that various authors have demonstrated their potential, especially for use at millimetre-wave frequencies [6, 7, 14, 15]. The method by Marcatili, which has been referred to as a 'classic paper' due to the number of times it has been cited in scientific work [16], has been proven in practice to provide good enough accuracy in practice and amenable to use for a wide variety of structures, despite being much less rigorous [1, 3, 5, 7].

However, the Marcatili method still requires many thousands of iterations to solve for the cutoff frequencies of just a single dielectric guide configuration, for example. This in itself represents a significant programming and time burden for the designer, potentially in the order of a few months. However, in this work, that burden was accepted and his method was programmed and used the method to compute the useful frequency range, propagation constant, and other fundamental guide characteristics for tens of thousands of sample dielectric guide configurations.

A practical range of material dielectric constants, representing suitable available materials [15] was chosen, along with a practical range of guide cross section dimensions and a number of popular dielectric guide types to represent the guide samples for this task.

Attempts at normalising the data representing the resulting guide characteristics for each sample revealed an important and interesting feature that has effectively enabled these results to be presented in the new, simple, and intuitive to use graphical manner presented in chapters 5 and 6; it was found that the data could be normalised to make it guide-size independent when the guide cross-section was fixed to one of a finite number of practical aspect ratios. This same advantage was then applied to other guide types, including image, trapped and inset guides, and the normalised guide characteristics of each of these was also derived.

First of all, the data for all these guide combinations has been presented in a set of plots of the normalised data, from which the reader can:

- Find a first-order guide design and quantify the tradeoffs in terms of the most important guiding characteristics;
- See and quantify the advantages of using one material (permittivity) over another;
- See and quantify the advantages of using one guide type over another;
- See and quantify the advantages of using one aspect over the other;
- Select a combination of these to suit any given design requirement;
- Be able to make changes and immediately see and quantify the changes;
- Make informed choices about the best guide for the job.

Further normalisation allowed the data to be very accurately represented by simple closed-form formulas. Because some corrections have been made to the data, the accuracy of these formulas is equivalent to or better than derived directly using the Marcatili method.

These formulas are extremely simple in form and can be used to accurately derive the guide characteristics for *any* guide height, most practical non-magnetic and low loss dielectric materials, and a range of popular dielectric guide types. The results are found with a

calculator in just a few key presses, whereas the alternatives represent a very significant computer programming task.

The only restriction is that the aspect ratio must be within the range 1:1 to 10:1. It is presumed that for new designs, this restriction will be acceptable for three basic reasons:

1. This range of aspects represents the widest practical range;
2. The change in guide characteristics is negligible outside this range;
3. There is no practical reason why an alternative aspect would be chosen e.g. 4.8:1 instead of 5:1.

A table of coefficients for these formulas has been provided for each of these four aspects and all four guide types. It is expected that, once the plots have been used to select a suitable guide configuration, only a single (or small number) set of coefficients will be needed to make the precise calculations. It is interesting to point out that although the data is discrete; the new formulas are effectively continuous.

Many examples demonstrating the use of the new formulas have been given for guide design and leaky wave antenna dimensioning. These examples have demonstrated the simplicity and effectiveness of the new method.

It is now feasible that within just few minutes, the reader can use the new method to get all of the information needed to dimension a working leaky wave antenna based on any of the common guide configurations. This was the original motivation behind this work – to make the selection of the guide dimensions easier and to derive a simpler method to obtain the propagation constant, which is needed to dimension the antenna.

As a minimum, the chosen guide or guides will serve as the basis on which to begin a computer-aided numerical simulation / parametric study. This latter stage would have been

necessary even if the characteristics were derived from a more rigorous alternative method, so nothing has been lost by choosing an approximate method to form the basis of these studies.

Owing to the fact that the results have been derived for guide types where the guide walls are surrounded by either a metal plane or air, the new method is much more applicable to situations where the guides are to be used as standalone structures. The leaky wave antenna studied in this thesis is such a structure, but it can also be embedded in other structures provided that the embedded walls are metalized.

The results are less applicable to the case where the dielectric guide is integrated into a MMIC circuit, because the guide will then more likely be surrounded, at least partly, by another dielectric, and the guide characteristics will be different. However, a wave will primarily travel within the highest dielectric constant material [14], therefore in theory, when the guiding material permittivity is much higher than that of a surrounding dielectric, the new method should produce a useful approximation.

Finally, the author believes that the new method and associated formulas are now in a form suitable for inclusion in a general engineering electromagnetics textbook covering transmission and or antennas.

7.10 References

[1] H. Jacobs and M. M. Chrepta, "Electronic phase shifter for millimeter-wave semiconductor dielectric integrated circuits," *IEEE Trans. Microwave Theory and Techniques*, vol. MTT-22, no. 4, pp. 411–417, Apr. 1974.

[2] A. Basu and T. Itoh, "Dielectric waveguide-based leaky-wave antenna at 212 GHz," *IEEE Trans. Antennas and Propagation*, vol. 46, no. 11, pp. 1665-1673, Nov. 1998.

[3] T.N. Trinh, R. Mittra and R.J. Paleta, "Horn image-guide leaky-wave antenna," *IEEE Trans. Microwave Theory and Techniques*, vol. MTT-29, no. 12, pp. 1310-1314, Dec. 1981.

[4] K. L. Klohn, R. E. Horn, H. Jacobs and E. Freibergs, "Silicon waveguide frequency scanning linear array antenna," *IEEE Trans. Microwave Theory and Techniques*, vol. MTT-26, no. 10, pp. 764–773, Oct. 1978.

[5] R. E. Horn, H. Jacobs, E. Freibergs and K. L. Klohn, "Electronic modulated beam-steerable silicon waveguide array antenna," *IEEE Trans. Microwave Theory and Techniques*, vol. MTT-28, no. 6, pp. 647–653, Jun. 1980.

[6] T. Itoh and B. Adelseck, "Trapped image guide for millimeter-wave circuits," *IEEE Trans. Microwave Theory and Techniques*, vol. MTT-28, no. 12, pp. 1433-1436, Dec. 1980.

[7] H. Jacobs, G. Novick, C. M. LoCascio and M. M. Chrepta, "Measurement of guide wavelength in rectangular dielectric waveguide," *IEEE Trans. Microwave Theory and Techniques*, vol. MTT-24, no. 11, pp. 815–820, Nov. 1976.

[8] S.P. Schlesinger and D.D. King, "Dielectric image lines," *IRE Trans. Microwave Theory and Techniques*, vol. MTT-6, pp. 291-299, Jul.1958.

[9] R. Mittra and R. Kastner, "A spectral domain approach for computing the radiation characteristics of a leaky wave antenna for millimeter waves," *IEEE Trans. Antennas and Propagation*, vol. AP-29, no. 4, pp. 652–654, Jul. 1981.

[10] S. Kobayashi, R. Lampe, R. Mittra and S. Ray, "Dielectric rod leaky-wave antennas for millimeter-wave applications," *IEEE Trans. Antennas and Propagation*, vol. AP-29, no. 5, pp. 822–824, Sep. 1981.

[11] J. Encinar, "Analysis and CAD techniques for periodic leaky-wave printed antennas: numerical and experimental results," International journal of Microwave and Millimetre-wave Computer-aided Engineering, vol. 4, no 1, pp. 88, 99. 1994.

[12] J. Jacobsen, "Analytical, numerical, and experimental investigation of guided waves on a periodically strip-loaded dielectric slab," *IEEE Trans. Antennas and Propagation*, vol. AP-18, no. 3, pp. 379-388, May. 1970.

[13] J. Encinar, "Mode-matching and pont-matching techniques applied to the analysis of metal-strip-loaded dielectric antennas," *IEEE Trans. Antennas and Propagation*, vol. 38, no. 9, pp. 1405-1412, Sep. 1990.

[14] W.V. McLevige, T. Itoh and R. Mittra, "New waveguide structures for millimeter-wave and optical integrated circuits," *IEEE Trans. Microwave Theory and Techniques*, vol. MTT-23, no. 10, pp. 788-794, Oct. 1975.

[15] F Schwering and A.A. Oliner, *Millimeter-wave antennas* in Antenna Handbook, Eds. Y.T. Lo and S.W. Lee, Van Nostrand Reinhold, New York, Chapter 17, 1988..

[16] E. A. J. Marcatili, "*Current Content*," Citation Classic number 21, May 21st, 1979.

8 DETERMINING ANTENNA CHARACTERISTICS

8.1 Introduction

8.1.1 Recent improvements in the theory of LWA radiation pattern control

In his very well cited but rarely implemented publication [1], the author pointed to the proceedings of a European Microwave conference in which Oliner et. al described the difficulty in independently controlling the phase and leakage constants of this type of antenna, and outlined an improvement. Ideally, the leakage would be shaped along the length of the antenna to achieve a desired field distribution that leads to a desired (probably low sidelobe level) radiation pattern.

The problem centred on the consequences of implementing control over this leakage constant, which is a function of the guide geometry and material permittivity, metal strip grating geometry and excitation frequency. One of these consequences is that the phase constant of the guided wave is modified, albeit very slightly, by the addition of the strips and, in particular, the width of these strips. They also noted that neglecting this variation in phase constant leads to degradation of the radiation pattern.

8.1.2 Most recent improvement

The improvement that the latter author published was an improvement in the procedure to automatically compensate for this change in phase constant; by making adjustments to the strip width and strip spacing. However, no detail about the procedure or proof was provided. In a later journal paper by the same author [2], a larger discussion and theoretical evidence was presented for a single antenna design i.e. one case, but no experimental results were provided, except to say that the experimental results showed no better sidelobe performance than that of the excitation waveguide. In other words, the experimental results showed none of the performance improvements described theoretically. This recent paper does though provide great insight into a number of other issues, especially the fact that the incorporation of higher spectral harmonics in numerical modelling degrades the theoretical sidelobe level

improvements brought about by ideal amplitude distributions designed upon the single main harmonic. This inclusion theoretically brings the theoretical radiation patterns closer to experimental ones in the sidelobe regions for this type of antenna. It should be said at this point that, although no theoretical radiation pattern exactly matches the experimental one in the sidelobe regions, such published improvement procedures do generally give some sidelobe level reduction. However, the improvement is usually much less than predicted.

8.1.3 Objectives

The consequences of the failure to implement such a strip spacing compensation procedure will be fully described and quantified using a new perturbation model in this present chapter. It will also be demonstrated how this change in phase constant can be modelled using well-known linear array theory. The new model will be used to quantify and compensate for these consequential effects for a larger number of cases and it will be shown how to tailor the model to any other case, including for the simple empirical strip width taper relation [3,4]. Results from the new model will be validated by comparing with HFSS simulation results for the same antenna designs, and against other published results. Finally, experiments will be carried out on a real antenna design to test the accuracy of the new model.

8.2 Problem Description

8.2.1 Overview

The existing compensation procedure has been cited many times [5,6] but never implemented in subsequent work on this type of antenna. Perhaps this was because it requires a significant amount of extra effort to add it to a numerical implementation, or that the true impact has not been fully presented and is perhaps not well understood.

8.2.2 Explanation

Although the problem has not been described very well by previous authors, the situation is relatively simple to explain as follows:

1. Introducing a finite size strip grating to the surface of dielectric waveguide presents an impenetrable boundary to the field on that particular guide wall. This causes a proportional change in the phase constant part of the longitudinal propagation constant k_z, often also expressed as β_0. By definition, the propagation constant β_0 or k_z is the rate of change of phase of the travelling wave. This wave is then described as *perturbed*. The associated propagation constant could also be described as being perturbed;
2. This change is directly proportional to the strip dimensions, but primarily the strip width W in the longitudinal direction. Here it is assumed that the length L of the strips is constant and extends across the full width a of the dielectric waveguide. In general, the strip length should be as long as possible to minimise the beamwidth in the H-plane (XY or Phi-plane), assuming that highest directivity is the goal. The strip thickness has been shown to have negligible affect on β_0 [6,7], therefore it is nor relevant here;
3. The phase difference between adjacent strip grating elements determines the angular direction of the main beam, in exactly the same way as for a phase-steered linear array antenna. If the rate of change of phase k_z is changed in a single unit cell, between the centres of two adjacent strips finite distance d apart, then the phase difference ($k_z d$) between these two elements also changes.

4. If the phase change between elements increases as a constant along the whole length of the antenna e.g. 5°, 10°, 15° etc., the radiation contributed by the individual elements will all point in the same direction, leading to a single main beam in the same direction. Such a progressive phase change dictates that the strip width be constant across all elements [8], or that the spacing is adjusted accordingly if the strip width is varied.
5. However, in many previous works the strips are arranged with a constant spacing *d* based on the wave being unperturbed [3,9,10,11]. In these cases it is assumed that the perturbation is small enough to be neglected. In many cases, this simplification was fit for the purpose of that work. In reality, the addition of finite width strips can cause a very significant change in propagation constant and therefore a proportional change in the phase difference and main beam angle, away from the designed value. These changes amount to errors because existing formulas (2-1) to (2-4) neglect the strip width.
6. However, if the strip width is a constant for all strip elements, then the phase error is constant and can be eliminated by decreasing the spacing *d* accordingly (by a constant) along the length of the antenna. This is done to achieve the required phase difference for the associated *designed* beam angle. This is the simple spacing compensation case.
7. The next case is when the strip width is varied along the length of the guide. In this case, neglecting the change in phase causes the phase difference to vary between adjacent strip elements and, as the previous authors pointed out, this leads to pattern degradation [2]. This is potentially caused by the individual elements radiating at slightly different angles. Of course, to compensate for this non-constant phase change, each adjacent pair of strip elements must have their spacing compensated individually in each unit cell to achieve a constant phase between strip centres, so that all the elements radiate at the same angle.
8. The existing formulas (2-1) to (2-4) can therefore be improved to take the finite strip width into account simply by using the adjusted strip spacing *d*.

8.2.3 Working in terms of physical parameters

These previous authors talk about this issue of slight change in propagation constant in terms of it being a function of the leakage constant α., which is extremely difficult to obtain both mathematically and experimentally. While this is true, it is only by virtue of the fact that the leakage constant is, in turn, controlled predominantly by the physical strip geometry and the strip width in particular. In the new model, developed next, it is this physical width that is used, rather than the resulting leakage. Many authors have shown both theoretically and experimentally that the leakage constant is a strong function of the strip width [3,5,12,13] and this is taken as justification of the theory used here. Using the physical strip width rather than its associated leakage constant also makes the problem amenable to study using linear phased array theory, as will be seen in the remainder of this chapter.

8.3 *New perturbed dielectric guide model*

8.3.1 Unperturbed model

As per bullet point 5 above, many previous works have assumed no perturbation of the travelling wave. In that case, a single unit cell of the model generally used is shown in Figure 8.1(a). From a propagation constant point of view, the model is treated as an entirely open guide; a dielectric guide with no continuous metal boundary on any of its sidewalls. All additional unit cells are identical from a guide perspective, except for the fact that the width *W* of the metal strip grating may vary. If the width is varied smoothly, increasing or decreasing it by some function, it is generally known as strip width tapering [14]. Independent of the strip width, this model uses the unperturbed longitudinal propagation constant kz_{open} for every unit cell as if the strips were not present (or infinitely narrow).

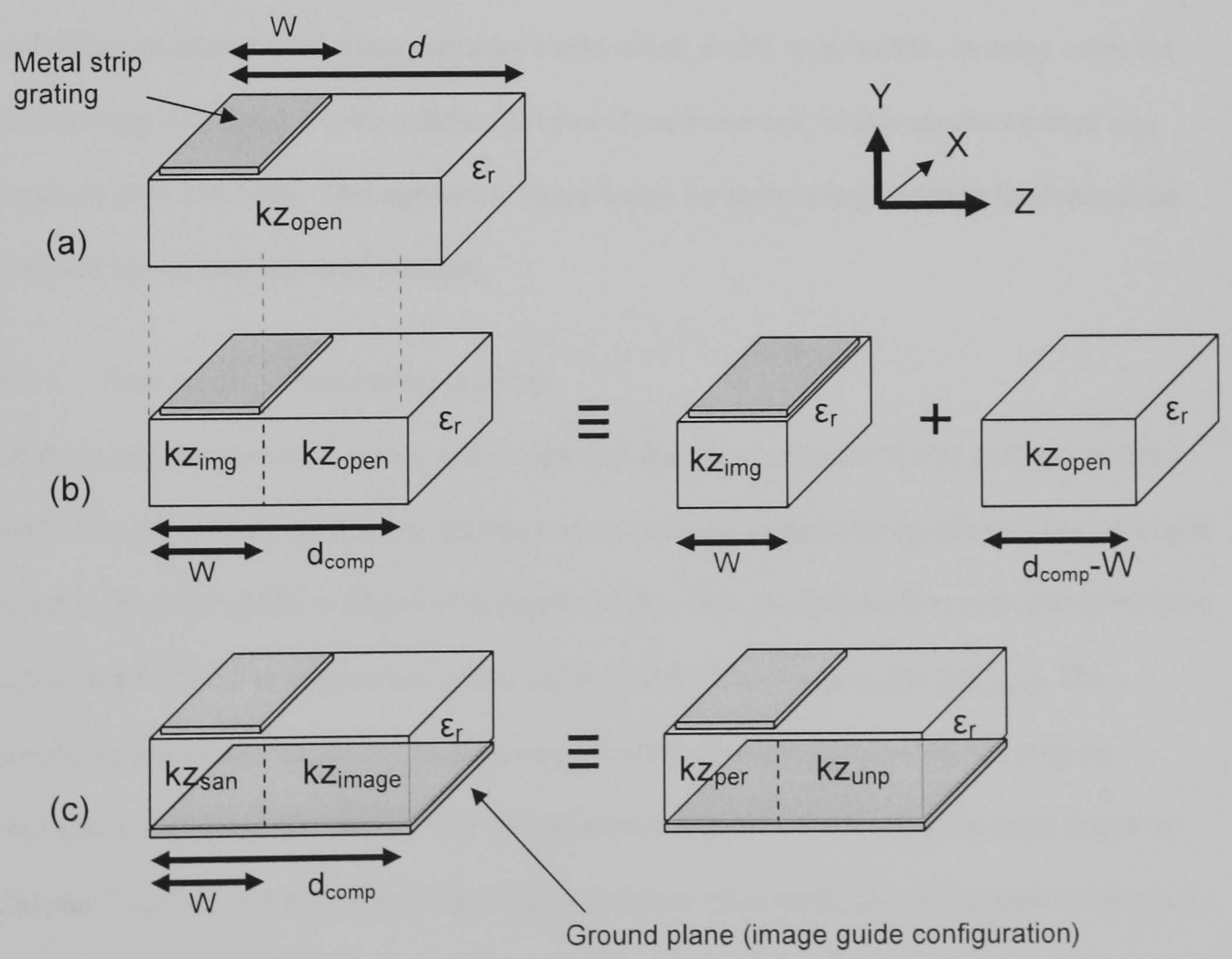

Figure 8.1 Dielectric guide section models (a) assumes no perturbation of wave (b) considers perturbation and adjusts spacing *d* to d_{comp} (c) considers perturbation for a different structure.

8.3.2 Useful range of strip widths

As demonstrated in Chapter 4 and in other publications [3,4], relatively narrow strips compared to the longitudinal guide wavelength in the order of $<0.2\lambda g$ radiate poorly. Further, the radiation per unit cell increases quite linearly and starts to peak at about $0.4\lambda g$, thereafter rolling off and decreasing at a similar rate to which it increased. This fact is also very well demonstrated for one example in [15]. In other words, the strip widths are likely to be far from negligible under real circumstances and model (a) is inadequate.

8.3.3 Practical strip coverage

If first of all, the case is studied where the antenna is to radiate approximately normal to the top and bottom surface, known as broadside, then it can be seen by inspection of (7-9) that the unit cell spacing d must equal one guided wavelength ($d \sim \lambda g$). This implies that in general, and taking guidance from these previous works about useful strip widths, in many cases the strip grating will cover a quite substantial area of each unit cell of waveguide section; say, between 20% and 50%. This appears to leave scope for quite a large change in propagation constant by the strip-covered sections.

8.3.4 New model incorporating speedup

Of great importance to this new model is the fact that these substantial size sections of open guide that are covered by the strip gratings are effectively image waveguide sections of length equal to the strip width, as depicted in Figure 8.1(b). This covered section must therefore have a different value of propagation constant equal to that of an image guide (kz_{image}). The remaining uncovered section of each unit cell is still considered an open guide with its propagation constant unchanged. The propagation constants of image guides were found in Chapter 7 earlier, and the formulas presented there, or other methods, can be used to obtain it. For the same size guide and the same material, it is now easy to show that the propagation constant of the image section is speeded up compared to the open section.

8.3.5 New model support for other dielectric guide types

Other guide configurations can be considered in the same way, such as that shown in Figure 8.1(c), where the guide is a perturbed image guide, and the perturbing strips effectively create sandwich sections and image guide sections.

8.3.6 Considering strip length

In this model, it is assumed that the strip extends across the full width of the guide so that the whole sidewall of the image guide section is covered in conductor. Very small departures from this situation in the order of, say, 10% will have an almost negligible effect. This can be explained by virtue of the fact that the field intensity inside the guide and the subsequent current distribution along the length of the strip (L) is cosinusoidal and is therefore low at the guide corners and strip ends compared to the centres [16]. Greater deviations will make the propagation constant approach that of the open guide section again, for example, as the strip length tends to zero. Although no specific mathematical relationship is offered here, the relationship between kz_{image}, L and kz_{open} it is likely to resemble $kz_{image}.\cos(L) = kz_{open}$ as $L \rightarrow 0$, assuming that the strip is always centred on the guide surface.

8.3.7 Examples to illustrate how the model might be used

The following examples serve to illustrate how the new model works and when it becomes essential by quantifying the change in phase for a single unit cell and two extremes of dielectric constant (ε_r). A number of issues surrounding the adoption of existing terminology are also highlighted and discussed.

8.3.7.1 Example 8.1, High dielectric constant case

ε_r = 12 (e.g. Silicon), kz_{image},= 567.5 and kz_{open} = 329.56 calculated for a guide 11.62mm wide x 5.76mm high operating at 10 GHz. Broadside radiation is required, which for model (a) gives a value of strip spacing $d = \lambda g = 2\pi / kz_{open}$ = 19.06 mm.

The values of kz were calculated using the new formulas introduced in Chapter 7 as follows. The required working frequency was taken as being the high frequency (fH) of single-mode operation for the image guide, allowing kz_{image} to be found directly using (7-1 or 7-1b) and the coefficients for a 2:1 aspect ratio. The high frequency of single mode operation for the open guide section is higher than for the image guide section according to Figure 6.8. The required operating frequency must therefore lie between the upper and lower bounds of the useful single-mode range (i.e. fL to fH), or even perhaps below it. In fact, it turns out to be somewhere in between. The simple procedure given in section 7.3.4.1 is therefore used to find the intermediate value of kz_{open} (i.e. work out the deviation from fL or fH, work out kz/GHz and then extrapolate to the required operating frequency).

8.3.7.2 Dilemma about which guide wavelength to use

First, when considering the more precise model of Figure 8.1(b) and a strip width of $W = 0.3$ λg, an interesting dilemma arises; should the guide wavelength λg for this strip be taken as that for the image guide (2π / kz_{image}) section, or as that of the unperturbed open guide as is normally done?

This matter has never been debated in literature before. If there is to be some kind of standard or benchmark for which to make comparison, it should probably be consistent with that used in similar works [3,14]. However, other authors like [17] use the operating wavelength λ_0 as a width reference and some use the ratio of the spacing to strip width W/d [7,15], while some just state the physical width, all completely unambiguous. There is no correct answer, except to be consistent throughout ones own work. In any case, it is trivial to convert from one to the other:

Taking $\lambda g = 2\pi$ / kz_{image} = 11.07 mm for the strip width, gives:

$W = 0.3 \times 11.07$ mm = 3.32 mm

This is equivalent to:

0.174 λg when λg is taken as 2π / kz_{open}

0.11 λ_0 at 10 GHz (≡ 30mm)

For the ratio W/d a similar dilemma about what value of d to use arises; the unperturbed value, or the compensated value d_{comp} that is adjusted from the value d to compensate for the change in kz brought about by adding the finite width strip. This time, the answer is simple because there are no existing benchmarks; use the compensated value d_{comp} if applying the compensation, otherwise use the uncompensated value d.

Now that the strip width has been found and know the rate of change of phase is known, the change in phase over that section can be worked out as:

$$kz_{image} \times W = 567.5 \text{ rad/m} \times 3.32 \text{ mm} = 1.8841 \text{ rads} \equiv 108°$$

For broadside operation, it is well known from array theory that the phase progression along adjacent pairs of elements (unit cells) must be zero. However, the high rate of phase change through the dielectric material over a finite length excludes this possibility. Instead, the strip spacing must be set so that the phase change between them is an integer multiples of 2π or 360°. In this example then, the remaining unperturbed open guide section of the unit cell must be a specific length to provide an additional change in phase of 4.4 rads or 252°.

Assuming fixed x and y axis geometry, the value kz_{open} rads/m over 4.4 radians is taken to give the gap between adjacent strips $d_{comp} - W$ as:

	$d_{comp} - W$	= 4.4 / 329.56 = 13.35 mm
therefore	d_{comp}	= 13.35 + 3.32 = 16.67 mm
giving	Δ	= 19.06 – 16.67 = 2.389 mm

End of example

8.3.7.3 High dielectric constant example results

From this result, it can be seen that for this relatively high dielectric constant and relatively narrow strip example, the error found by not compensating for the increased rate of change of phase caused by the introduction of the metal strip grating is very significant, at >12.5%.

More importantly, for this type of antenna, had the edge-to-edge strip spacing been arranged to be the uncompensated distance *d* apart, the main beam angle using (2-2 or 7-9) would have moved 13.1° away from the intended broadside angle in the forward endfire direction along the positive Z-axis. It is easy to show that increasing the strip width further increases this spacing error, equal to Δ, and vice-versa. The next example demonstrates the equivalent low dielectric constant case, to show that the error is proportionally lower.

8.3.7.4 Example 8.2, Low dielectric constant case

ε_r = 2 (e.g. Silicon), kz_{image} = 264 and kz_{open} = 244.23 calculated for the same guide as above 11.62mm wide x 5.76mm high operating at 10 GHz. Broadside radiation is required, which for model (a) gives a value of $d = \lambda g = 2\pi / kz_{open}$ = 25.726 mm.

Immediately, it can be seen that the difference between kz_{image} and kz_{open} is not as large in the previous example. This fact alone suggests that the phase change due to the introduction of the same electrical size (i.e. $W = 0.3\ \lambda g$) strip will be much lower for the low dielectric constant case compared to the high dielectric constant case. However, it is prudent to quantify the difference here:

$$W = 0.3 \times 23.8 \text{ mm} = 7.14 \text{ mm}$$

The change in phase over that section is therefore:

$$kz_{image} \times W = 264 \text{ rads/m} \times 7.14 \text{ mm} = 1.8841 \text{ rads} \equiv 108°$$

Note that this value is the same as in the previous example. For broadside operation, $d = \lambda_g = 2\pi / kz_{open}$ and the remaining unperturbed open guide section of the unit cell must be dimensioned to provide an additional change in phase of 4.4 rads or 252° again:

	$d_{comp} - W$	= 4.4 / 244.23 = 18.016 mm
and	d_{comp}	= 18 + 7.14 = 25.156 mm
giving	Δ	= 25.726 – 25.156 = 0.57 mm

8.3.7.5 Low dielectric constant example results

This gives rise to a much lower beam angle error of only 1.56° for this low value of $\varepsilon_r = 2$. It will be seen later that the difference between kz_{image} and kz_{open} and therefore this error Δ reduces with increased operating frequency. The examples above were for the same normalised strip width and so the impact of different strip widths was not seen. However, it will be seen later how the strip's physical width with respect to the spacing between adjacent strips also has a significant impact on the beam angle error.

End of example

8.4 *Developing the mathematical model*

The simple analytical examples presented above simply served to illustrate the problem of assuming that the guide is unperturbed when, in fact, there are finite width strips accelerating the change in phase. It was illustrated that this is a particularly bad assumption to make for high dielectric constant guides, but that the strip spacing can be shortened to compensate for any increased phase. That analysis will be expanded upon next; continuing with the analytical case where the antenna geometry is fixed and some of its radiation characteristics are derived. The synthesis case will then be developed, where the radiation characteristics are used to find the antenna geometry, as was done in the two examples. Useful mathematical expressions will be developed for both the analytical and synthesis cases.

8.4.1 Strip spacing for broadside beam

It is possible to put the compensated spacing d_{comp} in a more convenient form for broadside operation as follows. Referring to Figure 8.2(a), the phase difference from edge-to-edge or centre-to-centre must be equal to 2π. Of this, the image guide section advances the phase by kz_{image} x W radians, leaving the open guide section to make up the rest. This leads to the broadside spacing compensation expression (8-1).

$$2\pi - (kz_{image}.W) = kz_{open}.(d_{comp}-W)$$

(broadside case):
$$d_{comp} = \lambda_g = \frac{2\pi - (kz_{image}.W)}{kz_{open}} + W \quad \text{metres} \qquad (8\text{-}1)$$

8.4.2 Perturbed guide wavelength

Note that since this is the distance for one complete phase cycle, it is then also the guide wavelength (λ_g).

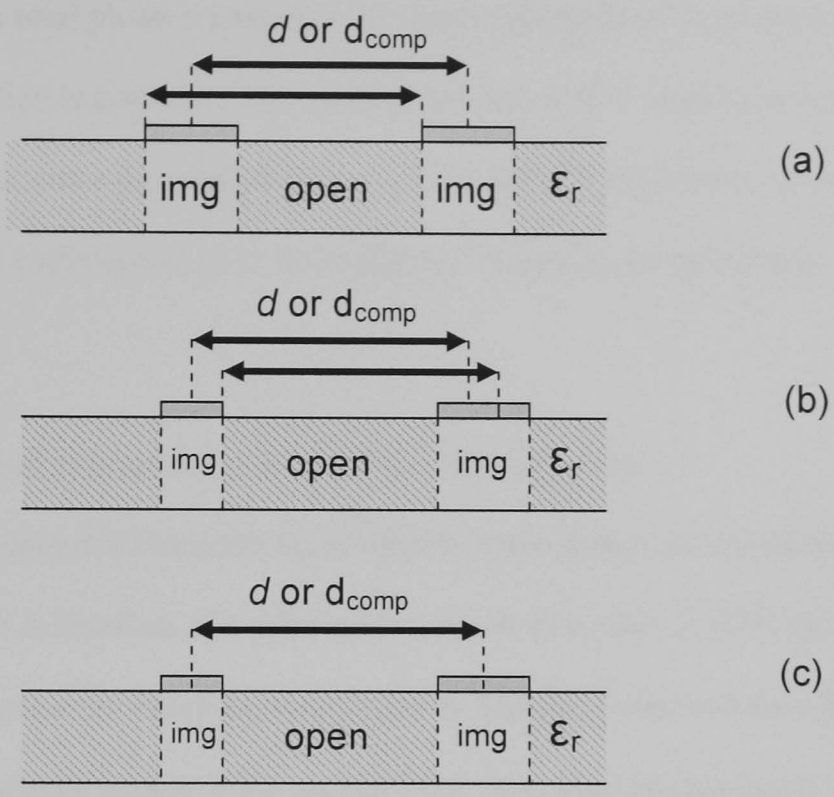

Figure 8.2 Demonstrates options for position of strip spacing (a) constant strip width case (b) simplification of variable strip width case (c) exact variable strip width case.

8.4.3 Beam angle error

Since the guide wavelength is known for the above case, it is easy to find the beam angle error using (2-2 or 7-9) when the spacing is not compensated, recognising that $kz = 2\pi / \lambda_g$. It can be seen by inspection of these formulas that when the compensated spacing d_{comp} is used the two terms in the brackets are equal, which is the condition for a broadside main beam angle. However, when the uncompensated spacing d is used along with λ_g, the two terms are no longer equal and the beam will point at a slightly different angle.

8.4.4 Oblique beam angles and phase components

When the antenna geometry including the strip spacing is known and the possibly oblique beam angle has to be determined, it is possible to take a similar approach to that above. In (8-1) the length of the open section is effectively determined (then W is added) so that the total phase equals 2π over the complete unit cell.

In this case, the total phase is unknown but can be determined from its component parts since all the information is available. The value of spacing will be seen to have particular importance here, since the total phase and the average (or equivalent) propagation constant developed next both depend on it. Referring to Figure 8.3, the total phase per unit cell Φ_d is given by (8-2).

8.4.5 Averaged propagation constant and antenna analysis

The average propagation constant kz_d is then the total phase over the same spacing distance d (8-4). Once this is obtained, it is then valid to insert this value in (7-9) along with the fixed distance or length d for which kz_d was found, to find the theoretical main beam angle. The same distance d must appear in the second term, otherwise this approach would be invalid, giving (8-5). This formula, with the new average kz term that takes into account the strip width, effectively fixes (2-2) and (7-9) so that they take the strip width into consideration. In this case, the strip width W is also assumed to be fixed, as are the propagation constants of the image and open guide sections, having been derived for a fixed guide geometry and dielectric material.

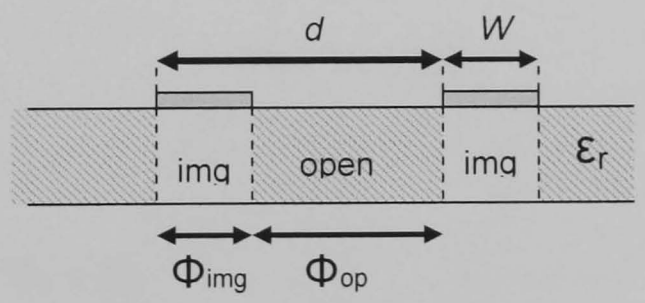

Figure 8.3 Perturbed phase shift model.

$$\phi_d = \phi_{img} + \phi_{op} = kz_{img}.W + kz_{op}.(d - W) \quad \text{rad or deg} \qquad (8\text{-}2)$$

$$kz_d = \frac{\phi_{img} + \phi_{op}}{d} \quad \text{rad/m or deg/m} \qquad (8\text{-}3)$$

$$kz_d = \frac{kz_{img}.W + kz_{op}.(d - W)}{d} \tag{8-4}$$

$$\theta_d = \cos^{-1}\left(\frac{kz_d}{k_0} + \frac{2n\pi}{k_0 d}\right) \quad \text{deg} \tag{8-5}$$

8.4.6 Relationship between beam angle and required strip spacing

At this point, it is important to lay down the conditions for the overall unit cell phase shift for beam angles about broadside (θ = 90°), and to understand how this affects the overall length of the unit cell, which of course is the strip spacing distance *d*. These situations are depicted in the complementary diagrams of Figures 8.4 and 8.5. From these, it can be seen that the conditions for a beam angle less than 90° (i.e. forward quadrant) requires that the total phase shift for a single unit cell must be greater than 2π radians. It can be seen from the second diagram that this effectively lengthens the unit cell and determines where to place the next strip.

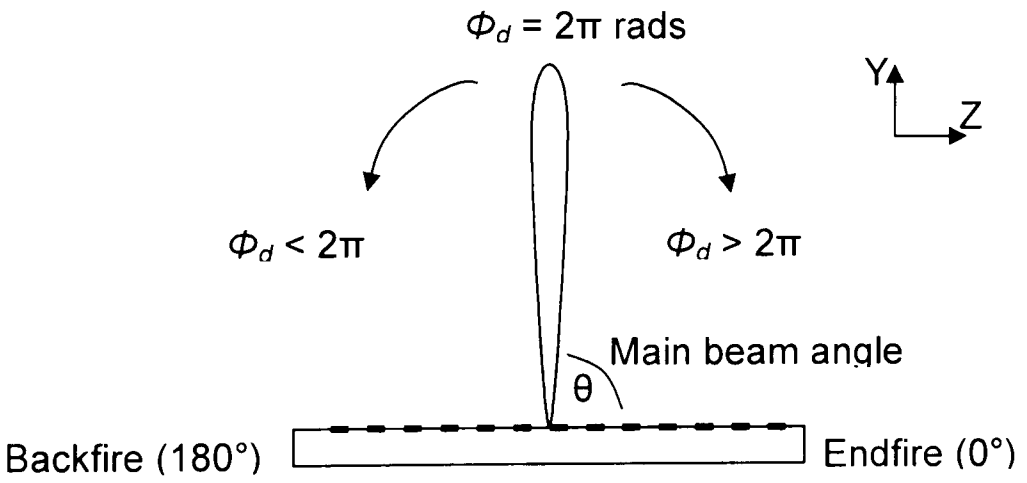

Figure 8.4 Demonstrates how the phase shift between strips (one unit cell) affects the main beam angle.

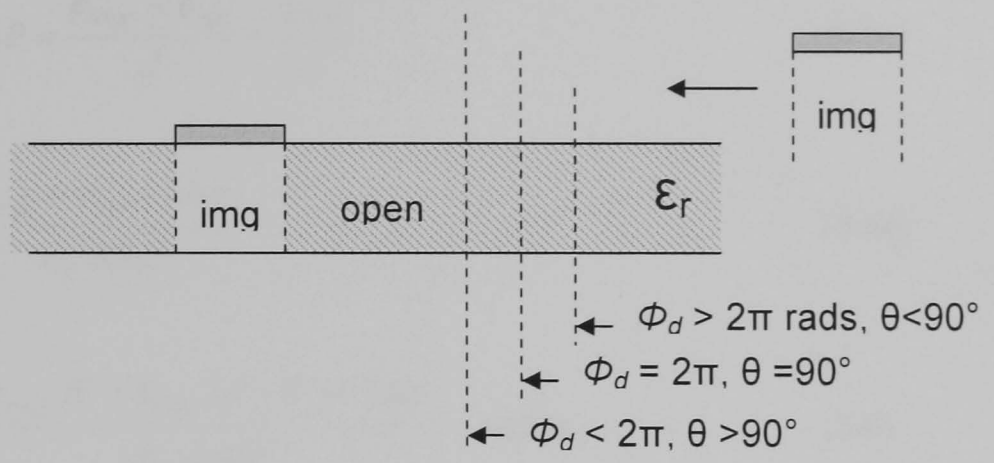

Figure 8.5 Demonstrates how the designed beam angle affects the strip spacing (unit cell length).

8.4.7 Swapping the excitation and endfire ends around

An interesting point to be made is that the spacing can be reduced, if the two ends of the antenna are exchanged, allowing the possibility of more elements to give higher directivity / narrower beamwidth or a shorter antenna. For example, a beam angle of 70°, which requires a large spacing, can be achieved by swapping ends on a 110° design, which potentially has a much shorter spacing. The greatest benefit will be found when $\theta << 90°$ and or $\varepsilon r >> 2$. Even the cross-sectional dimensions of the guide could be changed.

8.4.8 Antenna synthesis case

In the synthesis case, where a specific main beam angle at a specific operating frequency is the goal but where the antenna geometry (including strips) is unknown, the situation is not so straightforward; from inspection of (8-4, 8-5) it can be seen that there are at least four unknowns.

8.4.8.1 Iterative solution

Even if the waveguide geometry and strip width are chosen, there is still the problem of the interdependency between d and kz_d. By substituting (8-4) into (8-5), a transcendental equation is derived (8-6) that can be solved iteratively for the spacing that gives the required beam angle. Note that d appears in both sides. Interim stages are shown for convenience (8-6a,b).

$$k_0 \cos\theta = \frac{\phi_{img} + \phi_{op}}{d} + \frac{2n\pi}{d} \tag{8-6a}$$

$$d = \frac{\phi_{img} + \phi_{op} + 2n\pi}{k_0 \cos\theta} \tag{8-6b}$$

$$d = \frac{kz_{img}.W + kz_{op}.(d - W) + 2n\pi}{k_0 \cos\theta} \quad \text{metres} \tag{8-6}$$

8.4.8.2 Closed form solution

Such an iterative stage is undesirable because it has to be programmed. In any case, it turns out that closed form solution is available, that is also exact. It is found from the unperturbed case, where kz is a constant kz_{open} along the whole length of a unit cell, as in Figure 8.1(a), and as a modification of the simple broadside formula (8-1). Recognising that, as in general antenna array theory, it is the progressive phase between adjacent elements that sets the main beam angle, and that the only difference here is that the dielectric guide material controls the phase per unit length. The approach taken here is to derive an expression that finds this phase value.

Since the 2π term in (8-1) represents the total target phase for the unit cell, this may be replaced by different target total phase values, for other (non broadside) beam angles. Figure 8.5 depicts this situation. The goal then is to find an expression that gives the phase difference for any given beam angle. As mentioned above, the unperturbed model can be used; using (7-9), it is possible to find the spacing d for the same angle. Once this is known, the phase difference required between adjacent strips for a specified beam angle is also found (8-7). It is then possible to build up the same phase difference over other lengths with other propagation constants.

$$\phi_\theta = kz_{open}.d_\theta \qquad \text{rad or deg} \tag{8-7}$$

where $$d_\theta = \frac{-2n\pi}{kz_{open} - k_0.\cos\theta} \quad \text{metres} \tag{8-8}$$

The reader will note that (8-8) is actually the uncompensated spacing but it does not matter because only the total phase shift required to produce the desired beam angle is relevant here. not the spacing value and not the propagation constant. In other words, the unperturbed case is taken where it is assumed that the strips are infinitely narrow to get this phase.

Now, substituting (8-7) into (8-1) to replace the 2π term and simplifying gives the compensated strip element spacing:

$$d_{comp} = \frac{2\pi}{kz_{open} - k_0\cos\theta} - \frac{kz_{image}.W}{kz_{open}} + W \tag{8-9}$$

It is better to generalise this formula so that it may be used for any other guide configuration, for example that shown in Figure 8.1(c) to:

$$d_{comp} = \frac{2\pi}{kz_{unp} - k_0\cos\theta} - \frac{kz_{per}.W}{kz_{unp}} + W \tag{8-10}$$

Where kz_{per} is the perturbed section and kz_{unp} is the unperturbed section. As part validation, it can be seen that when $\theta = 90°$ (broadside), (8-9) and (8-10) both reduce to (8-1).

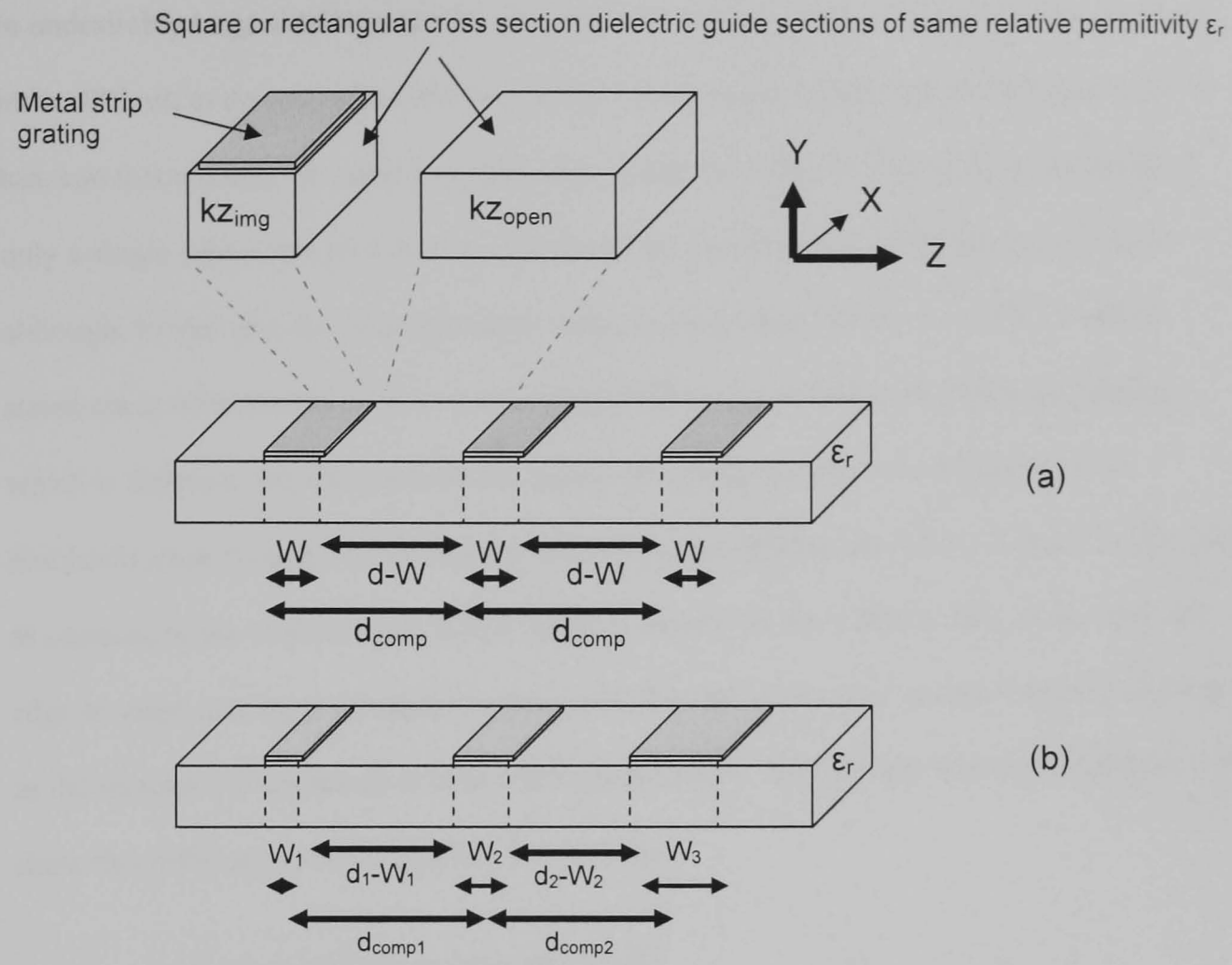

Figure 8.6 Depicts constant strip width (a) and variable strip width cases (b).

8.4.9 Variable strip width case

For the constant strip width case, the strip spacing is also a constant and the above formulas are only computed once per antenna no matter how many strips. However, when the strip width W is variable, each unit cell has to be considered and compensated for separately. Two situations now exist, one with constant strip width and constant spacing, and other where both these quantities vary, as depicted in Figure 8.6(a) and 8.6(b). The latter case will now be considered to highlight its particular complexities.

8.4.9.1 Constant versus variable strip width issues

As a reminder to the reader, a leaky-wave antenna with a constant strip width grating leads to an exponentially decaying field amplitude distribution along the length of the antenna, leading

to undesirably large sidelobes and filled nulls. The variable width alternative, which is much more difficult to design, allows the possibility of *shaping* the amplitude distribution. This in turn can theoretically be used to significantly reduce the sidelobe level [18]. Interestingly, only a single author has provided an analysis of the variable strip width antenna [3] and although. In that case the strip spacing is stated as bing taken 'between centres', but that statement is contradicted in an accompanying diagram by showing edge-to-edge spacing, which is different. [4] also misinforms by depicting edge-to-edge in a diagram. To be absolutely clear though, it only matters when the exact spacing model of Figure 8.2(c) is used as opposed to the model Figure 8.2(b). In other words, for the variable strip width case, the edge-to-edge spacing is an approximation, which tends to the exact centre-to-centre spacing as the increase (or decrease) in strip width tends to zero. An example later in this chapter will show this difference to be negligible for one case.

8.4.9.2 Synthesis formula for variable strip widths

Of course, (8-9) and (8-10) can in theory be used to set the phase difference between strips for all unit cells and any strip width W as per Figure 8.1(b) and (8-10) then becomes:

$$d_{comp\,n} = \frac{2\pi}{kz_{unp} - k_0 \cos\theta} - \frac{kz_{per}.W_n}{kz_{unp}} + W_n \qquad (8\text{-}11)$$

where n is the nth unit cell. However, a complexity arises which causes a small error. Consider the models Figure 8.2(b,c). In (8-11), only a single unit strip width per nth cell Wn is considered. In other words, the strip width increment (or decrement) in the next cell as in model Figure 8.2(b) is neglected. Simulations showed that in the variable strip width antenna case, it is the strip centre-to-centre spacing that sets the beam angle, and not the edge-to-edge spacing. It will be demonstrated shortly that as long as the width of the next strip does not change significantly, as is likely to be the case in practice, it can be neglected. However, it is easy to correct the error by replacing Wn everywhere by Wm where:

$$W_m = \frac{W_n}{2} + \frac{W_{n+1}}{2} \tag{8-12}$$

It is then convenient to express (8-1) in the form of (8-13) when the beam is to be pointed broadside:

$$d_{comp\,m} = \frac{2\pi}{kz_{unp}} + W_m\left(1 - \frac{kz_{per}}{kz_{unp}}\right) \tag{8-13}$$

Or, again, substituting in (8-8) to replace the 2π term gives the more useful oblique angled version:

$$d_{comp\,m} = \frac{2\pi}{kz_{unp} - k_0\cos\theta} + W_m\left(1 - \frac{kz_{per}}{kz_{unp}}\right) \tag{8-14}$$

8.4.10 Formulas for simple strip width taper

The same journal paper [3] published a simple empirical expression that the authors claim improves the radiation pattern (unquantified narrower beamwidth and lower sidelobes) beyond that of the constant strip width antenna. This particular expression, reproduced below as (8-15), has been cited many times by later works and according to one text book [4] is considered to be a rule-of-thumb. The text book itself contains a slightly modified version of this relation (starts with W = 0.145 instead of 0.15) but it is possible that the modification is a typing error.

$$W_n = [0.15 + 0.015(n-1)]\lambda_g \qquad n \le 18 \qquad (8\text{-}15)[4]$$

and $0.4\lambda g$ thereafter.

Consideration was given in the present work to providing an equivalent simple relation for the compensated spacing. The solution to this problem is to find the start value *dcomp1* and the next value *dcomp2* using (8-14). The remaining values *dcomp3*, *dcomp4* etc. can be found by adding the incremental value *dcomp2 – dcomp1* to the previous value.

i.e. $$d_n = d_1 + (d_2 - d_1)(n-1) \qquad (8\text{-}16)$$

where the values of d_n are found using (8-11) or (8-14). Note that the 'comp' label has been dropped here for the sake of clarity, and the subscripts n and m are interchangeable, depending on whether the approximate edge-edge or exact centre-centre case is used. In this case, when substituting the values of d_n into (8-16), the (d2 – d1) term simplifies and leads to (8-14) again but with the simple taper relation substituted for the Wm term and the new subscript n at the start of the formula as in (8-17).

$$d_n = [0.15 + 0.015(n-1)]\lambda_g \left(1 - \frac{kz_{per}}{kz_{unp}}\right) + \frac{2\pi}{kz_{unp} - k_0 \cos\theta} \qquad (8\text{-}17)$$

Of course, this mixture of terminology i.e. mixing wavelengths and propagation constants is somewhat inconvenient. However, the same dilemma introduced earlier appears again; which value of kz should be used to convert to the guide wavelength λ_g? The answer is not the same as before when it did not matter as long as consistency was maintained, because the empirical expression cited in the reference was clearly based on something; in this case the unperturbed propagation constant kz_{unp} i.e. $\lambda_g = 2\pi / kz_{unp}$. The correct form is then that of (8-18).

$$d_n = [0.15 + 0.015(n-1)]\frac{2\pi}{kz_{unp}} \left(1 - \frac{kz_{per}}{kz_{unp}}\right) + \frac{2\pi}{kz_{unp} - k_0 \cos\theta} \qquad (8\text{-}18)$$

This result meets the goal of a generating a simple relation to find the compensated spacing for the empirical taper expression. All the terms are constant except the width taper term in the square brackets which gives perhaps the most convenient expression yet, that of (8-19):

$$d_n = W_n R + S \qquad (8\text{-}19)$$

where Wn = (8-15), $R = \left(1 - \frac{kz_{per}}{kz_{unp}}\right)$ and $S = \frac{2\pi}{kz_{unp} - k_0 \cos\theta}$

In addition, it incorporates the calculation of the width *and* adjusts for oblique beam angles. It will therefore be extremely useful in practice to those designers that decide to use the taper expression. For broadside beams, (8-18) simplifies further as (8-20).

$$d_n = \left[\{0.15 + 0.015(n-1)\}\left(1 - \frac{kz_{per}}{kz_{unp}}\right) + 1\right]\frac{2\pi}{kz_{unp}} \qquad (8\text{-}20)$$

Note that in all cases, kz_{per} refers to the perturbed dielectric guide section i.e. covered by a metal strip and kz_{unp} is that section of a unit cell not covered by the strip. It is valid for the latter to have its sides or bottom covered by a continuous metal strip or plane, as in an image, trapped-image, inset guide and possibly other types of dielectric guide.

8.5 *Validation*

Three approaches will be taken to validate these theoretical results:

1. Correlate present results with other published results;
2. Correlate results with 3D structure simulation results;
3. Perform experiments and correlate results.

In this case, the simulations and experiments are performed on the same high dielectric constant model, which was shown earlier in this chapter to be the most extreme and therefore most important case.

8.5.1 Correlating with existing results

The comparison with other published results is limited to a single case where sufficient information was provided by that author against which a direct comparison can be made [2]. In that case a custom strip width taper arrangement was used which had a variable width increment and compensated by setting the spacing between each adjacent pair of strips accordingly. It is therefore a good test for the present theory, which provides the equivalent compensation. These are the only known results of this kind. It should be noted at this point that that author has not published the methodology in any great detail; only the resulting dimensions can be compared against. However, it is clear that in that case a circuit theory approach known as a transverse resonance formulation was been taken and all that is known about that compensation procedure is that it was embedded in that particular implementation to automatically find the propagation constant, leakage constant, strip width and strip spacing for a Taylor field amplitude distribution.

8.5.1.1 *Table of existing results*

The theoretical results from [2] were presented in a table for an antenna with 30 strips of variable width, the associated compensated spacing, and the propagation constant for the main radiated n = -1 space harmonic. The theoretical results showed a radiation pattern with first sidelobes down at -35dB compared to the main beam peak.

8.5.1.2 *Antenna design characteristics used by previous author*

The relevant antenna model parameters are as follows:

- Operating frequency — 38 GHz
- Material permittivity — $\varepsilon r = 3.5$
- Guide type — dielectric image guide
- Guide height — $b = 2.5$ mm
- Guide width — a = large
- Main beam direction — $\theta = 13°$ (from broadside)

It was assumed that a 'large' guide width means somewhere of the order of ten times the height, which was shown in Chapter 6 to be about the point when the dispersion characteristics become constant. In any case, various other aspect ratios were also compared against the results of the present formulas. The beam angle turned out to be 13° from broadside towards with endfire direction. Here, the explicit angle from endfire of 77° will be used to be consistent with the present work which takes the angle from endfire.

8.5.1.3 *Plotting the existing results data*

The compensated strip spacing values from [2] are plotted in Figure 8.7 as 'Encinar' for each value of strip width used by that author. It can be seen for this distribution that the widest strip width corresponds to the minimum strip spacing, which is what the present theory would suggest for a constant main beam angle.

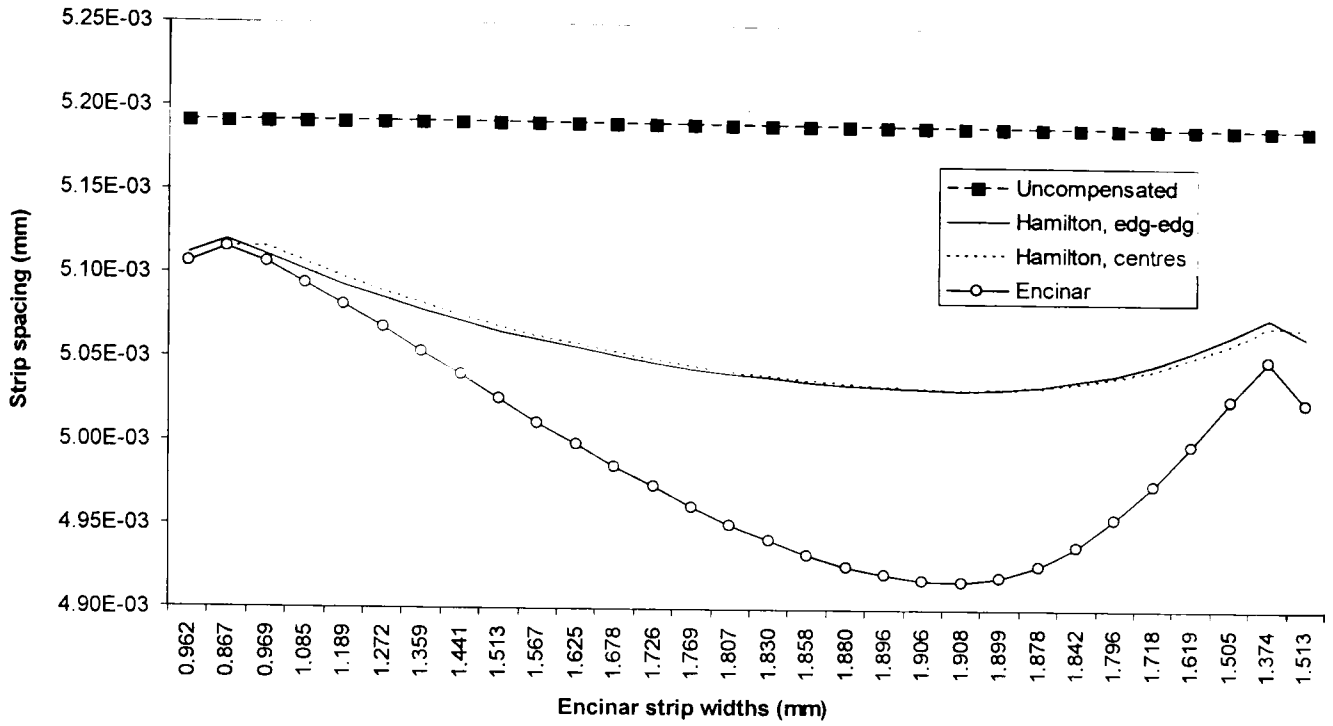

Figure 8.7 Comparing previous (Encinar) and current authors strip spacing results (*Hamilton*) for the same antenna model with variable strip widths. The uncompensated case is also shown.

8.5.1.4 Applying new compensation model to previous authors antenna design

To form a direct comparison between the previous author's results and the results of the new theory, the propagation constant must be computed for the unperturbed image guide section and the perturbed image section covered by the strip (sandwiched). This must only be done once, even though the length of the sections varies with strip spacing, because the height, width and guide material are constant. The Marcatili method, originally programmed for use in Chapter 5, was used find the respective propagation constant values for these two sections, based on a number of quite aspect ratios. These results are presented in Table 8.2. Once the free-space propagation constant is found as $k_0 = 2\pi f / c$, then all the information is available to find the *exact* compensated centre-centre strip spacing illustrated in Figure 8.2(c) using (8-14). The *simple* approximate case where the edge-edge spacing is used as per Figure 8.2(b) is also calculated for comparison using (8-11). The resulting compensated spacing values are plotted in Figure 8.7 based on the same strip widths as used by Encinar.

Table 8.2 Propagation constant for different guide aspect ratios.

	5:1	10:1	40:1	100:1	Units
Image guide	1358.2	1371.3	1376	1376.3	rad/m
Sandwich	1473.2	1485.3	1489.6	1489.9	

8.5.1.5 Comparison with previous author's results

It should be pointed out that the whole vertical scale is only about a quarter of a millimetre, which represents only about one thirtieth of the free-space wavelength. This implies that the results from the new formula are a relatively close match to the results presented by the previous author. From these results it can be seen that the results correlate extremely well at the two ends, but less so between. In addition, it can be seen that the difference between the edge-edge and centre-centre cases is negligible for this antenna model, but this might not be the case for models that use high permittivity materials.

8.5.1.6 Comparison with unperturbed results

The results from the unperturbed case, where the strip width is ignored (Figure 8.1a) is also found from (8-8) for the same beam angle, n = -1 harmonic, and the propagation constant found for the image guide. Of course, the result is a straight line since everything is a constant in that case. It can be seen that in this case the strip spacing is slightly longer, which is what would be expected since the speed up is neglected. The new formulas have put the curve approximately in the centre between the straight line and the Encinar curve, which indicates that there is definitely significant merit in using the new formulas.

8.5.1.7 Possible issues with previous author's results

There are a number of issues with the previous author's results that suggest a number of errors in that work. First of all, standard array theory suggests that the phase should be progressive across successive pairs of elements e.g. 300°, 600°, 900°. However, when applying the new model to find the phase between elements, it is found that the published values of strip width and spacing do *not* actually meet the progressive phase requirement. For example, the first

three strips give phase shifts of 7.135 and then 7.137 radians using (8-2) and the propagation constants for the 40:1 aspect ratio guide model.

$$\beta_{-1} = \beta_0 - \frac{2\pi}{d} \qquad \text{rad/m} \qquad (8\text{-}21)$$

8.5.1.7.1 Beta$_{-1}$ issue

The second issue with the previous author's results are that they show that the propagation constant for the n = -1 space harmonic β_{-1} is constant. This is sometimes used to specify the propagation constant for a given spacing as (8-21). No working out is provided in that case, but it is easy to see from the relationship that since d varies from unit cell to unit cell along the length of the antenna model, that β_0 must also vary. In this case β_0 is the same as kz used throughout this thesis, and since it is perturbed by variable width strips, it means that the average kz_d must be used as in (8-4). This can also be shown to vary along the length of the antenna model, which does align with the previous author's results. However, since all information is available to find the phase shifts, it can easily be shown by substituting kz_d for β_0 that β_{-1} is *not* constant for that set of data (by substitution of (8-4) into (8-21)). That author also specifies that when β_{-1} is *not* constant, the radiation pattern is degraded (it is assumed that this means that degradation is caused by a non-constant beam angle created by adjacent pairs of strips along the length of the antenna). It is felt that the author has mistakenly taken β_{-1} radians per metre as constant instead of specifying that the actual phase must be maintained constant as in standard array theory, which would be $\beta_{-1}.d$ radians in that case. Because of this mistake, the previous author's data produces non-constant $\beta_{-1}.d$ i.e. non-progressive phase shift along the antenna.

8.5.1.7.2 Dependency

The new formula however, does give $\beta_{-1}.d$ as constant for the range of strip widths, which agrees with array theory. In the unlikely event that there is merit in having β_{-1} maintained constant, it could easily be found by adding an iterative step to the new formula. Of course,

some of this speculation relies upon the present author's theory being correct. It is (8-4) that is key to this and it can be seen by inspection of that formula and its accompanying model Figure 8.1(b) that it is almost indisputably correct. The only real issue is that different methods for deriving the propagation constants might give different values. However, any differences in these values will be seen as a constant shift up or down of the curves shown in Figure 8.7; it will not change the shape.

8.5.1.7.3 Possible incorrect use of leakage constant by previous author

There is also a third issue; it appears that the previous author has incorrectly lumped the leakage constant (α) in with the phase information, although it is not clear how from the information given. It is thought that this might account for the difference between the previous author's original spacing distribution curve and the curves by the new formulas. Further, it is thought that the two new curves have the correct response, while the previous author's curve is wrong due to this third issue.

8.5.1.7.4 Propagation constant component parts

While, technically, the propagation constant is the sum of a phase constant and a leakage constant i.e. $kz = \beta + j\,\alpha$, array theory shows that only the phase part should be included in the derivation of the main beam angle and associated strip spacing. Even though the imaginary leakage constant is a function of the strip width (and other conditions), and the strip width is known to cause a change in phase (and kz), the phase and leakage parts act totally independently. The former controls the beam direction, while the latter controls directivity and beamwidth through an aperture efficiency and aperture distribution [17]. For these reasons the leakage is not relevant in this new model.

8.5.2 Correlating with simulation results

An equivalent antenna model was simulated with a high dielectric constant material, as used in experimental work, and with suitable geometry for operation at just under 6GHz, which

was the upper limit of available test equipment. The smallest possible aspect ratio of 1:1 was chosen to provide the widest operating frequency range, as demonstrated in Figure 6.10. A completely open guide was chosen because this is the easiest both to simulate and realise in practice. This setup was chosen to allow the greatest flexibility in subsequent experimental work.

8.5.2.1 Choosing suitable attributes

From the point of view of this chapter, the only way that the new theory can be correlated with the simulation results is to compare the simulated beam angles with the beam angles derived using the new theory, for the same strip widths, strip spacing, operating frequencies and antenna model. In the simulations, the relevant output is the radiation pattern data, from which the beam angles were extracted. In this case, the data was stored in 2 degree steps, implying that the actual peaks are within 2° of the stored values.

8.5.2.2 Computing the theoretical propagation constants

The respective propagation constants for the open and image sections were computed using the same Marcatili formula implementation as used earlier, and by the new propagation constant formulas presented in Chapter 7. These, of course, are required to test the new theory, and are required at every discrete operating frequency.

8.5.2.3 Comparing simulated and theoretical results

Figure 8.8 compares the results from the HFSS simulations, the results from the new perturbation theory that use the value of propagation constants found using both the new propagation constant formula (7-2b, 7-3b)(*Hamilton*) and Marcatili formula (*Ham/Marc*), and finally, the unperturbed uncompensated case using the Marcatili derived values for kz_{open}. The new theory finds the beam angle using (8-4) and (8-5). All these models used a fixed spacing, which happens to be 18 mm. The guide dimensions are 10.8 mm square and the length is not relevant in this scenario. Close scrutiny of the three curves for each frequency first of all shows that:

- while the new theory produces an essentially straight line relationship versus strip width, those from simulations show some curvature and non-linearity;
- in general, the results derived purely from the new (*Hamilton*) formulas are closer to the HFSS results;
- the *Hamilton* and *Ham/Marc* curves deviate as the strip width increases, and as the operating frequency increases;
- as the frequency increases, the slope of the HFSS curve decreases and shifts vertically downwards with respect to the two other curves;
- in general, the slope of the *Ham/Marc* curve is closer to the HFSS slope;
- HFSS curves around broadside (90°) have their slopes affected;

The horizontal straight lines representing the unperturbed beam angles where the strip width is not taken into consideration are also plotted, except for the lowest frequency which is off scale. In all these uncompensated cases the beam angle is significantly increased with respect to the simulated case and the two theoretical compensated cases. This is of course what would be expected. It also demonstrates that:

1. The unperturbed main beam angle case gives severe errors. For example, the error for the 8.33 mm strip widths (W/d ~ 0.5) is approaching 20°;
2. There is definitely merit in applying compensation.

8.5.2.4 Simulated curve anomalies

Drawing a straight line through the HFSS curves demonstrates that in all cases except the one that passes through broadside (HFSS, 5.8GHz), the actual points are no more than about 2° away. This implies that any anomalies in the curve could be purely a result of the 2° sample interval used in the simulations.

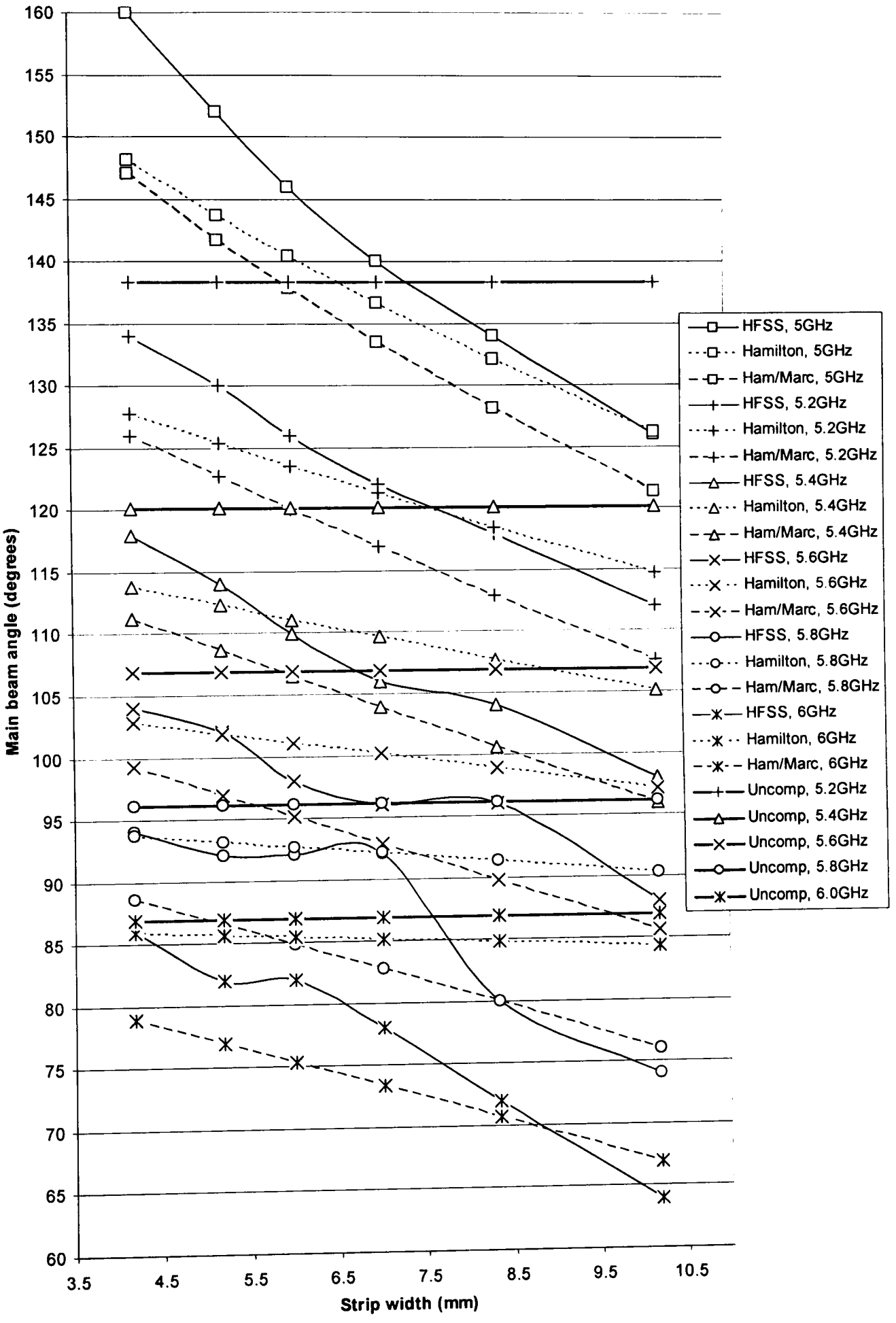

Figure 8.8 Compares simulated and theoretical beam angles for the practical range of frequencies and strip widths.

8.5.2.4.1 Broadside null effects apparent in simulation results

It is reasonable to assume that the initial flatness of the curve that passes through 90° is a side effect of the high input reflection coefficient and subsequent null that occurs at that angle [12,15]. The same flattening effect was seen in Figure 4.7 for a different simulated model. In Figure 8.8, it appear that the null might be having some affect up to about ±10° away for the HFSS 5.6GHz and HFSS 6GHz curves. The new formulas do not and cannot possess this feature, which appears to stop the beam steering in the vicinity of broadside. The beam angle then appears to increase more sharply beyond this in order to compensate and match the original slope.

8.5.2.5 Considering the accuracy of the theoretical results

Although the theoretical curves are generally only accurate to within 5 to 10° of the HFSS simulated curves, the improvement over the uncompensated case is still significant for this practical range of strip widths. If straight lines are drawn through the HFSS curves as mentioned above, the slopes of these do not align with the theoretical curves. This is potentially due, at least in part, to the calculated propagation constants being slightly different. In general, the slope of the HFSS curves decrease with frequency (except for the last two which seem to be affected by the null). The slopes of the theoretical curves also decrease to about the same extent. This happens because the difference between the propagation constant of the image guide section and the open guide section (of a unit cell) reduces with frequency.

8.5.2.6 Comparing the different theoretical curves

In theory, the two theoretical curves (*Hamilton* and *Ham/Marc*) for any given frequency should overlap almost perfectly. The fact that they deviate so much at the highest frequencies and widest strip widths implies that there is a problem. An investigation to find out why they differed so much revealed that the differences were due to the fact that the new propagation

constant formula produce an error, due to a slight curvature of the propagation constant curves between the high and low limits of the useful frequency range for large values of dielectric constant. Such an example of curvature can be seen in Figure 5.12. This requires quite a lengthy explanation, and will not be tackled here because the results still represent a great improvement.

8.5.2.7 Accounting for potential errors

The difference between the HFSS curves and the theoretical curves that used the Marcatili derived propagation constants, labelled as Ham/Mar, is interesting for a number of reasons. First of all, the Marcatili method used for the theoretical results is known to produce extremely accurate values when the operating frequency is close to or beyond the upper boundary of the useful frequency range [9]. This situation is satisfied for at least two frequencies for this antenna model; both the image guide section and the open guide section begin operating above their respective high frequencies at 5.8GHz. This implies that the Marcatili values *should* produce accurate results at least for the 5.8GHz and 6GHz Ham/Mar curves. Ideally then, these particular theoretical curves should correlate closely with the simulated versions. This is not the case, however, there is a strong possibility that these two curves are distorted by the broadside null effects and would otherwise agree closely with the results by the new theory.

8.5.3 Correlating with experimental results

As part of a series of experimental work, near field probing was carried out to try to measure the guide wavelength of the unperturbed guide, and perturbed guide with strips of different widths. The experimental method used here is presented in Chapter 9 along with other experimental work. The results are presented here in order to correlate with the new compensation / perturbation theory.

8.5.3.1 Comparing near field probing results with theoretical guide wavelengths

The aim was to try to qualify the theoretical speed up in propagation constant caused by each strip width. In theory, according to (8-1), the guide wavelength will decrease as a function of the distance over which this speed up occurs i.e. the strip width W, compared to if the strip was not present (or has zero width), because the phase cycle is completed over a shorter distance.

8.5.3.2 Irregular measured guide wavelengths

During near field probing experiments, the measured distances between the maxima and minima were found to become increasingly irregular as the strip width was increased. This was also the case when a continuous metal plane was used in place of the strips, simulating the maximum strip width case. This case gave the most irregular results, which gives cause for concern.

8.5.3.3 Accounting for the irregular wavelengths

In this near-field probing model, the spacing is fixed as per all the HFSS simulations and the subsequent experiments. When the strip widths are zero, as per the top of Figure 8.9, the propagation constant along the guide is such that the guide wavelength is simply 2π over that distance d. In this example, that makes the guide wavelength much greater than the spacing. In this figure, the spacing is in dimensionless units for simplicity.

8.5.3.3.1 Irregular wavelengths model

In this model, each of these unit lengths accounts for a single phase unit (Φ) when uncovered or two phase units i.e. two times speed up, when covered by part of a strip. One phase cycle or guide wavelength is equal to thirteen phase units ($\Phi = 13$). The physical number of unit lengths that it takes to make up the thirteen phase units is represented by dimensionless wavelength units (λ) and is shown as a white band. Each white band then represents a complete guide wavelength or phase cycle, the differences in length of which is effectively determined by how much of the strip each individual cycle passes through.

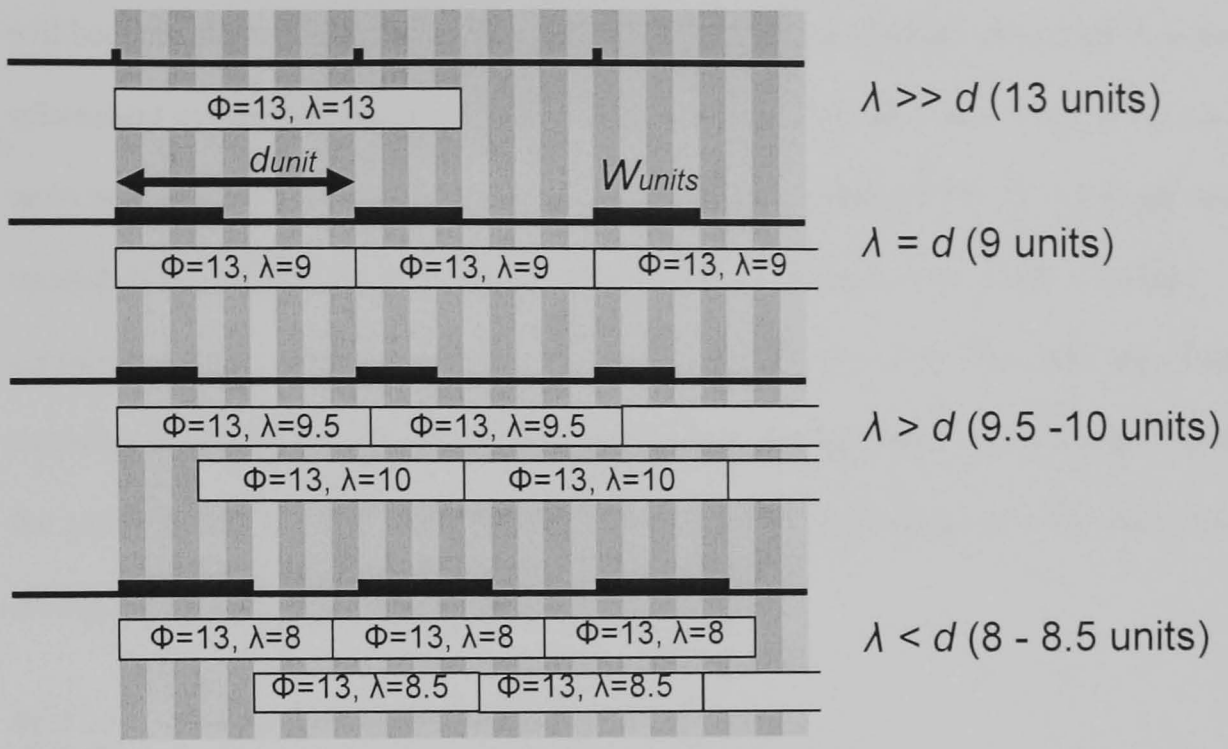

Figure 8.9 Demonstrates how full phase cycles along the length of the antenna are effected by the strip width used.

The point of this exercise is to demonstrate that the guide wavelength can vary along the length of this type of antenna, even with constant width strips and constant spacing. In theory, it will *not* vary when the spacing equals the guide wavelength. This situation is demonstrated in the medium strip width case in the figure. Here, every phase cycle is completed in $\lambda = d = 9$ units, and correlates exactly with the spacing along the whole length the antenna, even independently of the start position of the first cycle, or time. However, if the strip widths have unit length such that the cycles do not correlate with the spacing (are longer or shorter), then it is possible that some of the phase cycles along the length of the antenna receive contributions from more or less covered units. This causes a variation in cycle length and therefore guide wavelength along the antenna. The example at the bottom of the figure will serve to reinforce this concept, assuming initially that the start of the first cycle is aligned with the start of the first strip on the left side: initially, each cycle of 13 phase units has a length of 8 units, each as a result of passing through 5 covered units. The covered sections make up 5 x 2 =10 phase units which means that the cycle will complete after passing through three uncovered units.

Further along the length of the antenna, as represented by the lowest bands, the start of a cycle will become aligned with the trailing edge of a strip. Close scrutiny will reveal that the subsequent cycles then become slightly longer because they only pass through 4.5 covered units instead of 5. The covered sections only therefore contribute 4.5 x 2 = 9 phase units instead of 10. In that case, to complete a full cycle of 13 phase units needs a further contribution from 4 uncovered units, for a total length of 8.5 units. The guide wavelength has therefore increased from 8 units to 8.5 units at some distance down the antenna. Further down the antenna, it will reduce back to the original value and then up again, if the antenna is long enough and the transitions should be perfectly smooth.

8.5.3.3.2 Consequences for the standing wave

From the point of view of a standing wave, the cycles belonging to the backward travelling wave component should all see the same phase changes as their forward counterpart. In theory then, the two components should correlate exactly and add constructively; no matter what the strip width is and even if the resulting cycles are irregular (or vary smoothly). The reader can easily visualise this by assuming that the wave is reflected from the right hand side of Figure 8.9.

This all implies that the sinusoidal phase cycle is distorted as illustrated in Figure 8.10. Therefore, part of the cycle could change rapidly, while the rest might change slowly in comparison. Or, the cycle might have two or three rapidly changing parts and one or two slowly changing parts. Whatever the combination, this explains why the near field probing revealed some quite extreme irregularity between the distances between adjacent maxima and minima along the length of the antenna.

8.5.3.4 Quantifying the variations in guide wavelength

Previous chapters have demonstrated how the propagation constant changes with frequency, when covered by metal, as a function of the material permittivity, and finally, as a function of

its cross section. In general, the important parameters here are the relative propagation constant values of the covered and uncovered sections (the difference decreases with operating frequency), the spacing, and the ratio of covered to uncovered section. This parameter will allow determination of the maximum variation in guide wavelength.

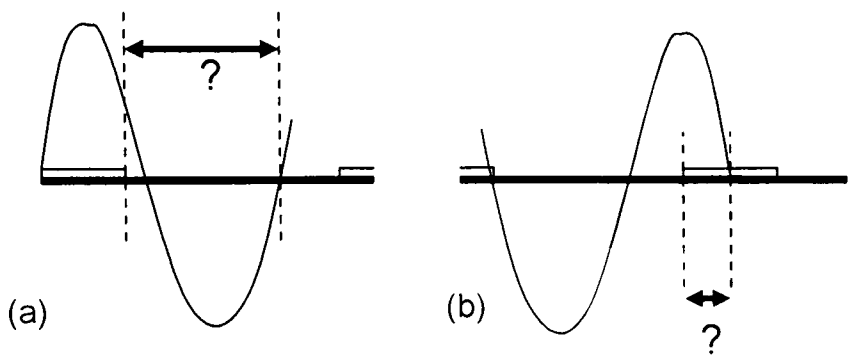

Figure 8.10 Illustrates the two conditions for finding the two limits of the variation in guide wavelength for the perturbed cases when (a) the phase cycles starts at the leading strip edge and (b) trailing edge.

$$\lambda_{gLO} = \frac{2\pi - kz_{open}(d-W)}{kz_{image}} + (d-W) \qquad \text{metres} \qquad (8\text{-}22)$$

The two limits are illustrated in Figure 8.10. In case (a) the phase cycle begins at the leading edge of a strip and ends some distance along the unperturbed section before the next strip. This distance can be found by the new formula (8-1). The other limit is found when the cycle begins at the trailing edge of a strip somewhere further along the antenna, as was demonstrated in Figure 8.9 and the example. In this case the cycle, excited by the same operating frequency, ends part way along the following strip. In that case, the form of (8-1) is unsuitable and must be rearranged as per (8-22) to deduce the limit. The maximum variation is then the difference between these two limits.

8.5.3.5 Approach taken for comparing experiment with theory

The actual measured results are presented in the chapter on experimental work. To eliminate the cycle irregularity, the maxima and minima values are averaged over multiple measured

cycles (typically around six). Figure 8.9 and its explanation have demonstrated the principle of varying guide wavelength. The theoretical wavelength has been taken as the mean of the maximum and minimum value, following this principle, and effectively assuming that the antenna is infinitely long (as opposed to six cycles long). In theory, this approach should allow a direct comparison between the measured values and theoretical values.

8.5.3.6 Comparing probing results with theoretical results

In Figure 8.11, the experimental near-field probing results are superimposed on top of the same theoretical results given in Figure 8.8 for an operating frequency of 5.8GHz. In addition, the calculated limits of the variation in guide wavelength are shown for comparison. The new *Ham/Mar_Lo* curve represents the limit calculated by (8-22) and the *Ham/Mar* curve is found by (8-1). This variation should be zero when the strip width is zero because there is nothing to change the wavelength. This is confirmed by the figure.

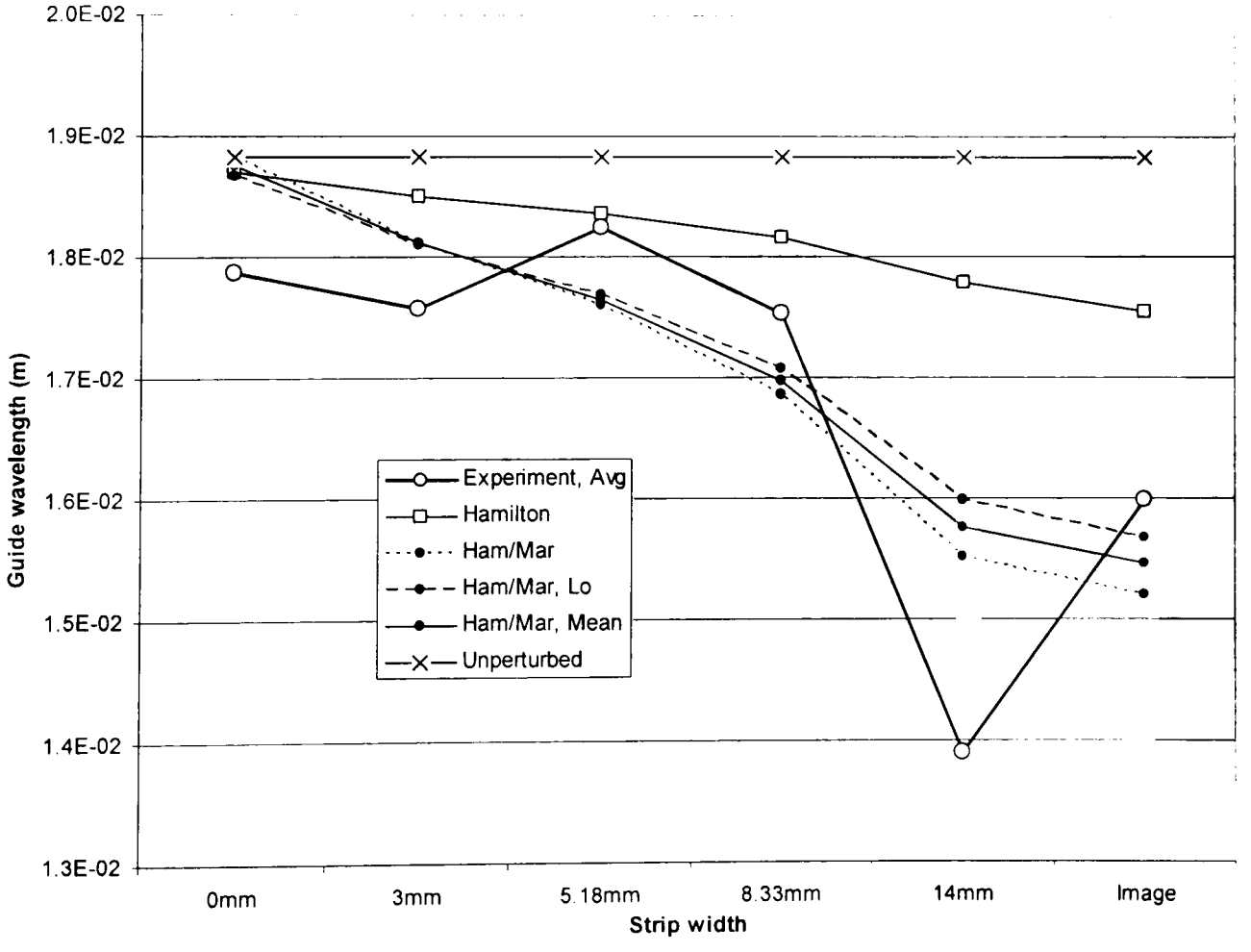

Figure 8.11 Shows experimental versus theoretical strip perturbed guide wavelength for a range of strip widths.

8.5.3.6.1 Results discussion

At this frequency, the *Hamilton* curve is relatively horizontal, as it was in the associated beam angle error curve of Figure 8.8. In theory, as mentioned above, this curve should essentially overlap the *Ham/Mar* curve. The explanation for this was also covered i.e. due to error the new kz formula at intermediate frequencies. The measured curve shows quite a different response. When the Marcatili kz values are used, the other three theoretical curves are close to the measured one, especially when it is considered that the measurement tolerance is thought to be in the order 0.5 to 1mm. Of these three, when the deviation theory is used, it can be seen that the difference between this (*Ham/Mar_Lo*) and the curve where the deviation in guide wavelength along the perturbed guide is ignored (*Ham/Mar*) is not very great, even when the strip width is so wide that it touches the next strip and forms a continuous image plane. In theory, the actual guide wavelength should exist somewhere between these two curves, estimated to be the mean value of these two (*Ham/Mar_Mean*). The continuous image plane situation exists when the strip width equals the guide wavelength, typically around $W \sim$ 15.5mm. The kink in these curves at $W = 14$mm only exists because the x-axis is not to scale. In reality, the image data points would be very close to the 14mm points.

8.5.3.6.2 Additional confidence in the new perturbation model

In the above example, all three theories correlate quite well with the measured results. This gives additional confidence in the new perturbation and compensation model presented in this chapter. Again, compared to the unperturbed case, both the measured and theoretical perturbed values compared to unperturbed imply that there is definite merit in using the model.

8.5.3.7 Influence of irregular wavelength on the new formulas

It should be said that the variation in guide wavelength has no impact on the compensation formulas developed in this chapter, or the associated beam angle calculations of Figure 8.8. It only effects near-field probing measurements, which is the only time when knowing the guide

wavelength is useful. The effects have only been quantified here for the situation where the strip width and the strip spacing are constant along the whole length of the antenna.

8.5.3.8 Near field probing and variable strip widths

The same formulas and analysis technique will apply to variable strip width and or strip spacing, except that every single unit cell (or a large sample) will have to be analysed independently. In this case, the simplicity of the method makes it amenable to working out in a spreadsheet program.

8.6 Conclusions

A new model consisting of a perturbed guide section in series with an unperturbed guide section is used to represent the unit cell of a metal strip grating leaky-wave antenna. This model demonstrated a step increase in the rate of change of phase, or propagation constant kz, caused by adding a strip of finite width to the unperturbed guide. Formulas were derived to compensate for this increase by reducing the strip spacing while maintaining the desired main beam angle constant. Since the cell length and the strip spacing are one in the same, this implies that the series unperturbed guide section is reduced in length according to the width of strip and the desired beam angle. This can also be done on a cell-by-cell basis if the strip width is varied along the length of the antenna. Linear array theory dictates that the phase across all unit cells is a constant (progressive), and it is this phase value that determines the main beam angle.

Once the strips have been arranged, the total phase value between the two ends of the unit cell, equal to the strip spacing d, is needed to plot the radiation pattern. The total phase is given by the average value of propagation constant kz_d over that length i.e. $kz_d\, d$. However, there is interdependence between kz_d and d according to the transcendental formula (8-6). Fortunately however, the required phase can be found independently from the unperturbed case using (8-7) for the desired beam angle and unperturbed propagation constant. Provided that this same phase value is achieved in the perturbed model, the same beam angle will be achieved. This finding was important to enabling this solution.

Now, assuming that the propagation constants have been calculated for the two sections for the guide material, guide dimensions and operating frequency, the target phase value can then be set by choosing the lengths of the perturbed and unperturbed guide sections accordingly. It is important that the strip width can be controlled separately because it is known to control the leakage, and it must be possible to separately design and vary the strip widths in order to achieve a desired aperture distribution along the length of the antenna. The new model

satisfies this requirement. For example, when the strip width is relatively wide, the strip spacing can be set to achieve the required total unit cell phase value. And, when the strip width is narrower, the spacing is increased accordingly to achieve the same phase value.

Simple formulas have been derived to make these compensations possible. In particular, the required spacing can be found using (8-10) for the constant strip width case, using (8-11) for the simple variable strip width case, (8-14) for the exact case or (8-19) for the well-known strip width taper formula (8-15). Once the spacing is found, the average propagation constant kz_d can then be found using (8-4). This average propagation constant can also be substituted into the well-known formula for calculating the main beam angle as per (8-5). This average propagation constant can also be used to plot the radiation pattern for the perturbed case by making the phase term Ψ for the array factor (2-1) equal to (8-23). These same values can also be used to improve the beam scanning and grating lobe formulas by substitution into (7-13) and (7-14) respectively to find those limits for the perturbed case.

$$\psi = d_{comp}\left(k_0 \sin\theta - kz_d\right) \qquad (8\text{-}23)$$

In this chapter it was demonstrated how the existing well-known unperturbed formulas normally associated with periodic grating leaky-wave antennas give significant error in all practical cases, and greater error for the higher dielectric constant materials. However, these new improvements to those formulas have been shown to represent the perturbed case accurately, and to eliminate this error in all cases. These improvements therefore represent a significant advancement for the analysis and design of this type of antenna.

8.7 References

[1] J. Encinar, M. Guglielmi and A.A Oliner, "Taper optimization for sidelobe control in millimeter-wave metal strip-loaded dielectric antennas," *URSI Radio Science meeting*, Syracuse, New York, pp. 379. Jun. 1988.

[2] J. Encinar, "Analysis and CAD techniques for periodic leaky-wave printed antennas: numerical and experimental results," International journal of Microwave and Millimetre-wave Computer-aided Engineering, vol. 4, no 1, pp. 88, 99. 1994.

[3] T.N. Trinh, R. Mittra and R.J. Paleta, "Horn image-guide leaky-wave antenna," *IEEE Trans. Microwave Theory and Techniques*, vol. MTT-29, no. 12, pp. 1310-1314, Dec. 1981.

[4] F. Schwering and A.A. Oliner, *Antenna Handbook*, Eds. Y.T. Lo and S.W. Lee, Van Nostrand Reinhold, New York, 1988.

[5] M. Ghomi, B. Lejay, J.L. Amalric and H. Baudrand, "Radiation characteristics of uniform and nonuniform dielectric leaky-wave antennas," *IEEE Trans. Antennas and Propagation*, vol. 41, no. 9, pp. 1177-1185, Sep. 1993.

[6] J. Encinar, "Mode-matching and pont-matching techniques applied to the analysis of metal-strip-loaded dielectric antennas," *IEEE Trans. Antennas and Propagation*, vol. 38, no. 9, pp. 1405-1412, Sep. 1990.

[7] M. Matsumoto, M. Tsutsumi and N. Kumagai, "Radiation characteristics of a dielectric slab waveguide periodically loaded with thick metal strips," *IEEE Trans. Microwave Theory and Techniques*, vol. MTT-35, no. 2, pp. 89-95, Feb. 1987.

[8] C.A. Balanis, "*Arrays*,"in Antenna Theory, Second edition, John Wiley & Sons, Ch. 6, p311, 1997.

[9] K. L. Klohn, R. E. Horn, H. Jacobs and E. Freibergs, "Silicon waveguide frequency scanning linear array antenna," *IEEE Trans. Microwave Theory and Techniques*, vol. MTT-26, no. 10, pp. 764–773, Oct. 1978.

[10] V.K. Varadan, V.V. Varadan, K.A. Jose and J.F Kelly, "Electronically steerable leaky wave antenna using a tunable ferroelectric material," *Smart Materials & Structures*, vol. 3, pp. 470-475, Jun. 1994.

[11] R. E. Horn, H. Jacobs, E. Freibergs and K. L. Klohn, "Electronic modulated beam-steerable silicon waveguide array antenna," *IEEE Trans. Microwave Theory and Techniques*, vol. MTT-28, no. 6, pp. 647–653, Jun. 1980.

[12] M. Guglielmi and D.R. Jackson, "Broadside radiation from periodic leaky-wave antennas," *IEEE Trans. Antennas and Propagation*, vol. 41, no. 1, pp. 31-37, Jan. 1993.

[13] J.L Gomez-Tornero, A.T Martinez, D.C. Rebenaque, M. Guglielmi and A.A. Melcon, "Design of tapered leaky-wave antennas in hybrid waveguide-planar technology for

millimeter waveband applications," *IEEE Trans. Antennas and Propagation*, vol. 53, no. 8, pp. 2563-2577, Aug. 2005.

[14] S. Kobayashi, R. Lampe, R. Mittra and S. Ray, "Dielectric rod leaky-wave antennas for millimeter-wave applications," *IEEE Trans. Antennas and Propagation*, vol. AP-29, no. 5, pp. 822–824, Sep. 1981.

[15] M. Guglielmi and G. Boccalone, "A novel theory for dielectric-inset waveguide leaky-wave antennas," *IEEE Trans. Antennas and Propagation*, vol. 39, no. 4, pp. 497-504, Apr. 1991.

[16] E. A. J. Marcatili, "Dielectric rectangular waveguide and directional coupler for integrated optics," *Bell Syst. Tech. J.*, vol. 48, no. 7, pp. 2071–2095, Sep. 1969.

[17] R. Mittra and R. Kastner, "A spectral domain approach for computing the radiation characteristics of a leaky wave antenna for millimeter waves," *IEEE Trans. Antennas and Propagation*, vol. AP-29, no. 4, pp. 652–654, Jul. 1981.

[18] R.C. Honey, "A flush-mounted leaky-wave antenna with predictable patterns," *IRE Trans. Antennas and Propagation*, vol. 7, iss. 4, pp. 320-329, Oct. 1959.

[19] W.V. McLevige, T. Itoh and R. Mittra, "New waveguide structures for millimeter-wave and optical integrated circuits," *IEEE Trans. Microwave Theory and Techniques*, vol. MTT-23, no. 10, pp. 788-794, Oct. 1975.

[20] T. Itoh and B. Adelseck, "Trapped image guide for millimeter-wave circuits," *IEEE Trans. Microwave Theory and Techniques*, vol. MTT-28, no. 12, pp. 1433-1436, Dec. 1980.

[21] T. Itoh, "Inverted strip dielectric waveguide for millimeter-wave integrated circuits," *IEEE Trans. Microwave Theory and Techniques*, vol. MTT-24, no. 11, pp. 821-827, Nov. 1976.

9 EXPERIMENTAL WORK

9.1 Introduction

In Chapter 8 it was shown that the highest value of dielectric constant gave the largest beam angle error compared to the unperturbed case using (2-2), and the majority of previous authors had used materials with a dielectric constant $\varepsilon r \sim 2.5$. Therefore D-16 Magnesium Titanate ($MgTiO_3$) with a high value of $\varepsilon r \sim 16$ was chosen for these experiments. This is a hard ceramic material, which can be purchased as a block and cut with a diamond saw, and is low-loss at millimetre-wave frequencies [1]. Attempts were made to manufacture this material from a powdered form but all these attempts failed, primarily because its granular shape (hexagonal plates) did not lend itself to being compacted sufficiently prior to sintering.

Available RF equipment limited the operating frequency to 6 GHz. Based on this constraint and the sizes of material available, two different open D-16 guides were designed with aspect ratios of 1:1 and 2:1 respectively. The guide designs were simulated using HFSS structure simulator software tool with metal strips added and the strips were spaced with a period equal to slightly less than the lowest calculated propagation constant. This period puts the main

beam angle close to broadside, but not *at* broadside. Simulations showed that the guide with a 1:1 aspect ratio gave the highest gain, therefore it was constructed. The guide specification was:

Useful frequency range	4.05 to 5.76 GHz
Propagation constant	84.9 to 335.5 rad/m
Guide wavelength	74mm to 18.72mm

Aluminium strips were laser cut from a 0.8mm thick sheet, which was the thinnest available. Water-jet cutting was also used to cut some of the strips and it was found that the edges had a sheer face, but fortunately they were straight on the cutting side. A template was laser cut to allow easy spacing of the strips, which were first placed on the sticky side of masking tape and then the set of strips was placed on the rod surface to realise the leaky-wave antenna. Various strip widths had been simulated, to quantify the error between the perturbed and unperturbed cases, as the simulation results showed in Chapters 4 and 8. The same range of strip widths as used in the simulations were cut and, in addition, a single set of tapered strips with widths designed using (8-15) were also cut. The main objectives of these experiments were to:

- Confirm the accuracy of the new guide formulas by correlating measured results with simulated results;
- Confirm the accuracy of the new strip width compensation formulas by measuring the change in phase and beam angle for a range of metal strip widths;
- Confirm the existence of asymmetry in the front and back main beam magnitudes;
- Confirm the affects caused by variations in start spacing.

9.2 Experimental setup

The LWA was excited by a conventional TE_{10}^{y} microwave horn antenna covered by a metal plate with a hole for inserting the dielectric guide, in the same manner as previous experimenters [2] to [7]. Such a configuration is deemed suitable because the excitation mode is similar to the TE_{11}^{y} mode in the dielectric guide [8]. For radiation pattern measurement, an open metal horn was used as the receiving antenna. The experimental setups are depicted in

Figure 9.1 for pattern measurement (a) reflection coefficient measurements (b) and near-field probing (c). The output power was measured on an Agilent E4407B spectrum Analyser, with the input signal generated by an Agilent E421B signal generator. Reflection coefficient measurements and near-field probing were carried out using an Agilent ES362B vector network analyser (VNA) as depicted. A standard gain horn antenna with 4 to 6 GHz range and a double-ridged guide antenna with 1 to 18 GHz range were used as the transmitting and receiving antennas respectively.

9.3 Reflection coefficient measurements

9.3.1 Issues with covered horn without guide inserted

Input reflection coefficient (S_{11}) measurements of the covered transmit horn (without the guide inserted) demonstrated almost total reflection across the useful frequency range of the dielectric rod, except for a few narrow regions of passband. These results are shown in Figure 9.2 over the useful operating frequency range calculated for this guide. The horn could not be successfully modelled with the guide because HFSS was not be able to cope with the large dimensions of the horn compared with the dielectric rod (HFSS tries to make the finite element mesh as dense as that of the rod, which makes the problem too large for HFSS to solve). In any case, no problems had been reported using this method except without the cover [9], and it was assumed that such a thin plate (1mm thick) would not have such an adverse effect on the passband.

It is immediately obvious from the plots that the covered horn curve *(Horn_covered)* is by far the dominant factor in determining the plotted S_{11} response. However, it is also apparent that other factors are causing variations. The covered horn method therefore appears to be quite inefficient for the excitation of the LWA, despite it being used by other experimenters. However, since the received signal was found to be sufficiently high above the noise floor, which was about -70dBm, relative power measurements could still be taken. A consequence of this passband problem is that the LWA would only be frequency steerable by a few degrees

across each of the narrow passbands, and that an analysis of the frequency dependence of the antenna would be extremely restricted.

Another possible consequence of this passband problem is that, since the majority of the transmit power is reflected back inside the covered horn mouth, that the dielectric guide might be insufficiently excited. And, since the LWA radiates and therefore looses power to radiated harmonics along the length of the guide, the physical aperture might only be partially illuminated. The consequences of limited aperture illumination would be a broader E-plane beamwidth, according to basic antenna theory.

9.3.2 Covered horn with guide inserted

Next, S_{11} measurements were taken with the 10.8 mm square dielectric guide inserted 10mm through the same dimension cut out in the horn cover, both with and without metal strips. The far end of the guide was supported by a polystyrene block.

Using an equivalent covered receive horn as depicted in Figure 9.1(b), the power received at the end of the rod was measured in order to determine which passbands could be used to excite the rod. It was assumed that, if power was received at the end of the rod without strips, then that frequency may be used to excite the antenna with strips.

However, it was found when displaying the S_{11} response over the frequency range 4 to 6 GHz on the VNA display that not all the previously found passbands appeared to be compatible with the dielectric guide. Further, the passbands were also affected by the strips. In general, the effect was to improve, generate or move different passbands. Another interesting finding was that the passbands shifted sideways slightly with a change of strip width or change of start spacing between the first strip and the horn cover, most notably at the higher frequency passbands. This phenomenon appeared to be cyclic. For example, as the set of strips (stuck to masking tape) were moved further away from the excitation horn, the high frequency passbands moved sideways to a slightly lower frequency e.g. by 10 MHz, and then back

again, and so on. This feature is seen in all the passband regions e.g. around 5.9 GHz in Figure 9.2. It is also interesting to note the S_{11} of the guide with a constant strip width made using aluminium tape, as seen in Figure 9.3. The only significant difference is that the passbands just below 5.2 and 5.6 GHz appear to be much wider.

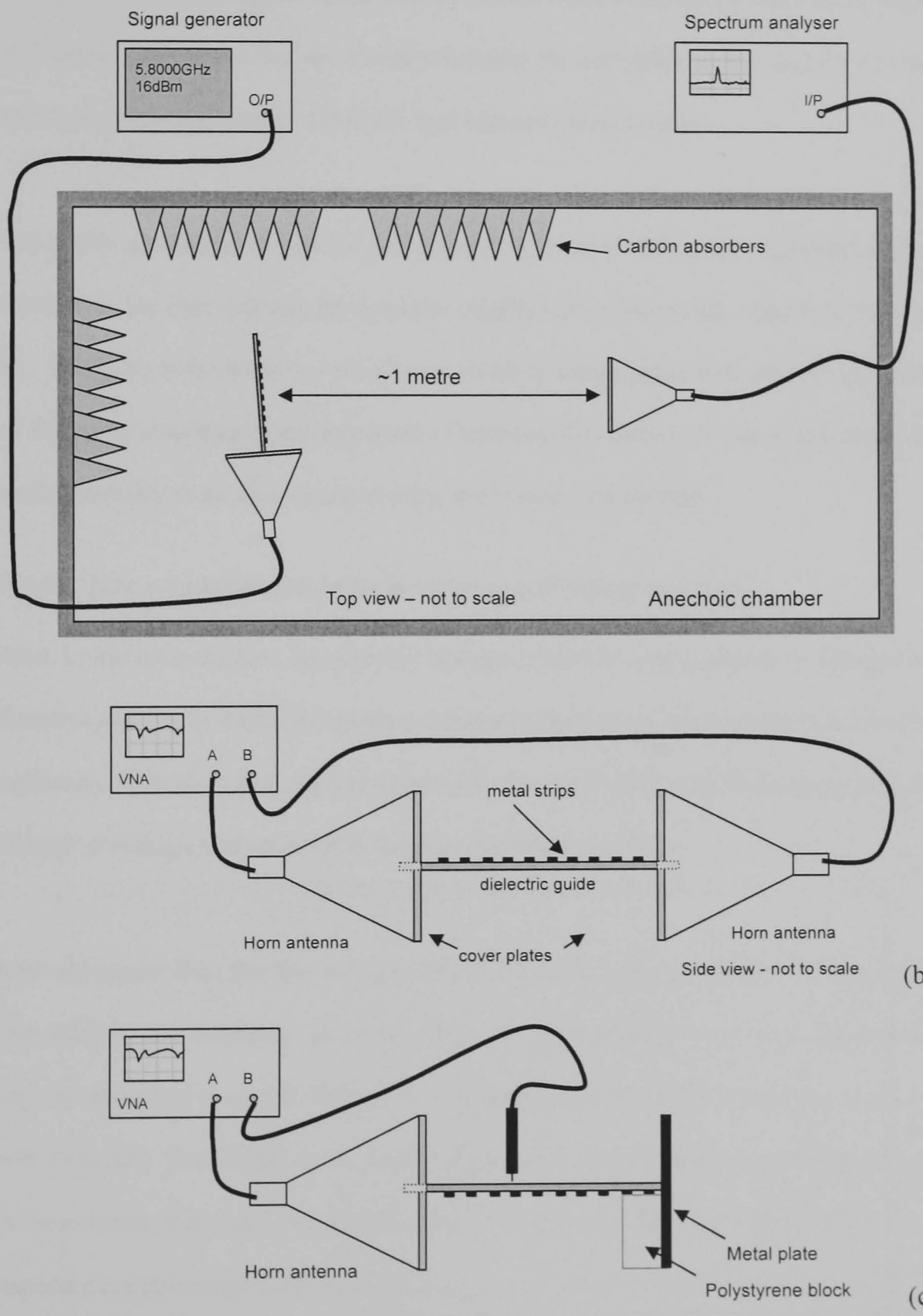

Figure 9.1 (a) radiation pattern measurement setup (b) reflection coefficient setup (c) near-field probing setup.

9.3.3 Confirmation of start spacing effects

By virtue of that fact that the input reflection coefficient is varying, the subsequent variation in received power could naturally lead to different aperture illuminations which would lead to different beamwidths which leads to different directivities as the frequencies, strip widths and start positions are changed. The measured effects tends to prove the simulation results given in Chapter 4 that show that the distance between the excitation source and the first strip, the start spacing, significantly affects the key antenna characteristics.

The earlier simulation results for other models presented in Chapter 4 demonstrated that an increase in the start spacing, for example, significantly changes the input reflection coefficient S_{11}. There, S_{11} was shown to vary almost perfectly sinusoidally at about twice the frequency of the guide wavelength and amplitude of between 0.15 and 0.25. The beam angle, directivity and asymmetry were also shown to vary in the same simulations.

9.3.4 New connection between start spacing and leakage constant

Also, in the same manner, because the leakage is known to be sensitive to changes in frequency and strip width (the guide geometry is fixed here), then it would seem to be extremely difficult at first sight to determine how much change in measurements is due to a change of leakage and how much is due to the reflection issue.

It would appear then that the leakage and the input reflection coefficient S_{11} are both controlled by the frequency, guide geometry and strip widths. These are naturally related anyway according to circuit theory since a higher input reflection means less energy going to port 2 via S21. The change in S_{11} with change in start spacing implies a change of impedance in the antenna. It appears then that the change in start spacing also gives a change in impedance. Interestingly, although the gain was shown to cycle in the same simulation results in Chapter 4, it cycled at about half the frequency of S_{11} therefore the situation is not as straight forward as saying that the change in impedance is the main factor in determining the

antenna characteristics. It is feasible then that the leakage could be a function of this implied impedance change, which would mean that the leakage is also a function of the start spacing. This connection has never been shown before.

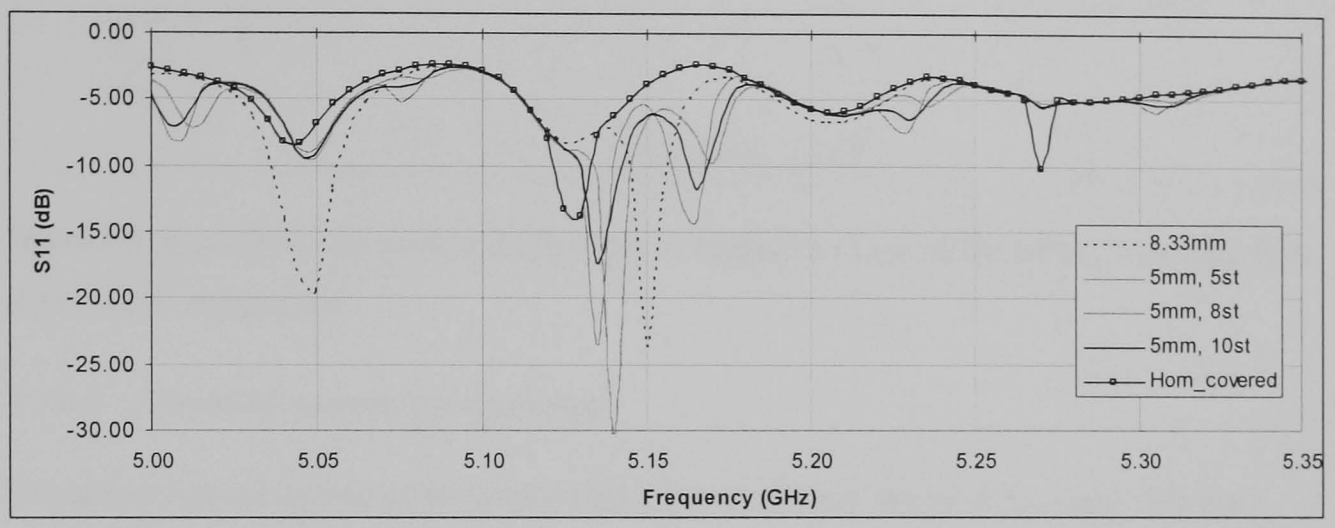

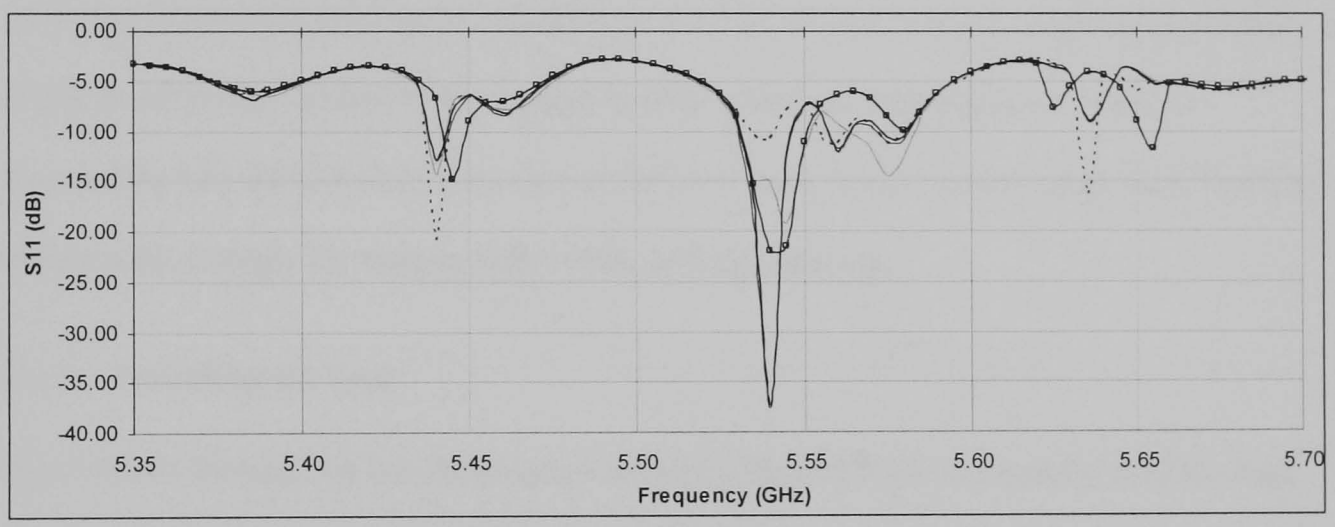

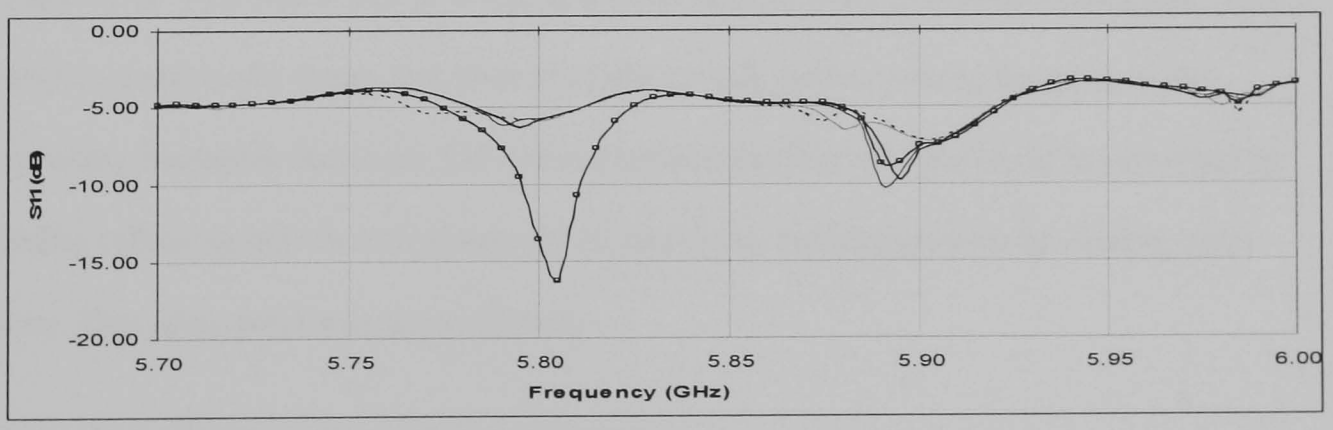

Figure 9.2 S_{11} curves for the covered horn and LWA with 5.18mm or 8.33mm wide strips. The 5.18mm strips start either 5mm, 8mm or 10mm away from the horn cover plate.

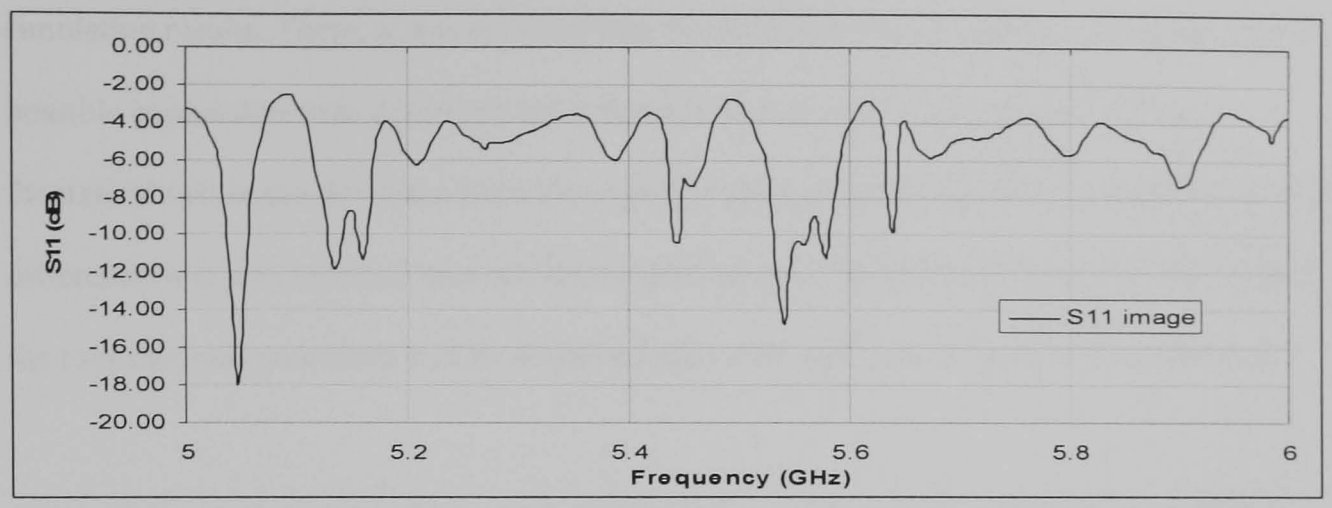

Figure 9.3 S_{11} curve for the guide with a contiguous metal strip replacing the strips i.e. the equivalent of a dielectric image guide.

9.3.4.1 Choosing operating frequencies

The author has not attempted to resolve this issue, choosing instead to be aware that the operating frequencies used in the experiments must be chosen carefully, and that the results might be adversely influenced by changes in strip width and start positions. The two frequencies 5.65 and 5.8 GHz were chosen for these experiments because they were found to radiate most strongly for various strip widths and start spacing.

9.3.5 Perturbing the field

Experiments showed that low frequencies seemed to be perturbed more easily than the high frequencies. This was found by bringing a metal plate in close proximity to the guide. This tends to confirm the theory that since the field extends further outside the guide as the operating frequency decreases, but it also demonstrates that the field could be perturbed by nearby reflecting objects and potentially impact on the radiation pattern by causing beam steer. This latter point was not confirmed.

9.4 Near-field probing measurements

The near-field probing was carried out to try to measure the guide wavelength for different width strips, including zero width and a contiguous metal strip (of aluminium tape). Previous authors have shown this to be a revealing measurement technique [9]. The most important results have already been presented in Chapter 8 to compare against theoretical and

simulation results. There, it was revealed that the measured wavelength was irregular, and a possible explanation was described and a formula was derived (8-22) to quantify the theoretical maximum deviation from the expected value found using (8-1). A small amount of difference was also reported between the theoretical and experimental results. In this chapter, the experimental procedure will be described and some additional results will be discussed.

It is prudent at this point to first explain that the guide wavelength is taken as the distance over which the phase changes by one full cycle (2π or 360°), irrespective of how the propagation constant kz might change over that cycle. This point is only made to draw attention to the fact that this rate sees a step change in kz at the transition to and from each strip, at least in the new model presented in chapter 8. One of the things to be considered next is if it is really a gradual change in kz, and if that might account for some of the difference between theoretical and experimental guide wavelengths.

The guide wavelength is of course is strongly related to the determination of the beam angle by the well-known formula (7-9), and is therefore related to the pattern measurements in this respect. However, it was also demonstrated in section 8.5.4 that the guide wavelength cannot be used to determine the beam angle directly unless the strip spacing period is made exactly the same distance. For oblique beam angles the total phase is needed over the whole period instead. The average propagation constant can be derived from the phase over the strip period using (8-3) and used instead of kz or λg in the respective forms of (7-9).

9.4.1 Near-field probing procedure

A standing wave was set up in the guide by placing a large metal plate at the end face of the VNA excited rod, as depicted in Figure 9.1(c). The S21 coefficient was measured using a probe connected to port 2 of the VNA. This probe was moved carefully along the centre of the rod to find the maxima and minima of the standing waves, using the edge of masking tape as a guide. These points were marked on the tape for later measurement with a ruler. Given that

the peaks and troughs are part of a sinusoid, they are slowly changing at those points and there is therefore some error in the measuring process, thought to be approximately ±1 mm or about ±5 % of the estimated guide wavelength of 18 mm.

9.4.1.1 Irregular distance between measured maxima

The measured results demonstrated that the distance between probed maxima and minima became increasingly irregular for strip widths >5.18mm. The continuous strip of metal tape gave the most irregularity. These values were averaged for use in the experimental curve of Figure 8.10. It is reasonable to assume that these average values for the wide strips and the continuous strip contain the greatest error therefore it is reasonable to think that it could be the reason that one of these values deviates quite far from the theoretical value. The theoretical values would then be an excellent match to the measured values.

9.4.1.2 Possible contribution from broadside null

The possible contribution of the broadside null effect was considered as a possible contributor to this wavelength irregularity. However, according to Figure 8.8, the beam angles should be well below broadside at 5.8 GHz for all these wide strip widths. The measured beam angles shown in Figure 9.6(h) next will also confirm this. The null effect is therefore discounted in this case.

9.5 Radiation pattern measurements

The radiation patterns were measured in an anechoic chamber for two constant strip widths and one tapered strip width arrangement with the spacing adjusted to equalise the phase between adjacent strip centres. The measured constant strip width patterns are compared side-by-side with HFSS simulated patterns for the same antenna models and the theoretical beam angles are also calculated and compared. The tapered strip version is compared with theory.

9.5.1 Constant strip width patterns

The measured radiation patterns are shown in Figures 9.4 and 9.5 for 5.6 and 5.8 GHz respectively, which were both found to fall within the available passbands. The measurements were taken at discrete points approximately 2° apart close to where the main beam was expected and wider increments further out. The pattern therefore appears to be more jagged than it actually is. The simulated patterns are shown at 5.6 and 5.8 GHz and are plotted with a 1° increment over the whole plot.

Comparing the measured and simulated results plots:

- The measured beamwidths are wide and are quite reminiscent of the simulated versions which are also wide compared to the typical, probably optimised, patterns presented by other authors;

This implies that the leakage is extremely high and the first few strips are radiating all the energy, or that the excitation power is low and the first few strips are radiating all the energy. The former case seems most likely since the HFSS simulation software shows an efficiency of 100% for remotely similar measured and simulated beamwidths and relative gains.

- In one case, the beamwidth appears narrow, like a typical pattern (5.6 GHz, W = 5.18mm).

It was demonstrated by other authors that the leakage is a strong function of the operating frequency, guide geometry and strip width and thickness [10,11]. It seems reasonable then to assume that in this case the leakage could be lower and the illuminated aperture much larger.

- The broadside null is extremely evident in all but one case (5.6 GHz, W = 8.33mm) from the experiments, but not at all evident from the simulation results for this model;

Since no previous authors have presented wide beamwidth patterns in their work, it is difficult to be sure if the measured pattern is normal. However, many authors have demonstrated the gain is very low at broadside so it seems reasonable to assume that if the beamwidth is wide and encompasses the broadside angle, that this null will exist as found. In Chapter 4, the

reduced gain at broadside was also demonstrated, and in those cases the gain was decreased but there were no nulls evident within the individual beams.

- The relative power levels for the two strip widths agree i.e. at 5.6 GHz the measured and simulated power is lower for the widest strip width and at 5.8 GHz the measured and simulated power is lower for the narrowest strip width;

Since the excitation horn antenna and cover plate were not simulated with the leaky-wave antenna, as explained in the introduction to this chapter, and this excitation method has been found to have some serious issues, the simulation and experimental results were not expected to match. However possible, it seems unlikely that the fact that they do is simply down to luck because they agree in all cases by similar relative amounts.

- Although the simulations show that the antenna should radiate more strongly at 5.6GHz than at 5.8GHz, the measured results do not agree;

Since the excitation issue is frequency sensitive, it is not surprising that the simulation and experimental results differ at these different frequencies.

- There are many spurious lobes present in the measured patterns;

Such spurious lobes are sometimes a result of *transmitted* internal reflections between the back of the strips and the opposite guide wall [3]. However, in this case it is feasible that they could also be reflections *received* from the anechoic chamber walls because the chamber was of the ferrite tile type and rated only for up 1 GHz. Early investigations using an open transmit horn and received horn had showed that the received power was at least 25dBm down when the transmit horn radiating in the 5 to 6 GHz region was pointed at the walls at oblique angles for which a reflection might be expected. In the experiments, carbon absorbing tiles were placed on the chamber walls as an added precaution. Despite these measures, it is feasible that such reflections could exist in the measured patterns because the received power

was relatively weak. Although feasible, it is therefore unlikely that spurious beams of half the magnitude or more could be reflections from the chamber walls.

- There is asymmetry between the magnitudes of the beams at each side of both simulated antennas. An asymmetry of about 2:1 is evident at 5.8 GHz, which is similar to that simulated. However, at 5.6 GHz perfect symmetry was measured;

Such asymmetry was seen in the current simulations and also in the simulation results seen in Chapter 4, where the results of a parametric simulation study were reported. Only one other author has pointed out this asymmetry but did not try to explain it [12] and it was also evident in the radiation patterns in a number of other references but not commented upon [5,13]. *These experimental measurements therefore tend to confirm the existence of asymmetry for the open dielectric waveguide type.* No satisfactory explanation has currently been found for this effect. In the optical case, a sawtooth grating has been used to eliminate the beam on one side of the grating [14]. However, this was due to the reflections and refraction on the angled surfaces, which did not offer clues for the metal strip grating case.

- In one case, the endfire radiation (0°) is higher than simulated;

Radiation at the endfire direction is normally attributed to inefficient radiation in the intended direction. This essentially translates to an aperture inefficiency. This will be explained in Chapter 10 when concluding about leakage from this type of structure.

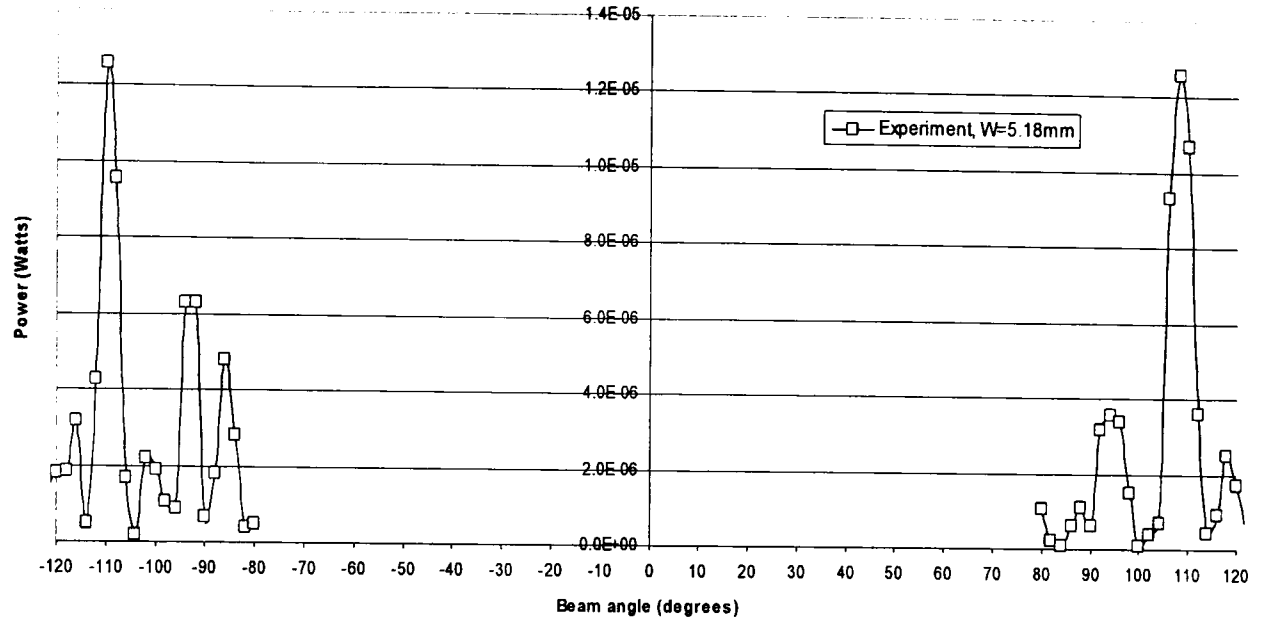

(a)

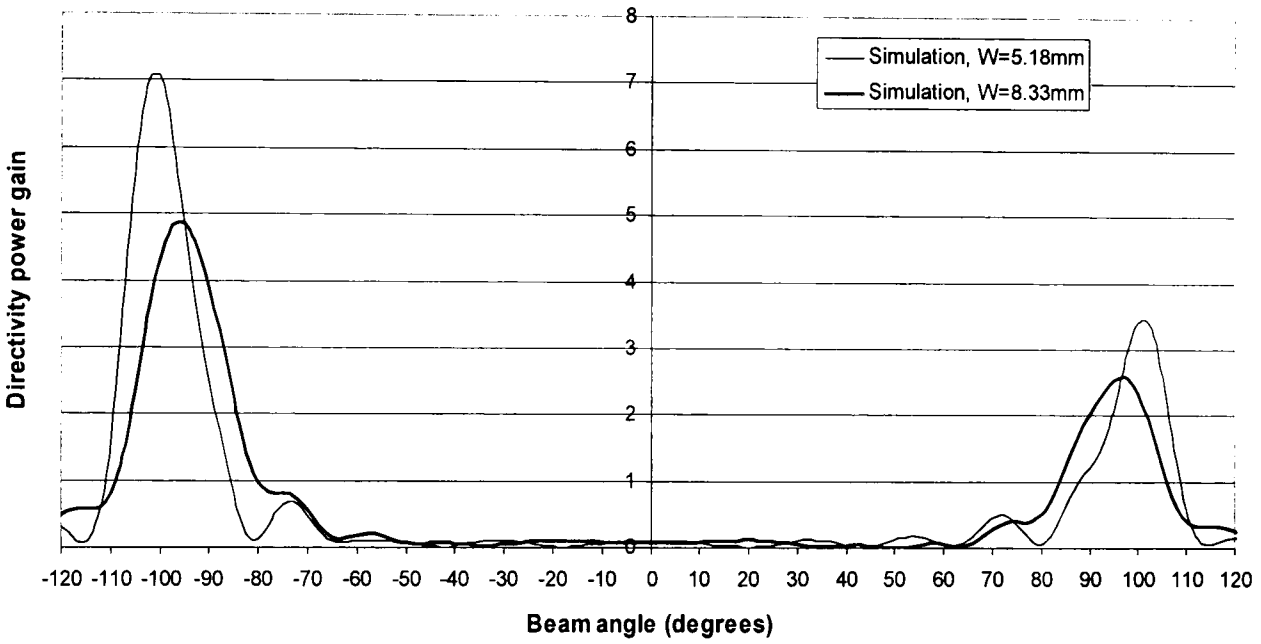

(b)

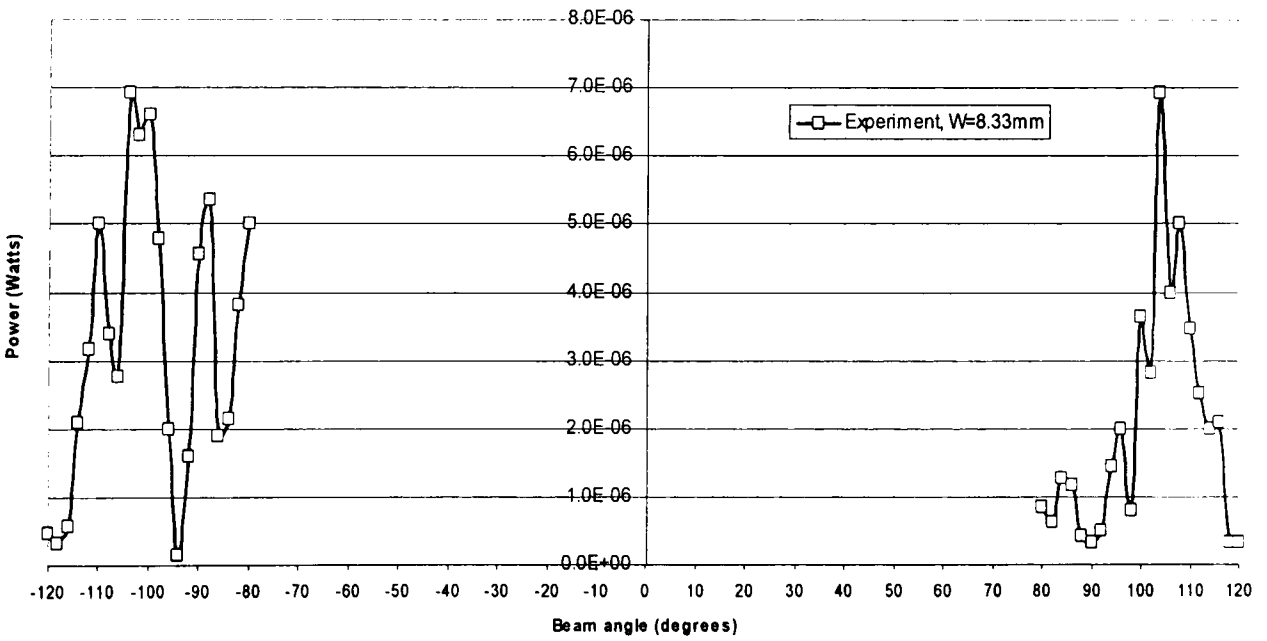

(c)

Figure 9.4 Radiation patterns at 5.6 GHz for different strip widths (a) measured with 5.18mm strips (b) simulated for 5.18mm and 8.33mm strips (c) measured with 8.33mm strips.

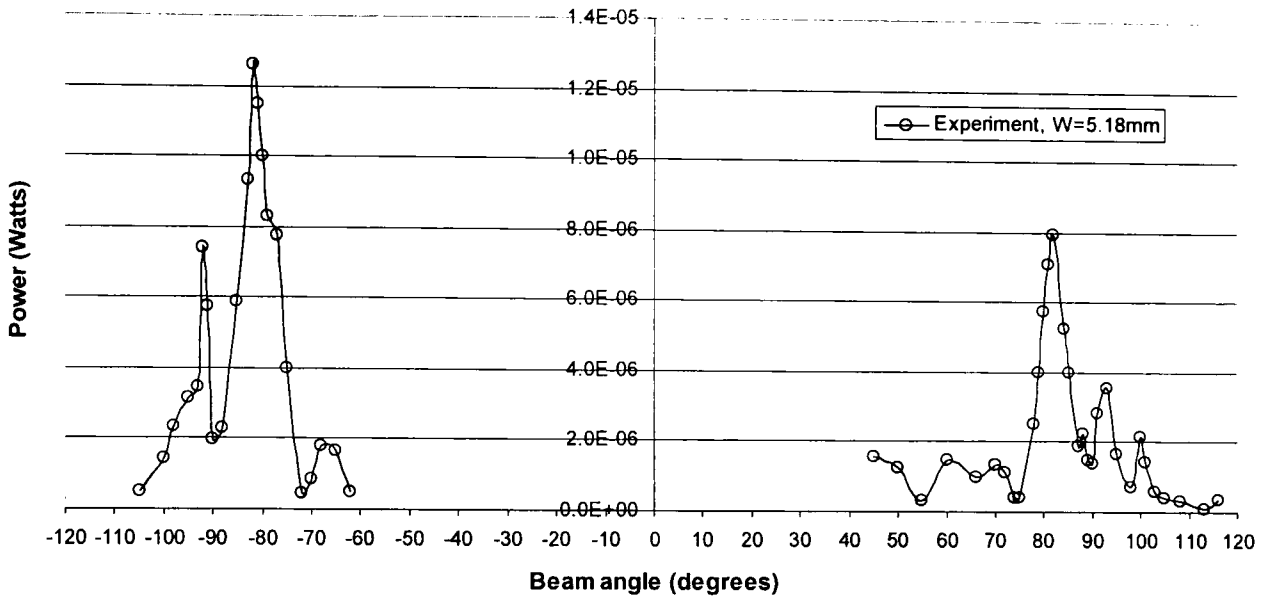

(d)

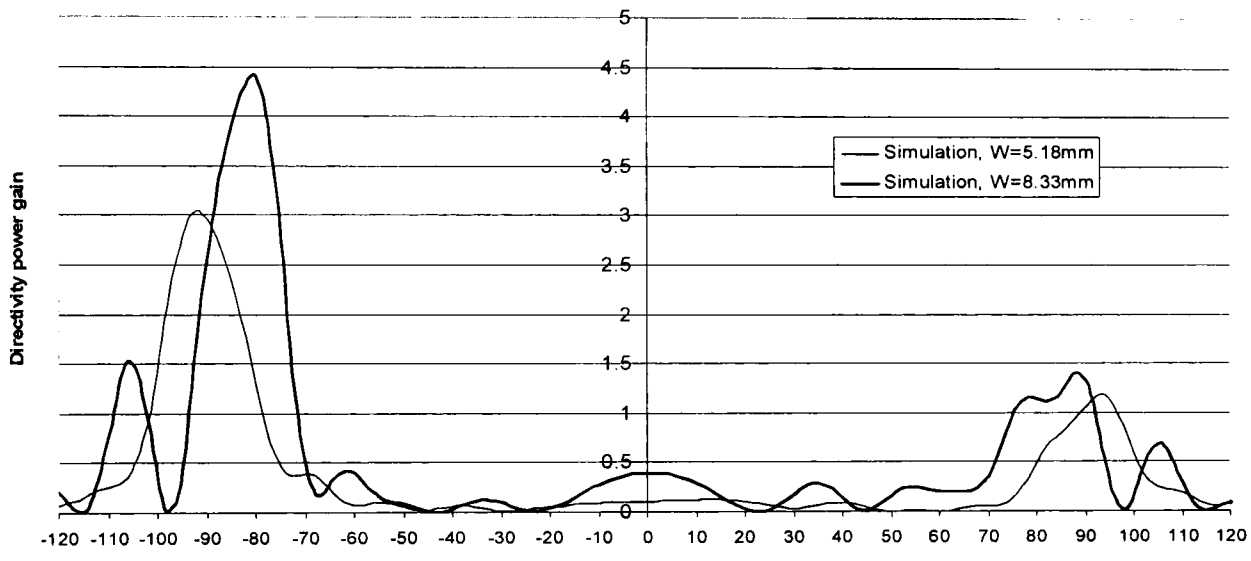

(e)

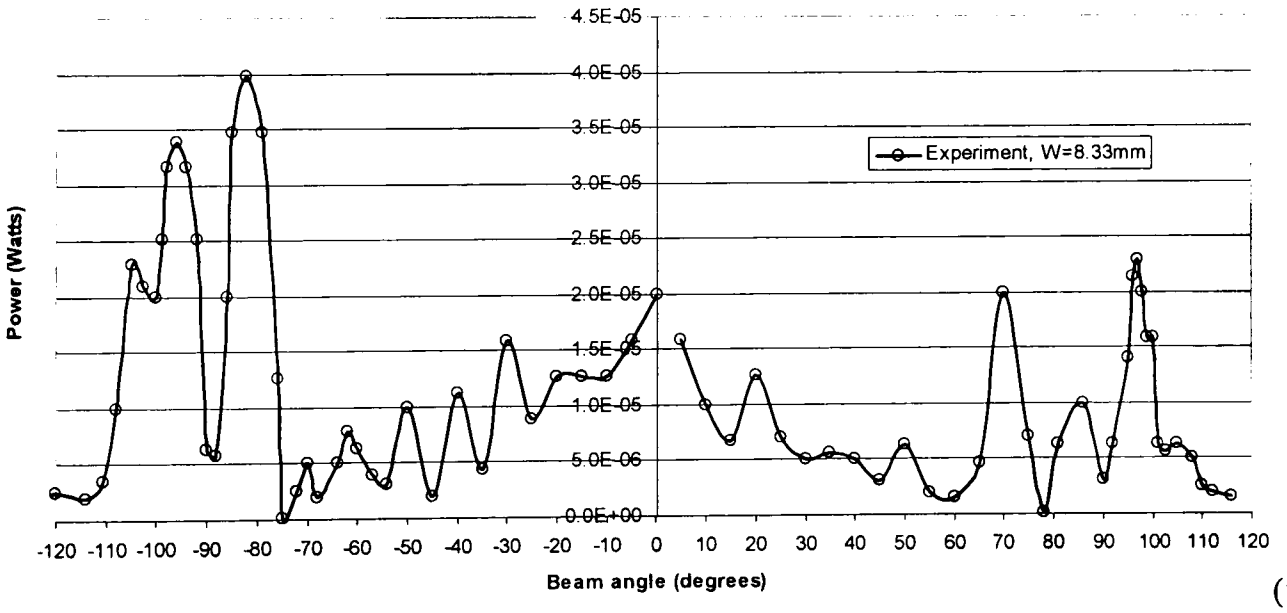

(f)

Figure 9.5 Radiation patterns at 5.8 GHz for different strip widths (d) measured with 5.18mm strips (e) simulated for 5.18mm and 8.33mm strips (f) measured with 8.33mm strips.

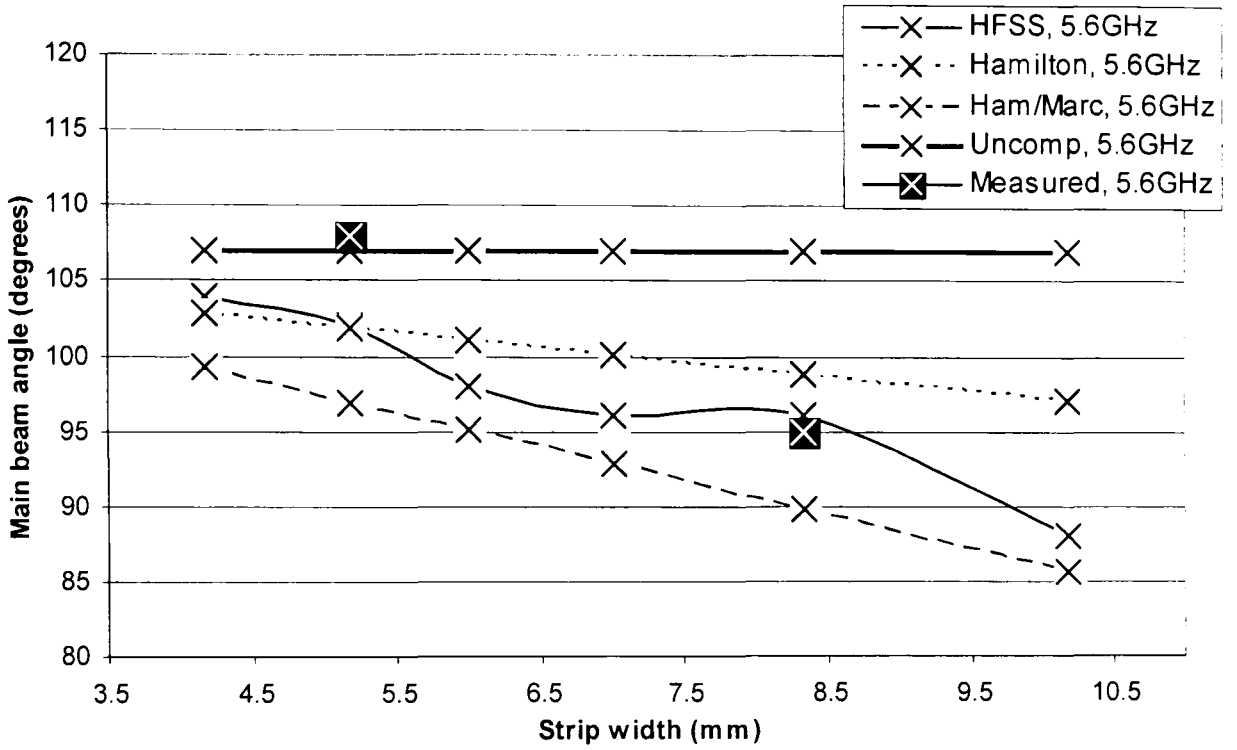

(g)

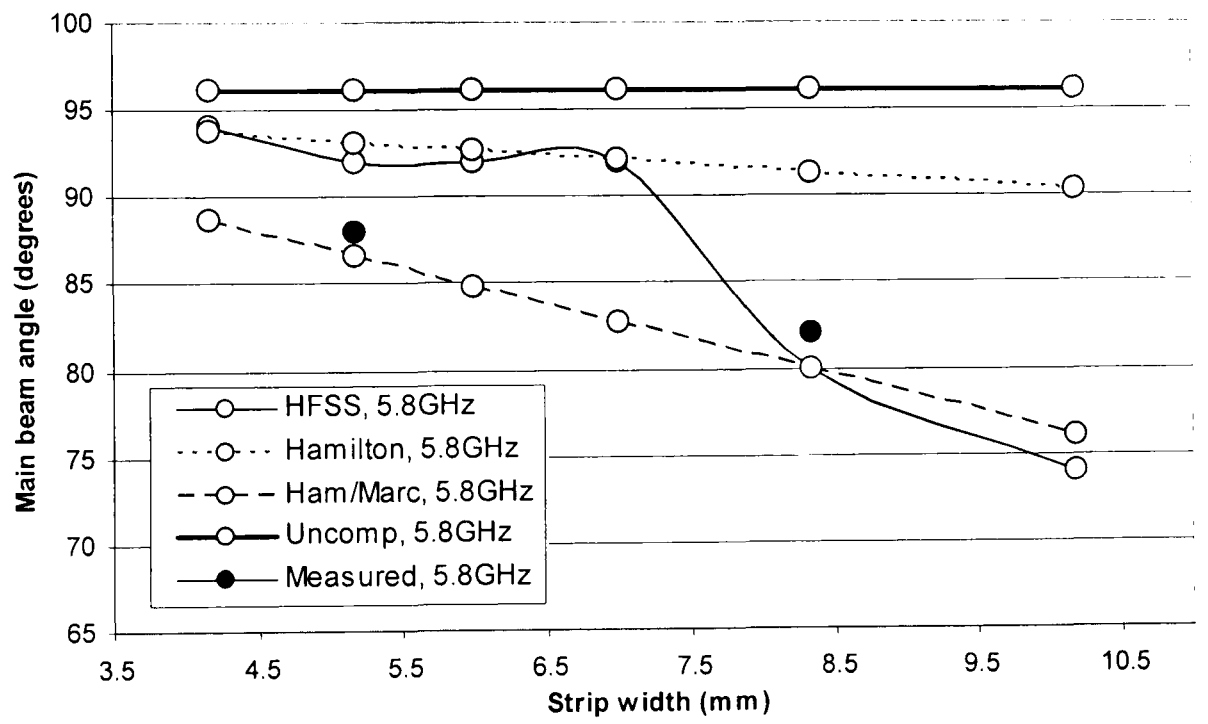

(h)

Figure 9.6 Measured, HFSS simulated and theoretical beam angles at 5.6 and 5.8 GHz. Theoretical values are assuming zero strip width (*uncomp*ensated case) and actual strip widths with spacing compensated accordingly using (8-4) and (8-5) with d = 18mm. In (8-4), the propagation constants are calculated using the new formulas from Table 7.2 and (7-4) labelled as *Hamilton* and the Marcatili formulas [15] labelled as *Ham/Marc.*

9.5.2 Tapered strip width pattern

Strips of a constant width spaced with a constant period should theoretically result in each strip radiating at the same angle into space. However, strips of varying widths should theoretically result in them all radiating at different angles. The same is true for a constant width and varying spacing. A simple experiment to plot the radiation pattern using the simple linear array formula using (2-1) for an array of point sources with tapered spacing demonstrated that the main beam is biased closely toward the highest angle.

A formula was derived in section 8.5 to adjust the spacing to compensate for the increase in phase caused by the introduction of any width strip, and for any desired main beam angle (8-11). This was extended to accommodate the well known empirical strip taper formula originally presented in [12] and its form is extremely simple and convenient to use (8-19).

The *exact* variable strip width case shown in Figure 8.2(c) was used to eliminate the error in the *simplified* variable strip width case. This was accomplished by finding the strip widths first using (8-15) and then using (8-12) to make the necessary adjustment so that half of the first strip and then half of the next strip are used per period. The strip spacing was then calculated for every period to give a constant main beam angle of 97.3° in this case, shown in Figure 9.7 as the *compensated* case. Also shown is the *uncompensated* case which shows what beam angle each strip in the taper would radiate at if they were spaced with a constant period of 18mm. Taking the above argument that the net beam angle will be biased toward the highest angle would result in a main beam around 90° in this case.

The error of approximately 7° minimum between the uncompensated and compensated spacing cases demonstrates the theoretical merit in adjusting the spacing for the empirical taper formula. However, experiments using the designed strip taper were unsuccessful, as can be seen in Figure 9.8 from the poor pattern measured.

Since the measured power levels were extremely low at the receiver, it is thought that the relative narrowness of the strips possibly coupled with low leakage efficiency for this structure might be the reasons why there is no discernable main beam. These taper experiments were therefore unsuccessful and the theoretical improvement could neither be proved nor disproved.

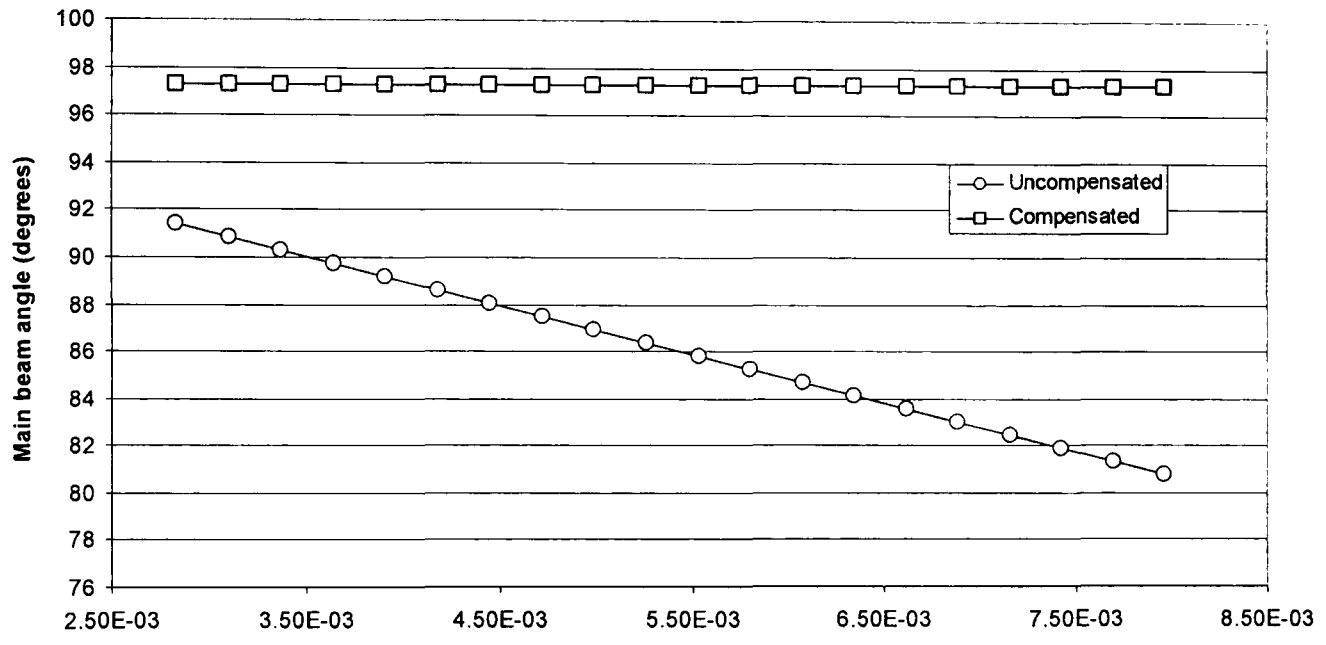

Figure 9.7 Shows the theoretical main beam angle versus strip widths for the case where the spacing is adjusted to maintain the phase between strip centres constant, and the case where the centre spacing is fixed (uncompensated).

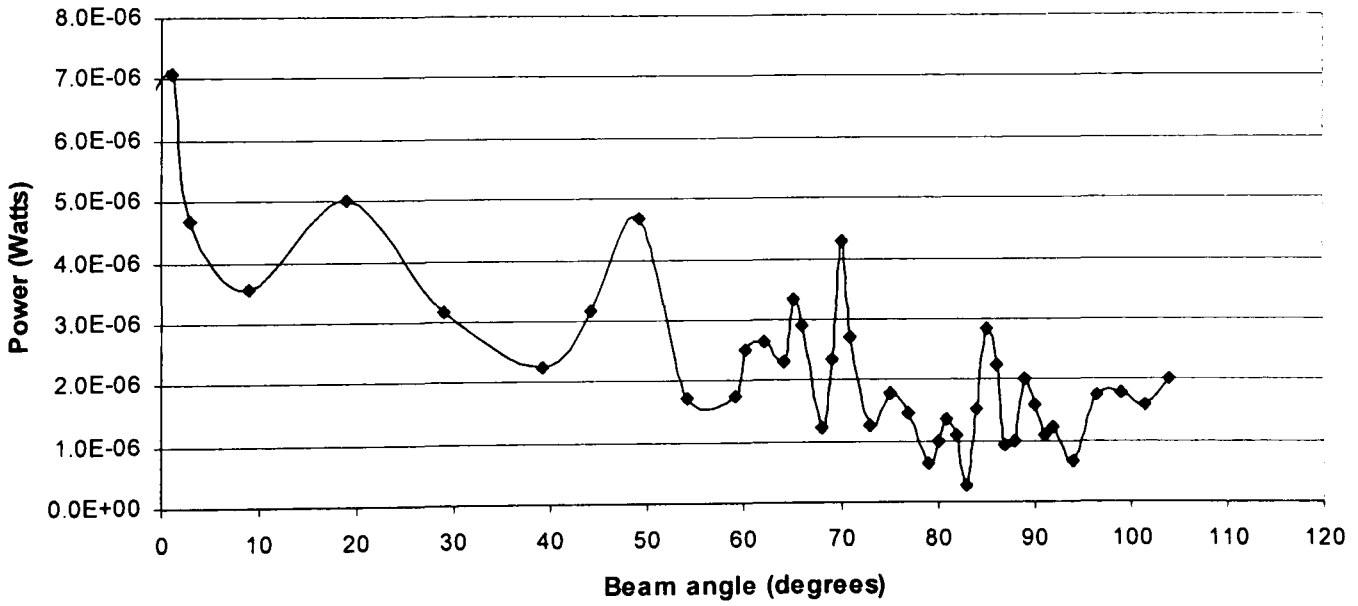

Figure 9.8 Radiation pattern for the tapered strip width model.

9.6 Conclusions

The existence of number of features of leaky-wave antennas that were found through simulations or theory have been confirmed by experiments, including:

- Change in input reflection coefficient with start spacing;
- Strip-side to back-side beam asymmetry;
- Decrease in guide wavelength with wider strips (increased propagation constant);

It was also found that the covered horn antenna excitation method is extremely frequency selective and only limited passbands existed for which experiments could be conducted. Input reflection coefficient measurements demonstrated that the passbands were found to move around with small changes in strip position, and in a cyclic manner as simulation results had suggested in Chapter 4.

Radiation pattern measurements showed wide E-plane beamwidths in the order of 20°. Ordinarily, the beamwidth would be expected to be in the order of ~5°. Interestingly, the beams that passed through broadside had a clear null in the lobe at that angle. The wide beamwidths are attributed to poor aperture efficiency and the poor aperture efficiency is thought to be a function of the unknown leakage of the waveguide design.

The measured main beam angles were compared with the theoretical unperturbed and compensated cases. The latter uses the strip width compensation formulas developed in Chapter 8 that takes the finite width of the strip in account when calculating the beam angle for a given spacing. The results demonstrated good agreement between the measured results, the compensation theory and simulation results. They also demonstrate categorically that the unperturbed case that ignores the strip width, gives a large and increasing error as the strip width is increased.

The compensation theory was then used to design an antenna with tapered strip widths. However, this antenna was found to radiate poorly in practice. It is thought that this was due to the relatively narrow strips along the length of the antenna.

9.7 References

[1] F. Schwering and A.A. Oliner, *Millimeter-wave antennas* in Antenna Handbook, Eds. Y.T. Lo and S.W. Lee, Van Nostrand Reinhold, New York, Chapter 17, 1988.

[2] K. L. Klohn, R. E. Horn, H. Jacobs and E. Freibergs, "Silicon waveguide frequency scanning linear array antenna," *IEEE Trans. Microwave Theory and Techniques*, vol. MTT-26, no. 10, pp. 764–773, Oct. 1978.

[3] T. Teshirogi, Y. Kawahara, A. Yamamoto, Y. Sekine, N. Baba and M. Kobayashi, "High efficiency dielectric slab leaky-wave antennas," *IEICE Trans. Communications*, vol. E84-B, no. 9, pp. 2387-2394, Sep. 2001.

[4] H. Jacobs and M. M. Chrepta, "Electronic phase shifter for millimeter-wave semiconductor dielectric integrated circuits," *IEEE Trans. Microwave Theory and Techniques*, vol. MTT-22, no. 4, pp. 411–417, Apr. 1974.

[5] S. Kobayashi, R. Lampe, R. Mittra and S. Ray, "Dielectric rod leaky-wave antennas for millimeter-wave applications," *IEEE Trans. Antennas and Propagation*, vol. AP-29, no. 5, pp. 822–824, Sep. 1981.

[6] L. Huang, J.C. Chiao and M.P. De Lisio, "An electronically switchable leaky wave antenna," *IEEE Trans. Antennas and Propagation*, vol. AP-48, no. 11, pp. 1769-1772, Nov. 2000.

[7] H. Schrank and N. Herscovici, "The shaped-beam polyrod antenna," *IEEE Antennas and Propagation Magazine*, vol. 36, no. 2, pp. 55-57, Apr. 1994.

[8] C. Salema, C. Fernandes and R.K. Jha, *Solid dielectric horn antennas*, Arctech House, 1998.

[9] A. Basu and T. Itoh, "Dielectric waveguide-based leaky-wave antenna at 212 GHz," *IEEE Trans. Antennas and Propagation*, vol. 46, no. 11, pp. 1665-1673, Nov. 1998.

[10] M. Guglielmi and G. Boccalone, "A novel theory for dielectric-inset waveguide leaky-wave antennas," *IEEE Trans. Antennas and Propagation*, vol. 39, no. 4, pp. 497-504, Apr. 1991.

[11] M. Matsumoto, M. Tsutsumi and N. Kumagai, "Radiation characteristics of a dielectric slab waveguide periodically loaded with thick metal strips," *IEEE Trans. Microwave Theory and Techniques*, vol. MTT-35, no. 2, pp. 89-95, Feb. 1987.

[12] T.N. Trinh, R. Mittra and R.J. Paleta, "Horn image-guide leaky-wave antenna," *IEEE Trans. Microwave Theory and Techniques*, vol. MTT-29, no. 12, pp. 1310-1314, Dec. 1981.

[13] J. Jacobsen, "Analytical, numerical, and experimental investigation of guided waves on a periodically strip-loaded dielectric slab," *IEEE Trans. Antennas and Propagation*, vol. AP-18, no. 3, pp. 379-388, May. 1970.

[14] D. Marcuse, "Exact theory of TE-wave scattering from blazed dielectric gratings." *Bell Syst. Tech. J.*, vol. 55, no. 9, pp. 1295–1317, Nov. 1976.

[15] E. A. J. Marcatili, "Dielectric rectangular waveguide and directional coupler for integrated optics," *Bell Syst. Tech. J.*, vol. 48, no. 7, pp. 2071–2095, Sep. 1969.

10 CONCLUSIONS & RECOMMENDATIONS

10.1 New way to represent dispersion characteristics of rectangular dielectric waveguides

The most popular antennas, especially those in wide use, most often have quite trivial formulas already developed that allow their design; these can be found in any antenna textbook. While this situation exists to a small extent for leaky-wave antennas when the dispersion characteristics for the supporting guide are known, it is these characteristics that are difficult to derive and there were no simple formulas until now.

10.1.1 Insufficient accuracy of existing formulas

It was proven in this work that existing formulas (2-1) to (2-4), which neglect the change in propagation constant caused by the introduction of the gratings, the metal strips in this case that cause the guide to radiate, are only remotely accurate for $\varepsilon r \sim 2$ and for very narrow strips. In all practical circumstances, the strips will never be narrow and so the error will be large. This error was quantified in Chapter 8 for a number of simulated guide models and then verified by experiment in Chapter 9.

10.1.2 Eliminating variables

Solutions for the dispersion characteristics exist for both the guide with gratings and without. The latter types are of course the easiest to derive, and perhaps the most popular version by Marcatili method for rectangular dielectric waveguides was chosen for use in this work. This turned out to be a good choice because the relative speed of implementation and computation allowed an extensive study of the characteristics for many different guide geometries and materials to be carried out. In addition, the Marcatili method allowed a further simplification to be made by imposing a cutoff frequency for the fundamental travelling wave mode. Solutions for specific structures including the gratings would have added many variables and considerably reduced the dimensions of such a study.

10.1.3 Enabling rapid guide selection

When beginning a leaky-wave antenna design, it is difficult to know where to start as far as designing a suitable guide is concerned. For example, if multiple suitable materials are available in different sizes and an antenna is required to operate at 10 GHz, it is difficult to know which material to choose and what dimensions to machine it into. When the guide might be placed on a ground plane or in a metal trough, this adds an extra dimension and makes the choice even more difficult. At millimetre wave frequencies, it might be advantageous to make the guide dimensions as large as possible to increase the success of machining small dimensions. At much lower frequencies, the smallest possible guide might be preferred to reduce the bulkiness. To solve this conundrum, the designer has to derive the dispersion characteristics for many different guide sizes and materials in order to converge on the most suitable combination. This represents a large time burden for the designer.

With this in mind, in Chapter 5 and 6, the dispersion characteristics were computed using the Marcatili method for a great number of different guide dimension and materials, including on ground planes and in troughs. Like Marcatili, whose solution was enabled and simplified by recognizing that the fields at the corners of the guides could be ignored, a further important

simplification was made by the present author that enabled the dispersion characteristics to be made guide-size independent. Further, it was discovered that the same normalisation factors that enabled this simplification could also be applied to the other guide types.

Marcatili's method only derives the propagation constant directly. The valid frequency range for any guide can only be found by an iteration process that computes this propagation constant until it reaches cutoff. Therefore, despite the fact that it represents a large simplification over an exact solution, it is still quite complex and represents a relatively significant programming task to implement. However, this programming task, which represents many months of work, was undertaken here to derive and then normalise the dispersion characteristics.

These new size-independent characteristics and their material dependence were then presented as plots, from which suitable choices of dimensions and materials can be derived by inspection in just a few minutes, and most importantly without the programming burden usually required to make that choice. This is believed to be the first time that the material dependence has been shown in this practical manner.

Another important ingredient that enabled both the guide size independence and limited the computational burden was the decision to limit the guide cross section to a small number of fixed aspect ratios. The chosen aspects were found to represent the complete practical range, because the change in characteristics was found to be negligible for aspects greater than about 10:1. Fixing the aspect ratio was considered acceptable here because such a choice could be made in a new design. In any case, it is good to limit the choice because the designer is most likely to choose one extreme or the other, or a compromise, rather than choose some obscure ratio in between. Analysis of existing designs is also immediately possible if the aspect is one of those used here, or can be estimated in other cases. Such standardisation has already been applied to standard metal waveguides, for which there are standard specification charts. For

the first time, an equivalent chart was also presented for open dielectric waveguides of the same dimensions.

10.1.4 New dispersion formulas

Additional normalisation, beyond that used to produce the plots, made the dispersion curves almost perfectly straight. This was another key finding, and again the same factors were found to apply to the other guide types. One of the main deliverables from this work is the resulting trivial straight line formulas, derived in Chapter 7, that allow the useful frequency range and propagation constant of the guides to be calculated. Twelve sets of coefficients were computed to represent each combination of the four practical aspect ratios and three common guide types studied. This is the first time that a simple formula has been derived for finding the frequency range of all these guide types directly and in closed form; it is key to the guide selection process.

10.1.5 Application of new method to other structures

This new way of representing dispersion characteristics and associated new formulas meet the goal of simplifying the once difficult task of deriving the characteristics needed to perform leaky-wave antenna analysis or design.

In principle, the same normalisation process and resulting straight-line representation could be applied to any set of dispersion curves provided that they are smoothly varying. The present author believes that there is equal merit in obtaining the dispersion characteristics for other useful structures, including perturbed structures, for a wide range of practical combinations of parameters. They should be presented in a practically useable form as plots and formulas as done in Chapters 6 and 7 of this work for unperturbed rectangular guide structures. Such knowledge can be then used as a parameter selection aid to assess quickly the response to parametric changes, and make changes, and form a working design. The same normalisation method should be used and any curved parts of the dispersion characteristics that cannot be

normalised to a fit a curve of straight line should be cut off, as was done for the E_{11} mode characteristics at the low frequencies in this work (see Figure 3.3). The process of normalisation is simplified by manipulating the captured dispersion data in a spreadsheet program and plotting the resulting curves.

The point of this whole exercise is for the specialist to use their significant insight and implementations to produce the data for a large number of practical cases to allow other workers to bypass most, if not all of the significant workload normally associated with the analysis or design. The other point is to allow a subject to be brought into wider use by giving less experienced engineers or scientists, like undergraduates, easy access to design data and without needing much background knowledge.

It is anticipated that this new way of representing the dispersion characteristics will apply immediately to other rectangular guides like the non-radiative dielectric (NRD) guide, various types of strip guide e.g. [1,2,3] and semi-rectangular guides embedded in MMIC substrates [4]. Some guide types such as the NRD guide [5] have physical asymmetry that effectively adds another dimension to the problem in the same way that the space between the guide walls and metal trough of the trapped image guide adds another dimension.

Careful consideration should be given to which parameters can be reduced to just a few discrete values and which need a wider range. For example, if the goal is to produce data for designing practical NRD guides, only the most important value(s) of asymmetry should be used. It would be a waste of effort to capture data for values that are inefficient. On the other hand, the choices of other parameters should not be too restrictive because part of the motivation is to fill in the gaps between currently published results that only consider certain values. It is likely that other guide shapes, such as circular, will use slightly different normalisation factors, but the process will be the same.

10.2 Improving accuracy of existing leaky-wave antenna design formulas

Choosing to solve for the dispersion characteristics of the bare dielectric guides themselves as opposed to the guide with strips for the antenna design usually implies that the radiation pattern and other characteristics will be computed by neglecting the strips entirely. This has been done by many previous authors [6] to [9] and is generally known as the unperturbed case.

However, it was realised once the dispersion characteristics had been solved for the completely open guide and image guide, that the strip covered open guide is effectively just a section of image guide. Theoretically then, the LWA unit cell consists of an open guide section in series with an image guide section of length equal to the strip width, each with different dispersion characteristics. This new model was presented and validated in Chapter 8. The error between the perturbed and unperturbed cases could then be found by computing and comparing the characteristics of the new model with the same unit cell length of open guide section. The error obviously increases as the difference between the propagation constant of these two sections increases, and as the length of these two sections of the unit cell changes. Now, since the propagation constant over a finite distance gives the phase, the total phase per unit cell can be found as the sum of that found for the open and image guide sections.

This is useful since the phase progression between adjacent unit cells sets the beam angle of this antenna, as determined by the usual linear array antenna factor (2-1). It is now possible to set the phase and therefore beam angle to any desired value by choice of strip width, strip spacing, guide dimensions and material.

It is important to point out, for the first time, that the propagation constant and therefore the guide wavelength actually changes within the unit cell in the perturbed case. This is especially interesting when it is considered that the simple well-known formulas for deriving the beam

angle, radiation pattern and strip spacing limits (2-1) to (2-4) are all based on a single contiguous value; effectively *analysis* formula for the unperturbed case.

With this in mind, and having shown that the unperturbed case can be extremely inaccurate, a formula for the average propagation constant was derived (8-4) that can be substituted for the constant propagation constant terms to correct the unperturbed formulas. In addition, a synthesis formula was derived to allow the strip geometry to be found for any desired beam angle (8-14). It was also demonstrated how to combine this with strip width taper formula for controlling the aperture distribution.

10.3 Reduced burden

The accuracy of dispersion formulas derived using the new method can only ever be as accurate as the dispersion results from which they are derived. In this case, the Marcatili method is known to produce results approaching the accuracy of an exact method as the operating frequency reaches the half way point of the single mode range. The new coefficients have been optimised to bring the results to within 1% of Marcatili's at the high frequency end. Also, Marcatili's method computes the cutoff of the first higher mode about 5% high, therefore this was compensated for in the new dispersion formulas, effectively making the new dispersion formulas more accurate at predicting the upper frequency limit for single-mode operation. At the low frequency end, where Marcatili's method is approximate, the new results are within 2%. This is deemed acceptable because the wave is poorly guided at the low frequency and should generally be avoided in practice anyway. This implies that the fact that the Marcatili method predicts a cutoff of the fundamental mode that does not really exist, and the new formulas predict the same cutoff, imposing such a cutoff is advantageous.

Other available methods for computing the perturbed dispersion characteristics are extremely rigorous and time-consuming to implement, and are only as accurate as their simplifications

allow. For example, the most widely used transverse equivalent network (TEN) model is only as accurate as the circuit representation of the perturbed guide section. This has only been proven by direct comparison with experimental results in one case for one type of guide. Even when the circuit is extended to incorporate higher spectral harmonics, the agreement with experimental results was shown to be no better [10]. The implication is that such a rigorous method does not give sufficient enough additional accuracy to justify its use over the new method presented in the current work. The rigorous perturbed methods do however find the complex leakage part of the propagation constant.

Since more rigorous methods represent quite a large increase in the time and complexity burden over the Marcatili method, and an even more extensive increase over the new formulas presented in this thesis, all with similar accuracy, the new formulas represent a significant advancement in LWA design and analysis. The simplicity of the new formulas, the fact that they are closed form and can be solved using a simple calculator, and the fact that very little background knowledge is required to use them makes them suitable for inclusion in general text books containing waveguide or antenna chapters. This reduced time and complexity makes dielectric waveguide analysis and LWA analysis accessible to a much wider, less specialist audience.

10.4 Further recommendations

10.4.1 Last piece of puzzle – leakage

A study of the leaky-wave antenna cannot be concluded without further discussing the complex part of the propagation constant, the leakage constant. This work has concentrated on simplifying the solution of the real part. However, the present author has studied the leakage enough during this work to believe that its solution can be simplified to a similar extent or, rather, that the optimum parameters for achieving highest leakage can be ascertained. This appears to be the last significant unsolved piece of the goal to simplify significantly the leaky-wave antenna analysis and design.

10.4.1.1 Large leakage variations

It was demonstrated in the parametric analysis results presented in Chapter 4 that the leakage and therefore directivity gain can be maximised for any LWA model by choice of strip width and spacing (around $W/d = 0.5$). However, the difference between the maximum directivity gain for one model was found to be completely different from another. This fact was reinforced by many additional simulation results, not presented in this work. A thorough early investigation carried out by inspecting the values of individual physical and electrical parameters and combinations of these parameters failed to reveal why some models gave high gain, while others gave low gain. These results tended to suggest extreme sensitivity to parametric changes, and a sense of randomness about which combinations of parameters were best. A key author has given one example of how the parameters affect the leakage in a dielectric grating LWA [11]. Those results are reproduced in Figure 10.1 to demonstrate that there will only be significant leakage for certain combinations of parameters, and their mostly parabolic relationships will lead to leakage and therefore gain peaks. This tends to explain the apparent randomness of the parametric study directivity gain results; the small change of parameter appears to result in a large change in leakage. Ideally, the antenna would be operated around these peaks where it is slowly varying. [12,13] give other specific examples.

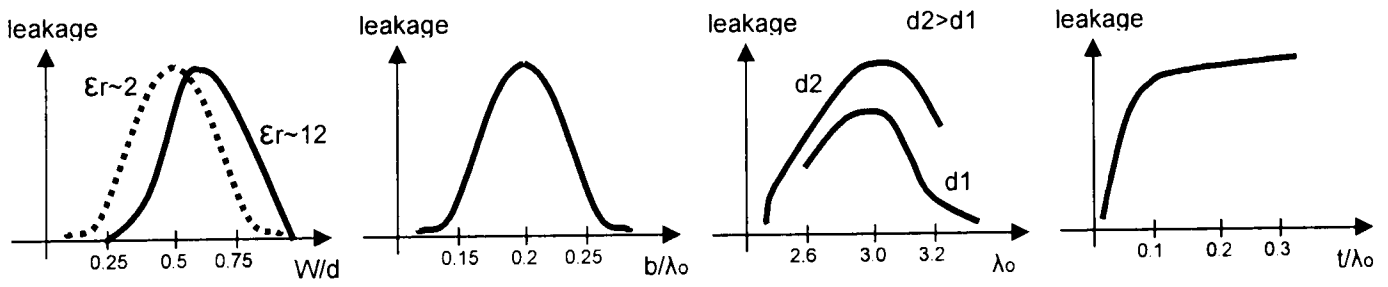

Figure 10.1 Results reproduced from [11] demonstrate relationships between leakage and strip width W, strip spacing d, guide height b, operating wavelength λ_o and dielectric grating thickness t on a $\varepsilon r = 12$ Silicon image guide (except where shown).

10.4.1.2 Importance of guide in establishing good leakage

The implication is that, besides the strip width and spacing, the guide dimensions and operating frequency play an extremely important role in establishing good leakage conditions.

This raises an interesting point: if the guide conditions for efficient leakage are unknown, it is impossible to know how many strips are needed to radiate such that there is little energy at the end of the guide. Of course, if this efficiency is unknown the antenna can be made or simulated with a very large number of strips e.g. 50 and then reduced in length until the gain is affected. However, if the efficiency is known, and the relationship between the leakage rate per unit strip width is known, the number of strips can be determined in advance. Moreover, if the conditions for highest leakage are known, then it will be possible to design the shortest antenna.

10.4.1.3 Leakage study recommended

A thorough structured study of the leakage constant is therefore recommended to determine what the optimum combinations of guide geometries, materials and single-mode operating frequencies are for obtaining maximum leakage from any given dielectric waveguide. The half peak -3dB points or a few other discrete points, for example, should also be found to gives some idea of the useful range without having to ascertain the whole shape of the curve. Most importantly, in order to reduce the dimensions of such a study, it is recommended that the same combinations of aspect ratios and materials used in the present work are used to reduce the number of variables. The overall goal should be to ascertain what combinations of parameters give high gain.

It is expected that it will be possible to normalise the guide cross section size as a function of the operating wavelength, as done in the present work, but this idea must be tested at the beginning of the study. Further, it is expected that, if the aspect ratio is fixed, that the size will be normalised to the guide height versus operating frequency again. Once the combination of parameters have been found for one type of guide, they should then be ascertained for other guide types studied in the present work. In that way, the results of the leakage study will then complement the present results to provide all the information needed to design a practical high-gain grating leaky-wave antenna.

It is also expected that the results of the leakage study may reveal that, for some combinations of guide types, dimensions and material dielectric constant, only a portion of the useful single-mode frequency range might give significant leakage. It is possible that some combinations might give no appreciable leakage over the whole range. Such low leakage conditions will be important to know for non-antenna applications of dielectric waveguides.

10.4.1.3.1 Protracted 3D approach

Now that the leakage study has been recommended and outlined, it remains to suggest possible approaches. Perhaps the most obvious but least practical approach is to implement a numerical method to solve for the leakage for a number of LWA models, to ascertain its leakage performance. The convergence of such a 3D solution is proportional to the number of samples, which given the large number of variables will be vast, and will take an impractical amount of time. This was already attempted to a limited attempt by the present author, from a gain perspective, but the results only indicated randomness as mentioned above. It is interesting to note that [14] found such issues for planar dielectric layered structures, and used genetic algorithms to obtain sets of parameters that maximised the gain. A new 2D+2D approach is suggested, along with supporting theory, which might enable the problem to be solved in a small fraction of the time. If this turns out not to work, it is possible that optical grating theory might hold some clues, or potentially even a solution to this problem, since it is known that one particular author [11] has programmed a method to find the leakage independently for the dielectric grating.

10.4.1.3.2 Recommended approach & new ideas

The recommended approach is to separate the problem into longitudinal and lateral parts. The longitudinal part is already solved i.e. the strip width and spacing in the longitudinal direction for achieving highest gain and therefore leakage is already largely known as described earlier.

The unsolved part requires finding the peaks of the average field intensity incident on a hypothetical thin narrow strip placed across the width of the guide. The conditions for peak leakage will be the same conditions for peak the peak field intensity. The following sections illustrate this theory and how scattering within the guide walls could obscure the results if not considered.

10.4.1.3.3 Possible leakage mechanisms

The present simulation results demonstrated that the leakage is also a function of the lateral strip length, usually equal to the width a of the guide or slightly less. This factor has not been mentioned by other authors. The implication is that the leakage a function of the strip surface area, or even volume. The present author believes that the leakage will be a strong function of the current density on the strips. Assuming that is the case, then the field intensity of the bound mode or modes in the vicinity of the strips must be ascertained. Some ideas about the potential controlling factors and specific objectives are presented next.

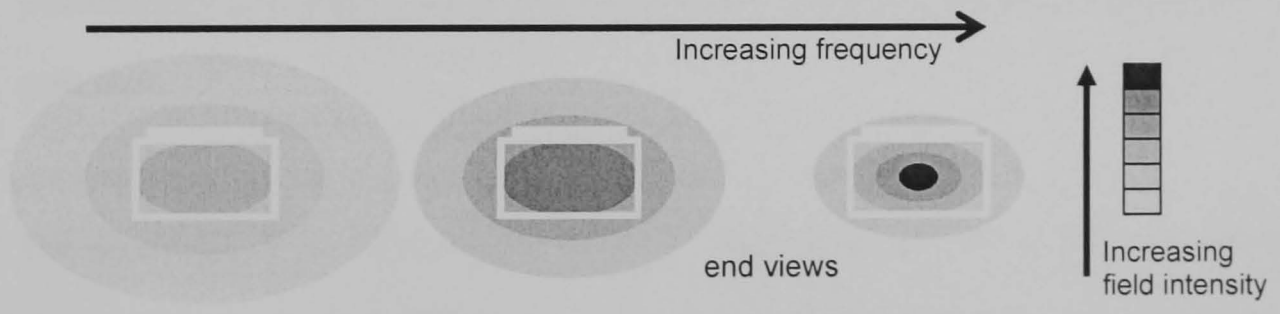

Figure 10.2 Field intensity versus operating frequency illustrates relative intensity in the vicinity of the metal strip.

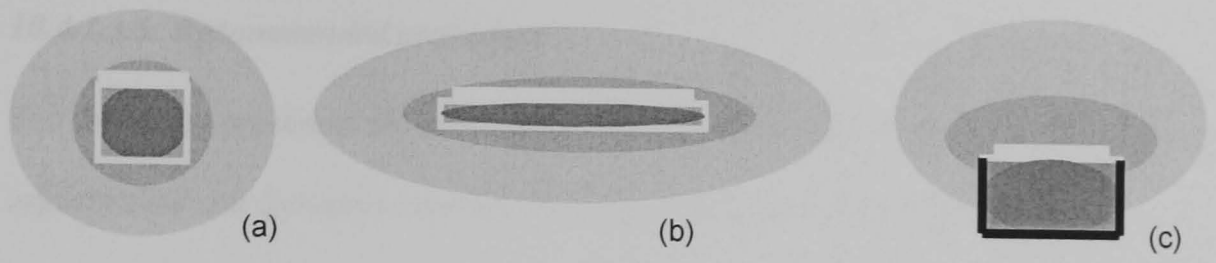

Figure 10.3 Field intensity for (a) narrow aspect (b) wide aspect (c) inset guide illustrates intensity along the metal strip.

10.4.1.3.4 Proposed objectives

At low frequencies approaching cutoff, a high proportion of field travels outside the guide walls. The field intensity is higher at high frequencies [15], as illustrated in Figure 10.2. If it is assumed that at some frequency the field intensity is a constant at the centre of all four sides of the guide cross-section as illustrated in Figure 10.3, then the intensity at the strip must be slowly changing for a large aspect and faster for the smallest aspect. This implies that the average intensity along the strip will be higher for the widest aspect, and most importantly that it will peak at some frequency dependent on the guide height and width. The objective would be to find out what the relationship is between the average intensity on the surface of the strip versus frequency, in the plane of the guide cross-section as illustrated, for various aspect ratios and various normalised guide heights (b/λ_o). Of particular interest is the frequency at which it peaks, and potentially the half power frequency to give some idea of range. In the longitudinal direction, the optimum strip width and spacing is known to a large extent already as described above, but this should be tested over the range of dielectric constants.

The advantages of the different guide types and aspect ratios in terms of guiding and antenna characteristics concerned with the real part of the propagation constant were summarised in Figure 6.17. This figure should ideally be updated with the findings from the proposed study of the leakage constant, the complex part.

10.4.1.3.5 Recommended procedure

The following procedure for ascertaining the leakage for the same range of guide types, sizes, aspect ratios and dielectric constant range as used in this work is recommended:

1. Starting with the 2:1 aspect ratio and a small number of dissimilar guide heights *b*, find and plot the average field intensity on the surface of the unperturbed guide wall of width 2*b* versus discrete frequency values within the single-mode range. The frequency ranges can be found quickly using the new formulas (7-1 or 7-1b). Do this for each guide height.
2. The results must be then be normalised such that the curves overlap as far as possible. In the present work, this was done by dividing the results by the guide height for the two frequency limits. However, the intermediate frequencies are of more interest here therefore it is suggested that the peak and -3dB intensity are divided by b/λo and plotted versus the dielectric constant. Hopefully, these curves will overlap to a great extent. If not, then other normalisation factors must be tried.
3. A mathematical representation of the resulting shape of the overlapping curves should then be found, or the shapes should be modified by some additional normalisation factor to alter its shape for a better fit to a simple curve formula, or straight line as done in the present case.
4. If successful, the same procedure should then be applied to the additional aspect ratios and guide types. Ideally, as in this work, the same formula could be used for all these combinations, but with different coefficients.

10.4.1.3.6 Possible effects of scattering on leakage

Scattering naturally occurs within the guide walls and theoretically increases with increased strip width, dielectric constant and frequency. This it is reported to produce spuriously directed radiation. It could be also be described as undesirable leakage and is potentially part of the reason why carefully designed theoretical patterns differ from measured patterns. In any case, it is possible that scattering might obscure the results of the proposed leakage study. For example, the theory used to derive the leakage constant or leakage peaks might not take

this into consideration. Therefore, it is proposed that the cancelling array presented in [16] is implemented in simulations or experiments to both establish how this scattering affects the leakage, how it then compares with theory and to eliminate it from the equation.

10.4.2 X-polarised case

When a dielectric guide is excited by a larger mouthed metal guide or horn antenna, it may be possible to rotate the guide cross-section so that the E_{11}^{x} mode is excited instead of E_{11}^{y}. The dispersion characteristics for the E_{11}^{x} mode have not been computed in this work, but the exact same process could be undertaken to find the associated coefficients if required.

10.4.3 Excitation methods

The experimental work reported in Chapter 9 highlighted how the excitation of the guide appeared to be a significant problem. In particular, the metal plate covered horn antenna excitation method used by many previous authors [7,9] has severely limited passbands and high attenuation. It is recommended that the efficiency of alternative methods is investigated, particularly for the higher dielectric constant materials where the problem is exacerbated.

10.4.4 Strip width tapering

The experimental work carried in Chapter 9 appears to demonstrate that the simple strip width taper formula radiates weakly. The main problem was probably that the dielectric guide conditions were not optimum as far as the leakage is concerned. However, the fact that the strip widths increase so slowly such that the optimum width and spacing was only achieved near the end of the antenna probably contributed to the poor radiation too. It is recommended other workers try increasing the strip width increment by two or three times, for example, and also start with a very large number of strips if the same problem is found. A large endfire beam is a good indication of this problem, and is easier to measure experimentally that the gain of an obliquely angled main beam because the guide can be pointed straight at the receiving antenna

10.5 Other applications for the new formulas

10.5.1 Dielectric grating antennas

The dielectric grating leaky-wave antenna is most easily analysed using the effective dielectric constant (EDC) method [17]. It is possible that the new dispersion formulas might potentially make the analysis even simpler if the antenna is modelled as shown in Figure 10.4. The propagation constants of the two sections can be modelled for example using a 2:1 aspect guide section in series with a 2.47:1 guide section, with the same guide width *a*. The 2.47:1 section will then have 81% of the height of the 2:1 section. The values can be found using the new dispersion formulas (7-1) to (7-3). This method has the added advantage of being able to dimension the guide sections automatically to be compatible with the operating frequency, and within the single-mode range. The beam angle can be set using the new perturbation formulas (8-4) and (8-5) and the maximum spacing period can be checked with the existing grating lobe test formula (2-4). Figure 5.10 demonstrates that the difference between kz*b for the 2:1 aspect and 2.47:1 aspect is a constant, which leads to the approximation kz2 ≈ 0.9 kz1, further simplifying the analysis. This procedure needs to be validated for this structure.

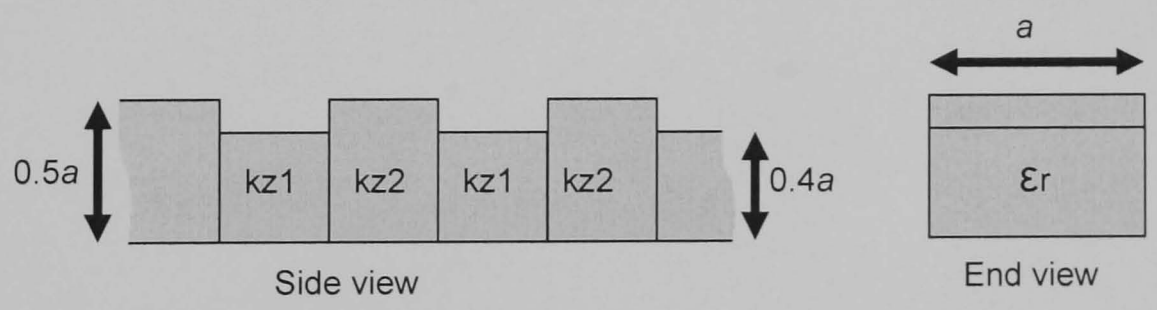

Figure 10.4 New proposed representation of dielectric grating LWA using series propagation constants instead of the effective dielectric constant.

10.5.2 Dielectric tapers and lenses

Other potential applications for the new dispersion formulas are for analysis and design of the tapering of dielectric rectangular rods, and potentially in the analysis of solid dielectric sectoral horn antennas and pyramidal horn lenses [18]. The simplest case is a transition from one physical guide dimension to another, in the same manner as metal waveguide taper

transitions, and to find the overlapping frequency range. The analysis of a smooth flare or taper can be approximately represented by discrete sections of dielectric, as illustrated in Figure 10.5. This type of procedure was used to analyse a tapered microstrip LWA in [19]. Of relevance to this work, the author of [20] stated that simulations (using HFSS) had demonstrated that despite the fact that the guide was excited at a frequency much higher than the single mode range, i.e. overmoded, none of these higher modes appeared to be coupled into the exciting metal waveguide. This implies that only the fundamental single-mode need be considered in the case of the tapered guide transition.

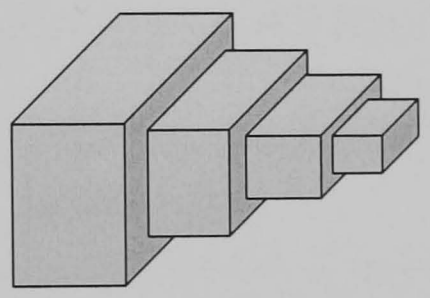

Figure 10.5 Proposed equivalent representation of smoothly tapered rectangular dielectric sections.

10.6 References

[1] W.V. McLevige, T. Itoh and R. Mittra, "New waveguide structures for millimeter-wave and optical integrated circuits," *IEEE Trans. Microwave Theory and Techniques*, vol. MTT-23, no. 10, pp. 788-794, Oct. 1975.

[2] W. Hong and Y.D. Lin, "Single-conductor strip leaky-wave antenna," *IEEE Trans. Antennas and Propagation*, vol. AP-52, no. 7, pp. 1783-1789, Jul. 2004.

[3] J.L Gomez-Tornero, G. Goussetis, A.P. Feresidis and A.A. Melcon, "Control of leaky-mode propagation and radiation in hybrid dielectric-waveguide printed-circuit technology: Experimental results," *IEEE Trans. Antennas and Propagation*, vol. 54, no. 11, pp. 3383-3390, Nov. 2006.

[4] E. A. J. Marcatili, "*Current Content*," Citation Classic number 21, May 21st, 1979.

[5] M.T. Lee, K.M. Luk, S.J. Xu and E.K.N Yung, "A double-slab leaky-wave NRD antenna," *IEEE Trans. Antennas and Propagation*, vol. AP-52, no. 9, pp. 2488-2491, Sep. 2004.

[6] T.N. Trinh, R. Mittra and R.J. Paleta, "Horn image-guide leaky-wave antenna," *IEEE Trans. Microwave Theory and Techniques*, vol. MTT-29, no. 12, pp. 1310-1314, Dec. 1981.

[7] K. L. Klohn, R. E. Horn, H. Jacobs and E. Freibergs, "Silicon waveguide frequency scanning linear array antenna," *IEEE Trans. Microwave Theory and Techniques*, vol. MTT-26, no. 10, pp. 764–773, Oct. 1978.

[8] R. E. Horn, H. Jacobs, E. Freibergs and K. L. Klohn, "Electronic modulated beam-steerable silicon waveguide array antenna," *IEEE Trans. Microwave Theory and Techniques*, vol. MTT-28, no. 6, pp. 647–653, Jun. 1980.

[9] L. Huang, J.C. Chiao and M.P. De Lisio, "An electronically switchable leaky wave antenna," *IEEE Trans. Antennas and Propagation*, vol. AP-48, no. 11, pp. 1769-1772, Nov. 2000.

[10] J. Encinar, "Analysis and CAD techniques for periodic leaky-wave printed antennas: numerical and experimental results," International journal of Microwave and Millimetre-wave Computer-aided Engineering, vol. 4, no 1, pp. 88, 99. 1994.

[11] F.K. Schwering and S.T. Peng, "Design of dielectric grating antennas for millimeter-wave applications," *IEEE Trans. Microwave Theory and Techniques*, vol. MTT-31, no. 2, pp. 199-208, Feb. 1983.

[12] M. Guglielmi and G. Boccalone, "A novel theory for dielectric-inset waveguide leaky-wave antennas," *IEEE Trans. Antennas and Propagation*, vol. 39, no. 4, pp. 497-504, Apr. 1991.

[13] J. Jacobsen, "Analytical, numerical, and experimental investigation of guided waves on a periodically strip-loaded dielectric slab," *IEEE Trans. Antennas and Propagation*, vol. AP-18, no. 3, pp. 379-388, May. 1970.

[14] D.R. Jackson, A.A. Oliner and A. Ip, "Laeky-wave propagation and radiation for a narrow-beam multiple-layer dielectric structure ," *IEEE Trans. Antennas and Propagation*, vol. 41, pp. 344-348, Mar. 1993.

[15] J. E. Goell, "A circular-harmonic computer analysis of rectangular dielectric waveguides," *Bell Syst. Tech. J.*, vol. 48, no. 7, pp. 2133–2159, Sep. 1969.

[16] T. Teshirogi, Y. Kawahara, A. Yamamoto, Y. Sekine, N. Baba and M. Kobayashi. "High efficiency dielectric slab leaky-wave antennas," *IEICE Trans. Communications*, vol. E84-B, no. 9, pp. 2387-2394, Sep. 2001.

[17] F. Schwering and A.A. Oliner, *Millimeter-wave antennas* in Antenna Handbook, Eds. Y.T. Lo and S.W. Lee, Van Nostrand Reinhold, New York, Chapter 17, 1988.

[18] C. Salema, C. Fernandes and R.K. Jha, *Solid dielectric horn antennas*, Arctech House, Chapters 4 and 7, 1998.

[19] W. Hong, T.L Chen, C.Y. Chang, J.W. Sheen and Y.D. Lin, "Broadband tapered microstrip leaky-wave antenna," *IEEE Trans. Antennas and Propagation*, vol. 51, no. 8, pp. 1922-1928, Aug. 2003.

[20] A. Basu and T. Itoh, "Dielectric waveguide-based leaky-wave antenna at 212 GHz," *IEEE Trans. Antennas and Propagation*, vol. 46, no. 11, pp. 1665-1673, Nov. 1998.

APPENDIX A

A.1 Marcatili method pseudocode

Implementation of Marcatili method to find the first two mode cutoff frequencies and their associated longitudinal propagation constants *kz* for a number of waveguide sizes with a large range of dielectric constants. As discussed in Chapter 3, the Marcatili method calculates the E_{21} mode cutoff frequency about 5% too high. This error is removed in this program by storing 95% of the original value, to give a more accurate high frequency limit (*fH*) for each guide. The low frequency (*fL*) value is taken at the E_{11} cutoff.

MAIN PROGRAM pseudocode for *MarcatiliPaperSingleMode_kz_1e.m* (see listing below)

```
For all GUIDE SIZES {list}
    For all MODES {list}
        For all MATERIALS {list}
            Find E11 & E21 CUTOFFS
            Find PROPAGATION CONSTS kzfL & kzE21
            Save RESULTS
        End
            If E21 mode, REMOVE ERROR
            Find NEW PROPAGATION CONST kzfH
            Save RESULTS
    End
End
```

.....

The following pseudocode is for finding CUTOFFS (this procedure forms part of the main program pseudocode above). Here, the frequency is incremented until the cutoff condition is met by kz. This frequency is then the cutoff frequency for that particular guide size, material and mode number.

```
For START FREQ to LARGE NUMBER {size, mode, material}
    Solve TRANSCENDENTAL EQN for kx
    Solve TRANSCENDENTAL EQN for ky
    Compute kz
    Break if CUTOFF CONDITION kz ≥k0, else
End
```

.....

The following pseudocode illustrates the procedure for finding PROPAGATION CONSTs by solving Marcatili's TRANSCENDENTAL EQNs (this procedure forms part of the CUTOFF pseudocode above). Here, the starting value of kx (or ky) is incremented until both sides of the equation are equal. This is then the solution of the Transcendental equation for kx (or ky) for that particular guide size, material and mode number.

```
For kx = 1 to LARGE NUMBER {size, mode, material}

        Compute Marcatili eqn (3-2) at current value of kx, size, mode, material
        Break if LEFT SIDE = RIGHT SIDE, else
End
```

.....

The following is optimized pseudocode for finding CUTOFFS. This procedure is an alternative significantly faster version of the one above. In this version, the start frequency is seeded with a value just under the expected value. Then, the frequency is increased in large increments, and then in small increments. Without this code, the solve time for a sample of approximately 100 samples is >24 hours using an Intel Pentium 4 processor with 3GHz clock speed. With this code, it takes less than one hour, depending on various factors.

```
Compute ROUGH (under) CUTOFF FREQUENCY

For ROUGH FREQ to LARGE NUMBER with medium increment{size, mode, material}

        Solve TRANSCENDENTAL EQN for rough value of kx
        Solve TRANSCENDENTAL EQN for rough value of ky
        Compute ROUGH kz, CLOSER FREQ
        Break if CUTOFF CONDITION kz ≥k0, else

        End

For CLOSER FREQ to LARGE NUMBER with small increment{size, mode, material}

        Solve TRANSCENDENTAL EQN for kx, starting with rough kx
        Solve TRANSCENDENTAL EQN for ky, starting with rough ky
        Compute ACCURATE kz
        Break if CUTOFF CONDITION kz ≥k0, else
End
```

A.2 Dispersion characteristics code listing

```
% Calculates the cutoff frequency of modes using the Marcatili equations for a range of materials (εr).
% Set to find 1ST TWO MODES (E11 & E21), AND εr = 2 TO 16 for all guide sizes from WG10 TO 25 (15 sizes).
% Uses a two-stage search process to find the cutoffs, with variable granularity to speed up the program at the high
% frequencies. Implements a 2-stage transverse propagation constant (kx, ky) computation with high accuracy.
% Enables computation of dispersion characteristics of multiple waveguide aspect ratios (integer aspects only).

starttime = clock;

% <<<<<<<< INPUTS >>>>>>>
%p=1 replaced by a for loop to auto cycle
q=1; % mode number q of pq mode, fixed to 1 in this case, but can be changed manually for other modes
ErMat_min = 2;      % integers only
ErMat_max = 16;   % CAUTION: will take a long time to compute for many values of εr.
f_min = 0.01e9;      % start value used for searching for the cutoff freq for each mode using the Marcatili approx
% formula (freq_app loop). This value is modified (*0.8) and used as the start point in the Marcatili exact formula
% to speed up the trancendental equation solving times (freq loop).
f_max = 500e9; % cursary end value (never reaches it because if statement breaks the loop before this point, at the
% cutoff freq)
%f_incr = 0.5e9; % 0.1 provides reasonable accuracy and short times up to about 9 mins.
f_incr = 0.01e9; % frequency step resolution. 0.01 is most accurate practical value. Any smaller would take days to
% complete.
gap = 0.95; % multiplier to set the desired distance below the E21 mode
numtypes = 1; % number of waveguide types to include from the waveguide type array
aspect = 1; % aspect ratio, aspect:1
% <<<<<<<< END of INPUTS >>>>>>>

% allocate array space and zero it
depth = (ErMat_max - ErMat_min) + 3;
fullwidth = numtypes*2+1;
narrowwidth = numtypes+1;
f_app_results = zeros(depth, fullwidth);
kz_app_results = zeros(depth, fullwidth);
freq_results = zeros(depth, fullwidth);
kz_results = zeros(depth, fullwidth);
kz_fH_results = zeros(depth, narrowwidth);
fout_results = zeros(depth, narrowwidth);

a=0;      b=0;      fout=0;   kz_fH=0;

% guide dimensions next, separated into guide width a and height b.
size_a = [0.1651 0.10922 0.08636 0.072 0.05817 0.04755 0.0404 0.03485 0.0284988      0.02286  0.01905
          0.0158 0.012954    0.010668 0.00711 0.0056896 0.0047752 0.00376 0.0030988 0.00254 0.002032
          0.001651 0.0012954 0.0008636];
size_b = [0.08255 0.05461 0.04318 0.034 0.02908 0.02215 0.0202 0.0157988 0.0126238 0.01016 0.009525
           0.0079 0.006477 0.004318 0.00356 0.0028448 0.0023876 0.00188 0.0015494 0.00127 0.001016
          0.0008255 0.0006477 0.0004318];

for type = 1:1:numtypes
          a =  size_b(type);% * aspect; % wguide dimensions are converted to correct units
          b =  size_b(type);
%type

% alternative for loop to allow manual entry of height b
% size_b = [0.001];              % enter guide height in mm
% for type = 1:1:numtypes
% a =  size_b(type) * aspect;  % makes a a multiple of height b

for p = 1:1:2 % cycles thru mode number p of pq mode

% put a and b values at head of columns, in all arrays
f_app_results (2, p+(2*type)-1) = a; % row 2 (row 1 is empty)
f_app_results (3, p+(2*type)-1) = b; % row 3 (row 1 is empty)
kz_app_results (2, p+(2*type)-1) = a;
```

```
kz_app_results (3, p+(2*type)-1) = b;
freq_results (2, p+(2*type)-1) = a;
freq_results (3, p+(2*type)-1) = b;
kz_results (2, p+(2*type)-1) = a;
kz_results (3, p+(2*type)-1) = b;
kz_fH_results (2, type+1) = a;
kz_fH_results (3, type+1) = b;
fout_results (2, type+1) = a;
fout_results (3, type+1) = b;
%p

for ErMat = ErMat_min:1:ErMat_max % cycles thru min to max values of εr

IrMat = sqrt(ErMat);% Index of refraction of Silicon material (εr=12)
IrAir = 1;       % Index of refraction of air
%ErMat
% place εr value at start of each row in column 1, starting at the 4th row down.
f_app_results (ErMat+2, 1) = ErMat;
kz_app_results (ErMat+2, 1) = ErMat;
freq_results (ErMat+2, 1) = ErMat;
kz_results (ErMat+2, 1) = ErMat;
kz_fH_results (ErMat+2, 1) = ErMat;
fout_results (ErMat+2, 1) = ErMat;

% YYYYYYYYYYYYYYYYYYYYYYYYYYYYYYYYYYYYYYYYYYYYYYYYYYYYYYYYYYYYY
% search for the approx cutoff using the Marcatili 'approx' formula (only
% used to compare with results of 'exact' formula in Excel analysis.

    for freq_app = f_min:f_incr:f_max

Lamda0 = 299792458 / freq_app; % convert to wavelengths
k1 =  (2*pi*IrMat)/ Lamda0;
ko =  (2*pi)/ Lamda0;
A = Lamda0 / (2*sqrt(IrMat^2-IrAir^2)); % =1.51e-3

kz_approx = sqrt(k1^2 - ((pi*p/a)^2 * (1+((A+A)/(pi*a)))^-2) - ((pi*q/b)^2 *
(1+(((IrAir^2*A)+(IrAir^2*A))/(pi*b*IrMat^2)))^-2));
if kz_approx >= ko, break, end
    end % end of freq loop

f_app_results (ErMat+2, p+(2*type)-1) = freq_app; % store approx cutoff starting 4 rows down. for every εr value
and waveguide type
kz_app_results (ErMat+2, p+(2*type)-1) = kz_approx; % store approx kz

%OOOOOOOOOOOOOOOOOOOOOOOOOOOOOOOOOOOOOOOOOOOOOOOOOOOOOOOOOOOO
% search for the exact cutoff using the Marcatili 'exact' formula. Uses the
% approx value * 0.8 as the start value to speed up the solution.
% Uses a rough search stage followed by another using the finer freq incr.
rough_incr = freq_app / sqrt(freq_app/f_incr);
  % rough search stage
  for roughfreq = freq_app*0.6:rough_incr:f_max
Lamda0 = 299792458 / roughfreq; % Operating wavelength
k1 =  (2*pi*IrMat)/ Lamda0;
ko =  (2*pi)/ Lamda0;
A = Lamda0 / (2*sqrt(IrMat^2-IrAir^2)); % =1.51e-3

for kx_rough = 0.1:0.1:10000
Xdir_fieldattenconst =  1 / sqrt((pi/A)^2-kx_rough^2);
rightsideX = ((pi*p) - atan(kx_rough * Xdir_fieldattenconst) - atan(kx_rough * Xdir_fieldattenconst));
leftsideX = kx_rough * a;
crossoverX = rightsideX - leftsideX;
if crossoverX <=0 , break, end
end % end of kx loop

for kx = kx_rough-0.1:0.001:10000
Xdir_fieldattenconst =  1 / sqrt((pi/A)^2-kx^2);
rightsideX = ((pi*p) - atan(kx * Xdir_fieldattenconst) - atan(kx * Xdir_fieldattenconst));
```

```
leftsideX = kx * a;
crossoverX = rightsideX - leftsideX;
if crossoverX <=0 , break, end
end % end of kx loop

for ky_rough = 0.1:0.1:10000
Ydir_fieldattenconst = 1 / sqrt((pi/A)^2-ky_rough^2);
rightsideY = (pi*q) - atan((IrAir^2/IrMat^2) * ky_rough * Ydir_fieldattenconst) - atan((IrAir^2/IrMat^2) *
ky_rough * Ydir_fieldattenconst);
leftsideY = ky_rough * b;
crossoverY = rightsideY - leftsideY;
if crossoverY <=0 , break, end
end % end of ky loop

for ky = ky_rough-0.1:0.001:10000
Ydir_fieldattenconst = 1 / sqrt((pi/A)^2-ky^2);
rightsideY = (pi*q) - atan((IrAir^2/IrMat^2) * ky * Ydir_fieldattenconst) - atan((IrAir^2/IrMat^2) * ky *
Ydir_fieldattenconst);
leftsideY = ky * b;
crossoverY = rightsideY - leftsideY;
if crossoverY <=0 , break, end
end % end of ky loop

kz = sqrt(k1^2 - kx^2 - ky^2);
if kz >= ko, break, end
   end % end of freq loop

   % fine search stage
   for freq = roughfreq-rough_incr:f_incr:f_max
Lamda0 = 299792458 / freq; % Operating wavelength
k1 =  (2*pi*IrMat)/ Lamda0;
ko =  (2*pi)/ Lamda0;
A = Lamda0 / (2*sqrt(IrMat^2-IrAir^2)); % =1.51e-3

for kx_rough = 0.1:0.1:10000
Xdir_fieldattenconst =  1 / sqrt((pi/A)^2-kx_rough^2);
rightsideX = ((pi*p) - atan(kx_rough * Xdir_fieldattenconst) - atan(kx_rough * Xdir_fieldattenconst));
leftsideX = kx_rough * a;
crossoverX = rightsideX - leftsideX;
if crossoverX <=0 , break, end
end % end of kx loop

for kx = kx_rough-0.1:0.001:10000
Xdir_fieldattenconst =  1 / sqrt((pi/A)^2-kx^2);
rightsideX = ((pi*p) - atan(kx * Xdir_fieldattenconst) - atan(kx * Xdir_fieldattenconst));
leftsideX = kx * a;
crossoverX = rightsideX - leftsideX;
if crossoverX <=0 , break, end
end % end of kx loop

for ky_rough = 0.1:0.1:10000
Ydir_fieldattenconst = 1 / sqrt((pi/A)^2-ky_rough^2);
rightsideY = (pi*q) - atan((IrAir^2/IrMat^2) * ky_rough * Ydir_fieldattenconst) - atan((IrAir^2/IrMat^2) *
ky_rough * Ydir_fieldattenconst);
leftsideY = ky_rough * b;
crossoverY = rightsideY - leftsideY;
if crossoverY <=0 , break, end
end % end of ky loop

for ky = ky_rough-0.1:0.001:10000
Ydir_fieldattenconst = 1 / sqrt((pi/A)^2-ky^2);
rightsideY = (pi*q) - atan((IrAir^2/IrMat^2) * ky * Ydir_fieldattenconst) - atan((IrAir^2/IrMat^2) * ky *
Ydir_fieldattenconst);
leftsideY = ky * b;
crossoverY = rightsideY - leftsideY;
if crossoverY <=0 , break, end
end % end of ky loop
```

```
kz = sqrt(k1^2 - kx^2 - ky^2);
if kz >= ko, break, end
   end % end of freq loop

freq_results (ErMat+2, p+(2*type)-1) = freq;% store exact cutoff starting 4 rows down, for every εr value and
waveguide type
kz_results (ErMat+2, p+(2*type)-1) = kz;

%OOOOOOOOOOOOOOOOOOOOOOOOOOOOOOOOOOOOOOOOOOOOOOOOOOOOOOOOOOOOOOOO
% this procedure finds kz using 0.95*fc_E21 as the operating frequency.
%This gives us a suitable value of fH for the E11 mode. The kz value
%calculated next using the transcendental equations from Marcatili gives us
%kz_fH(E11), as distinct from kz_E21 found in "MarcatiliPaperVersusFREQ1e.m".
% kz_fL(E11) is that found for the cutoff of the E11 mode in "...FREQ1e.m",
% stored in the kz_results array for p=1.

for fakeloop = 1:1:1 % this fake loop is only for enabling the if test on the next line
if p==1 , break, end % i.e. we are only interested in the E21 mode freq, not 11 (Epq)
%p=1; % however, we need kz for the E11 mode (at the E21 mode freq, or preferably below by some gap).
freqin = freq;
fout = freq * gap;
kz_in = kz;
Lamda_fH = 299792458 / fout; % Compute wavelength for 0.95* the E21 cutoff freq found in previous proc
kone_fH =  (2*pi*IrMat)/ Lamda_fH; % find k1 based on fH
A_fH = Lamda_fH / (2*sqrt(IrMat^2-IrAir^2)); % find A based on fH

for kx_rough = 0.1:0.1:10000
Xdir_fieldattenconst =  1 / sqrt((pi/A_fH)^2-kx_rough^2);
rightsideX = ((pi) - atan(kx_rough * Xdir_fieldattenconst) - atan(kx_rough * Xdir_fieldattenconst));
leftsideX = kx_rough * a;
crossoverX = rightsideX - leftsideX;
if crossoverX <=0 , break, end
end % end of kx loop

for kx = kx_rough-0.1:0.001:10000
Xdir_fieldattenconst =  1 / sqrt((pi/A_fH)^2-kx^2);
rightsideX = ((pi) - atan(kx * Xdir_fieldattenconst) - atan(kx * Xdir_fieldattenconst));
leftsideX = kx * a;
crossoverX = rightsideX - leftsideX;
if crossoverX <=0 , break, end
end % end of kx loop

for ky_rough = 0.1:0.1:10000
Ydir_fieldattenconst = 1 / sqrt((pi/A_fH)^2-ky_rough^2);
rightsideY = (pi) - atan((IrAir^2/IrMat^2) * ky_rough * Ydir_fieldattenconst) - atan((IrAir^2/IrMat^2) * ky_rough
* Ydir_fieldattenconst);
leftsideY = ky_rough * b;
crossoverY = rightsideY - leftsideY;
if crossoverY <=0 , break, end
end % end of ky loop

for ky = ky_rough-0.1:0.001:10000
Ydir_fieldattenconst = 1 / sqrt((pi/A_fH)^2-ky^2);
rightsideY = (pi) - atan((IrAir^2/IrMat^2) * ky * Ydir_fieldattenconst) - atan((IrAir^2/IrMat^2) * ky *
Ydir_fieldattenconst);
leftsideY = ky * b;
crossoverY = rightsideY - leftsideY;
if crossoverY <=0 , break, end
end % end of ky loop

kz_fH = sqrt(kone_fH^2 - kx^2 - ky^2);
end % end of fakeloop

fout_results (ErMat+2, type+1) = fout;% store exact freq*0.95 starting 4 rows down and 1 column in, for every εr
value and waveguide type
```

```
kz_fH_results (ErMat+2, type+1) = kz_fH; % store E11 mode kz for the high frequency fH i.e. 0.95* the E21
cutoff
%kkkkkkkkkkkkkkkkkkkkkkkkkkkkkkkkkkkkkkkkkkkkkkkkkkkkkkkkkkkkkkkkkkkkkkkkkkkkkkkkkkkkkkkkkkkk

end % end of εr loop
end % end of p loop
end % end of wguide type (sizes) loop
endtime = clock;
t = endtime - starttime

% END OF LISTING
```

A.3 Code listing for guides with metal sides

```
% This version implements the extensions to the Marcatili formulas to allow metal walls to be represented
% for image guides, trapped image guides and inset (trough) guides etc.
% This version also calculates kz/GHz for each type and εr, removes the
% approximate kz and cutoff frequency storage, and puts the fH and kz_fH
% values in the freq_results and kz_results arrays, overwriting the E21 results
% instead of having using dedicated arrays fout_results and kz_fH_results.
% Note that in some cases, it appears as if Matlab has crashed as it stops writing to the screen.
% However, IT HAS NOT CRASHED!! Windows also reports "not responding" if the task manager is called up.

warning off MATLAB:divideByZero
starttime = clock;
%hold on

% <<<<<<<< INPUTS >>>>>>>
%p=1 replaced by a for loop to auto cycle
q=1; % mode number q of pq mode, fixed in this case
ErMat_min = 2;
ErMat_max = 16;
f_min = 0.01e9; % start value used for searching for the cutoff freq for each mode using the Marcatili approx
% formula (freq_app loop). This value is modified (*0.8) and used as the start point in the Marcatili exact formula
% to speed up the trancendental equation solving times (freq loop).
f_max = 600e9; % cursary end value (never reaches it because if statement breaks the loop before this point, at the
% cutoff freq)
%f_incr = 0.5e9; % 0.1 provides reasonable accuracy and short times up to about 9 mins.
f_incr = 0.001e9; % frequency step resolution. 0.01 is most accurate practical value. Any smaller would take days
% to complete.
gap = 0.95; % multiplier to set the desired distance below the E21 mode
numtypes_start = 1;
numtypes_finish = 1; % number of waveguide sizes to include from the waveguide type array, 24 max
nummodes = 2;
aspect = 5; % aspect ratio, aspect:1. Only enabled when line112 is enabled as a=b*aspect.

% //////////////// OPEN GUIDE //////////////// 1hr16mins 1:1
h3 = inf; % no gnd plane, L side
h5 = inf; % no gnd plane, R side
t2 = inf; % no gnd plane, top
t4 = inf; % no gnd plane, btm
compensator = 0.5 % maybe even 0.85
% //////////////// IMAGE GUIDE //////////////// 4.5mins for 11types, all εr. 19mins 5to 1 4types all εr.
%h3 = 1000; %inf; % no gnd plane, L side
%h5 = 1000;%inf; % no gnd plane, R side
%t2 = 1000;%inf; % no gnd plane, top
%t4 = 0; % gnd plane, btm
```

```
%compensator = 0.5 %  std size image guide. Check that kz_fL/ko is unity. Reduce if necessary. Increasing speeds
up solving time.
% ////////////////// INSET GUIDE ////////////////// 28mins for 11 types, all εr std sizes. 1hr35mins for 1:1
%h3 = 0; % gnd plane, L side
%h5 = 0; % gnd plane, R side
%t2 = inf; % no gnd plane, top
%t4 = 0; % gnd plane, btm
%compensator = 0.4 % 0.65 for 1:1 & 2:1. 0.4 for 5:1.
% ////////////////// TRAPPED IMAGE GUIDE ////////////////// 13mins std
% sides=a, 19mins std sides=b/2, 32mins1to1 sides=b, 27mins sides=b/4, 39mins b/32
%%h3 = a; % gnd plane, L side NEED THIS LINE AT START OF 'TYPE' LOOP
%%h5 = a; % gnd plane, R side NEED THIS LINE AT START OF 'TYPE' LOOP
%t2 = inf; % no gnd plane, top
%t4 = 0; % gnd plane, btm
%compensator = 0.55
% <<<<<<<< END of INPUTS >>>>>>>

% allocate array space and zero it
depth = (ErMat_max - ErMat_min) + 3;
fullwidth = numtypes_finish*2+1;
narrowwidth = numtypes_finish+1;
freq_results = zeros(depth, fullwidth);
kz_results = zeros(depth, fullwidth);
kz_GHz_results = zeros(depth, narrowwidth);
kz_ko_results = zeros(depth, fullwidth);
a=0;
b=0;
fout=0;
kz_fH=0;
%       wg6  wg10   wg12   wg13  wg14      wg15    wg16   wg19    wg20    wg25    wr6
size_a = [0.1651  0.072  0.04755 0.0404 0.03485   0.0284988 0.02286 0.012954 0.010668 0.00376 0.001651];
size_b = [0.08255 0.034  0.02215 0.0202 0.0157988 0.0126238 0.01016 0.006477 0.004318 0.00188 0.0008255];
% takes 25mins to do all 11 types for εr=2to6
%for type = 1:1:numtypes
 for type = numtypes_start:1:numtypes_finish

a =  size_b(type) * aspect; %* 1e-3; % wguide dimensions are converted to correct units - THIS ENABLES A
% FIXED ASPECT RATIO WITH THE b VALUES AS THE REFERENCE
b =  size_b(type); %* 1e-3;

for p = 1:1:nummodes % cycles thru mode number p of pq mode

% put a and b values at head of columns, in all arrays
freq_results (2, p+(2*type)-1) = a;
freq_results (3, p+(2*type)-1) = b;
kz_results (2, p+(2*type)-1) = a;
kz_results (3, p+(2*type)-1) = b;
kz_GHz_results (2, type+1) = a;
kz_GHz_results (3, type+1) = b;
kz_ko_results (2, p+(2*type)-1) = a;
kz_ko_results (3, p+(2*type)-1) = b;

        for ErMat = ErMat_min:1:ErMat_max % cycles thru min to max values of εr
IrMat = sqrt(ErMat);% Index of refraction of Silicon material (εr=12)
IrAir = 1;        % Index of refraction of air

% place εr value at start of each row in column 1, starting at the 4th row down.
freq_results (ErMat+2, 1) = ErMat;
kz_results (ErMat+2, 1) = ErMat;
kz_GHz_results (ErMat+2, 1) = ErMat;
kz_ko_results (ErMat+2, 1) = ErMat;

%YYYYYYYYYYYYYYYYYYYYYYYYYYYYYYYYYYYYYYYYYYYYYYYYY
% search for the approx cutoff using the Marcatili 'approx' formula (only
% used to compare with results of 'exact' formula in Excel analysis.
freq_app = f_min;
```

```
      %for freq_app = f_min:f_incr*10:f_max
      for freq_app = freq_app:f_incr*10:f_max
Lamda0 = 299792458 / freq_app; % convert to wavelengths
k1 =  (2*pi*IrMat)/ Lamda0;
ko =  (2*pi)/ Lamda0;
A = Lamda0 / (2*sqrt(IrMat^2-IrAir^2)); % =1.51e-3

kz_approx = sqrt(k1^2 - ((pi*p/a)^2 * (1+((A+A)/(pi*a)))^-2) - ((pi*q/b)^2 *
(1+(((IrAir^2*A)+(IrAir^2*A))/(pi*b*IrMat^2)))^-2));
if kz_approx >= ko, break, end
      end % end of freq_app loop

%YYYYYYYYYYYYYYYYYYYYYYYYYYYYYYYYYYYYYYYYYYYYYYYYYYYYYYYYYYYYYYYYYYYYYY
% search for the exact cutoff using the Marcatili 'exact' formula. Uses the
% approx value * 0.8 as the start value to speed up the solution.
% Uses a rough search stage followed by another using the finer freq incr.
rough_incr = freq_app / sqrt(freq_app/f_incr);

% rough search stage
   for roughfreq = freq_app*compensator:rough_incr/10:f_max

Lamda0 = 299792458 / roughfreq; % Operating wavelength
k1 =  (2*pi*IrMat)/ Lamda0;
ko =  (2*pi)/ Lamda0;
A = Lamda0 / (2*sqrt(IrMat^2-IrAir^2)); % =1.51e-3

for kx_rough = 1:1:10000
Xdir_fieldattenconst =  1 / sqrt((pi/A)^2-kx_rough^2);
Xdir_fieldattenconst));
rightsideX = ((pi*p) - atan(kx_rough * Xdir_fieldattenconst*tanh(h3/Xdir_fieldattenconst)) - atan(kx_rough *
Xdir_fieldattenconst*tanh(h5/Xdir_fieldattenconst)));
leftsideX = kx_rough * a;
crossoverX = rightsideX - leftsideX;
if crossoverX <=0 , break, end
end % end of kx loop

for ky_rough = 1:1:10000
Ydir_fieldattenconst = 1 / sqrt((pi/A)^2-ky_rough^2);
atan((IrAir^2/IrMat^2) * ky_rough * Ydir_fieldattenconst);
rightsideY = (pi*q) - atan((ky_rough * Ydir_fieldattenconst * coth(t2/Ydir_fieldattenconst))/ErMat) -
atan((ky_rough * Ydir_fieldattenconst * coth(t4/Ydir_fieldattenconst))/ErMat);
leftsideY = ky_rough * b;
crossoverY = rightsideY - leftsideY;
if crossoverY <=0 , break, end
end % end of ky loop

kz_rough = sqrt(k1^2 - kx_rough^2 - ky_rough^2);
if kz_rough >= ko, break, end
   end % end of freq loop

% fine search stage
   for freq = roughfreq-rough_incr:f_incr:f_max
Lamda0 = 299792458 / freq; % Operating wavelength
k1 =  (2*pi*IrMat)/ Lamda0;
ko =  (2*pi)/ Lamda0;
A = Lamda0 / (2*sqrt(IrMat^2-IrAir^2)); % =1.51e-3

for kx = kx_rough-1:0.001:10000
Xdir_fieldattenconst =  1 / sqrt((pi/A)^2-kx^2);
Xdir_fieldattenconst));
rightsideX = ((pi*p) - atan(kx * Xdir_fieldattenconst*tanh(h3/Xdir_fieldattenconst)) - atan(kx *
Xdir_fieldattenconst*tanh(h5/Xdir_fieldattenconst)));
leftsideX = kx * a;
crossoverX = rightsideX - leftsideX;
if crossoverX <=0 , break, end
end % end of kx loop
```

```
for ky = ky_rough-1:0.001:10000
Ydir_fieldattenconst = 1 / sqrt((pi/A)^2-ky^2);
atan((IrAir^2/IrMat^2) * ky * Ydir_fieldattenconst);
rightsideY = (pi*q) - atan((ky * Ydir_fieldattenconst * coth(t2/Ydir_fieldattenconst))/ErMat) - atan((ky *
Ydir_fieldattenconst * coth(t4/Ydir_fieldattenconst))/ErMat);
leftsideY = ky * b;
crossoverY = rightsideY - leftsideY;
if crossoverY <=0 , break, end
end % end of ky loop

kz = sqrt(k1^2 - kx^2 - ky^2);
ko;
%plot(ErMat, kz/ko, '-rx')
%plot(ErMat, kz, '-rx')
%plot(ErMat, ko, '-bx')
if kz >= ko, break, end
   end % end of freq loop
%freq_app
%roughfreq

%freq
freq_results (ErMat+2, p+(2*type)-1) = freq;% store exact cutoff starting 4 rows down, for every εr value and
waveguide type
kz_results (ErMat+2, p+(2*type)-1) = kz;

%jjjjjjjjjjjjjjjjjjjjjjjjjjjjjjjjjjjjjjjjjjjjjjjjjjjjjjjjjjjjjjjj
%>>>>>>>>>>> this proc finds kz using gap*fc_E21 as the operating frequency.
%This gives us a suitable value of fH for the E11 mode. The kz value
%calculated next using the transcendental equations from Marcatili gives us
%kz_fH(E11), as distinct from kz_E21 found in "MarcatiliPaperVersusFREQ1e.m".
% kz_fL(E11) is that found for the cutoff of the E11 mode in "...FREQ1e.m",
% stored in the kz_results array for p=1.

for fakeloop = 1:1:1 % this fake loop is only for enabling the if test on the next line
if p==1 , break, end % i.e. we are only interested in the E21 mode freq (p=2), not E11 (Epq),
% because we want to borrow the E21 cutoff frequency and use it as the upper operating freq (fH) of the E11
mode.

freqin = freq;
fout = freq * gap;
kz_in = kz;
Lamda_fH = 299792458 / fout; % Compute wavelength for 0.95* the E21 cutoff freq found in previous proc
kone_fH =  (2*pi*IrMat)/ Lamda_fH; % find k1 based on fH
A_fH = Lamda_fH / (2*sqrt(IrMat^2-IrAir^2)); % find A based on fH

for kx_rough = 0.1:0.1:10000
Xdir_fieldattenconst =  1 / sqrt((pi/A_fH)^2-kx_rough^2);
Xdir_fieldattenconst));
rightsideX = (pi - atan(kx_rough * Xdir_fieldattenconst*tanh(h3/Xdir_fieldattenconst)) - atan(kx_rough *
Xdir_fieldattenconst*tanh(h5/Xdir_fieldattenconst)));
leftsideX = kx_rough * a;
crossoverX = rightsideX - leftsideX;
if crossoverX <=0 , break, end
end % end of kx loop

for kx = kx_rough-0.1:0.001:10000
Xdir_fieldattenconst =  1 / sqrt((pi/A_fH)^2-kx^2);
Xdir_fieldattenconst));
rightsideX = (pi - atan(kx * Xdir_fieldattenconst*tanh(h3/Xdir_fieldattenconst)) - atan(kx *
Xdir_fieldattenconst*tanh(h5/Xdir_fieldattenconst)));
leftsideX = kx * a;
crossoverX = rightsideX - leftsideX;
if crossoverX <=0 , break, end
end % end of kx loop

for ky_rough = 0.1:0.1:10000
Ydir_fieldattenconst = 1 / sqrt((pi/A_fH)^2-ky_rough^2);
```

```
atan((IrAir^2/IrMat^2) * ky_rough * Ydir_fieldattenconst);
rightsideY = pi - atan((ky_rough * Ydir_fieldattenconst * coth(t2/Ydir_fieldattenconst))/ErMat) - atan((ky_rough
* Ydir_fieldattenconst * coth(t4/Ydir_fieldattenconst))/ErMat);
leftsideY = ky_rough * b;
crossoverY = rightsideY - leftsideY;
if crossoverY <=0 , break, end
end % end of ky loop

for ky = ky_rough-0.1:0.001:10000
Ydir_fieldattenconst = 1 / sqrt((pi/A_fH)^2-ky^2);
atan((IrAir^2/IrMat^2) * ky * Ydir_fieldattenconst);
rightsideY = pi - atan((ky * Ydir_fieldattenconst * coth(t2/Ydir_fieldattenconst))/ErMat) - atan((ky *
Ydir_fieldattenconst * coth(t4/Ydir_fieldattenconst))/ErMat);
leftsideY = ky * b;
crossoverY = rightsideY - leftsideY;
if crossoverY <=0 , break, end
end % end of ky loop

kz_fH = sqrt(kone_fH^2 - kx^2 - ky^2);
freq_results (ErMat+2, 2+(2*type)-1) = fout;% store exact cutoff starting 4 rows down, for every εr value and
waveguide type
kz_results (ErMat+2, 2+(2*type)-1) = kz_fH;

end % end of fakeloop

%&&&&&&&&&&&&&&&&&&&&&&&&&&&&&&&&&&&&&&&&&&&&&&&&&&&&&&&&&&&&&&&&&&&&&&&&
end % end of εr loop
end % end of p loop
end % end of wguide type (sizes) loop

%&&&&&&&&&&&&&&&&&&&&&&&&&&&&&&&&&&&&&&&&&&&&&&&&&&&&&&&&&&&&&&&&&&&&&&&&
% Calc kz/GHz and store in array
for down = ErMat_min+2:1:ErMat_max+2
   for across = numtypes_start+1:1:numtypes_finish+1
      kzdelta = kz_results(down, 2*across-2) - kz_results(down, 2*across-1);
      fcdelta = freq_results(down, 2*across-2) - freq_results(down, 2*across-1);
      kz_GHz_results (down, across) = kzdelta/fcdelta * 1e9;
   end
end
%&&&&&&&&&&&&&&&&&&&&&&&&&&&&&&&&&&&&&&&&&&&&&&&&&&&&&&&&&&&&&&&&&&&&&&&&
% Calc kz/ko and store in array
for down = ErMat_min+2:1:ErMat_max+2
   for across = numtypes_start:1:numtypes_finish
      for pee = 0:1:1
      kzed = kz_results(down, 2*across+pee);
      knort = freq_results(down, 2*across+pee) * 2*pi/299792458;
      kz_ko_results (down, 2*across+pee) = kzed/knort;
      end
   end
end
kz_ko_results
endtime = clock;
t = endtime - starttime
```

% END OF LISTING

A.4 Code listing for plotting kz from fL to fH

```
%_____________________________________________________
warning off %MATLAB:divideByZero
starttime = clock;
hold on
% <<<<<<<< INPUTS >>>>>>>
q=1; % mode number q of pq mode, fixed in this case
ErMat_min = 16;
ErMat_max = 16;
f_min = 0.01e9; % start value used for searching for the cutoff freq for each mode using the Marcatili approx formula (freq_app loop). This value is modified (*0.8) and used as the start point in the Marcatili exact formula to speed up the trancendental equation solving times (freq loop).
f_max = 600e9; % cursary end value (never reaches it because if statement breaks the loop before this point, at the cutoff freq)
%f_incr = 0.5e9; % 0.1 provides reasonable accuracy and short times up to about 9 mins.
f_incr = 0.001e9; % frequency step resolution. 0.01 is most accurate practical value. Any smaller would take days to complete.
gap = 0.95; % multiplier to set the desired distance below the E21 mode
numtypes_start = 3;
numtypes_finish = 3; % number of waveguide sizes to include from the waveguide type array, 24 max
nummodes = 2;
%aspect = 5; % aspect ratio, aspect:1. Only enabled when line112 is enabled as a=b*aspect.

% ////////////////// OPEN GUIDE ////////////////// 1hr16mins 1:1
h3 = inf; % no gnd plane, L side
h5 = inf; % no gnd plane, R side
t2 = inf; % no gnd plane, top
t4 = inf; % no gnd plane, btm
% ////////////////// IMAGE GUIDE ////////////////// 4.5mins for 11types, all εr. 19mins 5to 1 4types all εr.
%h3 = 1000; %inf; % no gnd plane, L side
%h5 = 1000;%inf; % no gnd plane, R side
%t2 = 1000;%inf; % no gnd plane, top
%t4 = 0; % gnd plane, btm
% ////////////////// INSET GUIDE ////////////////// 28mins for 11 types, all εr std sizes. 1hr35mins for 1:1
%h3 = 0; % gnd plane, L side
%h5 = 0; % gnd plane, R side
%t2 = inf; % no gnd plane, top
%t4 = 0; % gnd plane, btm
% ////////////////// TRAPPED IMAGE GUIDE ////////////////// 13mins std
% sides=a, 19mins std sides=b/2, 32mins1to1 sides=b, 27mins sides=b/4, 39mins b/32
%%h3 = a; % gnd plane, L side NEED THIS LINE AT START OF 'TYPE' LOOP
%%h5 = a; % gnd plane, R side NEED THIS LINE AT START OF 'TYPE' LOOP
%t2 = inf; % no gnd plane, top
%t4 = 0; % gnd plane, btm
% <<<<<<<< END of INPUTS >>>>>>>

% allocate array space and zero it
depth = (ErMat_max - ErMat_min) + 3;
fullwidth = numtypes_finish*2+1;
narrowwidth = numtypes_finish+1;
%f_app_results = zeros(depth, fullwidth);
%kz_app_results = zeros(depth, fullwidth);
%kz_fH_results = zeros(depth, narrowwidth);
%fout_results = zeros(depth, narrowwidth);
freq_results = zeros(depth, fullwidth);
kz_results = zeros(depth, fullwidth);
kz_GHz_results = zeros(depth, narrowwidth);
kz_ko_results = zeros(depth, fullwidth);
a=0;
b=0;
fout=0;
kz_fH=0;
size_a = [0.02286 0.010668 0.00376];
size_b = [0.01016 0.004318 0.00188];
```

```
%for type = 1:1:numtypes
 for type = numtypes_start:1:numtypes_finish
%a =  size_a(type);% * aspect; %* 1e-3; % wguide dimensions are converted to correct units - THIS ENABLES A
FIXED ASPECT RATIO WITH THE b VALUES AS THE REFERENCE
a =  size_a(type); %* 1e-3; % wguide dimensions are converted to correct units
b =  size_b(type); %* 1e-3;
%h3 = b/16; % gnd plane, L side NEED THIS LINE AT START OF 'TYPE' LOOP
%h5 = b/16; % gnd plane, R side NEED THIS LINE AT START OF 'TYPE' LOOP
type

        for ErMat = ErMat_min:1:ErMat_max % cycles thru min to max values of εr
IrMat = sqrt(ErMat);% Index of refraction of Silicon material (εr=12)
IrAir = 1;        % Index of refraction of air
%ErMat
% place εr value at start of each row in column 1, starting at the 4th row down.
%f_app_results (ErMat+2, 1) = ErMat;
%kz_app_results (ErMat+2, 1) = ErMat;
%kz_fH_results (ErMat+2, 1) = ErMat;
%fout_results (ErMat+2, 1) = ErMat;
freq_results (ErMat+2, 1) = ErMat;
kz_results (ErMat+2, 1) = ErMat;
kz_GHz_results (ErMat+2, 1) = ErMat;
kz_ko_results (ErMat+2, 1) = ErMat;

for p = 1:1:nummodes % cycles thru mode number p of pq mode
   % put a and b values at head of columns, in all arrays
%f_app_results (2, p+(2*type)-1) = a; % row 2 (row 1 is empty)
%f_app_results (3, p+(2*type)-1) = b; % row 3 (row 1 is empty)
%kz_app_results (2, p+(2*type)-1) = a;
%kz_app_results (3, p+(2*type)-1) = b;
%kz_fH_results (2, type+1) = a;
%kz_fH_results (3, type+1) = b;
%fout_results (2, type+1) = a;
%fout_results (3, type+1) = b;
freq_results (2, p+(2*type)-1) = a;
freq_results (3, p+(2*type)-1) = b;
kz_results (2, p+(2*type)-1) = a;
kz_results (3, p+(2*type)-1) = b;
kz_GHz_results (2, type+1) = a;
kz_GHz_results (3, type+1) = b;
kz_ko_results (2, p+(2*type)-1) = a;
kz_ko_results (3, p+(2*type)-1) = b;
p

%
YYYYYYYYYYYYYYYYYYYYYYYYYYYYYYYYYYYYYYYYYYYYYYYYYYYYYYYYYYY
% find approx cutoff using my own curve fitting formula (see sheet 'image
% 5to1' of the spreadsheet "Marcatili Cutoff Analysis-part2.xls"

if p == 1, nrtr=90e6;  % 73e6 for 5:1, 48e6 for inset,image10:1, 65 for open 10:1
else nrtr = 105e6;     % 83e6 for 5:1, 63e6 for inset,image10:1, 90 for open 10:1
end
freq_app = nrtr/(ErMat^0.5*b);
%

%OOOOOOOOOOOOOOOOOOOOOOOOOOOOOOOOOOOOOOOOOOOOOOOOOOOOOOOOO
% search for the exact cutoff using the Marcatili 'exact' formula. Uses the
% approx value * 0.8 as the start value to speed up the solution.
% Uses a rough search stage followed by another using the finer freq incr.
rough_incr = (freq_app) / sqrt(freq_app/f_incr);
   % rough search stage
   %for roughfreq = freq_app*compensator:rough_incr/10:f_max
for roughfreq = freq_app:rough_incr:f_max
     % roughfreq
Lamda0 = 299792458 / roughfreq; % Operating wavelength
```

```
k1 =  (2*pi*IrMat)/ Lamda0;
ko =  (2*pi)/ Lamda0;
A = Lamda0 / (2*sqrt(IrMat^2-IrAir^2)); % =1.51e-3

for kx_rough = 1:.1:10000
Xdir_fieldattenconst =  1 / sqrt((pi/A)^2-kx_rough^2);
%rightsideX = ((pi*p) - atan(kx_rough * Xdir_fieldattenconst) - atan(kx_rough * Xdir_fieldattenconst));
rightsideX = ((pi*p) - atan(kx_rough * Xdir_fieldattenconst*tanh(h3/Xdir_fieldattenconst)) - atan(kx_rough *
Xdir_fieldattenconst*tanh(h5/Xdir_fieldattenconst)));
leftsideX = kx_rough * a;
crossoverX = rightsideX - leftsideX;
if crossoverX <=0 , break, end
end % end of kx loop

for ky_rough = 1:.1:10000
Ydir_fieldattenconst = 1 / sqrt((pi/A)^2-ky_rough^2);
%rightsideY = (pi*q) - atan((IrAir^2/IrMat^2) * ky_rough * Ydir_fieldattenconst) - atan((IrAir^2/IrMat^2) *
ky_rough * Ydir_fieldattenconst);
rightsideY = (pi*q) - atan((ky_rough * Ydir_fieldattenconst * coth(t2/Ydir_fieldattenconst))/ErMat) -
atan((ky_rough * Ydir_fieldattenconst * coth(t4/Ydir_fieldattenconst))/ErMat);
leftsideY = ky_rough * b;
crossoverY = rightsideY - leftsideY;
if crossoverY <=0 , break, end
end % end of ky loop

kz_rough = sqrt(k1^2 - kx_rough^2 - ky_rough^2);
if kz_rough >= ko, break, end
   end % end of freq loop
%diff=roughfreq/freq_app


   % fine search stage
   for freq = roughfreq-rough_incr:f_incr:f_max
Lamda0 = 299792458 / freq; % Operating wavelength
k1 =  (2*pi*IrMat)/ Lamda0;
ko =  (2*pi)/ Lamda0;
A = Lamda0 / (2*sqrt(IrMat^2-IrAir^2)); % =1.51e-3

for kx = kx_rough-1:0.001:10000
Xdir_fieldattenconst =  1 / sqrt((pi/A)^2-kx^2);
%rightsideX = ((pi*p) - atan(kx * Xdir_fieldattenconst) - atan(kx * Xdir_fieldattenconst));
rightsideX = ((pi*p) - atan(kx * Xdir_fieldattenconst*tanh(h3/Xdir_fieldattenconst)) - atan(kx *
Xdir_fieldattenconst*tanh(h5/Xdir_fieldattenconst)));
leftsideX = kx * a;
crossoverX = rightsideX - leftsideX;
if crossoverX <=0 , break, end
end % end of kx loop

for ky = ky_rough-1:0.001:10000
Ydir_fieldattenconst = 1 / sqrt((pi/A)^2-ky^2);
%rightsideY = (pi*q) - atan((IrAir^2/IrMat^2) * ky * Ydir_fieldattenconst) - atan((IrAir^2/IrMat^2) * ky *
Ydir_fieldattenconst);
rightsideY = (pi*q) - atan((ky * Ydir_fieldattenconst * coth(t2/Ydir_fieldattenconst))/ErMat) - atan((ky *
Ydir_fieldattenconst * coth(t4/Ydir_fieldattenconst))/ErMat);
leftsideY = ky * b;
crossoverY = rightsideY - leftsideY;
if crossoverY <=0 , break, end
end % end of ky loop

%roughfreq
%rough_incr
%diff2=roughfreq-rough_incr
%freq
kz = sqrt(k1^2 - kx^2 - ky^2);
ko;
%plot(ErMat, kz/ko, '-rx')
%plot(ErMat, kz, '-rx')
```

```
%plot(ErMat, ko, '-bx')
if kz >= ko, break, end
   end % end of freq loop


   if p==1 , freq_results (ErMat+2, p+(2*type)-1) = freq;% store exact cutoff starting 4 rows down, for every εr
value and waveguide type
      kz_results (ErMat+2, p+(2*type)-1) = kz
   else freq_results (ErMat+2, p+(2*type)-1) = freq * 0.95;
   end
% note that we dont have to recompute the value of kz for the new 0.95E21
% freq just calcd because we are going to calc it below for all freqs
% between the E11 and the 0.95E21!!
%OOOOOOOOOOOOOOOOOOOOOOOOOOOOOOOOOOOOOOOOOOOOOOOOOOOOOOOOOOOOOOOOOO

   end % end of mode (p) loop

%staat = freq_results(ErMat+2, 1+(2*type)-1)
staat = freq_results(ErMat+2, 2*type); % 2 4 6 8
finis = freq_results(ErMat+2, 2*type+1); % 3 5 7 9
   %for curve_freq = staat:(fout-staat)/20:fout
for curve_freq = staat:(finis-staat)/10:finis
Lamda_fH = 299792458 / curve_freq; % Compute wavelength for 0.95* the E21 cutoff freq found in previous
proc
kone =  (2*pi*IrMat)/ Lamda_fH; % find k1 based on fH
ko =  (2*pi)/ Lamda_fH;
A_fH = Lamda_fH / (2*sqrt(IrMat^2-IrAir^2)); % find A based on fH

for kx_rough = 0.1:0.1:10000
Xdir_fieldattenconst =  1 / sqrt((pi/A_fH)^2-kx_rough^2);
%rightsideX = ((pi*p) - atan(kx_rough * Xdir_fieldattenconst) - atan(kx_rough * Xdir_fieldattenconst));
rightsideX = (pi - atan(kx_rough * Xdir_fieldattenconst*tanh(h3/Xdir_fieldattenconst)) - atan(kx_rough *
Xdir_fieldattenconst*tanh(h5/Xdir_fieldattenconst)));
leftsideX = kx_rough * a;
crossoverX = rightsideX - leftsideX;
if crossoverX <=0 , break, end
end % end of kx loop

for kx = kx_rough-0.1:0.001:10000
Xdir_fieldattenconst =  1 / sqrt((pi/A_fH)^2-kx^2);
%rightsideX = ((pi*p) - atan(kx * Xdir_fieldattenconst) - atan(kx * Xdir_fieldattenconst));
rightsideX = (pi - atan(kx * Xdir_fieldattenconst*tanh(h3/Xdir_fieldattenconst)) - atan(kx *
Xdir_fieldattenconst*tanh(h5/Xdir_fieldattenconst)));
leftsideX = kx * a;
crossoverX = rightsideX - leftsideX;
if crossoverX <=0 , break, end
end % end of kx loop

for ky_rough = 0.1:0.1:10000
Ydir_fieldattenconst = 1 / sqrt((pi/A_fH)^2-ky_rough^2);
rightsideY = pi - atan((ky_rough * Ydir_fieldattenconst * coth(t2/Ydir_fieldattenconst))/ErMat) - atan((ky_rough
* Ydir_fieldattenconst * coth(t4/Ydir_fieldattenconst))/ErMat);
leftsideY = ky_rough * b;
crossoverY = rightsideY - leftsideY;
if crossoverY <=0 , break, end
end % end of ky loop

for ky = ky_rough-0.1:0.001:10000
Ydir_fieldattenconst = 1 / sqrt((pi/A_fH)^2-ky^2);
rightsideY = pi - atan((ky * Ydir_fieldattenconst * coth(t2/Ydir_fieldattenconst))/ErMat) - atan((ky *
Ydir_fieldattenconst * coth(t4/Ydir_fieldattenconst))/ErMat);
leftsideY = ky * b;
crossoverY = rightsideY - leftsideY;
if crossoverY <=0 , break, end
end % end of ky loop
curve_freq
kz_curve = sqrt(kone^2 - kx^2 - ky^2)
```

```
plot(curve_freq, kz_curve, '-ko')
%plot(curve_freq, kz_curve/ko, '-ko')
%%plot(ErMat, kz_curve/ko, '-kx')

%&&&&&&&&&&&&&&&&&&&&&&&&&&&&&&&&&&&&&&&&&&&&&&&&&&&&&&&&&&&&&&&&&&&&&&&&&&&&
end % end of curve_freq loop
kz_results (ErMat+2, 2*type+1) = kz_curve;


end % end of εr loop
end % end of wguide type (sizes) loop

% display results in command window
%delta = kz - ko
%delta_rough = kz_rough - ko
%roughfreq
%freq

%&&&&&&&&&&&&&&&&&&&&&&&&&&&&&&&&&&&&&&&&&&&&&&&&&&&&&&&&&&&&&&&&&&&&&&&&&&&&
% Calc kz/GHz and store in array
for down = ErMat_min+2:1:ErMat_max+2
   for across = numtypes_start+1:1:numtypes_finish+1
      kzdelta = kz_results(down, 2*across-2) - kz_results(down, 2*across-1);
      fcdelta = freq_results(down, 2*across-2) - freq_results(down, 2*across-1);
      kz_GHz_results (down, across) = kzdelta/fcdelta * 1e9;
   end
end
%&&&&&&&&&&&&&&&&&&&&&&&&&&&&&&&&&&&&&&&&&&&&&&&&&&&&&&&&&&&&&&&&&&&&&&&&&&&&
% Calc kz/ko and store in array
for down = ErMat_min+2:1:ErMat_max+2
   for across = numtypes_start:1:numtypes_finish
      for pee = 0:1:1
      kzed = kz_results(down, 2*across+pee);
      knort = freq_results(down, 2*across+pee) * 2*pi/299792458;
      kz_ko_results (down, 2*across+pee) = kzed/knort;
      end
   end
end
kz_ko_results
endtime = clock;
t = endtime - starttime


% END OF LISTING
```

A.5 Example output

The above listing generates and stores the results in arrays in memory. These were exported to a spreadsheet for further analysis.In this case, the Matlab *getmatrix* function was installed in Microsoft Excel and then used to import array the values from Matlab into Excel. The results were captured in the manner shown below. In this case, the rows represent values of dielectric constant from 2 to 12.

	kz_results					freq_results				
	wg20 fL	wg20 fH	wg25 fL	wg25 fH		wg20 fL	wg20 fH	wg25 fL	wg25 fH	
	0.010668	0.010668	0.00376	0.00376		0.010668	0.010668	0.00376	0.00376	width
Er	0.004318	0.004318	0.00188	0.00188		0.004318	0.004318	0.00188	0.00188	height
2	447.9182	725.1688	1078.935	1898.938	2	2.12E+10	3.04E+10	5.15E+10	7.82E+10	
3	351.9282	595.36	865.147	1560.965	3	1.68E+10	2.3E+10	4.13E+10	5.85E+10	
4	309.9937	536.9834	761.7077	1417.69	4	1.48E+10	1.96E+10	3.63E+10	4.94E+10	
5	284.8672	502.8985	693.8176	1328.944	5	1.36E+10	1.74E+10	3.31E+10	4.37E+10	
6	265.5638	479.559	643.1358	1273.751	6	1.27E+10	1.59E+10	3.07E+10	3.97E+10	
7	249.505	462.0472	604.1414	1230.459	7	1.19E+10	1.47E+10	2.88E+10	3.66E+10	
8	236.5496	446.2359	571.0617	1196.629	8	1.13E+10	1.37E+10	2.72E+10	3.42E+10	
9	225.88	435.3835	543.5099	1172.64	9	1.08E+10	1.3E+10	2.59E+10	3.22E+10	
10	216.9666	426.372	520.0819	1149.768	10	1.03E+10	1.23E+10	2.48E+10	3.05E+10	
11	208.0705	418.9743	498.4629	1133.843	11	9.92E+09	1.18E+10	2.38E+10	2.91E+10	
12	201.1252	412.4253	480.9195	1116.856	12	9.6E+09	1.13E+10	2.29E+10	2.78E+10	
13	194.2262	404.6776	463.8704	1105.332	13	9.26E+09	1.08E+10	2.21E+10	2.67E+10	
14	188.1083	400.0866	448.8057	1092.015	14	8.96E+09	1.04E+10	2.14E+10	2.58E+10	
15	183.3872	395.7149	436.3145	1083.507	15	8.74E+09	1.01E+10	2.08E+10	2.49E+10	
16	178.1602	392.1866	423.5881	1076.245	16	8.49E+09	9.78E+09	2.02E+10	2.41E+10	

Table A.1 Example output from program listings showing values of computed propagation constant *kz* and useful frequency range (*fL* to *fH*) for a number of guide sizes and range of material dielectric constant.

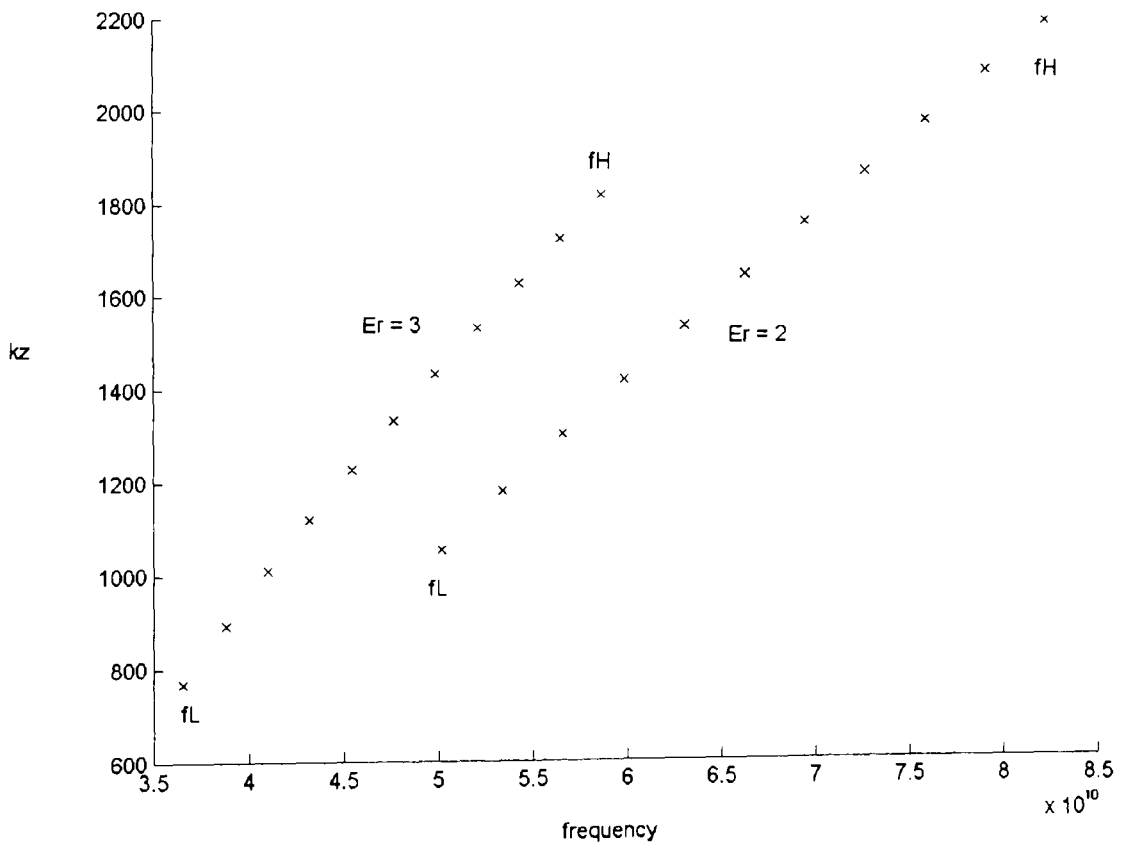

Figure A.1 Example plot output from program listing A.4. showing values of propagation constant *kz* over the computed useful frequency range from *fL* to *fH*.

APPENDIX B

The following plots show the results from attempts to normalise the frequency and propagation constant data captured in Chapter 5.

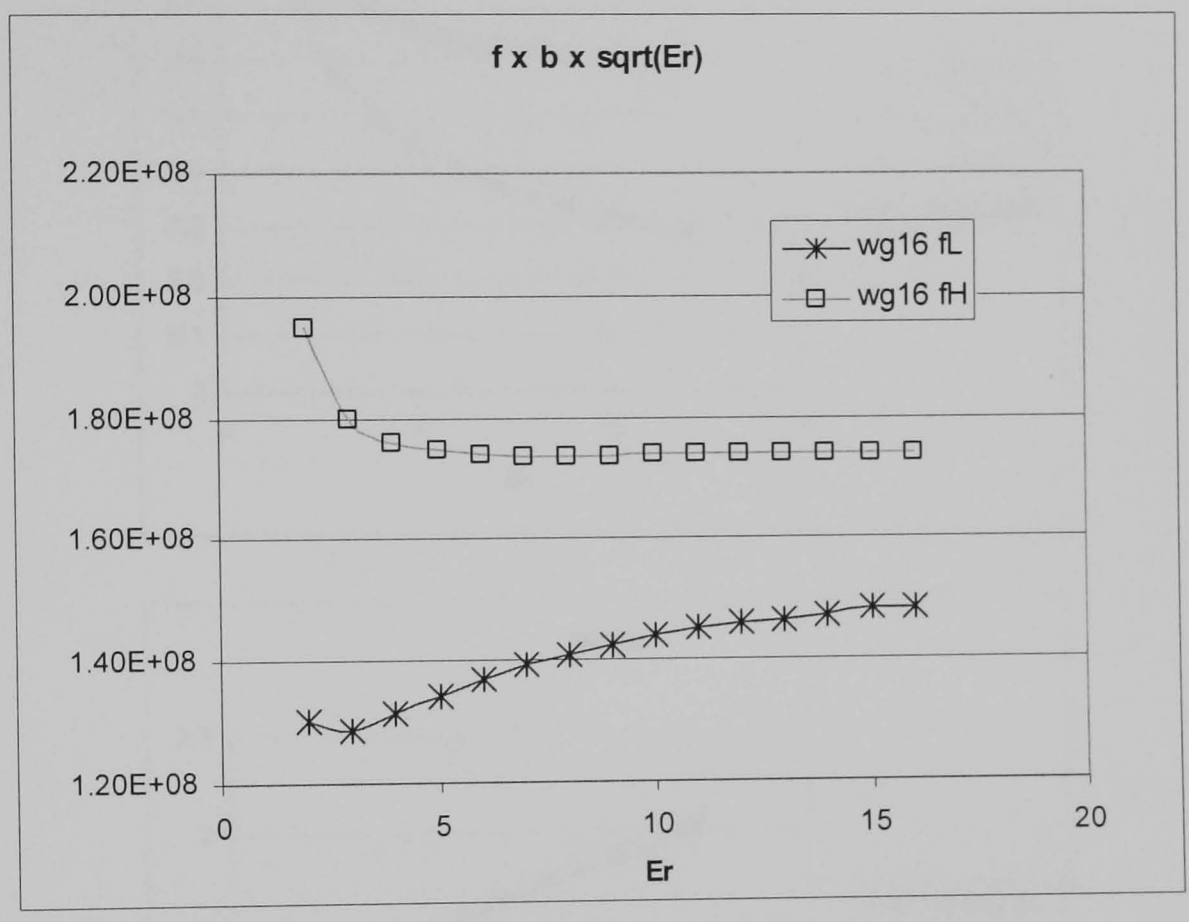

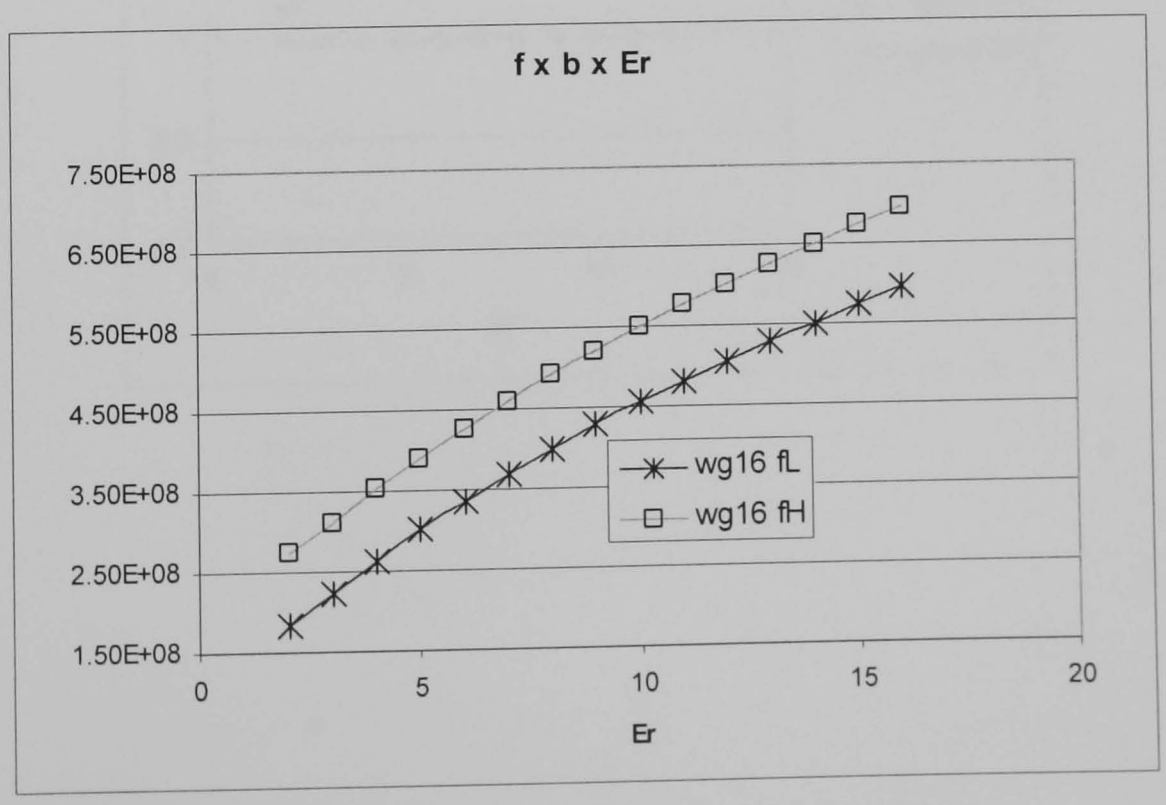

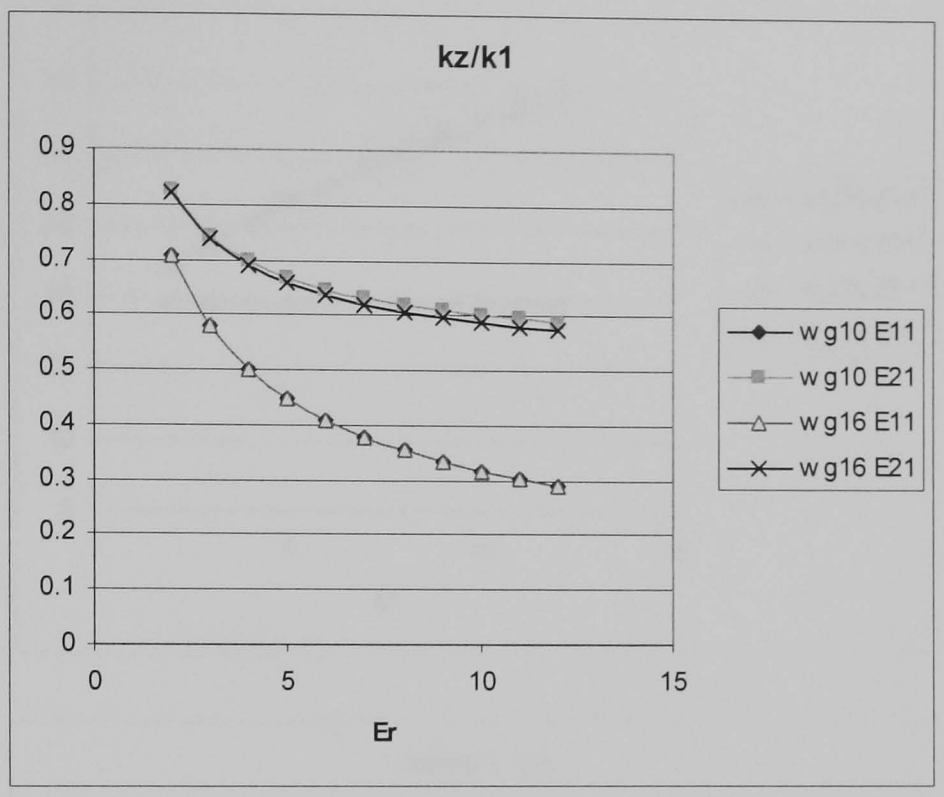
kz/k1
0.9
0.8
0.7
0.6
0.5
0.4
0.3
0.2
0.1
0
0
5
10
15
Er
w g10 E11
w g10 E21
w g16 E11
w g16 E21

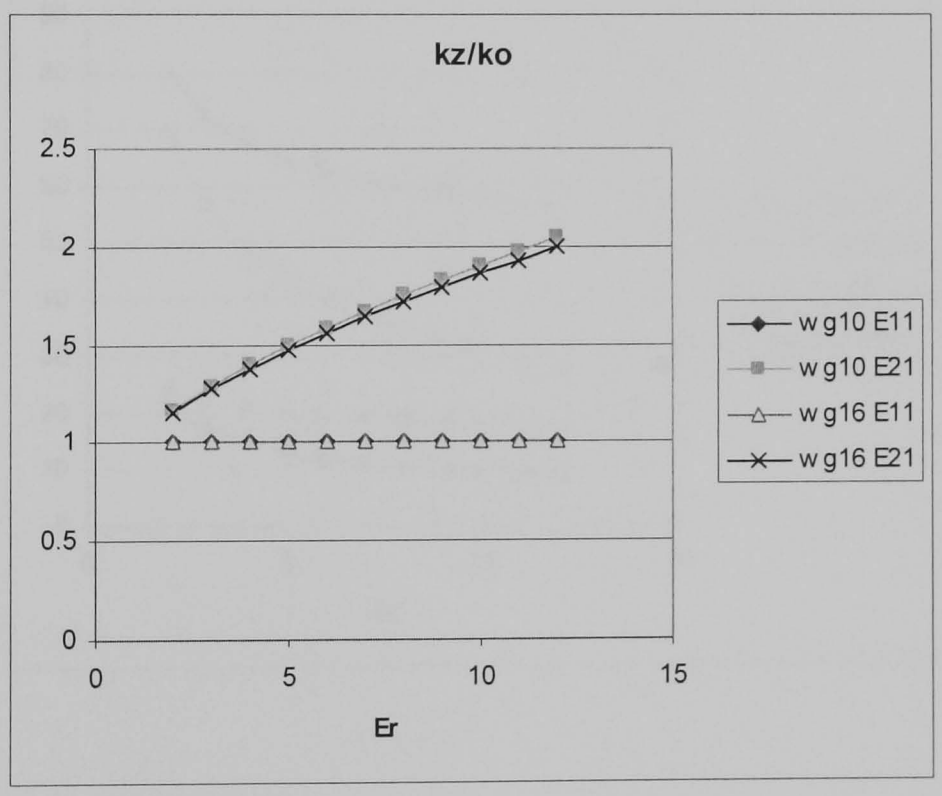
kz/ko
2.5
2
1.5
1
0.5
0
0
5
10
15
Er
w g10 E11
w g10 E21
w g16 E11
w g16 E21

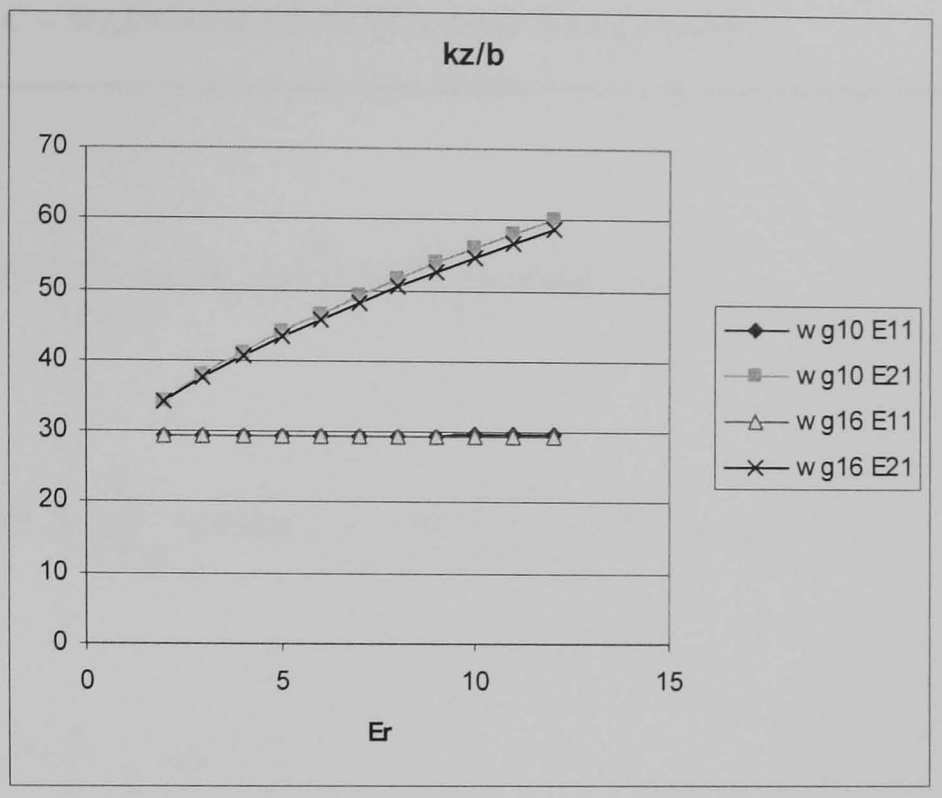
kz/b
70
60
50
40
30
20
10
0
0
5
10
15
Er
w g10 E11
w g10 E21
w g16 E11
w g16 E21

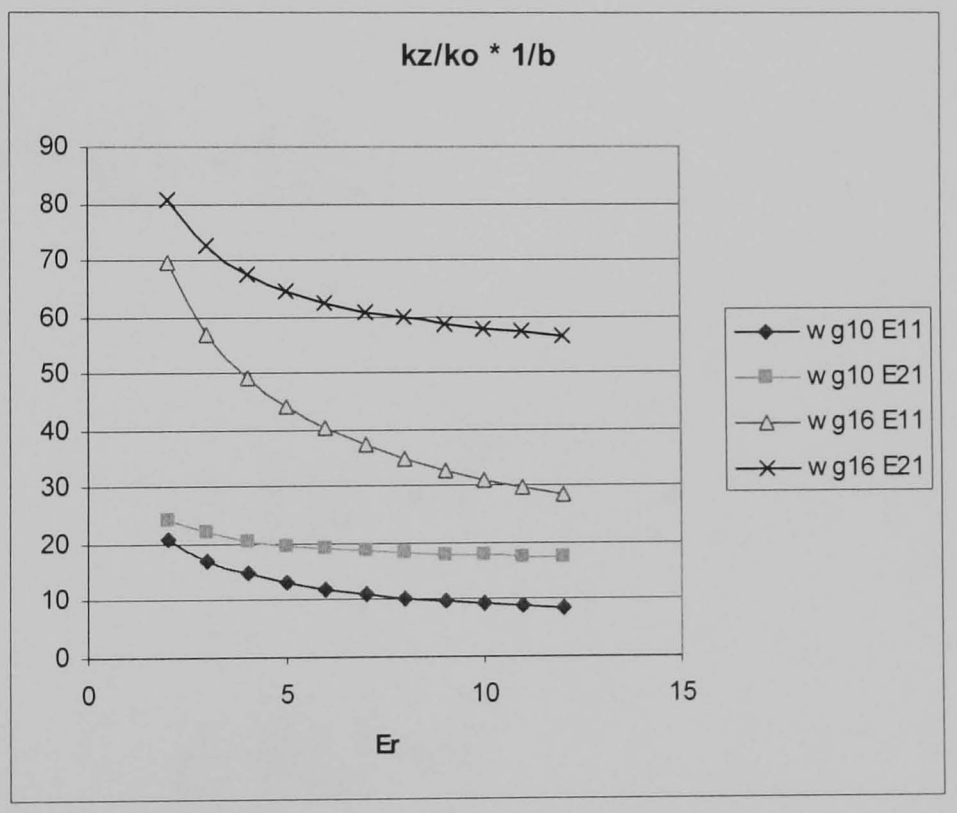
kz/ko * 1/b
90
80
70
60
50
40
30
20
10
0
0
5
10
15
Er
w g10 E11
w g10 E21
w g16 E11
w g16 E21

APPENDIX C – MARCATILI FORMULAS & EXTENSIONS

$$k_x a = \pi - \tan^{-1}\left(\frac{k_x}{k_{x3}}\tanh(k_{x3_x} h_3)\right) - \tan^{-1}\left(\frac{k_x}{k_{x5}}\tanh(k_{x5_x} h_5)\right) \tag{C.1}$$

$$k_y b = \pi - \tan^{-1}\left(\frac{k_y}{\varepsilon_r k_{y2}}\coth(k_{y2_x} t_2)\right) - \tan^{-1}\left(\frac{k_y}{\varepsilon_r k_{y4}}\coth(k_{y4_x} t_4)\right) \tag{C.2}$$

$$k_x a = \pi - \tan^{-1}\left(\frac{k_x}{k_{x3}}\right) - \tan^{-1}\left(\frac{k_x}{k_{x5}}\right) \tag{C.3}$$

$$k_y b = \pi - \tan^{-1}\left(\frac{k_y}{\varepsilon_r k_{y2}}\right) - \tan^{-1}\left(\frac{k_y}{\varepsilon_r k_{y4}}\right) \tag{C.4}$$

where

$$\frac{1}{k_{x3,5}} = \left[\left(\frac{\pi}{A_{3,5}}\right)^2 - {k_x}^2\right]^{-0.5} \tag{C.5}$$

$$\frac{1}{k_{y2,4}} = \left[\left(\frac{\pi}{A_{2,4}}\right)^2 - {k_y}^2\right]^{-0.5} \tag{C.6}$$

and

$$A_{2,3,4,5} = \left(\frac{f}{2c(\varepsilon_r - \varepsilon_{2,3,4,5})^{0.5}}\right) \tag{C.7}$$

APPENDIX D

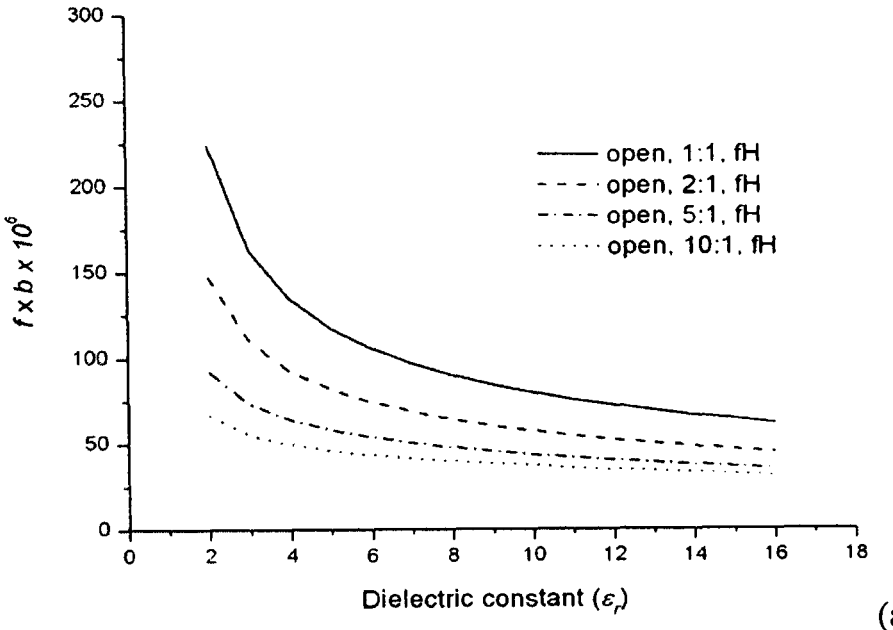

(a)

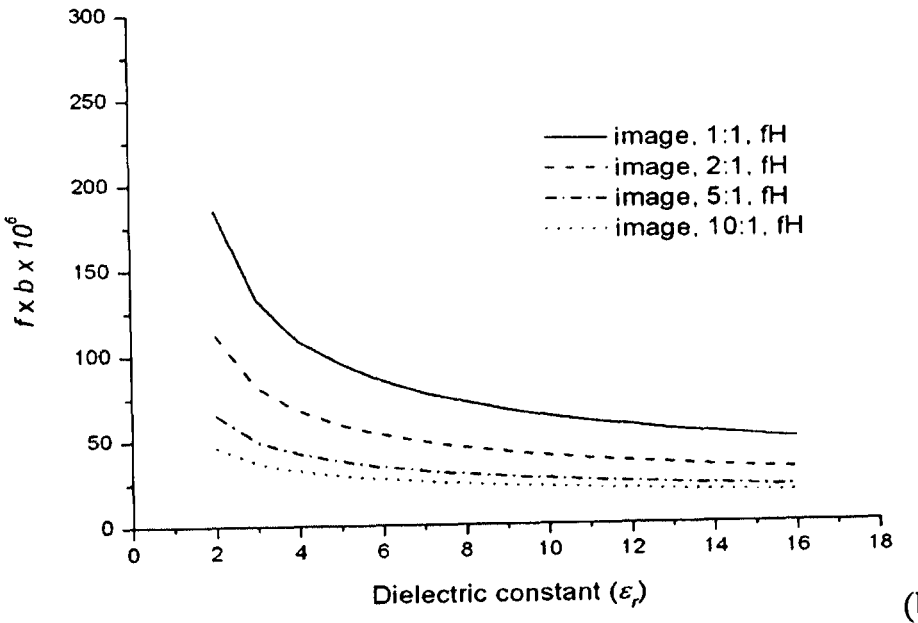

(b)

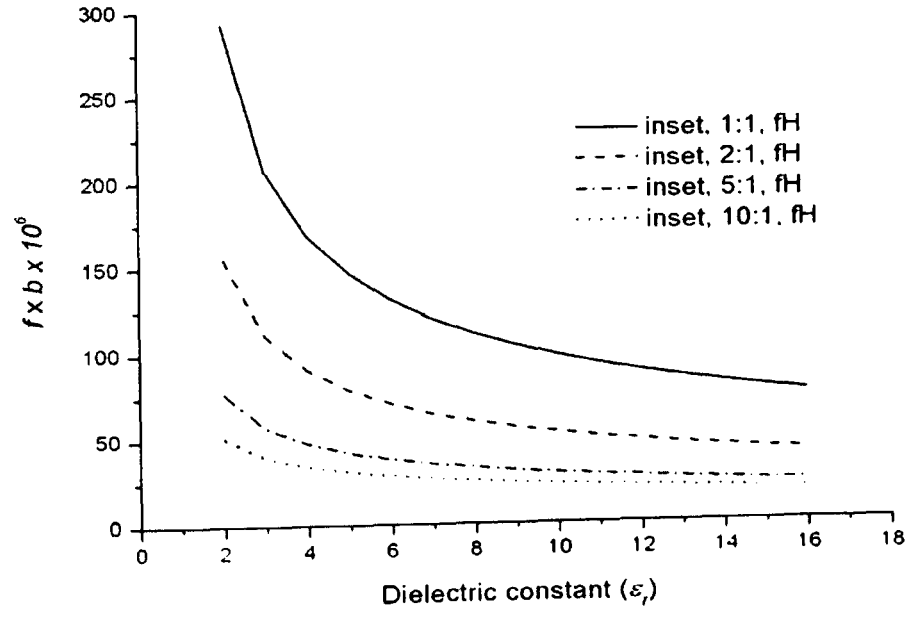

(c)

Figure D.1 Height-independent frequency range (fL to fH) for rectangular dielectric waveguides of fixed type and varying aspect ratios for (a) open guide (b) image guide (c) inset guide.

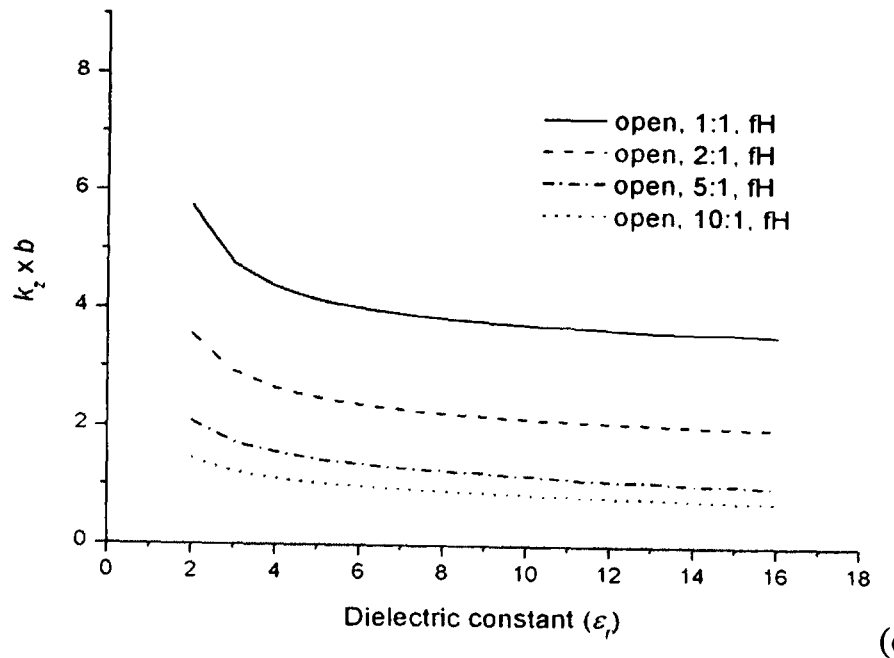

(d)

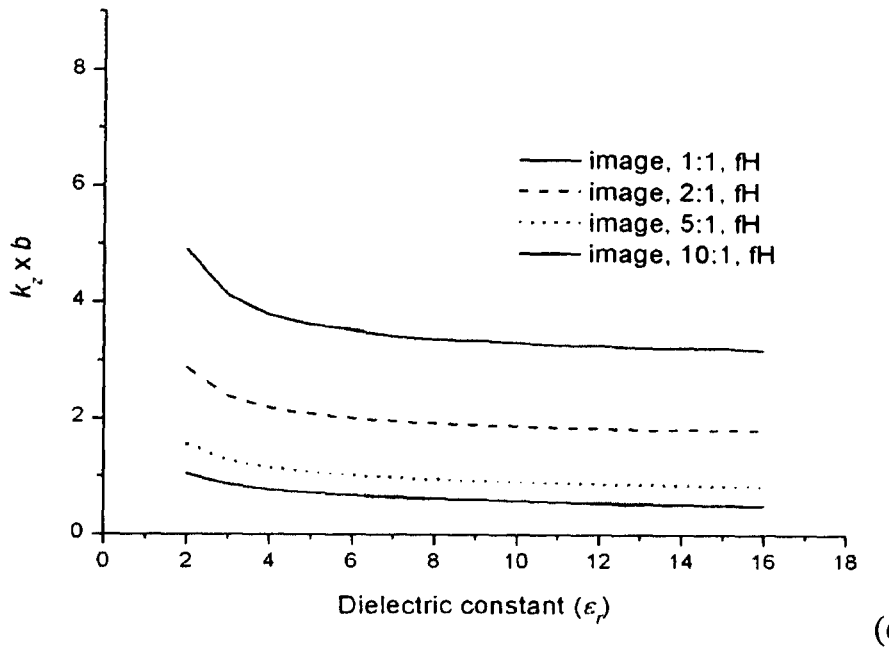

(e)

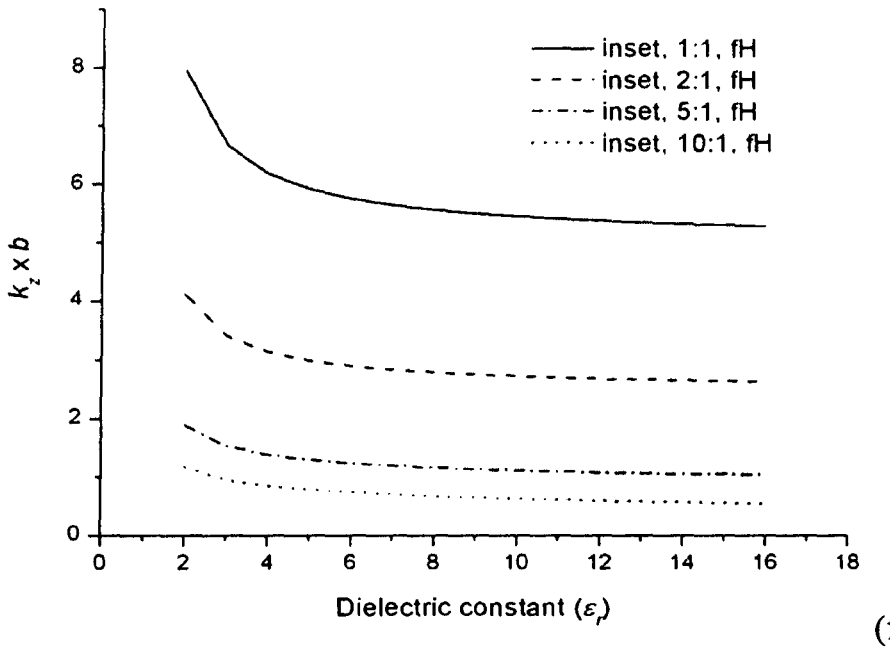

(f)

Figure D.2 Height-independent longitudinal propagation constant *kz* at both ends of the frequency range (*fL* to *fH*) for rectangular dielectric waveguides of fixed type and varying aspect ratios (d) open guide (e) image guide (f) inset guide.

APPENDIX E – WORKED EXAMPLE RESULTS

Refer to section 6.5

Rectangular dielectric guide of Er = 2, operating frequency to 10 GHz.

Column→	A	B	C	D	E	F	G	H	I	J	K	L	M	N	O
OPEN	fL*b	fH*b	b	fL	fH	Δf_GHz	kz_L	kz_H	Δkz	kz_L*b	kz_H*b	λg_L	λg_H	kz/GHz	Δf*Δkz
1:1	1.29E+08	2.24E+08	2.24E-02	5.74E+09	1.00E+10	4.26	120.33	257.87	137.54	2.70	5.78	5.22E-02	2.44E-02	32.30	585.73
2:1	9.65E+07	1.47E+08	1.47E-02	6.58E+09	1.00E+10	3.42	137.87	243.05	105.18	2.02	3.57	4.56E-02	2.59E-02	30.74	359.88
5:1	8.38E+07	9.16E+07	9.16E-03	9.15E+09	1.00E+10	0.85	191.78	228.23	36.44	1.76	2.09	3.28E-02	2.75E-02	42.90	30.96
10:1	4.81E+07	6.65E+07	6.65E-03	7.23E+09	1.00E+10	2.77	151.62	213.41	61.79	1.01	1.42	4.14E-02	2.94E-02	22.34	170.91
IMAGE															
1:1	8.73E+07	1.85E+08	1.85E-02	4.72E+09	1.00E+10	5.28	98.98	263.80	164.81	1.83	4.88	6.35E-02	2.38E-02	31.23	869.76
2:1	6.46E+07	1.12E+08	1.12E-02	5.78E+09	1.00E+10	4.22	121.18	256.39	135.21	1.35	2.86	5.19E-02	2.45E-02	32.05	570.37
5:1	5.15E+07	6.47E+07	6.47E-03	7.97E+09	1.00E+10	2.03	166.98	238.60	71.62	1.08	1.54	3.76E-02	2.63E-02	35.23	145.59
10:1	3.29E+07	4.61E+07	4.61E-03	7.13E+09	1.00E+10	2.87	149.36	223.78	74.42	0.69	1.03	4.21E-02	2.81E-02	25.90	213.85
INSET															
1:1	1.63E+08	2.92E+08	2.92E-02	5.58E+09	1.00E+10	4.42	116.97	271.21	154.23	3.42	7.92	5.37E-02	2.32E-02	34.90	681.54
2:1	9.40E+07	1.55E+08	1.55E-02	6.09E+09	1.00E+10	3.91	127.57	263.80	136.22	1.97	4.08	4.93E-02	2.38E-02	34.81	533.04
5:1	5.36E+07	7.67E+07	7.67E-03	6.98E+09	1.00E+10	3.02	146.32	244.53	98.21	1.12	1.88	4.29E-02	2.57E-02	32.54	296.43
10:1	3.71E+07	5.07E+07	5.07E-03	7.32E+09	1.00E+10	2.68	153.36	229.71	76.35	0.78	1.17	4.10E-02	2.74E-02	28.46	204.85

P	Q	R	S	T	U	V	W	X	Y	Z	AA	AB	AC	AD
d_{90}	θ_{fL}°	θ_{fH}°	sweep°	deg/GHz	$Mtest_H$	fH*d	fHmax	k0max	k0max[1]	fH for bsi	β ..	β ..*d	β ..*d [2]	Vol cm^3
0.033227	124.85	70.85	54.00939	26.40	0.514	1.301E+09	3.917E+10	820.86	210.231	0.024366	68.769	1.676	5.107	15.073
0.032890	112.42	75.47	36.95333	10.80	0.345	1.878E+09	5.692E+10	1192.94	321.172	0.025852	52.588	1.359	5.418	12.917
0.029919	95.45	85.01	10.4399	12.29	0.186	3.371E+09	1.127E+11	2361.07	514.620	0.027530	18.222	0.502	5.770	12.578
0.034426	101.76	81.52	20.23518	7.32	0.037	1.644E+10	4.776E+11	10009.46	708.971	0.029442	30.896	0.910	6.171	13.254
0.034639	146.36	37.36	109.001	25.20	0.584	1.159E+09	3.346E+10	701.29	254.850	0.023818	82.407	1.963	4.992	10.257
0.033283	123.91	71.18	52.72966	26.34	0.496	1.343E+09	4.034E+10	845.43	421.793	0.024507	67.605	1.657	5.136	7.489
0.030983	102.38	80.16	22.22136	10.93	0.296	2.165E+09	6.989E+10	1464.80	728.341	0.026333	35.810	0.943	5.519	6.279
0.033677	104.43	79.77	24.653	8.58	0.140	4.426E+09	1.314E+11	2754.56	1021.352	0.028077	37.211	1.045	5.885	6.386
0.032373	131.24	39.20	92.0426	27.36	0.674	1.020E+09	3.150E+10	660.15	161.364	0.023168	77.117	1.787	4.856	25.585
0.032109	122.27	42.46	79.81282	28.05	0.584	1.159E+09	3.610E+10	756.56	305.003	0.023818	68.111	1.622	4.992	14.323
0.032151	109.61	76.45	33.15704	19.76	0.361	1.798E+09	5.593E+10	1172.13	614.223	0.025695	49.103	1.262	5.385	8.829
0.032805	104.42	79.50	24.91028	9.28	0.201	3.122E+09	9.518E+10	1994.79	928.826	0.027353	38.177	1.044	5.733	7.722

Column→	P	Q	R	S	T	U	V	W	X	Y	Z	AA	AB	AC	AD
Row ↓	d±	θ_{fL}°	θ_{fH}°	sweep°	deg/GHz	$Mtest_H$	fH*d	fHmax	k0max	k0max[1]	fH for bsi	β ..	β ..*d	β ..*d [2]	Vol cm^3
13	**0.0370**	114.28	65.16	49.13	25.47	0.514	1.301E+09	3.517E+10	737.15	210.231	0.024366	88.052	2.145	5.107	15.073
14	**0.0350**	107.58	72.36	35.23	10.30	0.345	1.878E+09	5.365E+10	1124.41	321.172	0.025852	63.528	1.642	5.418	12.917
15	**0.0299**	95.45	85.01	10.44	12.29	0.186	3.371E+09	1.127E+11	2361.07	514.620	0.027530	18.222	0.502	5.770	12.578
16	0.034426	101.76	81.52	20.24	7.32	0.037	1.644E+10	4.776E+11	10009.46	708.971	0.029442	30.896	0.910	6.171	13.254
17	**0.0350**	144.45	36.72	107.74	25.12	0.584	1.159E+09	3.312E+10	694.06	254.850	0.023818	84.276	2.007	4.992	10.257
18	**0.0370**	113.67	65.60	48.06	25.43	0.496	1.343E+09	3.629E+10	760.49	421.793	0.024507	66.570	1.617	5.136	7.489
19	**0.0315**	101.22	79.24	21.98	10.81	0.296	2.165E+09	6.874E+10	1440.78	728.341	0.026333	39.136	1.031	5.519	6.279
20	**0.0345**	102.67	78.53	24.14	8.40	0.140	4.426E+09	1.283E+11	2688.86	1021.352	0.028077	41.660	1.170	5.885	6.386
21	**0.0310**	137.12	42.30	94.81	27.65	0.674	1.020E+09	3.289E+10	689.38	161.364	0.023168	68.522	1.587	4.856	25.585
22	**0.0297**	131.17	48.65	82.51	28.46	0.584	1.159E+09	3.903E+10	817.91	305.003	0.023818	52.241	1.244	4.992	14.323
23	**0.0310**	112.65	78.48	34.17	19.71	0.361	1.798E+09	5.800E+10	1215.66	614.223	0.025695	41.846	1.075	5.385	8.829
24	**0.0335**	102.89	78.40	24.49	9.13	0.201	3.122E+09	9.320E+10	1953.40	928.826	0.027353	42.152	1.153	5.733	7.722

			Rectangular dielectric guide of Er = 12, operating frequency to 10 GHz.												
Column→	A	B	C	D	E	F	G	H	I	J	K	L	M	N	O
OPEN	**fL*b**	**fH*b**	**b**	**fL**	**fH**	**Δf_GHz**	**kz_{fL}**	**kz_{H}**	**Δkz**	**kz_{L}*b**	**kz_{H}*b**	**λg_{fL}**	**λg_{H}**	**kz/GHz**	**Δf*Δkz**
1:1	5.06E+07	7.27E+07	7.27E-03	6.96E+09	1.00E+10	3.04	145.82	510.64	364.82	1.06	3.71	4.31E-02	1.23E-02	119.91	1109.89
2:1	4.36E+07	5.26E+07	5.26E-03	8.30E+09	1.00E+10	1.70	173.90	395.69	221.78	0.91	2.08	3.61E-02	1.59E-02	130.27	377.59
5:1	3.72E+07	4.06E+07	4.06E-03	9.16E+09	1.00E+10	0.84	191.97	262.58	70.61	0.78	1.07	3.27E-02	2.39E-02	83.99	59.37
10:1	3.14E+07	3.56E+07	3.56E-03	8.84E+09	1.00E+10	1.16	185.20	220.23	35.03	0.66	0.78	3.39E-02	2.85E-02	30.10	40.77
IMAGE															
1:1	3.12E+07	5.76E+07	5.76E-03	5.42E+09	1.00E+10	4.58	113.60	567.51	453.92	0.65	3.27	5.53E-02	1.11E-02	99.11	2078.95
2:1	2.53E+07	3.65E+07	3.65E-03	6.94E+09	1.00E+10	3.06	145.54	510.03	364.50	0.53	1.86	4.32E-02	1.23E-02	119.27	1113.94
5:1	2.13E+07	2.44E+07	2.44E-03	8.74E+09	1.00E+10	1.26	183.27	357.57	174.30	0.45	0.87	3.43E-02	1.76E-02	138.81	218.86
10:1	1.84E+07	2.05E+07	2.05E-03	8.97E+09	1.00E+10	1.03	188.02	254.71	66.69	0.38	0.52	3.34E-02	2.47E-02	64.82	68.61
INSET															
1:1	5.05E+07	8.89E+07	8.89E-03	5.68E+09	1.00E+10	4.32	119.14	606.84	487.70	1.06	5.40	5.27E-02	1.04E-02	113.01	2104.65
2:1	3.12E+07	4.78E+07	4.78E-03	6.52E+09	1.00E+10	3.48	136.70	561.46	424.76	0.65	2.68	4.60E-02	1.12E-02	122.14	1477.15
5:1	2.22E+07	2.66E+07	2.66E-03	8.32E+09	1.00E+10	1.68	174.47	402.34	227.87	0.46	1.07	3.60E-02	1.56E-02	135.99	381.85
10:1	1.89E+07	2.10E+07	2.10E-03	8.99E+09	1.00E+10	1.01	188.35	275.29	86.93	0.40	0.58	3.34E-02	2.28E-02	85.80	88.08

P	Q	R	S	T	U	V	W	X	Y	Z	AA	AB	AC	AD
d_{90}	**θ_{fL}°**	**θ_{fH}°**	**sweep°**	**deg/GHz**	**$Mtest_{H}$**	**fH*d**	**fHmax**	**k0max**	**k0max[1]**	**fH for bsi**	**$\beta_{,}$**	**$\beta_{,}$*d**	**$\beta_{,}$*d [2]**	**Vol cm³**
0.019143	194.53	7.45	187.0792	61.49	0.449	2.09E+08	1.09E+10	228.51	195.315	0.012305	182.408	2.244	2.579	1.588
0.022062	129.62	58.06	71.56145	42.03	0.233	3.38E+08	1.53E+10	320.74	270.312	0.015879	110.891	1.761	3.328	1.658
0.027646	100.60	80.30	20.29686	24.14	0.052	1.19E+09	4.29E+10	898.84	349.693	0.023929	35.307	0.845	5.015	2.476
0.030996	95.43	85.21	10.2214	8.78	0.009	5.90E+09	1.90E+11	3992.13	399.615	0.028530	17.516	0.500	5.980	3.793
0.018450	266.34	-4.75	271.0914	59.19	0.576	1.76E+08	**9.51E+09**	199.41	246.816	0.011071	226.958	2.513	2.320	0.994
0.019169	194.61	7.49	187.1175	61.23	0.447	2.09E+08	1.09E+10	228.65	389.599	0.012319	182.250	2.245	2.582	0.798
0.023235	118.39	65.43	52.96476	42.18	0.174	4.25E+08	1.83E+10	382.99	583.052	0.017572	87.150	1.531	3.683	0.891
0.028383	100.22	80.85	19.37002	18.83	0.043	1.39E+09	4.91E+10	1028.08	694.452	0.024668	33.345	0.823	5.170	1.256
0.017310	272.68	-9.41	282.0884	65.37	0.671	1.58E+08	**9.14E+09**	191.51	159.803	0.010354	243.849	2.525	2.170	2.372
0.017999	213.62	-0.76	214.3797	61.65	0.562	1.79E+08	**9.92E+09**	207.92	297.248	0.011191	212.381	2.377	2.345	1.371
0.021786	130.77	27.15	103.6199	61.84	0.244	3.26E+08	1.50E+10	313.58	533.543	0.015617	113.937	1.779	3.273	1.064
0.027104	103.34	78.03	25.31243	24.98	0.066	9.56E+08	3.53E+10	739.51	676.167	0.022824	43.467	0.992	4.784	1.325

Column→	P	Q	R	S	T	U	V	W	X	Y	Z	AA	AB	AC	AD
Row ↓	**d±**	**θ_{fL}°**	**θ_{fH}°**	**sweep°**	**deg/GHz**	**$Mtest_{H}$**	**fH*d**	**fHmax**	**k0max**	**k0max[1]**	**fH for bsi**	**$\beta_{,}$**	**$\beta_{,}$*d**	**$\beta_{,}$*d [2]**	**Vol cm³**
1	0.021300	181.31	-1.66	182.97	60.14	0.449	2.09E+08	**9.80E+09**	205.36	195.315	0.012305	215.654	2.654	2.579	1.588
2	0.022030	129.80	58.19	71.61	42.06	0.233	3.38E+08	1.53E+10	321.20	270.312	0.015879	110.475	1.754	3.328	1.658
3	0.027646	100.60	80.30	20.30	24.14	0.052	1.19E+09	4.29E+10	898.84	349.693	0.023929	35.307	0.845	5.015	2.476
4	0.030996	95.43	85.21	10.22	8.78	0.009	5.90E+09	1.90E+11	3992.13	399.615	0.028530	17.516	0.500	5.980	3.793
5	0.023000	203.88	-23.85	227.73	49.72	0.576	1.76E+08	**7.63E+09**	159.96	246.816	0.011071	294.330	3.259	2.320	0.994
6	0.021300	181.54	-1.49	183.04	59.89	0.447	2.09E+08	**9.82E+09**	205.77	389.599	0.012319	215.049	2.649	2.582	0.798
7	0.023700	116.52	63.82	52.70	41.97	0.174	4.25E+08	1.79E+10	375.47	583.052	0.017572	92.455	1.625	3.683	0.891
8	0.028383	100.22	80.85	19.37	18.83	0.043	1.39E+09	4.91E+10	1028.08	694.452	0.024668	33.345	0.823	5.170	1.256
9	0.020400	215.82	-25.20	241.02	62.73	0.671	1.58E+08	**7.75E+09**	162.50	159.803	0.010354	298.839	3.094	2.170	2.372
10	0.020650	193.05	-13.13	206.18	59.29	0.562	1.79E+08	**8.65E+09**	181.23	297.248	0.011191	257.191	2.878	2.345	1.371
11	0.019800	144.97	36.47	108.50	64.75	0.244	3.26E+08	1.65E+10	345.04	533.543	0.015617	85.008	1.328	3.273	1.064
12	0.027410	102.53	77.31	25.23	24.90	0.066	9.56E+08	3.49E+10	731.25	676.167	0.022824	46.056	1.051	4.784	1.325

APPENDIX F – NEW DIELECTRIC WAVEGUIDE SPECIFICATIONS CHART

Refer to section 7.3.6.

Waveguide size designations		**Size, mm**	**Frequency range coefficients**		**Longitudinal propagation constant coefficients**
U.K.	U.S.A	width a, height b	f_L	f_H	kz_{fH}
WG 6	WR650	165.1, 82.55	U=131, V=4	U=152, V=93	P=0.68, Q=0.40
WG 8	WR430	109.22, 54.61	U=131, V=4	U=152, V=93	P=0.68, Q=0.40
WG 9A	WR340	86.36, 43.18	U=131, V=4	U=152, V=93	P=0.68, Q=0.40
WG 10	WR284	72.14, 34	U=129, V=4	U=149, V=90	P=0.66, Q=0.45
WG 11A	WR229	58.17, 29.08	U=131, V=4	U=152, V=93	P=0.68, Q=0.40
WG 12	WR187	47.55, 22.15	U=128, V=4	U=148, V=89	P=0.65, Q=0.46
WG 13	WR159	40.39, 20.19	U=131, V=4	U=152, V=93	P=0.68, Q=0.40
WG 14	WR137	34.85, 15.8	U=127, V=4	U=147, V=85	P=0.64, Q=0.49
WG 15	WR112	28.5, 12.624	U=127, V=6	U=146, V=82	P=0.64, Q=0.47
WG 16	WR90	22.86, 10.16	U=127, V=6	U=146, V=82	P=0.64, Q=0.47
WG 17	WR75	19.05, 9.525	U=131, V=4	U=152, V=93	P=0.68, Q=0.40
WG 18	WR62	15.8, 7.9	U=131, V=4	U=152, V=93	P=0.68, Q=0.40
WG 19	WR51	12.954, 6.477	U=131, V=4	U=152, V=93	P=0.68, Q=0.40
WG 20	WR42	10.688, 4.318	U=124, V=7	U=142, V=72	P=0.60, Q=0.56
WG 22	WR28	7.11, 3.56	U=131, V=4	U=152, V=93	P=0.68, Q=0.40
WG 23	WR22	5.7, 2.85	U=131, V=4	U=152, V=93	P=0.68, Q=0.40
WG 24	WR19	4.78, 2.39	U=131, V=4	U=152, V=93	P=0.68, Q=0.40
WG 25	WR15	3.76, 1.88	U=131, V=4	U=152, V=93	P=0.68, Q=0.40
WG 26	WR12	3.1, 1.55	U=131, V=4	U=152, V=93	P=0.68, Q=0.40
WG 27	WR10	2.54, 1.27	U=131, V=4	U=152, V=93	P=0.68, Q=0.40
WG 28	WR8	2.03, 1.016	U=131, V=4	U=152, V=93	P=0.68, Q=0.40
	WR6	1.65, 0.826	U=131, V=4	U=152, V=93	P=0.68, Q=0.40
	WR5	1.3, 0.65	U=131, V=4	U=152, V=93	P=0.68, Q=0.40
	WR3	0.86, 0.43	U=131, V=4	U=152, V=93	P=0.68, Q=0.40

$$f_{L,H} = \frac{(U\varepsilon_r + V)\times 10^6}{b\varepsilon_r^{1.45}} \quad (1) \qquad kz_{fL} = \frac{2\pi f_L}{c} \quad (2) \qquad kz_{fH} = \frac{2\pi f_H}{c\varepsilon_r^{0.6}}(P\varepsilon_r + Q) \quad (3) \qquad kz_{GHz} = 10(\varepsilon_r + 1) \quad (4)$$

b is the dielectric waveguide height in mm
ε_r is the relative dielectric constant of the waveguide material
c is the speed of light, approximately 299.79×10^6 m/s

Note: kz equations (2,3) are only valid at fL and fH respectively. Use (4) to find intermediate values of kz by interpolation between fL and fH, or projection beyond fH.

APPENDIX G – DIELECTRIC GUIDE FREQUENCY RANGE OVERLAP

Refer to section 7.3.6.

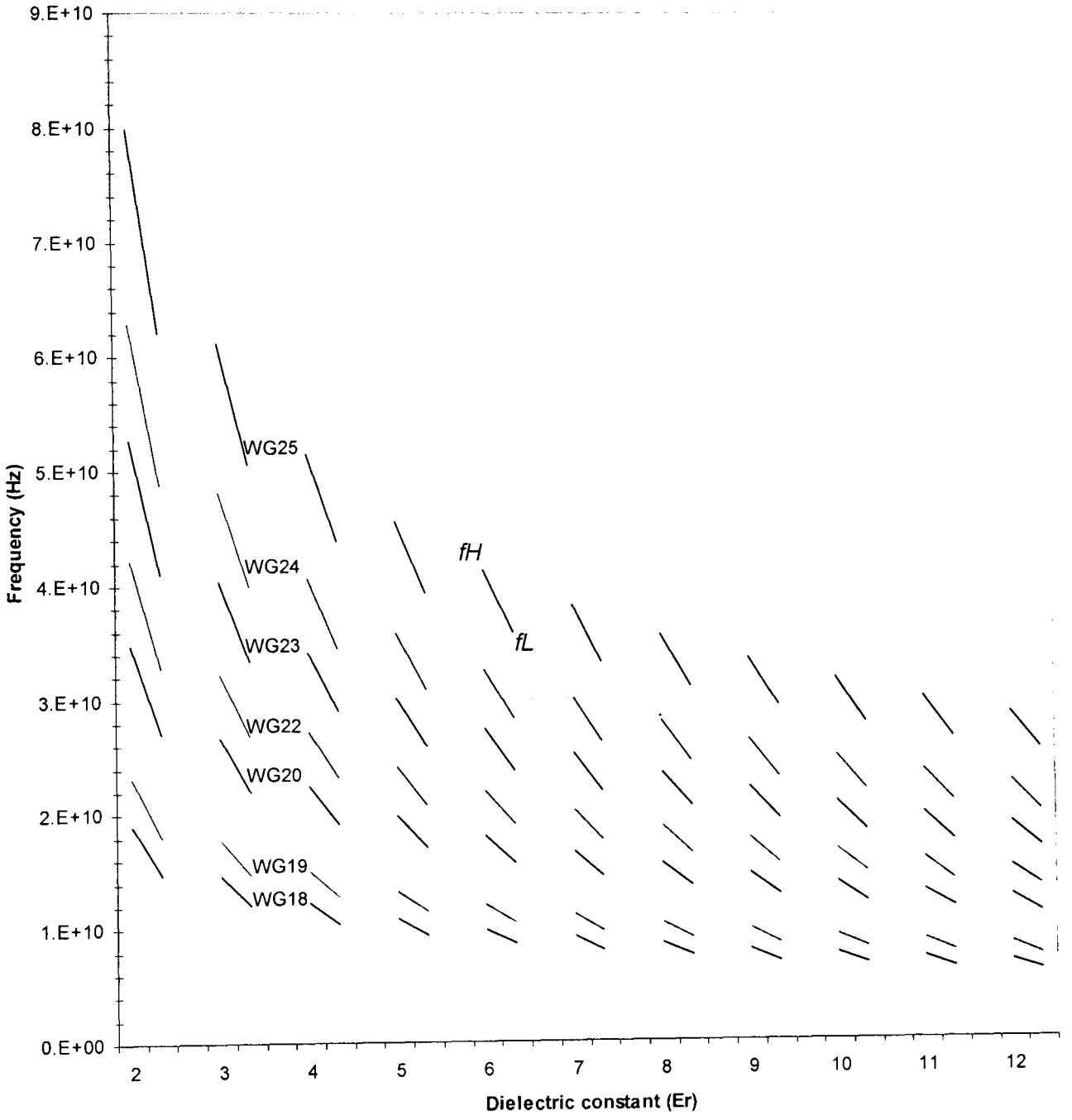

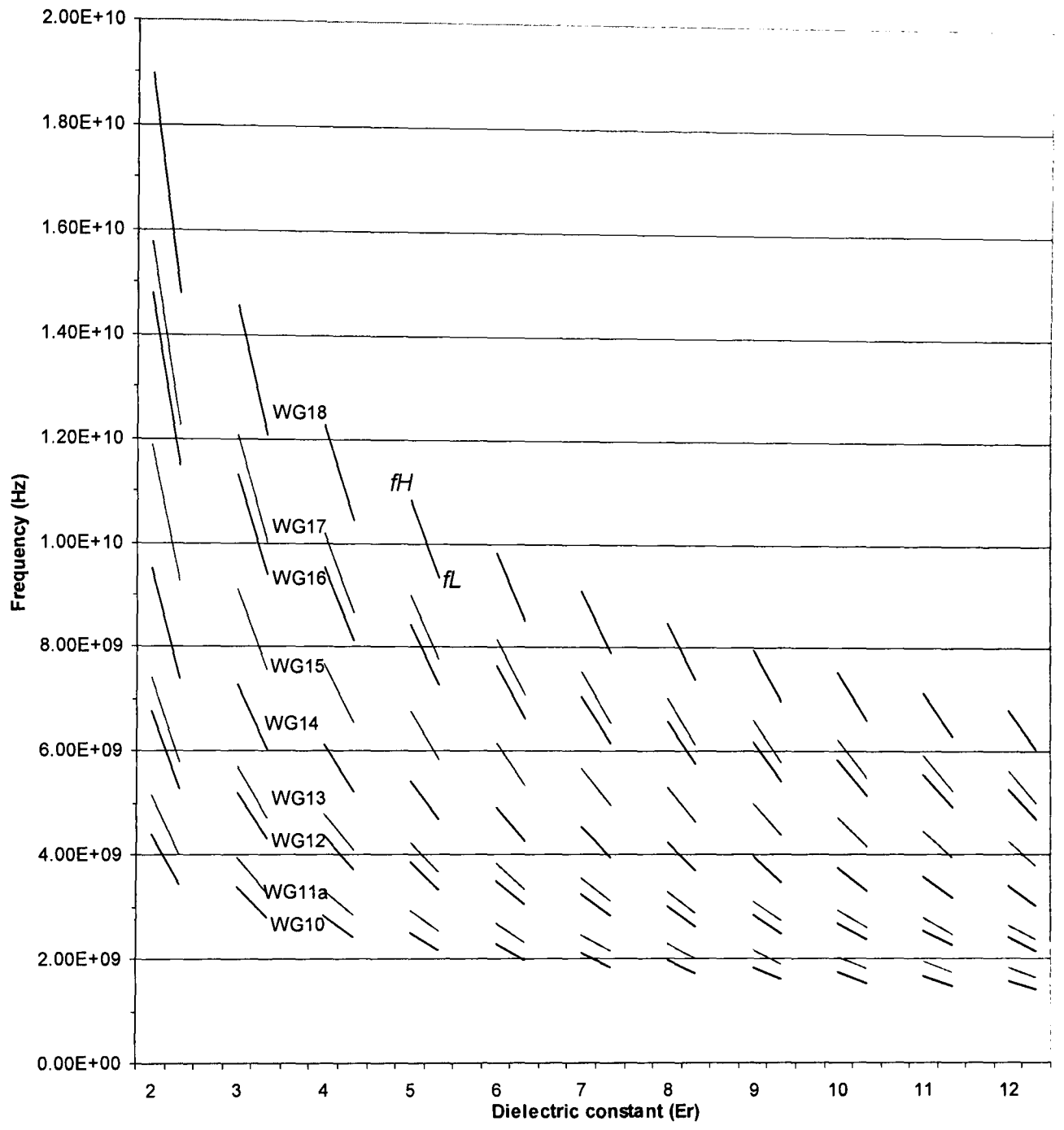
2.00E+10
1.80E+10
1.60E+10
1.40E+10
1.20E+10
1.00E+10
8.00E+09
6.00E+09
4.00E+09
2.00E+09
0.00E+00
Frequency (Hz)
WG18
WG17
WG16
WG15
WG14
WG13
WG12
WG11a
WG10
fH
fL
2
3
4
5
6
7
8
9
10
11
12
Dielectric constant (Er)

APPENDIX H – NEAR-FIELD PROBING MEASUREMENTS

Refer to section 9.4.

	Near-field probing measurements (wavelength in guide in mm)									
Strip width										Average
0mm	16.5	18	18	19						17.875
3.33mm	17.4	18.6	17.6	16.7						17.575
5mm	18	18.5								18.25
6mm	15.8	18.2	20.5	16.5	17.7	18.8	18	18	17.5	17.88889
7mm	18	18	18.9	18	17.5	19				18.23333
8.33mm	17.8	17	17.8							17.53333
14mm	17	11.5	13.2							13.9
Continuous	10	13.2	15	23.5	9.2	10.5	22.5	24		15.9875

APPENDIX I – PUBLICATIONS

TITLE: **SIMPLE ESTIMATION FORMULAS FOR RECTANGULAR DIELECTRIC WAVEGUIDE SINGLE-MODE RANGE AND PROPAGATION CONSTANT**

AUTHORS: Dean P. Hamilton, Roger J. Green and Mark S. Leeson
School of Engineering
University of Warwick
Coventry, CV4 7AL, England

PUBLICATION: Microwave and Optical Technology Letters, Wiley
MANUSCRIPT I.D.: MOP-06-0776
SUBMITTED for PUBLICATION: 10th Jul. 2006
ACCEPTED for PUBLICATION: 19th Oct. 2006
PUBLISHED: Mar. 2007 (Vol. 49, No. 3)

ABSTRACT

Closed-form formulas for estimating the single-mode frequency range and propagation constant of open rectangular dielectric waveguides are presented. The formulas are based on curve fitting to normalized results by the popular Marcatili method, suitably modified to reduce error. Excellent agreement with independent experimental data is reported.